2.12.2 GNF-J Certification Tests

Normal conditions of transport (NCT) and hypothetical accident conditions (HAC) certification testing of the RAJ-II package was also performed by GNF-J as part of obtaining a Type AF certificate of compliance in Japan [Ref. 5]. For the U.S. testing, the GNF-J certification tests were utilized to determine the worst-case test orientations for the certification tests identified in Section 2.12.1. This appendix summarizes the GNF-J RAJ-II certification tests.

2.12.2.1 Certification Test Units

Two certification test units (CTUs) were utilized for the GNF-J RAJ-II tests. Each CTU was fabricated in accordance with the Packaging General Arrangement Drawings found in Section 1.3.2, with the following exceptions:

1. The lateral wood bolsters on each end were not installed. Elimination of these wood bolsters is conservative for the free drops.

2. Maximum content weight was 560 kg (1,235 lbs), which results in a maximum package weight of 1,490 kg (3,285 lbs). This weight reduction is less than 8% lower than the maximum gross weight of the RAJ-II package, and will result in higher impact forces. The small difference in weight will have an insignificant effect on the free drop response of the package and/or fuel assembly.

One simulated fuel assembly and one dummy weight were utilized in each CTU to simulate the payload contents. Accelerometers were installed on the CTUs to measure and record each free drop impact. No accelerometers were used for the puncture drop tests.

2.12.2.2 Test Orientations

Since the RAJ-II package relies on the fuel cladding as the containment boundary, free drop and puncture drop orientations that could damage the fuel cladding and potentially breach the containment boundary should be included in the test series. In addition, orientations that could damage the package and/or the fuel assemblies such that an unsafe criticality geometry would exist should be included in the test series. Free drop orientations that could result in this type of damage include:

1. Vertical drop on the package end – maximizes axial impact acceleration to a fuel assembly, potentially buckling and failing the fuel cladding (containment boundary).

2. Horizontal drop of the package – maximizes lateral impact acceleration on a fuel assembly, potentially bending and failing the fuel cladding (containment boundary).

3. CG-over-corner of the package – maximizes deformation of outer container (OC).

All of these orientations were included in the free drop test series of the package.

Puncture drop orientations that could potentially breach the containment boundary (cladding) include:

1. Horizontal puncture drop on the center of the package – maximizes puncture impact onto fuel pins and potentially shearing and failure of the fuel cladding (containment boundary).

2. Vertical puncture drop on the end of the package – maximizes puncture impact onto the fuel assembly

Because of the end internal structure and wood dunnage in the outer container, the puncture drop on the end will not result in any significant deformation of the fuel assembly or the inner container. Therefore, this puncture drop orientation is bounded by the horizontal puncture drop on the center of the package.

The free drop tests included NCT drops of 0.3 meters (1 foot) and 1.2 meters (4 feet) prior to performing the 9-meter (30-foot) HAC free drop on each CTU. The horizontal puncture drop test was only performed on CTU 2J.

Two certification test series were performed. Three free drop tests were performed on CTU 1J, and three free drop and one puncture drop tests were performed on CTU 2J. The test series for each CTU is summarized in Table 2-10. All drop tests were performed at ambient temperature.

2.12.2.3 Test Performance

Free drop and puncture testing was performed at two test facilities in Japan. At one facility, the drop pad consisted of a 32-mm (1.26-inch) thick steel plate that was embedded in a 1-meter (40-inch) thick concrete and steel support structure, with an overall length of 8 meters (26 feet). The other drop pad consisted of a 50-mm (1.97-inch) thick × 5-meter (16.4-feet) × 5-meter (16.4-feet) steel plate that was embedded in a 450-mm (12-inch) thick × 8.5-meter (27.9-feet) wide concrete and steel structure. The mass of each drop pad constituted an essentially unyielding surface for the CTUs, which weighed approximately 1,490 kg (3,285 lbs).

2.12.2.3.1 CTU 1J

CTU 1J was tested for a total of six free drop tests at heights of 0.3 meters (1 foot), 1.2 meters (4 feet), and 9 meters (30 feet). Figures 2-43 through 2-48 sequentially photo-document the CTU 1J tests.

The maximum resultant accumulated deformation, ~163 mm (~6 inches) occurred in the OC body corner. This orientation resulted in the maximum impact acceleration of 203g. No failure of the cladding (containment boundary) occurred from this test series.

2.12.2.3.2 CTU 2J

The testing of CTU 2J focused on free drop orientations not addressed by the CTU 1J tests. In addition, a HAC puncture drop test and HAC thermal test were performed. A total of three free drop tests at heights of 0.3 meters (1 foot), 1.2 meters (4 feet), and 9 meters (30 feet) were performed. Figures 2-49 and 2-50 sequentially photo-document the CTU 2J tests.

The maximum resultant accumulated deformation, ~19 mm (~.8 inches) occurred in the OC body corner. This orientation resulted in the maximum impact acceleration of 145g. No failure of the cladding (containment boundary) occurred from this test series.

2.12.2.4 Test Summaries

Two 0.3-meter (1-foot), four 1.2-meter (4-foot), three 9-meter (30-foot) free drops, one 1-meter (40-inch) puncture drop, and one HAC thermal test were performed on two CTUs. The packages retained the fuel assemblies and protected the fuel. There was no visual damage or loss of fuel pellets from the simulated fuel assemblies from both CTUs. A summary of the test results is provided in Table 2-13.

Table 2-12 GNF-J CTU Test Series Summary

CTU	Drop Height, m (ft)	Test Description	Purpose
1J	0.3 (1)	Free drop, CG-over-bottom end lower corner	Normal operation impact on OC body corner.
	1.2 (4)	NCT free drop, CG-over-bottom end lower corner	Impart initial deformation in same orientation as subsequent HAC free drop
		NCT free drop, horizontal on OC lid	Impart initial deformation in same orientation as planned HAC free drop
		NCT free drop, vertical, bottom end	Impart initial deformation in same orientation as subsequent HAC free drop
	9 (30)	HAC free drop, CG-over-bottom end lower corner	Maximize OC body deformation; potentially fail fuel rod and breach cladding.
		HAC free drop, vertical, bottom end	Maximize axial impact loads on fuel assemblies, potentially buckle fuel rod and breach cladding.
2J	0.3 (1)	Free drop, CG-over-lid corner	Normal operation impact on OC lid/body corner interface.
	1.2 (4)	NCT free drop, horizontal on lid	Impart initial deformation in same orientation as subsequent HAC free drop
	9 (30)	HAC free drop, horizontal on lid	Maximize lateral impact loads on fuel assemblies, potentially breaching cladding.
	1 (3.3)	HAC puncture drop, horizontal on OC lid	Impact directly on HAC free drop damage; attempt to rupture fuel cladding.
	N/A	HAC thermal test	Demonstrate thermal performance of package.

Table 2-13 GNF-J CTU Test Series Results

CTU	Drop Height, m (ft)	Test Description	Result
1J	0.3 (1)	Free drop, CG-over-bottom end lower corner	Combined deformation of ~40 mm (~1.6 inches) of bottom corner.
	1.2 (4)	NCT free drop, CG-over-bottom end lower corner	
		NCT free drop, horizontal on OC lid	No significant deformation.
		NCT free drop, vertical, bottom end	Impacted end deformed ~3.9 mm (~0.2 inches)
	9 (30)	HAC free drop, CG-over-bottom end lower corner	Impacted OC bottom corner deformed ~163 mm (~6 inches), OC lid corner ~101 mm (~4 inches). Maximum acceleration of 203g.
		HAC free drop, vertical, bottom end	IC body/lid deformed ~2 - 81 mm (~0.08 - 3 inches) in length, U-shaped lifting bar on fuel assembly bent due to contact with wood end dunnage. Maximum acceleration of 58g.
2J	0.3 (1)	Free drop, CG-over-lid corner	Combined deformation of ~2.9 mm (~0.1 inches) of lid corner.
	1.2 (4)	NCT free drop, horizontal on lid	
	9 (30)	HAC free drop, horizontal on lid	Impacted side deformed ~2 - 19 mm (~0.08 -0.8 inches), localized weld failure of OC lid flange/OC lid sheet interface, no failure of OC lid bolts. Maximum acceleration of 145g.
	1 (3.3)	HAC puncture drop, horizontal on OC lid	~100 mm deep × ~2,000 mm (~4 inches × ~79 inches) wide indention in OC lid, no breach of OC lid sheet.
	N/A	HAC thermal test	No failure of simulated fuel assembly cladding.

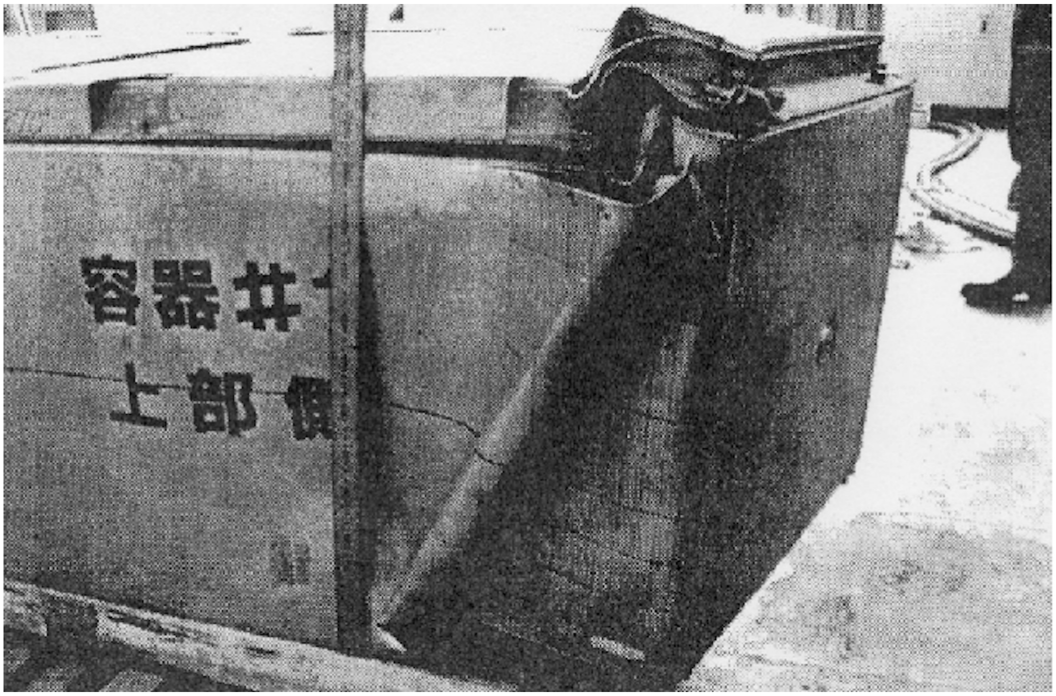

Figure 2-43 CTU 1J 9 m CG-Over-Bottom Corner Free Drop: View of Impacted Corner

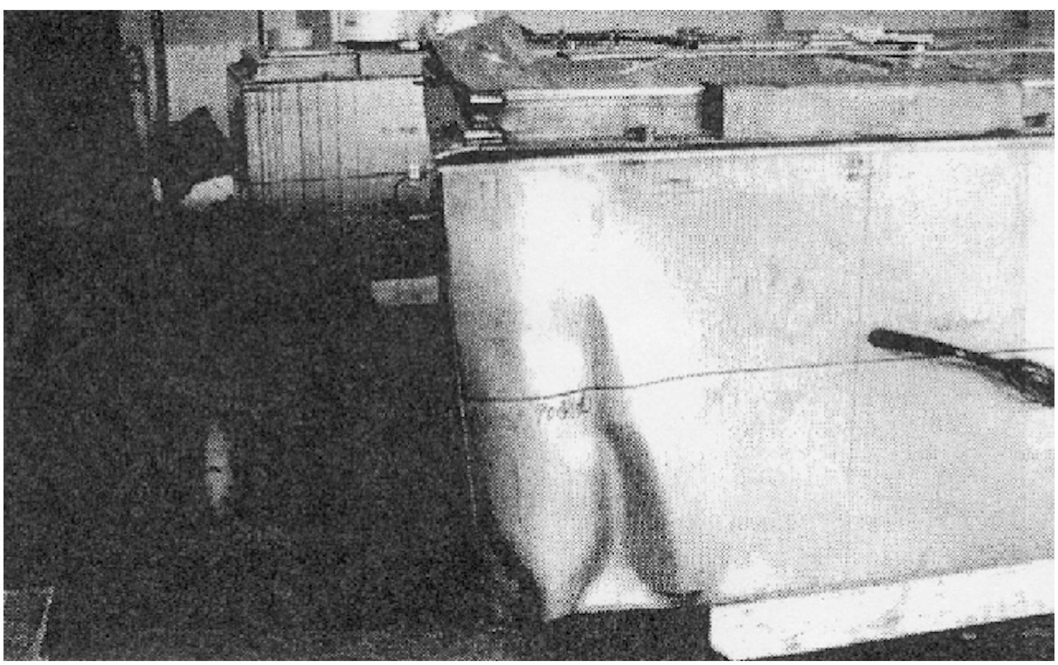

Figure 2-44 CTU 1J 9 m CG-Over-Bottom Corner Free Drop: View of Opposite Corner

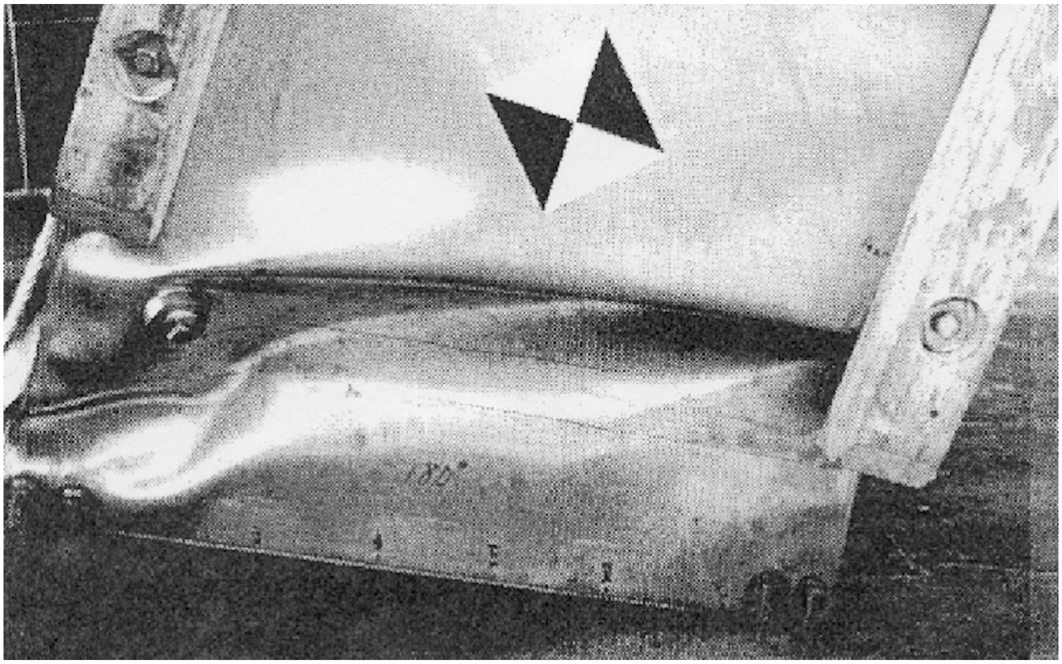

Figure 2-45 CTU 1J 9 m CG-Over-Bottom Corner Free Drop: View of Bottom

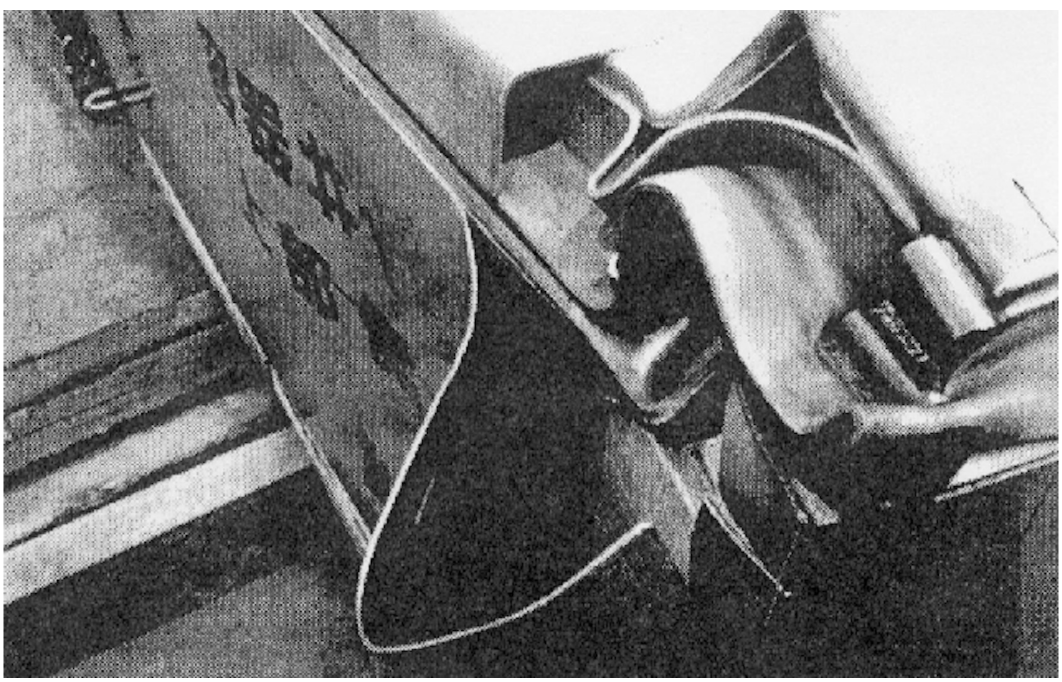

Figure 2-46 CTU 1J 9 m CG-Over-Bottom Corner Free Drop: Close-up View of Top Corner

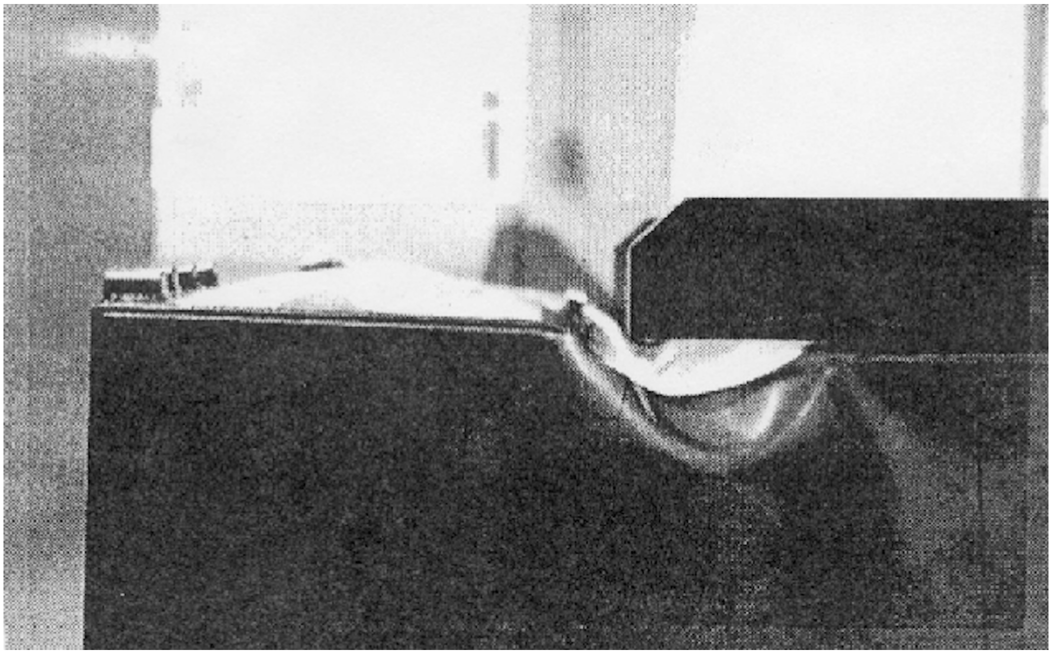

Figure 2-47 CTU 1J 9-m Vertical End Drop: Close-up Side View of Bottom Damage

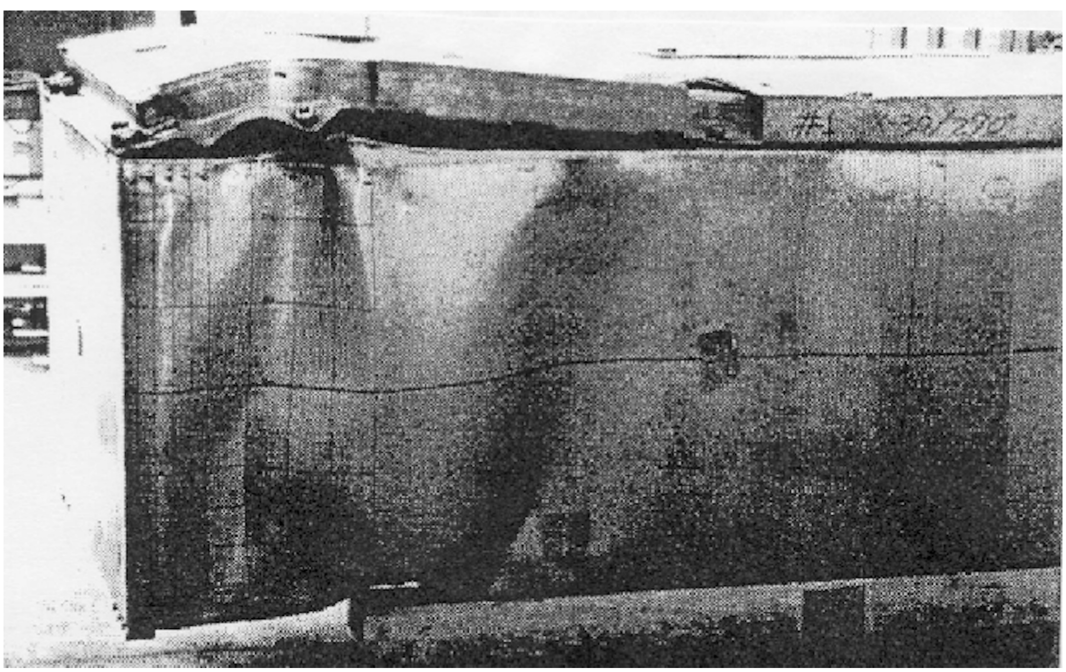

Figure 2-48 CTU 1J 9-m Vertical End Drop: Overall View of Damage

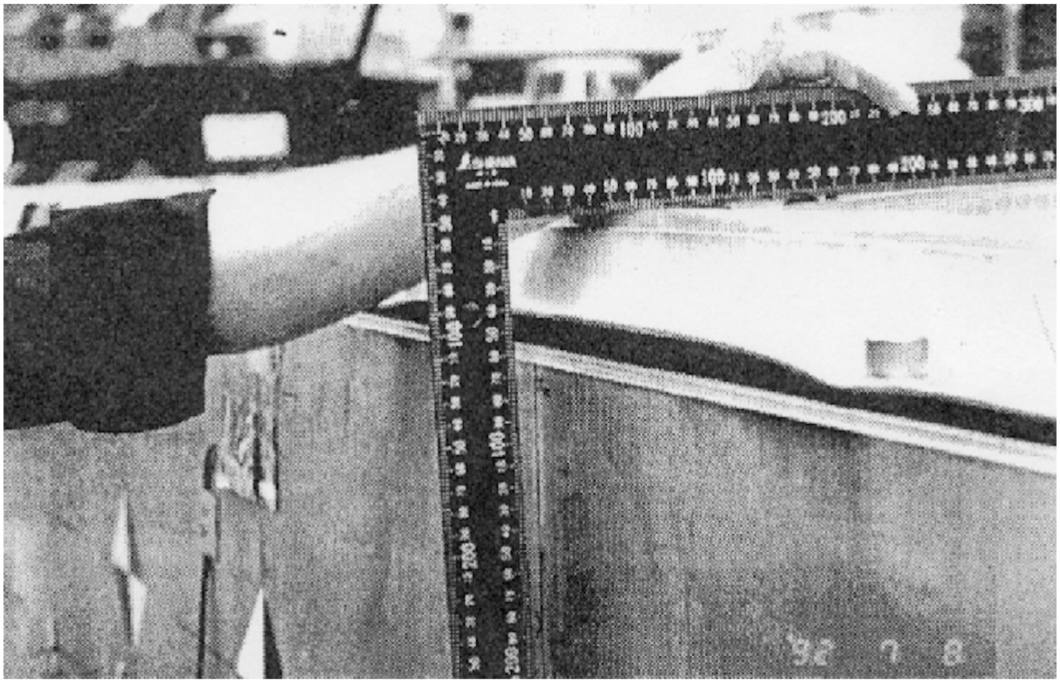

Figure 2-49 CTU 2J 9-m Horizontal Free Drop: Close-up Side View of Damage

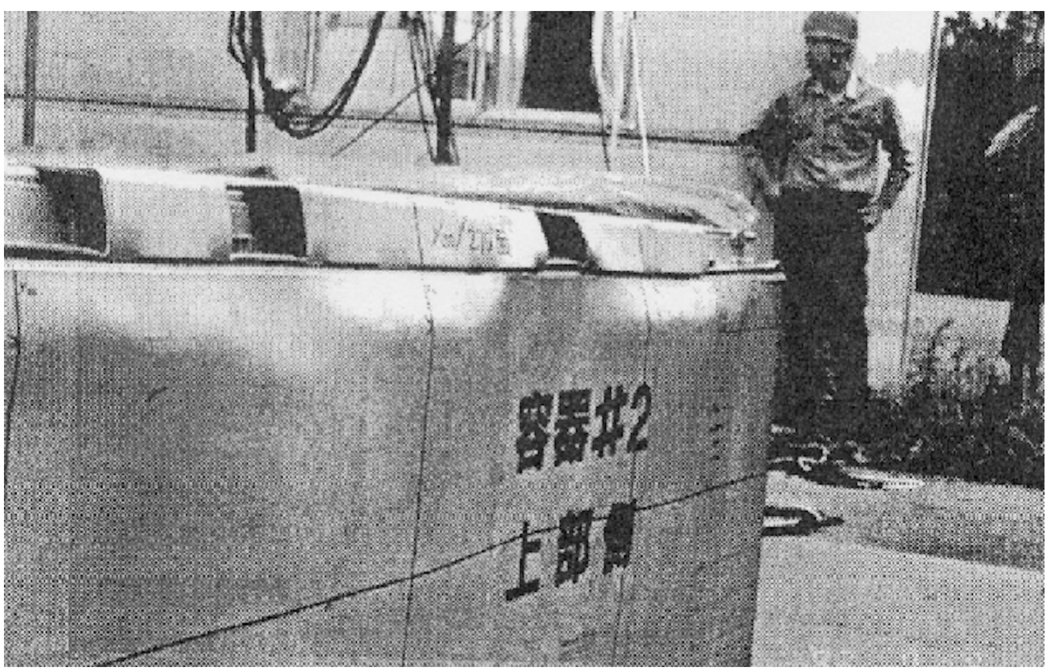

Figure 2-50 CTU 2J 9-m Horizontal Free Drop: Overall Side View of Damage

2.12.3 Outer Container Gasket Sealing Capability

The outer container for the RAJ-II packaging utilizes a 5 mm thick × 40 mm wide × 11,360 mm long, 50 shore durometer, solid elastomer gasket. As shown in Section 1.3.2, Packaging General Arrangement Drawings, the gasket is attached to the flange of the outer container lid. The outer container lid is secured to the outer container body by twenty-four (24) M14 × 2, Type 304 stainless steel bolts, which are tightened to "wrench tight or as defined in user procedures".

2.12.3.1 Seal Evaluation for NCT

Since a specific tightening torque is not specified, the maximum bolt tension will be based on the minimum yield strength of the stainless steel.

The maximum force, F_b, in each lid bolt will be:

$$F_b = S_y(A_t)$$

where:

S_y = 206.8 MPa (30.0 ksi), Minimum yield strength (Ref. Table 2-2)

A_t = 115 mm^2 (0.1783 in^2), Tensile area for M14 × 2 bolt

Substituting these values into the above equation yields a bolt force of 23,794 N (5,349 lb_f). The total compressive force applied to the gasket, F_{gasket}, is then:

$$F_{gasket} = (24)F_b = (24)(23{,}794) = 571{,}056 \text{ N } (128{,}378 \text{ lb}_f)$$

For the applied bolt force, the gasket compressive area, A_{gasket}, is 40 × 11,360 = 454,400 mm^2 (704.3 in^2). Conservatively neglecting any deflection of the 4-mm thick lid flange between the lid bolts, the resultant compressive stress on the gasket is then:

$$\sigma_{gasket} = \frac{571{,}056}{454{,}400} = 1.257 \text{ MPa (182 psi)}$$

The shape factor, s, for the 5 × 40 gasket is:

$$s = \frac{\text{One Load Area}}{\text{Total Free Area}} = \frac{\text{Width}}{2(\text{thickness})} = \frac{40}{10} = 4.0$$

From Figure 5-12 of Handbook of Molded and Extruded Rubber [Ref. 6], the percent compressive deflection of the 50-durometer natural rubber gasket with s = 4.0 at 182 psi compressive stress is approximately 3%, or 0.15 mm (0.006 in), which is minimal.

To determine whether the gasket is compressed with the applied bolt force, the compression modulus and the linear spring rate for the gasket is computed. Equation 3-7 of Handbook of Molded and Extruded Rubber, the linear spring rate, K_L, for the rubber gasket is:

$$K_L = \frac{E_c(A)}{h}$$

where:

E_c = Compression modulus

A = 454,400 mm^2 (704 in^2), Compression area of gasket

h = 5 mm (0.197 in), height of gasket

The compression modulus is extracted from Figure 5-20 of the Handbook of Molded and Extruded Rubber for a shape factor "s" of 4.0 and an approximate compression of 3% for the 50 durometer gasket. From this figure, the compression modulus is interpolated to be 6,912 psi (47.7 MPa). The linear spring rate of the gasket is then:

$$K_L = \frac{6{,}912(704)}{0.197} = 24.7 \times 10^6 \text{ lb}_f/\text{in } (4.33 \times 10^6 \text{ N/mm})$$

To compress the gasket 0.15 mm (0.006 in), the required force in the bolts is:

$$24F_{bolt} = K_L\Delta = 24.7 \times 10^6(0.006) = 148{,}200 \text{ lb}_f \text{ (659,226 N)}$$
$$\Rightarrow F_{bolt} = 6{,}175 \text{ lb}_f \text{ (27,468 N)}$$

Since the resultant bolt force required to compress the gasket 3% is greater than the yield strength of the lid bolts, the gasket will not be compressed to the estimated 3% compression.

To determine the estimated gasket compression with the maximum lid bolt force at yield strength (23,794 N [5,349 lb_f]), the linear spring rate will be computed for zero compression and then compared to the applied maximum force. From Figure 5-20 of the Handbook of Molded and Extruded Rubber for a shape factor "s" of 4.0, the compression modulus at zero compression will be:

$$E_c = 9{,}000(0.75) = 6{,}750 \text{ psi (46.5 MPa)}$$

For zero compression and this compression modulus, the linear spring rate is:

$$K_L = \frac{6{,}750(704)}{0.197} = 24.1 \times 10^6 \text{ lb}_f/\text{in } (4.22 \times 10^6 \text{ N/mm})$$

The resultant deformation of the gasket for this spring rate with the maximum bolt force is:

$$\Delta_{gasket} = \frac{24(F_{bolt})}{K_L} = \frac{24(23{,}794)}{4.22 \times 10^6} = 0.135 \text{ mm } (0.005 \text{ in})$$

This deformation is approximately 2.7% compression of the gasket. Prototypic seal testing in support of the TRUPACT-II package [Ref. 7] has demonstrated that a pressure seal requires a minimum of 10% – 12% compression. Section 3.6, *Squeeze*, of the Parker O-ring Handbook [Ref. 8] states that "*The minimum squeeze for all seals, regardless of cross-section should be about 0.2 mm (0.007 inches). The reason is that with a very light squeeze almost all elastomers quickly take 100% compression set.*" Based on these test results and the recommendations of Parker, the outer lid gasket will not form a pressure retaining seal.

2.12.3.2 Closure Bolt Evaluation for HAC

No credit is taken for the sealing capabilities of the outer container during HAC. However, it is necessary to predict the performance of the closure bolts during HAC impact conditions. To estimate the load applied to the lid of the outer container, it is assumed the loaded inner container weight is conservatively applied to the lid during a top impact event without the benefit of the inner container hold down clamps. The maximum force due to impact, F_{bi}, in each lid bolt is:

$$F_{bi} = S_U (A_t) = 59{,}484 \text{ N } (13{,}373 \text{ lb}_f)$$

where:

S_U = 571 MPa (75.0 ksi), ultimate tensile strength (Ref. Table 2-2)
A_t = 115 mm^2 (0.1783 in^2), Tensile area for M14 × 2 bolt

Based on accelerations during drop testing [Ref. 9] the total impact load applied to the closure bolts is calculated as follows:

$$F_i = \frac{Wg}{24} = 58{,}795 \text{ N } (13{,}213 \text{ lb}_f)$$

where:

W = 992 kg (2187 lb), weight of the inner container (Ref. Table 2-1)
g = 145 g [Ref. 9]

Comparison of the allowable force per bolt (59,484 N) and the total impact load per bolt (58,795 N) shows there is sufficient bolt strength to retain the lid during a top impact event.

2.12.4 References

1. Lustman, Benjamin, et al., *The Metallurgy of Zirconium, First Edition,* McGraw-Hill Book Company, Inc., 1955.

2. Shigley, Joseph E., and Mischke, Charles R., Mechanical Engineering Design, Fifth Edition, McGraw-Hill, Inc., 1989.

3. Framatome ANP MOX Material Properties Manual 51-5010288-03.

4. Framatome ANP MOX Material Properties Manual 51-5010288-02.

5. Global Nuclear Fuel - Japan (fka Japan Nuclear Fuel Co., Ltd), *Application for Approval of Packaging, Type RAJ-II*, STO-M00-034, dated September 26, 2000.

6. *Handbook of Molded and Extruded Rubber, Third Edition*, Goodyear Tire & Rubber Company.

7. U. S. Department of Energy (DOE), *Safety Analysis Report for the TRUPACT-II Shipping Package*, USNRC Certificate of Compliance 71-9218, U.S Department of Energy, Carlsbad Field Office, Carlsbad, New Mexico.

8. ORD 5700A/US, *Parker O-ring Handbook*, 2001, Parker Hannifin Corporation, Lexington, KY.

9. *Drop Tests Report for Demonstrating Ability to Withstand Accident Transport Conditions, RAJ-III (Europe Validation),* 12247-R-1E Rev. 0, Transnuclear, 1999.

10. “Atlas of Stress-Strain Curves”, ASM International, Materials Park, OH, 2004.

11. *LS-DYNA Keyword User’s Manual*, Version 971, Livermore Software Technology Corporation, Livermore CA, May 2007.

12. “ASME Boiler and Pressure Vessel Code, Section II, Part D, Materials, “American Society of Mechanical Engineers, July 1, 2010.

13. Honeycomb and Ethafoam Compression Test Results, Test Report GEN015-08-05-59922-1, Stork Herron Testing Laboratories, 5404 E. Schaaf Road, Cleveland, OH 44131 USA.

14. Hoadley, R. Bruce, “Understanding Wood: A Craftsman’s Guide to Wood Technology”, ISBN 1-56158-358-8, The Taunton Press, Inc., Newtown, CT, 2000.

15. “Wood Handbook – Wood as an Engineering Material”, General Technical Report FPL-GTR-113, United States Department of Agriculture, Forest Products Laboratory, One Gifford Pinchot Drive, Madison, WI 53705–2398.

16. Test Procedure, RAJ-II Vibration Test, TR63107-08N, National Technical Systems, September 2007, eDRF Section 0000-0071-3905, Global Nuclear Fuels, Wilmington, NC.

17. Mindlin, R.D., *Dynamic of Package Cushioning*, Bell Telephone System Technical Publications Monograph B-1369, Bell Telephone Laboratories, July 1945.

18. Blodgett, O.W., *Design of Welded Structures*, The James F. Lincoln Arc Welding Foundation, Cleveland Ohio, March 1996.

19. "Instrumented Drop Tests with Shipping Container (RA-3D) for New Fuel Bundles," Test Report No. III.3/20554, Federal Institute for Materials Research and Testing (BAM), Technical Group III.3 Safety of Shipping and Storage, Berlin, Germany, 1998.

2.12.5 RAJ-II Impact Analysis

A finite element model of the RAJ-II was developed to investigate the performance of the package during conditions not evaluated during the regulatory testing sequence. This appendix specifically addresses the following:

- It is noted that a difference in mass exists between the original drop tests performed in Japan (8×8 and 9×9 fuel) and the test performed in the United States (10×10 fuel). It is recognized the difference is minimal (7.7%), but must be considered when evaluating the side/top drop orientations.
- Drop testing of the package did not consider the full operating temperature range for the shock absorbing materials as defined by IAEA. The evaluation should consider cold conditions, i.e., -40°C, to maximum temperature during normal transport, 77°C.
- Evaluate the package at the maximum slapdown (whiplash) angle and compare the results to the side drop results and show how the regulatory testing is bounding.

The purpose of this appendix is to document the impact analysis of the RAJ-II package during hypothetical accident conditions using the explicit finite element analysis code LS-DYNA. Drop test data from the Japanese RAJ-II and RA-3D testing programs are used to provide a comparison with the analyzed cases and benchmark the model.

2.12.5.1 LS-DYNA Finite Element Model

The solid model of the RAJ-II was developed using Autodesk Inventor. The Inventor model was developed from the RAJ-II fabrication drawings. The model is constructed of solid objects that represent the crushable materials and surfaces for most steel components. Surfaces are two-dimensional objects that represent the center plane of the original solid surface. Figure 2-51 shows the Inventor solid model.

The finite element model is generated by importing the Inventor solid model into ANSYS Workbench and meshed using the Workbench meshing tools. Once meshed in Workbench, an ANSYS classic input file is created and opened in ANSYS 11.0 Mechanical using the ANSYS LS-DYNA PrepPost license where real constants are assigned to model components that are equivalent to LS-DYNA part definitions and generic MESH200 elements are converted to

ANSYS SOLID164 and SHELL163 explicit elements. Once the finite element model is completed, the ANSYS 'EDWRITE' command is issued to save the nodes and elements into the standard LS-DYNA keyword file format. The resulting LS-DYNA model is imported into the LSTC LS-PREPOST, which is launched from the LS-DYNA manager to ensure elements are translated from ANSYS properly. The keyword file is then edited to include control cards, database cards, material cards, and boundary condition cards. Figures 2-52 through 2-54 show the fully assembled model and each individual part.

The materials properties in the following section are based on laboratory test results and open literature. To ensure accuracy of the material model, the top drop analysis results are compared to the Japanese RAJ-II top drop test results (refer to Section 2.12.2.3).

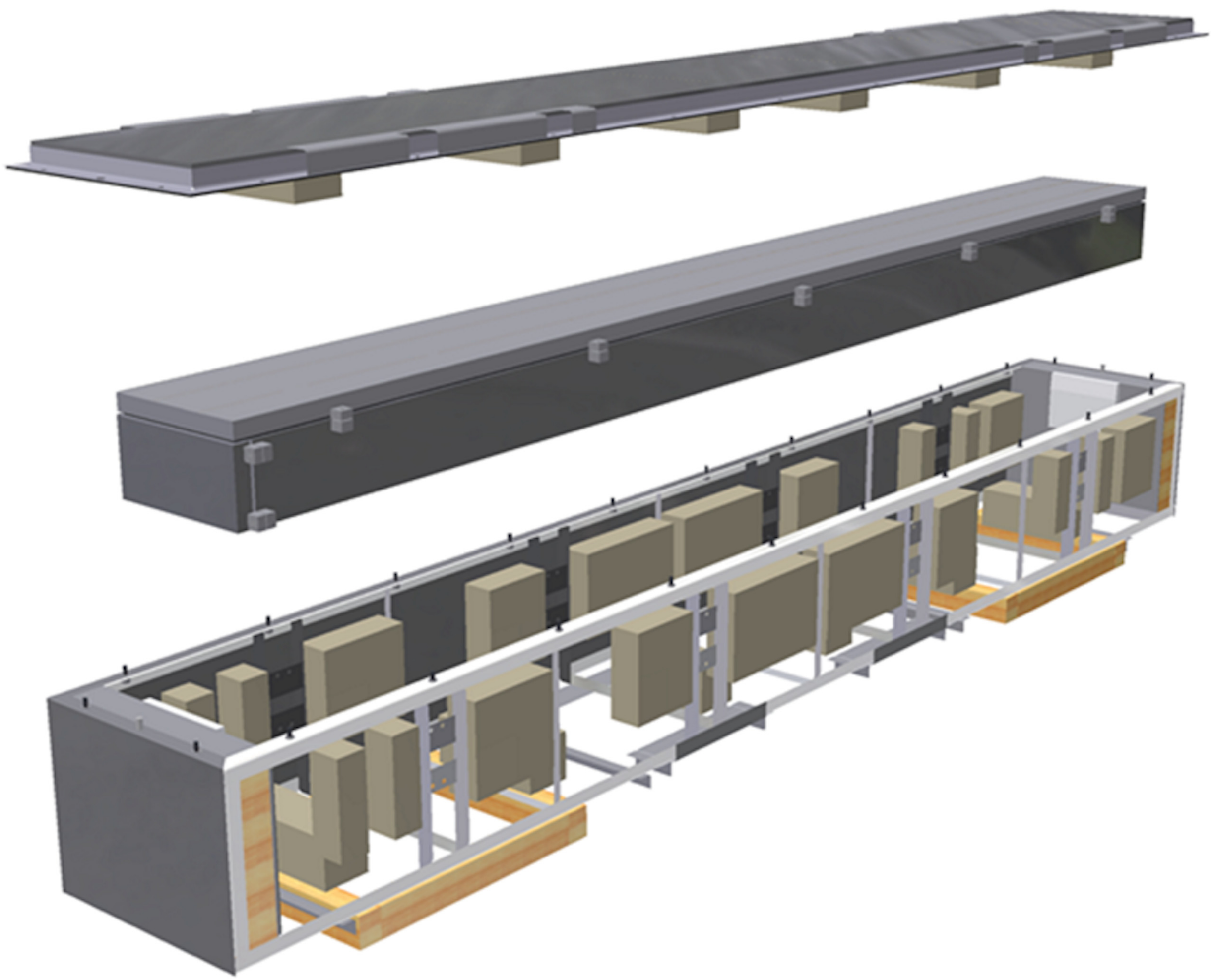

Figure 2-51 RAJ-II Solid Model

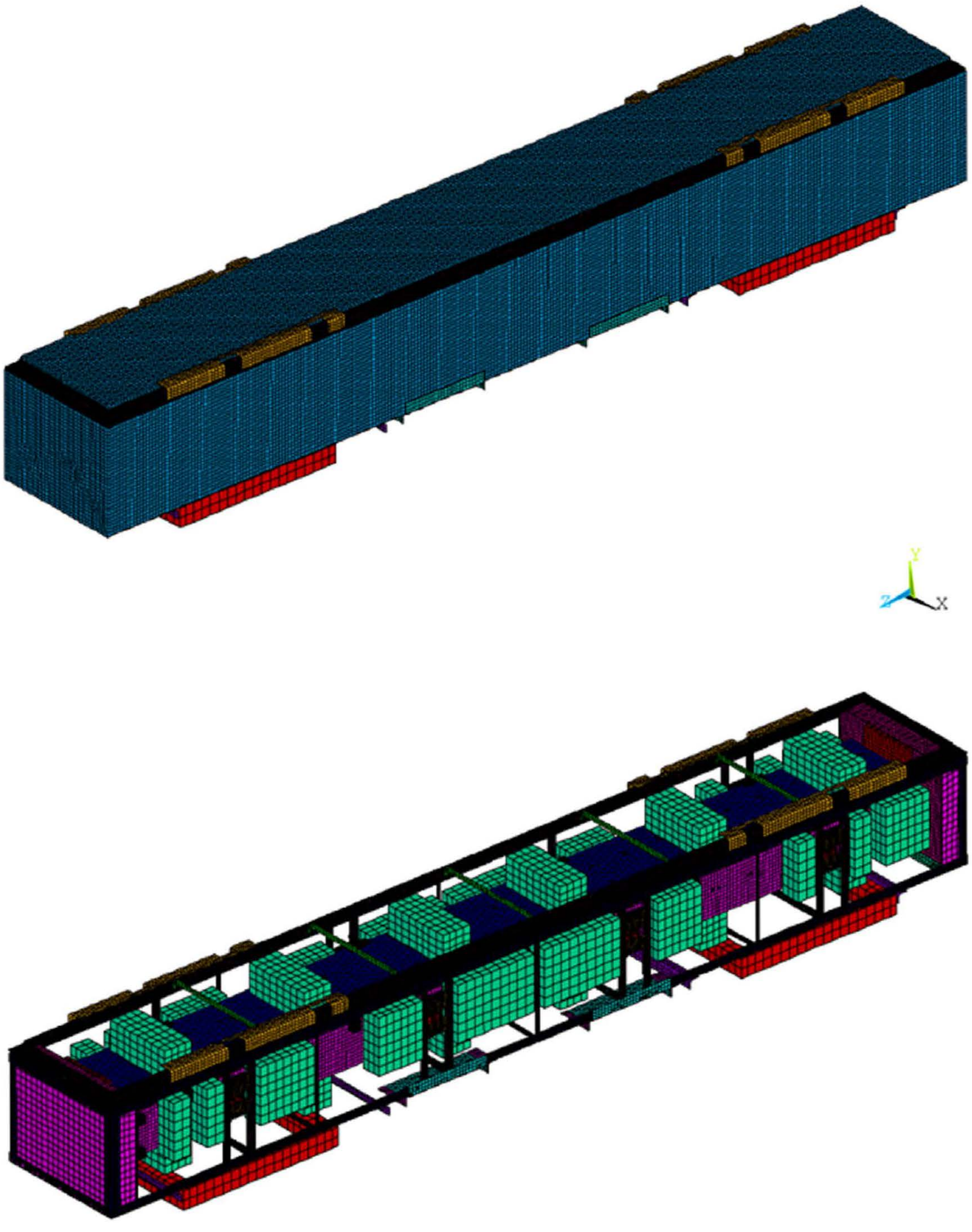

Figure 2-52 RAJ-II LS-DYNA Finite Element Model Assembly

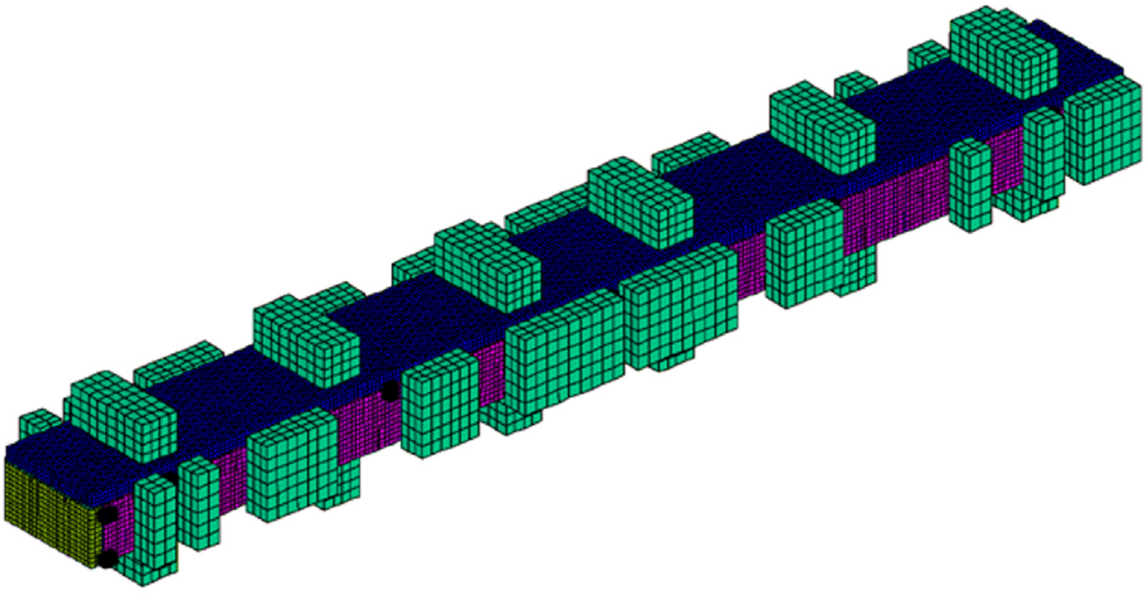

Figure 2-53 Inner Container Assembly with Honeycomb Blocks

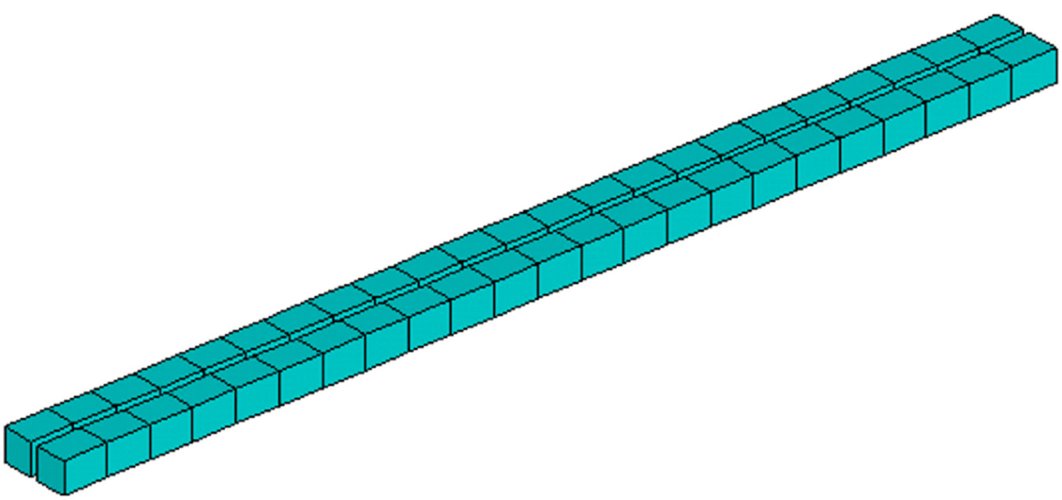

Figure 2-54 Rigid Fuel Bundle Payload

2.12.5.2 Material Properties

The structural components of the RAJ-II are constructed of 304 stainless steel, Paper Honeycomb, Balsa, Hemlock, flexible polyurethane foams, and Aluminum Silicate.

Stainless Steel: Steel components are modeled with 304 stainless steel properties [Ref. 10] as an elasto-plastic material using the LS-DYNA material model *MAT_PIECEWISE_LINEAR_PLASTICITY [Ref. 11]. The total true stress and plastic true strain are inputted into LS-DYNA. Stainless steel properties are stable through a temperature range of -20 to 100°F [Ref. 12]. The properties used in this analysis are:

Table 2-14 304 Stainless Steel Stress-Strain Properties at 100°F

Total True Stress (psi)	Total True Stress (in/in)
30000	0.0000
35070	0.0020
92300	0.2624
107100	0.3365
115735	0.3819
119250	0.4055
121600	0.4187
160000	0.6931

Paper Honeycomb: The paper honeycomb used for impact protection is constructed of resin impregnated kraft paper of uniform density. Honeycomb properties were obtain by laboratory testing at –40°C, 21°C, and 77°C representing cold, ambient, and hot conditions [Ref. 13]. The honeycomb is modeled using the LS-DYNA material *MAT_HONEYCOMB. The stress versus relative volume properties used in this analysis is:

Table 2-15 Paper Honeycomb True Stress versus Volume Properties

Relative Volume	Stress (psi) at 77°F	Stress (psi) at 21°C	Stress (psi) at -40°C
0.140	152	201	215
0.200	152	201	215
0.247	145	198	198
0.341	140	191	197
0.435	132	169	173
0.529	122	130	154
0.624	109	104	153
0.718	98	77	144
0.812	84	59	120
0.906	77	55	77
1.000	67	40	62
1.100	67	40	62
0.140	152	201	215

Benchmarking of the honeycomb properties was accomplished by comparing the measured crush of obtained following the physical top drop test of the RAJ-II. The measured crush of 2.25 inches Figure 2-38 provides a direct comparison to the LS-DYNA results of 2.30 inches. To account for the peak acceleration and proper material stiffness, the instantaneous modulus of elasticity, E, was increased until the peak acceleration equaled 145g (Figure 2-55).

Ethafoam: The Ethafoam is used to line the inner container to provide vibration protection for the fuel bundles. Ethafoam properties were obtained by laboratory testing at –40°C, 21°C, and 77°C representing cold, ambient, and hot conditions [Ref. 13]. The Ethafoam is modeled using the LS-DYNA material *MAT_CRUSHABLE_FOAM.

Table 2-16 Ethafoam True Stress versus Volumetric Stress Properties

Volumetric Strain	Stress (psi) at 77°F	Stress (psi) at 21°C	Stress (psi) at -40°C
0.000	0	0	0
0.014	3	9	11
0.028	5	12	15
0.042	7	13	17
0.056	9	15	19
0.071	11	18	23
0.085	15	23	27
0.099	20	29	35
0.113	28	41	47
0.127	42	63	70
0.134	55	84	91
0.140	152	201	215

Balsa and Hemlock: Balsa wood is used for primary impact protection during the end drop, and hemlock is used to separate the inner container shells.

To bound the temperature effects, and grain direction, the hot stress-strain data is taken from the weaker perpendicular to grain direction, and the ambient and cold properties are taken from the stronger parallel to grain direction [Ref. 14]. The ambient curve is benchmarked from the crush measured following the end drop. To ensure the maximum acceleration is achieved, the cold properties are increased by approximately 30%. The Benchmarking of the balsa properties is discussed in Figure 2-66 and below. Hemlock is a soft wood that has properties similar to balsa wood [Ref. 15]. The hemlock is modeled to provide separation of the steel shells and to include the mass of the part. However, hemlock provides little impact protection. Even though hemlock is a higher density than balsa wood, the difference is insignificant. Thus, hemlock can be modeled with balsa properties.

Benchmarking of the balsa properties was accomplished by comparing the measured crush to the LS-DYNA model. To make the comparison, a core sample measurement of the end drop CTU was made. The core sample showed that the balsa block crushed 2 inches, which agrees with the LS-DYNA results.

The materials are modeled using the LS-DYNA material *MAT_CRUSHABLE_FOAM. The stress-strain properties used in this analysis are:

Table 2-17 Balsa Wood True Stress versus Strain Properties

Volumetric Strain	Stress (psi) at 77°F	Stress (psi) at 21°C	Stress (psi) at -40°C
0.000	0	0	0
0.010	66	665	1500
0.025	90	1065	1900
0.050	98	1265	2000
0.075	100	1365	2010
0.100	102	1405	2020
0.200	110	1555	2060
0.300	118	1695	2160
0.400	126	1835	2260
0.500	134	1980	2360
0.600	153	2260	2710
0.700	360	4260	7218

Aluminum Silicate: Aluminum silicate is used as an insulating material between the inner container shells. The properties for the aluminum silicate insulation are derived from the manufacturer's data sheet and account for the behavior of the material when compressed to a solid height, while air is pressed out of the fabric/ceramic layers. The crushable foam material model is used for stability. Aluminum silicate is modeled to include the mass of the material but provides little energy absorption. The stress-strain properties used in this analysis are:

Table 2-18 Aluminum Silicate True Stress versus Strain Properties

Strain (in/in)	Stress (psi)
0.00	0
0.05	42
0.10	50
0.15	57
0.30	300
0.50	1000
0.70	100000
0.90	500000

Fuel Bundle Payload: The fuel bundles are modeled as rigid bodies to ensure no energy is dissipated by the contents. The fuel bundles are modeled using the LS-DYNA material *MAT_RIGID. The bundle mass is based upon the range of designs shipped in the RAJ-II. Analyzed fuel bundle weights are based on actual design weights. The following table provides a comparison of the fuel bundle weights evaluated. These weights are chosen, because they provide the best comparison between actual tests performed on the RAJ-II and RA-3D and the LS-DYNA results.

Table 2-19 Fuel Bundle Properties

Product Name	Type	Weight, kg (lb)
GE11	9x9	249 (549)
GE14	10x10	266 (587)
GE14 Channeled	10x10	298 (658)

To show that the use of a rigid fuel payload is conservative, an LS-DYNA top drop analysis was performed using elastic properties for the fuel bundle payload and compared with data from the original Japanese RAJ-II drop testing program. For both test and analysis, data was collected at accelerometer locations at the center of the fuel bundle. The same solid brick model used for the rigid case was used for the elastic fuel bundle case with a representative modulus of elasticity to simulate the stiffness properties.

Acceleration time histories were recorded at the center of the bundle close to the location of the physical accelerometer in the drop test. Figure 2-56 is an overlay of drop test and LS-DYNA analysis results.

Figure 2-56 compares the Japanese top drop test results (black line) filtered at 500 Hz with LS-DYNA filtered acceleration time-history results ranging from 25 Hz to 500 Hz. The rigid fuel bundle result is also provided for comparison (red line).

Referring to the Japanese top drop, the plot shows additional sinusoidal waves on top of the primary impact responses. This resulted from the actual fuel bundle geometry as the individual rods responded to the impact. The Japanese top drop is also represented by a sixth order polynomial curve fit (gray dashed line). The shape and duration of the curve fit matches the LS-DYNA results.

From results of shaker table testing (fully loaded RAJ-II), road testing vibration studies, flow induced vibration testing of fuel bundles, and seismic testing of fuel bundles, it was determined that the natural frequency of the fuel bundle was approximately 10 Hz [Ref. 16]. Because the fuel bundles are the largest, non-stationary mass in the system, the fuel bundles drive the natural frequency of the RAJ-II package. For conservatism, the analysis assumed the natural frequency of the package to be less than 25 Hz. Using a Butterworth filter and evaluating the results at 25 Hz resulted in a maximum acceleration of 66g. Therefore, performing the evaluation with a rigid fuel payload is conservative for the following reasons:

- *All of the energy was absorbed by the crushable materials of the package with no loss to the contents.*
- *The LS-DYNA results were checked by integrating the acceleration time history to verify the velocity thus the kinetic energy.*
- *Using rigid properties avoided the need to aggressively filter the results which in many cases could skew the analysis results, if too few data points were requested for the LS-DYNA NODOUT file.*

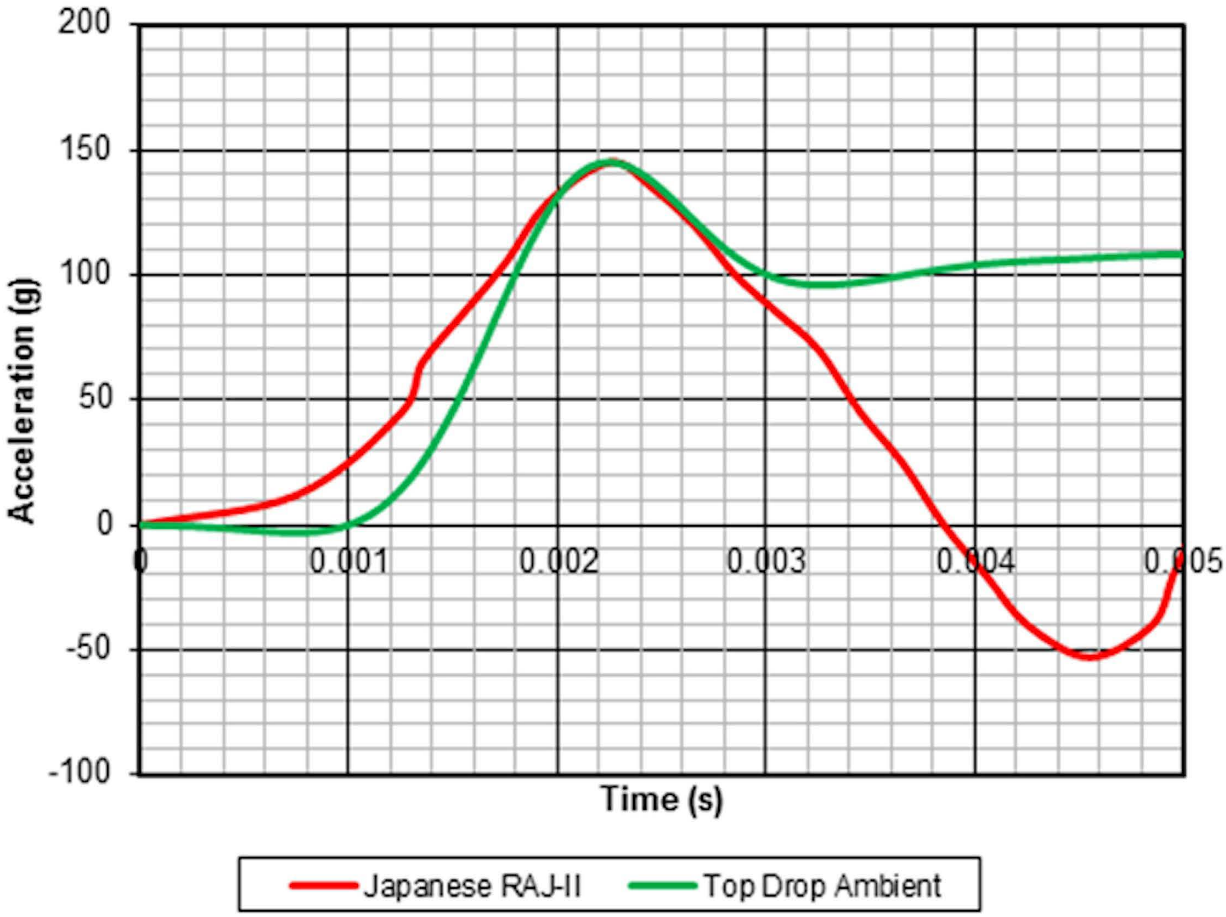

Figure 2-55 Comparison of Japanese RAJ-II Drop Test and LS-DYNA Results

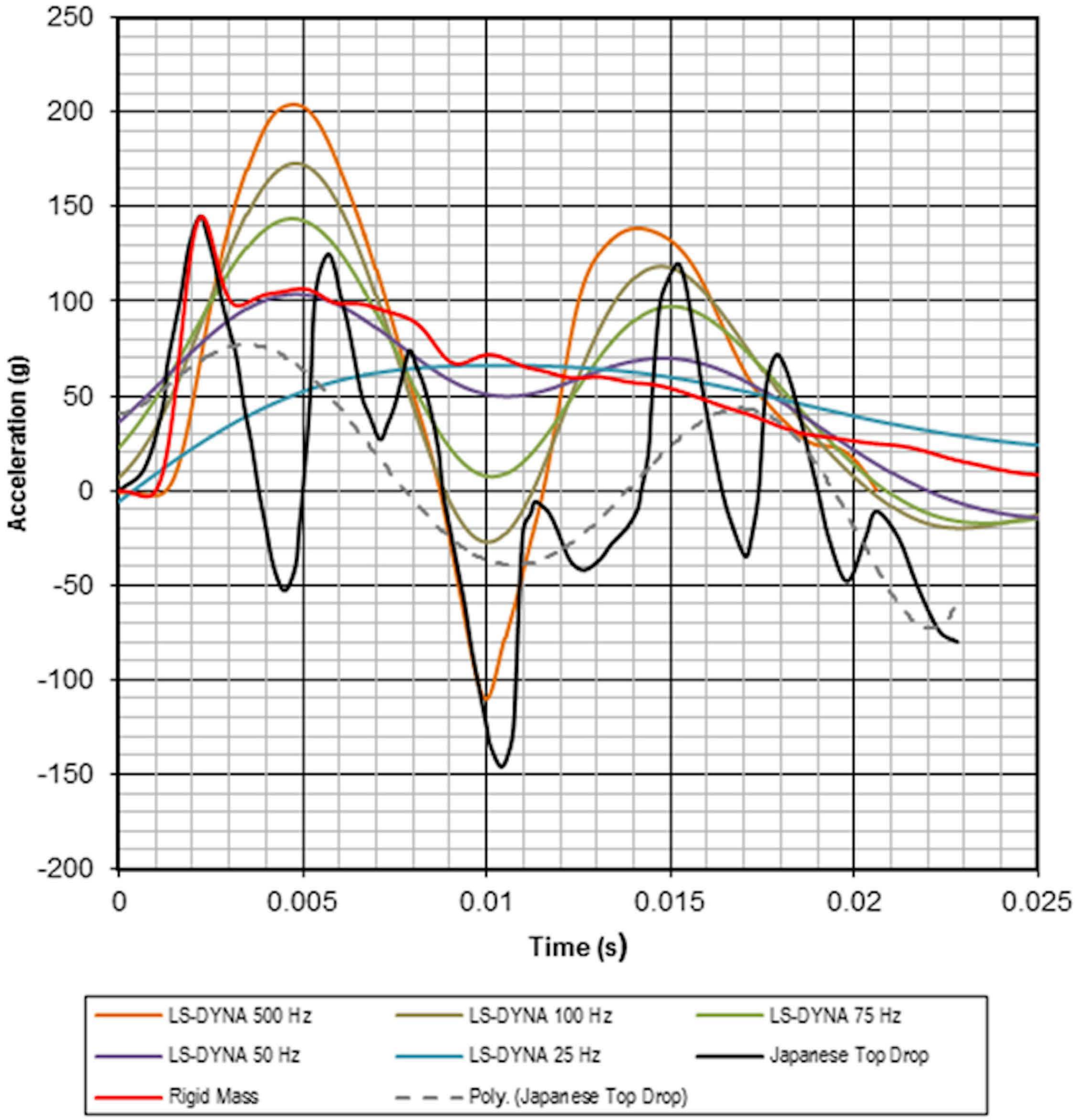

Figure 2-56 Comparison of Japanese RAJ-II Drop Test and LS-DYNA Elastic Analyses

2.12.5.3 Boundary Conditions

The LS-DYNA command *RIGIDWALL_GEOMETRIC_FLAT is used to define the infinitely rigid impact plane. The rigid wall definition is provided in the following table.

Table 2-20 Rigid Wall Definitions

Drop Orienta-tion	XT	YT	ZT	XH	YH	ZH	XHEV	YHEV	ZHEV
Corner	0.000	25.065	-101.600	0.000	25.065	0.000	0.000	0.000	-101.600
End	0.000	25.065	-100.000	0.000	25.065	0.000	0.000	0.000	-100.000
Side	-14.200	0.000	0.000	0.000	0.000	0.000	0.000	0.000	0.000
Slapdown	0.000	25.065	0.000	0.000	20.000	0.000	0.000	0.000	0.000
Top	0.000	25.065	0.000	0.000	20.000	0.000	0.000	0.000	0.000

The LS-DYNA card *CONTACT_AUTOMATIC_SINGLE_SURFACE defines all interfaces within the model except the welds. LS-DYNA automatically simulates both impact and sliding along interfaces. For this analysis, the non-default soft constraint method is used which calculates the stiffness of the linear contact springs based on the nodal masses that come into contact and the global time step size. The stiffness is found by taking the nodal mass divided by the square of the time step size with a scale factor to ensure stability. The SOFT=2 option invokes a segment-based contact algorithm which has it origins in Pinball contact developed by Belytschko. With this contact algorithm, contact between surfaces uses two 4-node segments. When contact occurs, forces are applied to the eight-node set to resist segment penetration. This method has the effect of distributing forces more realistically.

To simulate connectivity between parts, the LS-DYNA surface-to-surface contact card *CONTACT_TIED_SURFACE_TO_SURFACE is used. For the top and side drop cases, an initial velocity (*INITIAL_VELOCITY) is applied to the model to simulate the 360 in (9.1 m) free drop. Knowing that the potential and kinetic energies are equal on impact, the initial velocity is

$$\frac{1}{2}MV^2 = Mgh$$

$$V = \sqrt{2gh} = \sqrt{2\left(386.4\frac{\text{in}}{\text{sec}^2}\right)(360\text{ in})} = 527.5\frac{\text{in}}{\text{sec}^2}$$

For the 35° slapdown / whiplash analysis the kinetic energy is a function of the distance the center of gravity of the package has to travel to contact the impact plane (see Figure 2-57). Therefore, the kinetic energy is the calculated by adding the drop height 360 in (9.1 m) to the distance from the center of gravity to the impact plane. Therefore, the effective drop height of the whiplash is 426.54 in (10.83 m) as compared to the top drops 372.36 in (9.46 m).

The drop energy is calculated by multiplying the drop height times the weight. For the LS-DYNA model the total weight is 2,653 lb (11,801 N). Therefore, the total energy absorbed during impact is 1.1316E+06 lbf-in (1.2785E+05 N-m) for the whiplash case as compared to 9.8783E+05 lbf-in (1.1161E+05 N-m) for the top drop. To simulate the whiplash in LS-DYNA, an angular velocity, omega, is applied at the point of impact using the LS-DYNA command *INITIAL_ VELOCITY_ GENERATION. The angular velocity was increased for mass added to individual elements during the solution process to decrease run time. The final angular velocity is -5.05153 rad/s.

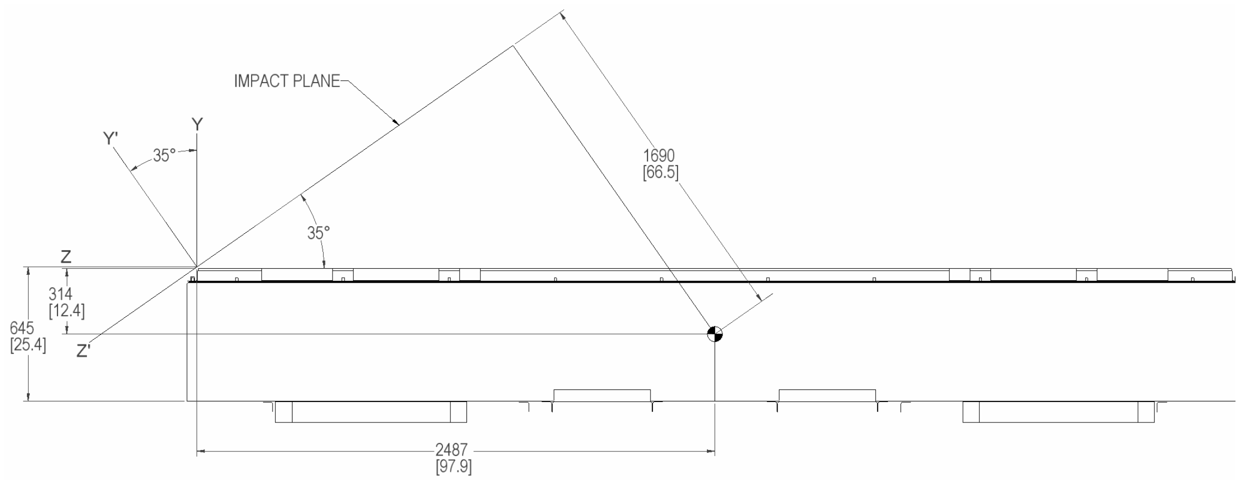

Figure 2-57 Slapdown / Whiplash Geometry

2.12.5.4 Results of RAJ-II Impact Analysis

Nodal output is stored by LS-DYNA using the *DATABASE_HISTORY_NODE command. Post-processing of results is accomplished by starting the program LS-PREPOST from the LS-DYNA manager. Nodal output of the node representing the acceleration is stored as a text file database by LS-DYNA that are post-processed using the LS-PREPOST command ASCII and opening the NODOUT file. For this evaluation, a series of nodes located are tracked. One node is place on the fuel bundle to determine the maximum acceleration.

Side Drop: The LS-DYNA analysis shows that variations in payload weight cause an increase in accelerations of up to +5% when the lightest fuel bundles are evaluated and a decrease in accelerations of approximately 9% that results from the heaviest bundle configuration. The LS-DYNA analysis shows that the temperature variations in the shock absorbing materials affect transmissibility. The maximum acceleration occurs when the temperature is -40°C.

The RAJ-II side drop acceleration time histories at cold, ambient, and hot conditions are presented in Figure 2-58. Because of the crush characteristics of the honeycomb, the maximum acceleration occurs when the lightest fuel weight at coldest temperature (-40°C) is used. The peak acceleration reported during the side drop is 339.6g at 500 Hz.

<u>Top Drop</u>: Figure 2-59 provides a comparison of the RAJ-II top drop at cold, ambient, and hot conditions. Like the side drop, the combination of extreme cold temperatures (-40°C) and lights bundle weight results in the maximum acceleration. The peak acceleration reported during the top drop is 186.0g at 500 Hz.

<u>End Drop:</u> Figure 2-60 provides a comparison of the RAJ-II corner drop at cold, ambient, and hot conditions. Like the top and side drops, the combination of extreme cold temperatures (-40°C) and lightest bundle weight results in the maximum acceleration. The peak acceleration reported during the top drop is 377.8g at 500 Hz.

<u>Corner Drop:</u> Figure 2-61 provides a comparison of the RAJ-II corner drop at cold, ambient, and hot conditions. Like the other cases, the combination of extreme cold temperatures (-40°C) and lightest bundle weight results in the maximum acceleration. The peak acceleration reported during the top drop is 227.7g at 500 Hz. Comparing the corner and end drop results, the corner drop results in lower peak acceleration, because the small initial projected contact area.

<u>Whiplash/Slapdown</u>: Figure 2-62 compares the whiplash and top drop results. The analysis results show that RAJ-II is more efficient during the whiplash event than the flat top drop. During the whiplash, honeycomb surface area is initially only available at the point impact and gradually increases as the impact progresses. During the flat top or side drops, all area contacts the inner container at impact initiation. Therefore, the initial peak acceleration is much higher during the flat top or side drops than when the container impacts at an angle.

.

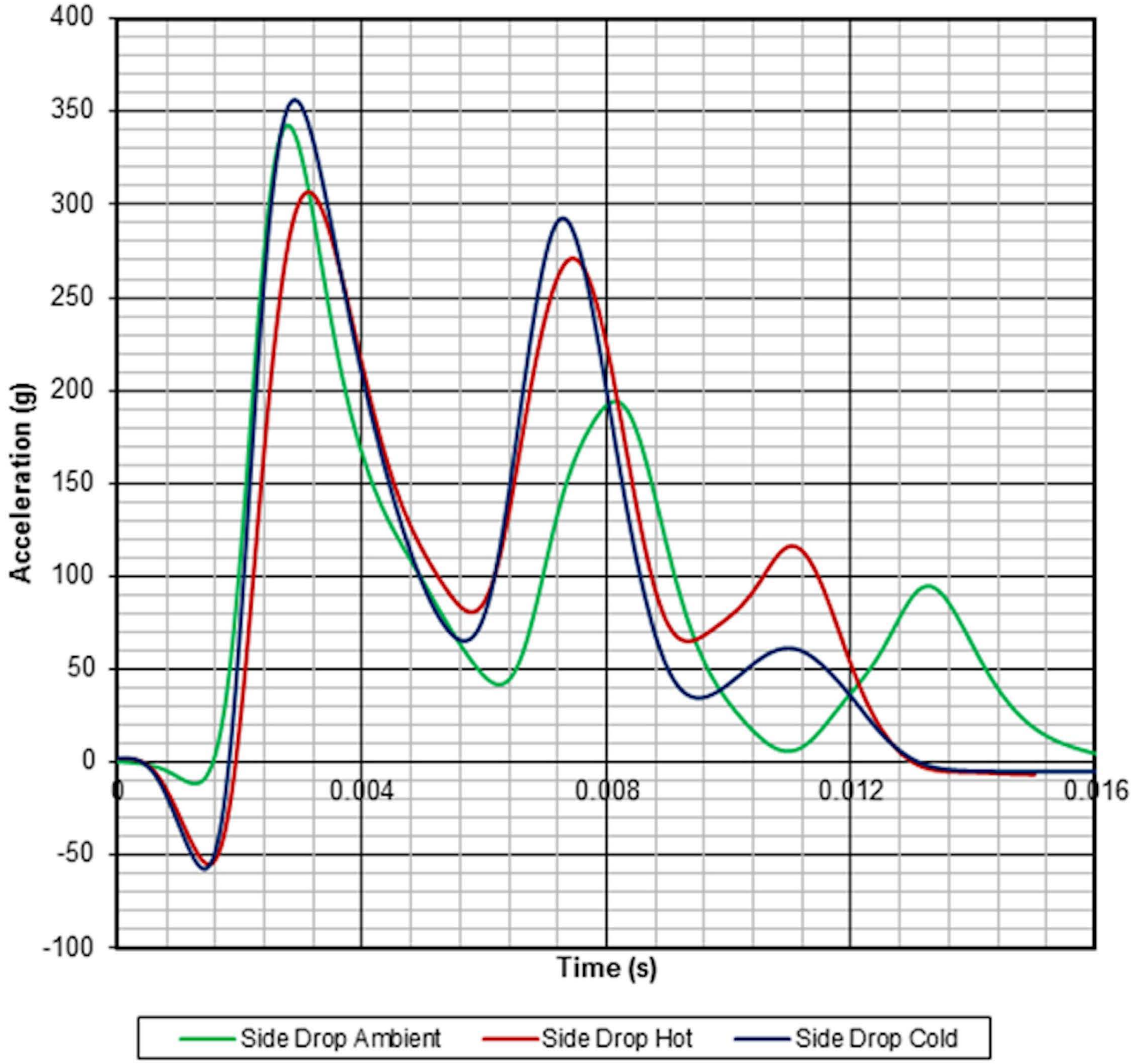

Figure 2-58 Comparison of Side Drop Accelerations at Cold, Ambient, and Hot Conditions

.

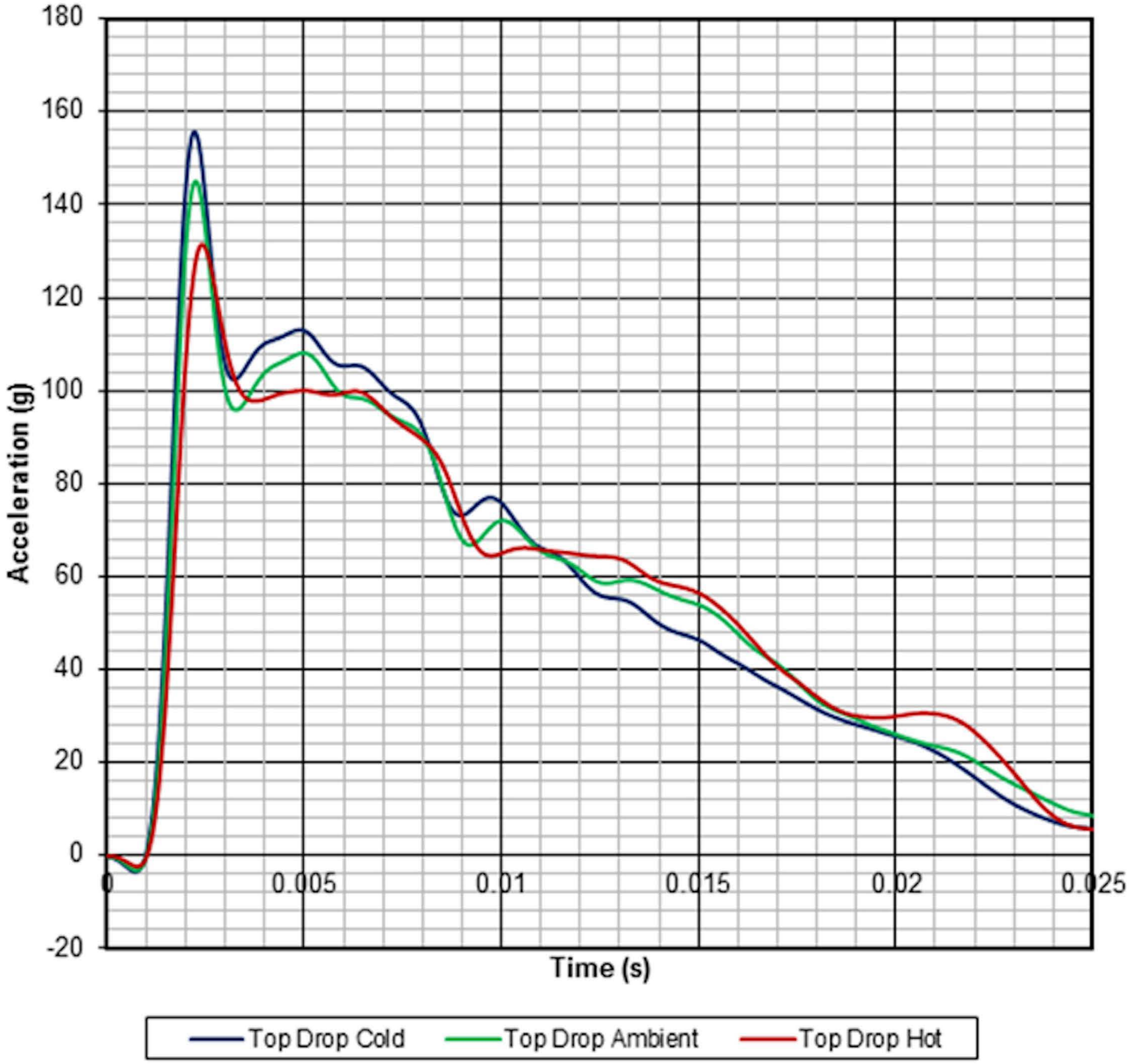

Figure 2-59 Comparison of Top Drop Accelerations at Cold, Ambient, and Hot Conditions

.

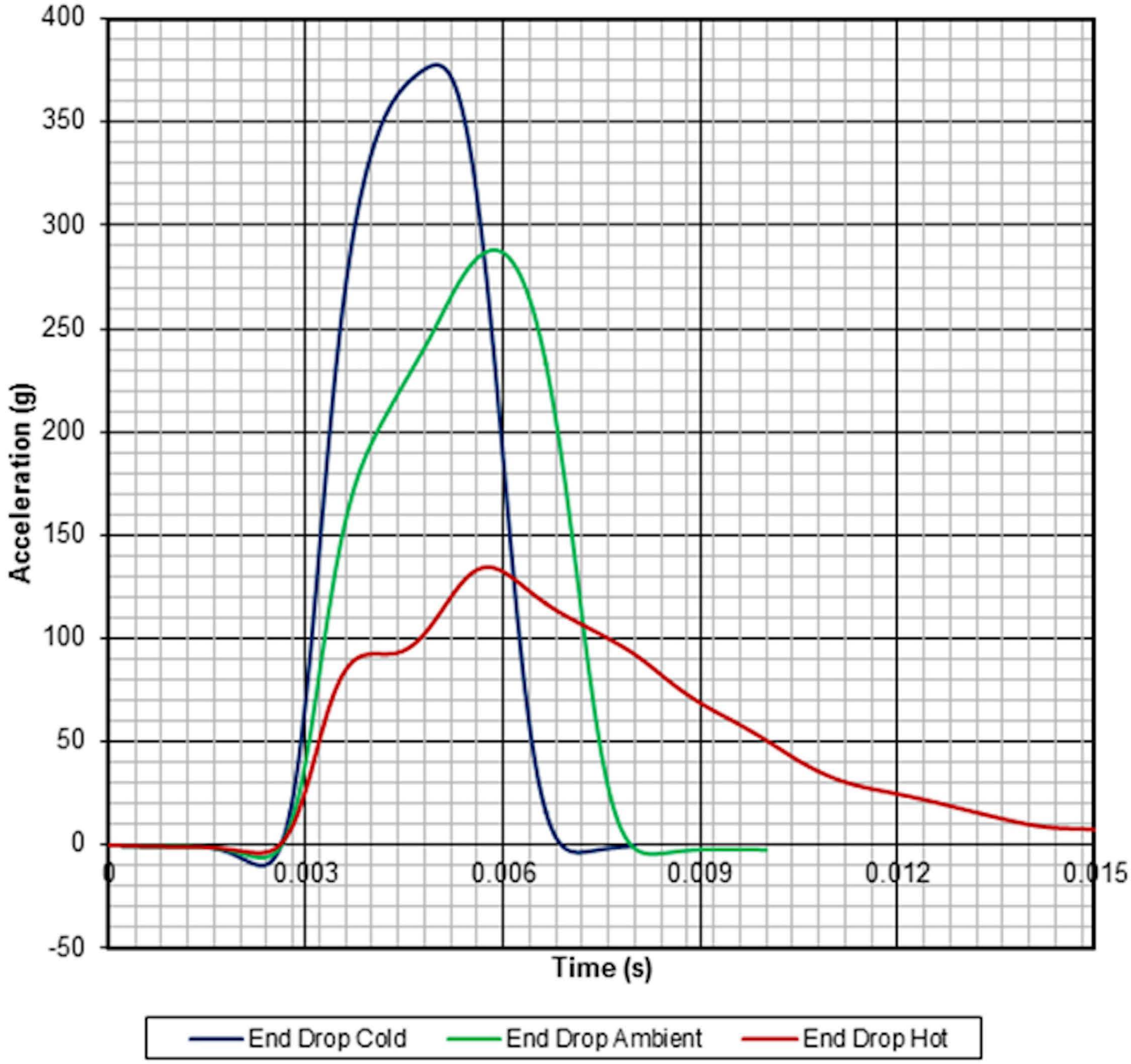

Figure 2-60 Comparison of End Drop Accelerations at Cold, Ambient, and Hot Conditions

.

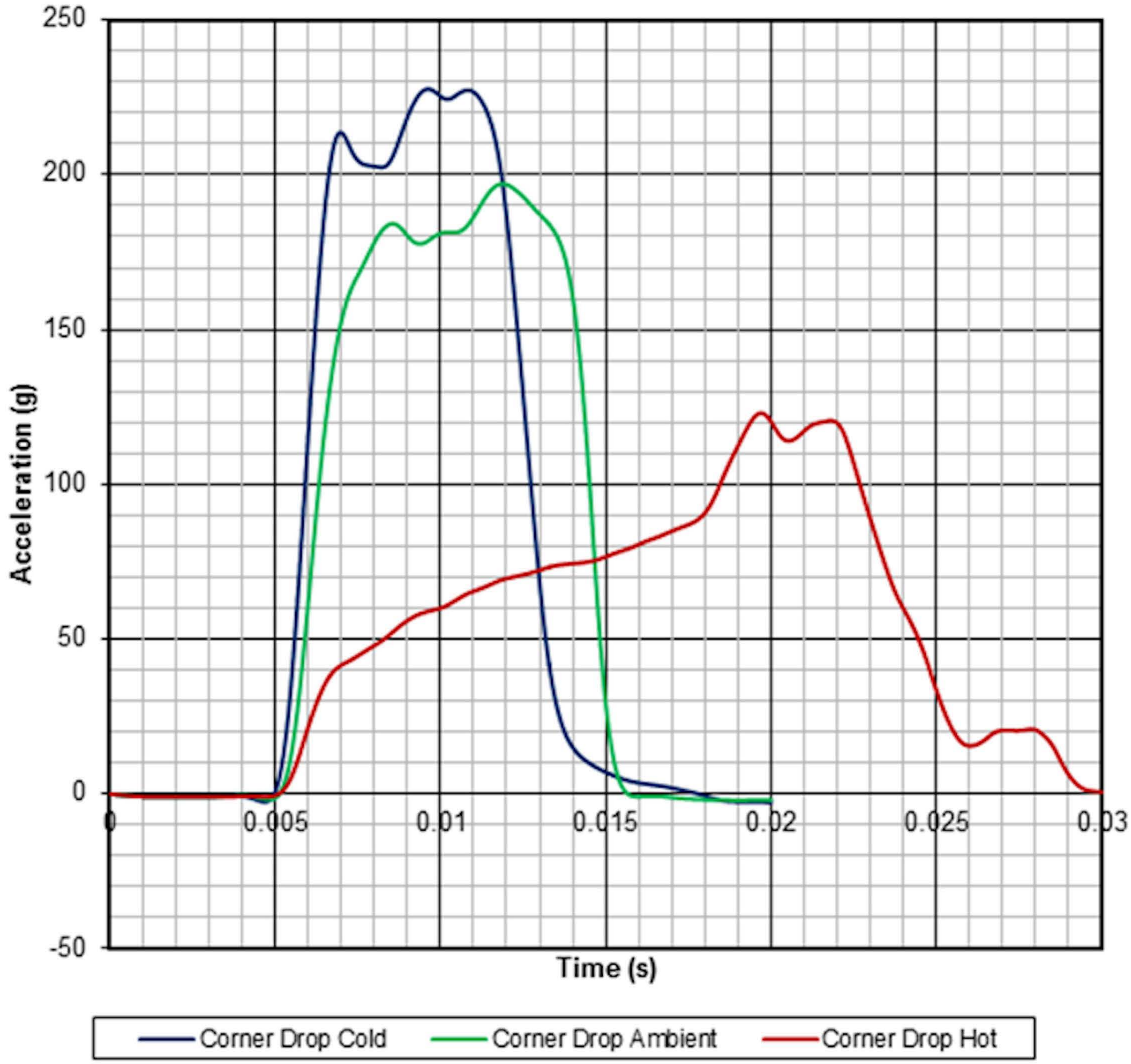

Figure 2-61 Comparison of Corner Drop Accelerations at Cold, Ambient, and Hot Conditions

.

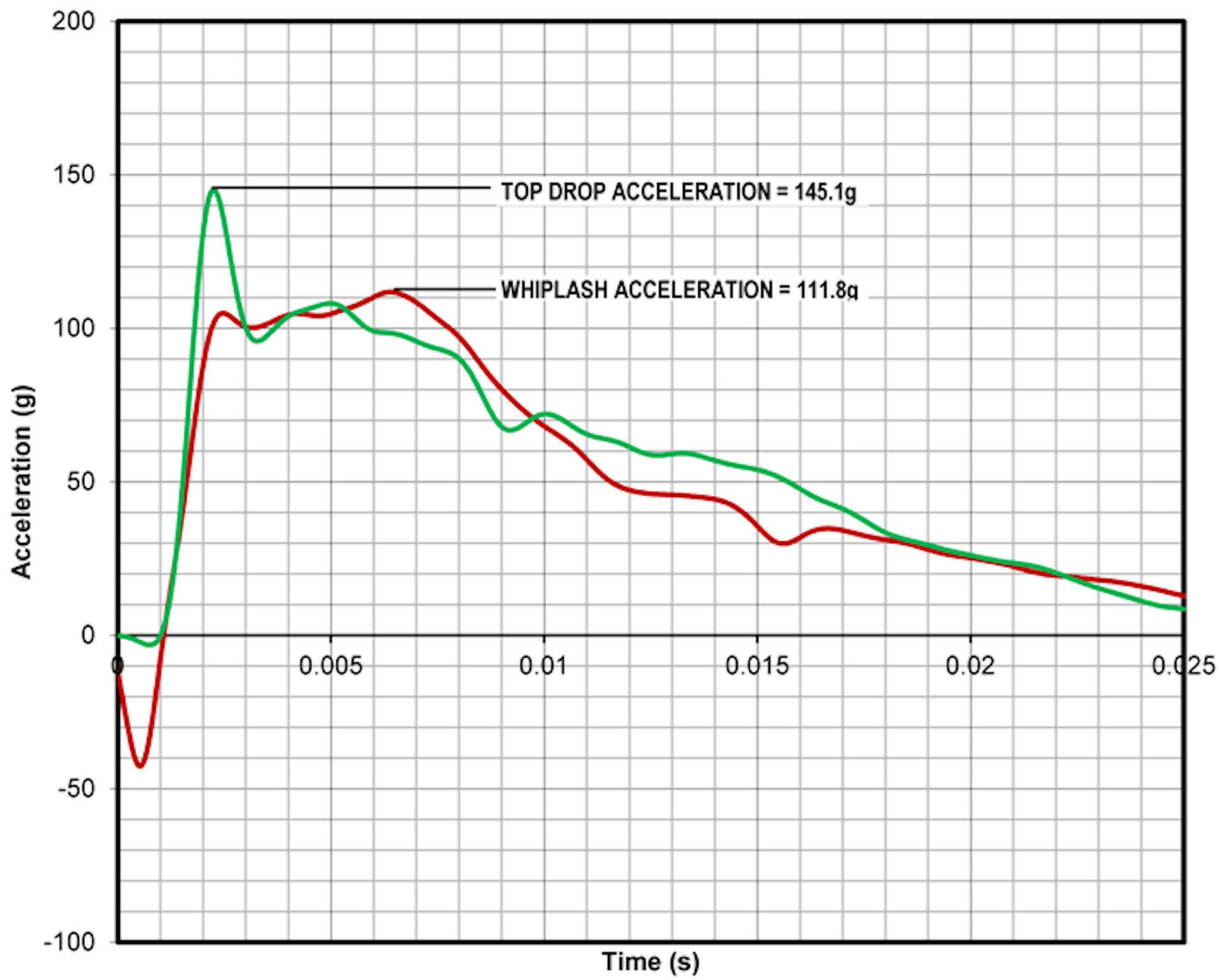

Figure 2-62 Comparison of Slapdown / Whiplash and Top Drop Accelerations

2.12.5.5 Benchmarking

The following table provides a summary of the available drop test data and accelerometer location. The referenced figures compare the acceleration time history at the physical sensor location on the CTU and corresponding FEA overlay plot.

Table 2-21 Package Drop Test Orientation and Accelerometer Location

Package	Test Location	Drop Orientation	Acceleration (G)	Sensor Location	Reference
RAJ-II	Japan	Horizontal top drop	145	Center of bundle	Figure 2-63
RAJ-II	Japan	Horizontal top drop	194	Inner container outer shell	Figure 2-64
RAJ-3D	Spain	Horizontal side drop	487	Upper tie plate	Figure 2-65
RAJ-II	Japan	Vertical end drop	303	Inner container outer shell	Figure 2-66
RAJ-II	Japan	Vertical CG over corner	203	Lower tie plate	Figure 2-67
RAJ-3D	Spain	Vertical CG over corner	195	Inner container outer shell	Figure 2-67

Figure 2-65 provides a comparison of the RAJ-II side impact and the RA-3D side drop results over an impact duration of approximately 15 milliseconds. The plots shows that the RAJ-II and RA-3D respond similarly during drop events and provide good evidence that the LS-DYNA results are realistic. However, because of the simple geometry of the RAJ-II and RA-3D honeycomb, it is possible to perform an alternate calculation to benchmark the results. Reasonable estimates of the drop accelerations is possible by using the methodology presented in Mindlin [Ref. 17].

$$G_m = DLF \times \sqrt{\frac{2hk_2}{W_2}},\ \text{Absolute value of maximum acceleration of packaged article}$$

Where,

h = Drop height (in)

W_2 = Weight of the packaged article (lb)

$k_2 = \frac{P_m}{x_2}$, Spring rate for a linear elastic material (lb/in)

$P_m = \frac{\sigma}{A}$, Maximum force exerted on the packaged article by cushioning (lb)

σ = Crush strength of the material (psi)

A = Projected area of the honeycomb (in^2)

x_2 = Downward displacement (kn)

DLF = Dynamic load factor

The following table is a summary of the calculations used to estimate the accelerations of the RA-3D and RAJ-II.

Table 2-22 Side Drop Accelerometer Estimates using Classic Methodology

Variable	Units	RAJ-II	RA-3D	Notes
G_m	g	**367.81**	**507.81**	
h	in	360.00	360.00	
W_2	lb	2187.00	2094.39	
k_2	lb/in	102730.70	187526.31	
P_m	lb	359352.00	309905.69	
σ	psi	322.00	205.00	
A	in^2	1116.00	1511.74	
x_c	in	3.50	1.65	Derived from compressed honeycomb distance
DLF		2.00	2.00	DLF from Blodgett [Ref. 18, p 2.8-3]

Figure 2-68 shows a comparison of RAJ-II LS-DYNA side drop results, RA-3D side drop test results, and the estimated results by alternate calculations. The alternate calculation confirms that the RA-3D test and RAJ-II LS-DYNA results reasonably predict the acceleration response of the packaged article.

The following curve shows the results of Japanese top drop test and LS-DYNA analysis results. The sensor location for both the analysis and test was on the fuel bundle. As the test curve shows, the sensor recorded the elastic response of the bundle during the impact. This data was chosen as the initial benchmark to verify the LS-DYNA honeycomb model, because the measured honeycomb crush of 2.25 inches (Figure 2-38) provides a direct comparison to the LS-DYNA results of 2.30 inches.

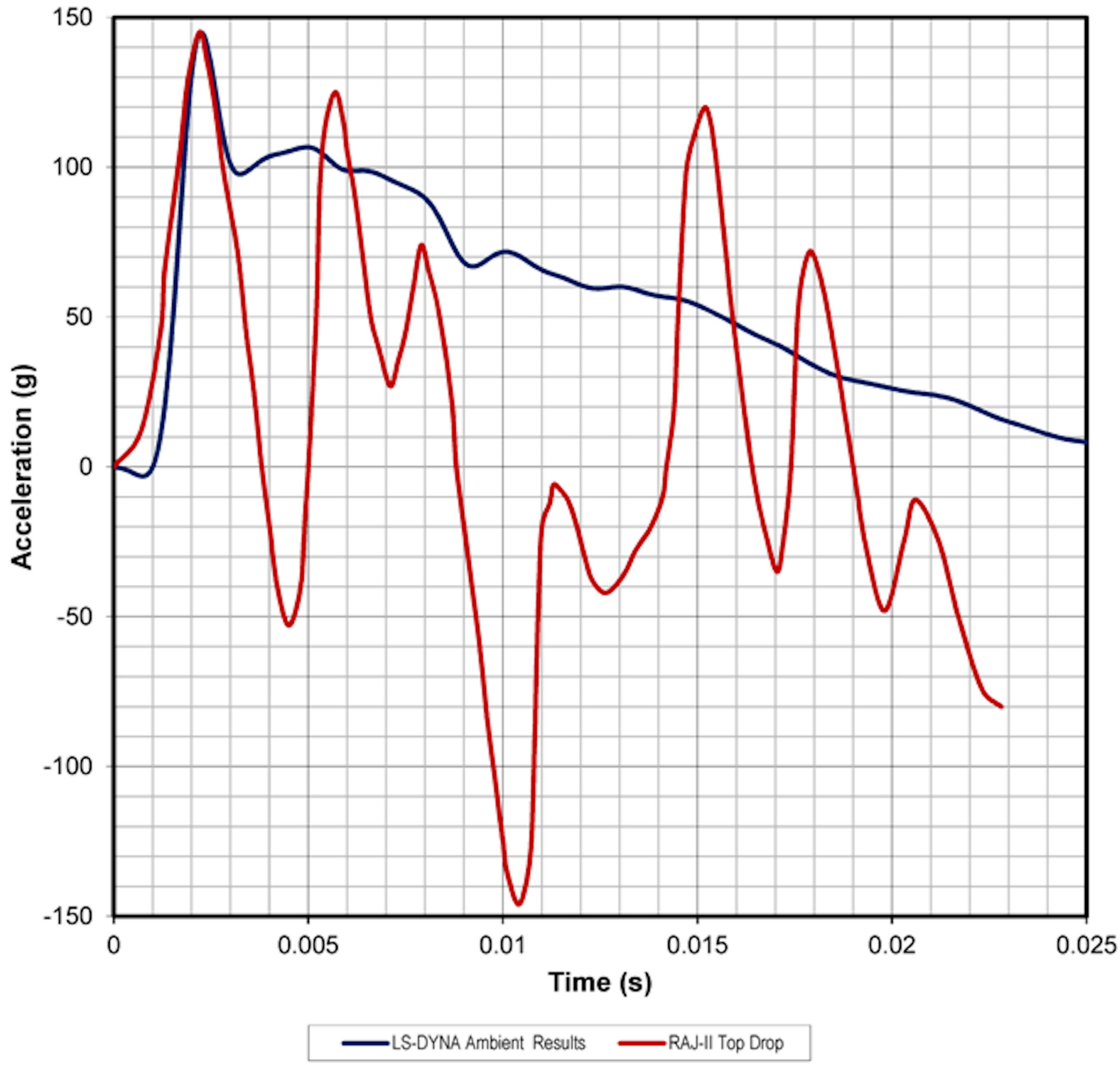

Figure 2-63 Comparison of Japanese RAJ-II Top Drop and LS-DYNA Results (Center of Bundle)

The following figure is a comparison of the Japanese RAJ-II top drop with the accelerometer located on the side of the inner container. Because the exact location of the sensor is not documented, an average of four nodes along the length of the inner container is used to represent the LS-DYNA responses. The LS-DYNA results show good agreement with the drop test results.

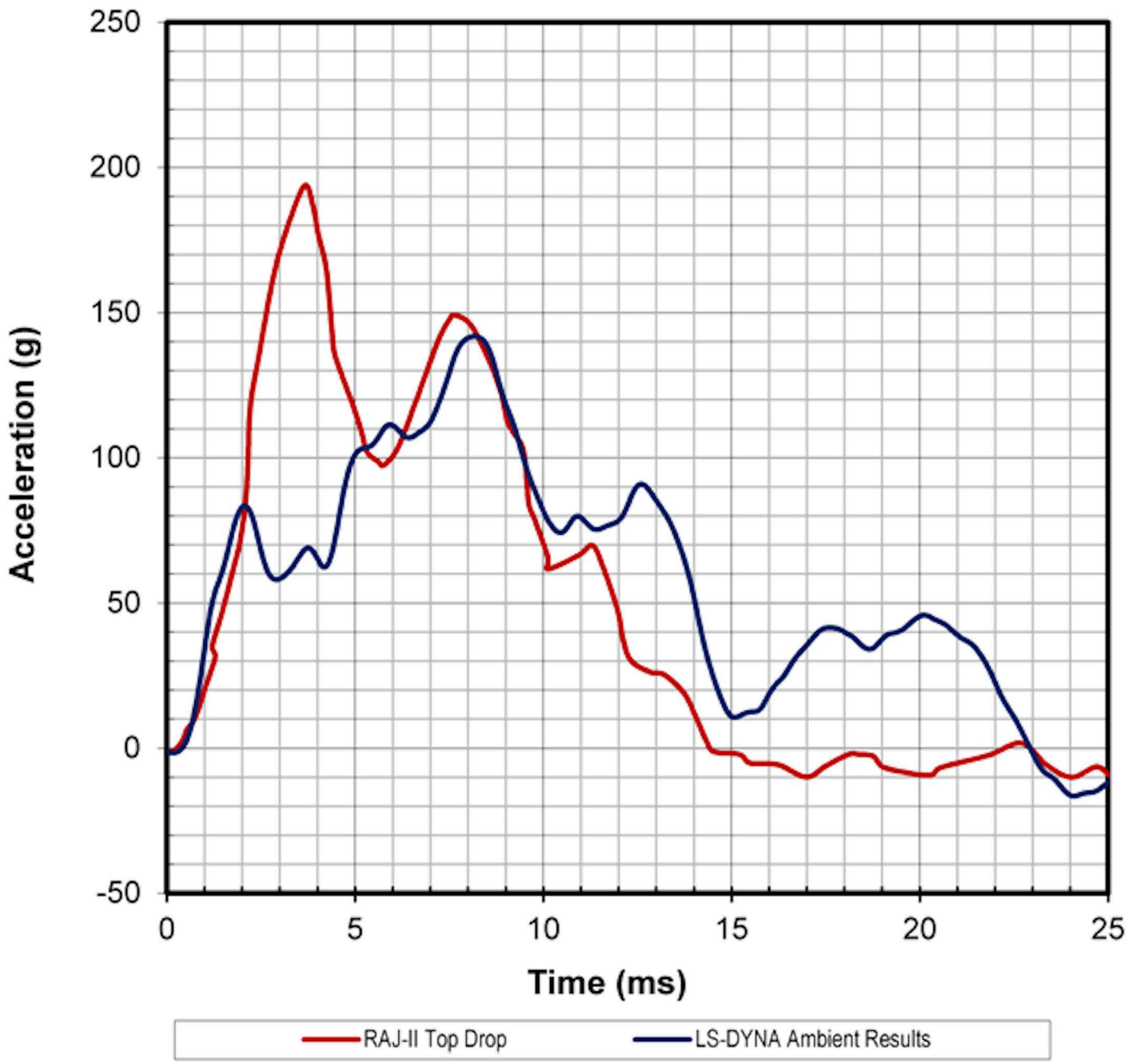

Figure 2-64 Comparison of Japanese RAJ-II Top Drop and LS-DYNA Results (Inner Container Shell)

Following the completion of the top drop analysis, where the material properties were benchmarked, the honeycomb properties were copied to the side drop model and the side drop analysis was completed. However, accelerometer data was not available for the side drop case during either of the two RAJ-II testing programs. The best comparison for the RAJ-II side drop case was the data available from the Spanish test program for the RA-3D [Ref. 19]. As the following figure shows, the LS-DYNA analysis properly captured the response of the initial impact and subsequent secondary responses of the fuel bundles, as the crushable materials in the inner container deforms and flexes.

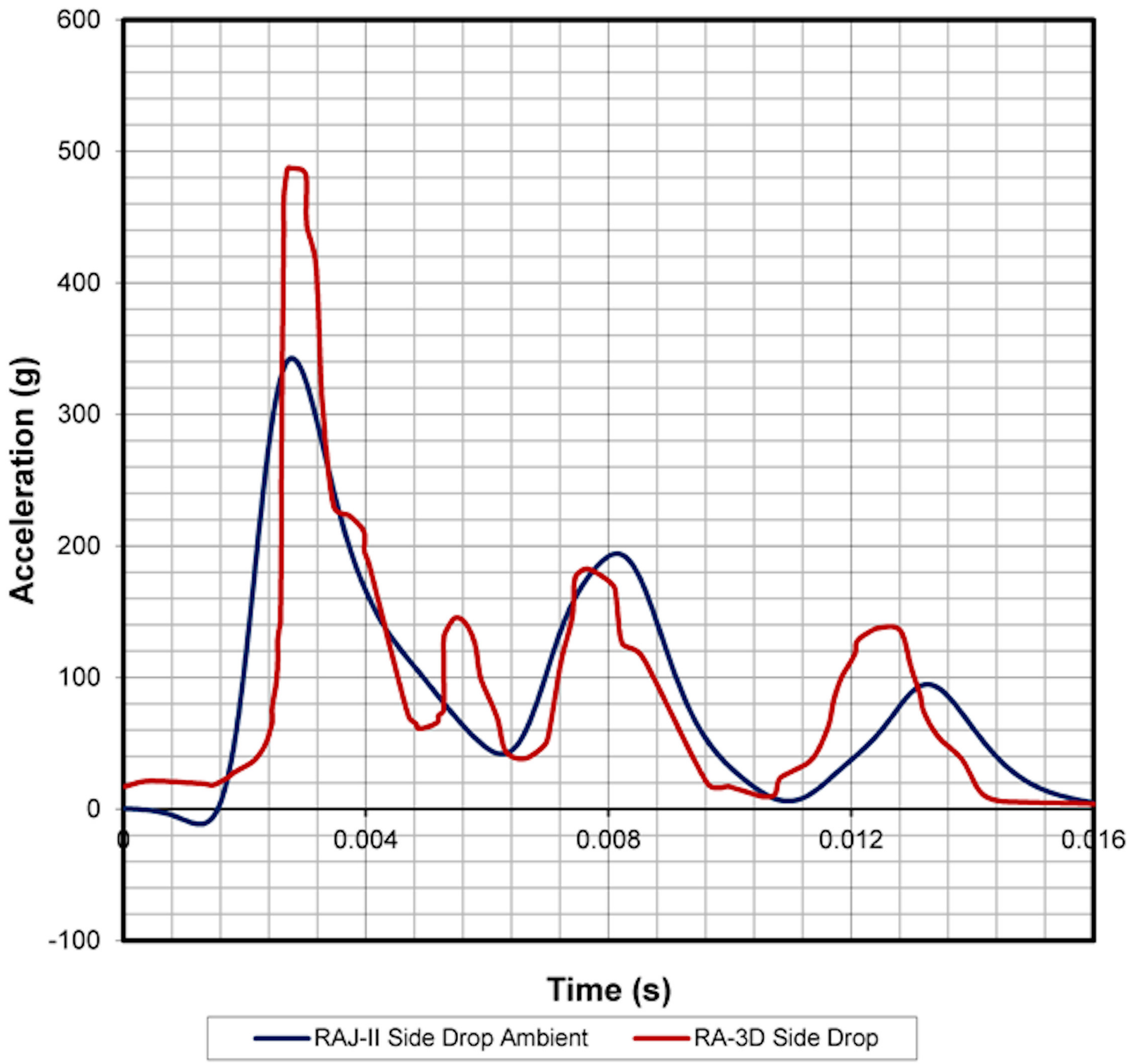

Figure 2-65 Comparison of RA-3D Side Drop and LS-DYNA Results

The following figure represents the end drop of the package and the crushing of the balsa blocks located at the end of the container. Benchmarking of the balsa properties was accomplished by taking measurements from the balsa post impact and comparing to the LS-DYNA results. Evaluation of the CTU shows that a maximum crush of 2 inches occurs under the point of impact, which agrees with the LS-DYNA results.

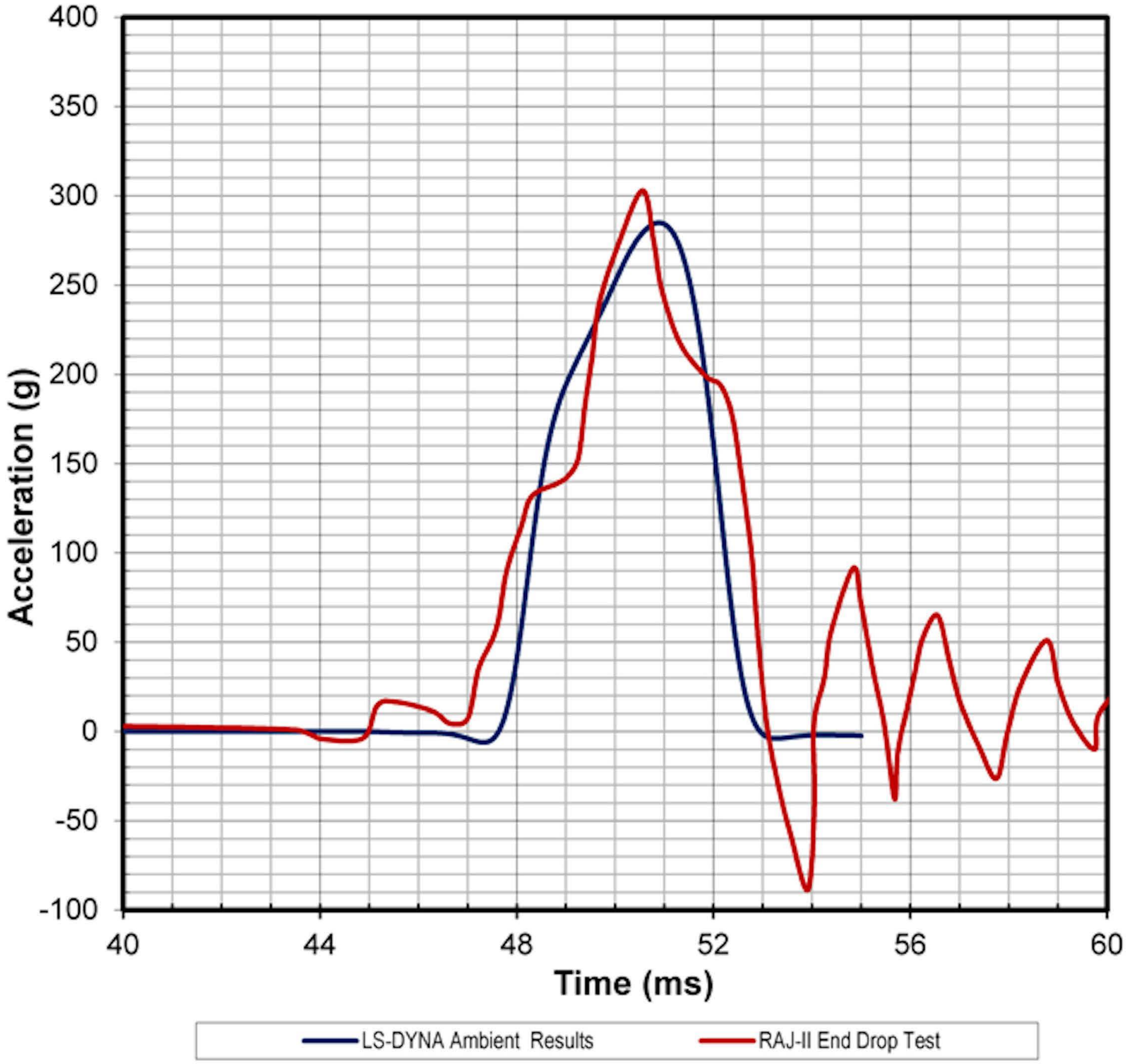

Figure 2-66 Comparison of RAJ-II End Drop and LS-DYNA Results

Using the balsa properties used for the end drop case, the corner drop evaluation was performed. As the results shows, the magnitude, and pulse duration compared favorably with the Japanese RAJ-II corner drop and RA-3D corner drop cases. It was observed that the corner drop acceleration is less than the end drop, because of corner deformation at the point of impact and the smaller initial contact area.

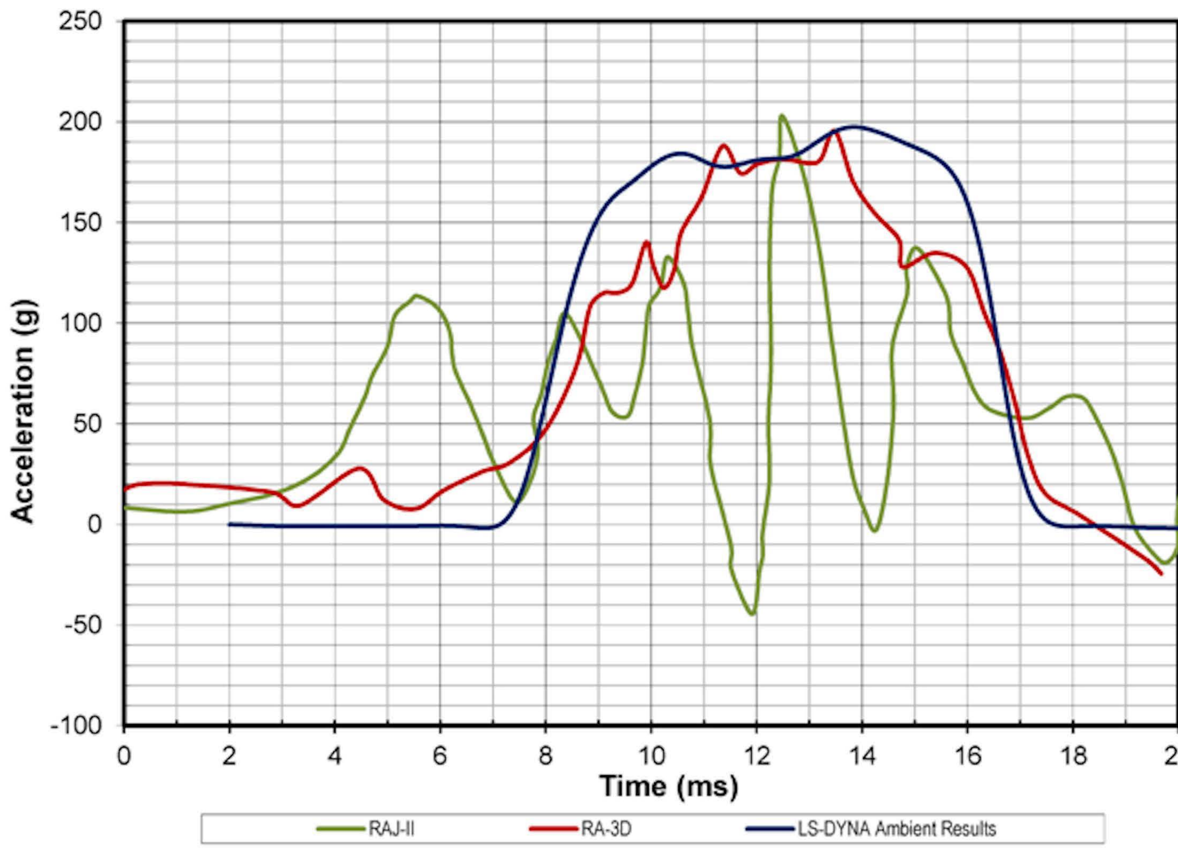

Figure 2-67 Comparison of RAJ-II and RA-3D Corner Drop and LS-DYNA Results

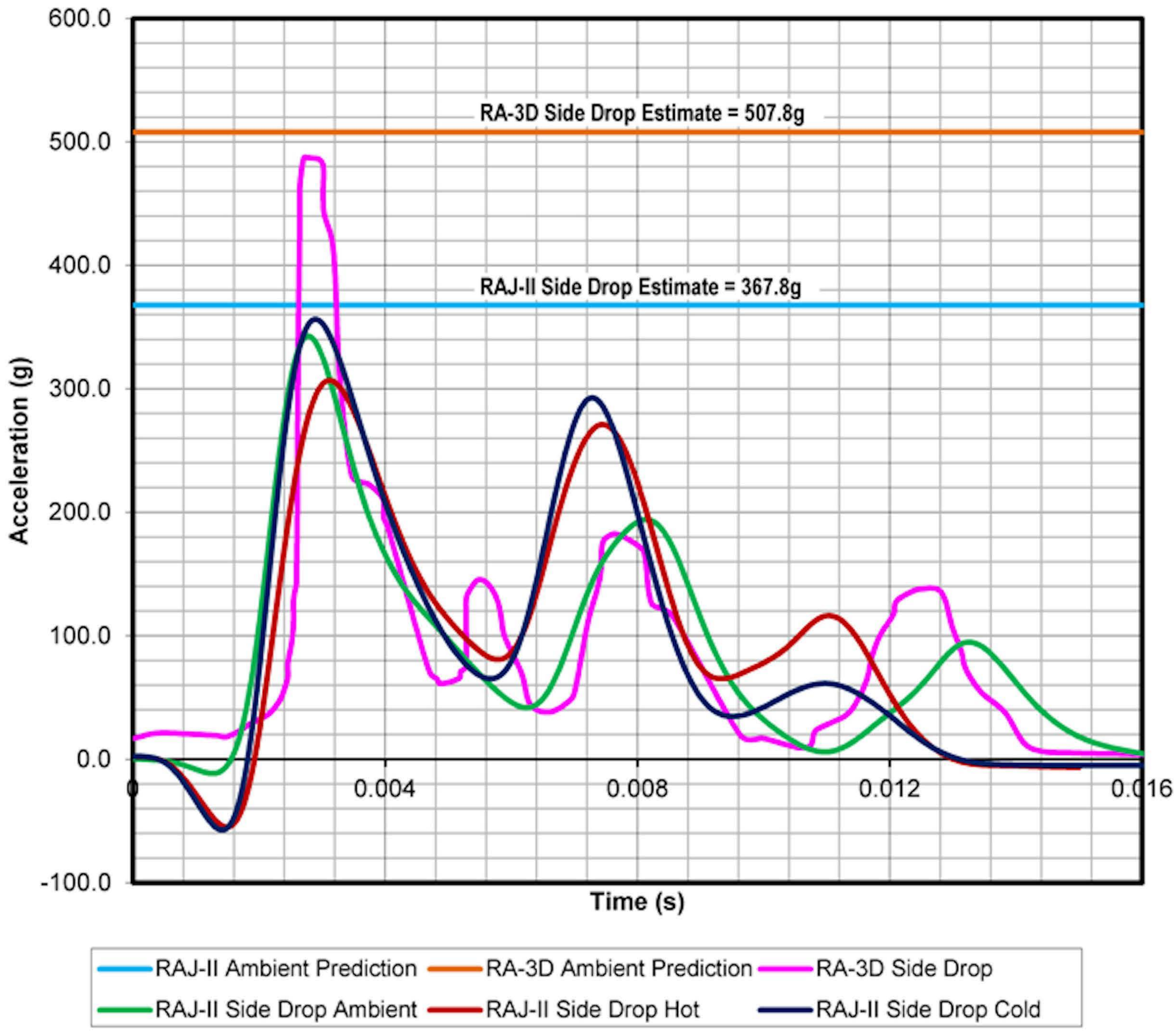

Figure 2-68 Benchmark Comparison of RAJ-II LS-DYNA Side Drop Analyses, RA-3D Drop Test, and Estimated Fuel Bundle Accelerations

2.12.5.6 Conclusions

The RAJ-II impact evaluation concludes:

1. The mass effects associated with variations in bundles design influence the acceleration. The analysis shows that the lightest fuel bundle weight results in the highest accelerations.

2. The effects of temperature on the crushable materials have results similar to mass variations. Extreme cold conditions, -40°C, result in stiffer properties and higher accelerations.

3. The combination of the lightest fuel bundle and extreme cold conditions results in the highest accelerations.

4. The hot evaluations results show there is sufficient crushable material to resist the impact without bottoming out.

5. The combination of the heaviest fuel bundle and hot conditions results in the lowest accelerations. This evaluation shows that the honeycomb has enough energy absorbing capacity to protest the fuel during hot conditions.

6. Comparison of the corner and end drop results show that the end drop is bounding because of the smaller contact area during the corner drop.

7. The slapdown/whiplash evaluation shows that the accelerations are less than the flat drop orientation, because crushing of the honeycomb occurs incrementally.

8. Comparison of the RAJ-II and RA-3D design shows that the RA-3D is a conservative analog for the RAJ-II, see Section 2.12.7 for further detail.

9. The bounding analyses and testing show, that small variations in honeycomb and foam crush strength do not adversely affect the acceleration results. For example, the results of the hot impact analyses, where crush properties are minimum show that there is sufficient crush strength and capacity to protect the inner container. This supports the damage limits specified in Section 8.2.4, where foam cushioning material may have up to 5% of the total volume damaged or absent and individual honeycomb blocks may have volume up to 10% damaged or absent.

10. The analysis and testing show the longest impact duration recorded is less than 20 milliseconds. The natural frequency of the fuel bundle is approximately 10 Hertz, which translates to a pulse length of 100 milliseconds. The impact event is completed, before the fuel bundle can respond to the shockwave generated during the impact, and the majority of energy is absorbed by the packaging materials. Therefore, the damage to the fuel bundle is minimal.

11. The requirements of IAEA TS-R-1 paragraph 725 and 10 CFR 71.73 are met.

2.12.6 Lower Tie Plate (LTP) and Cladding Impact Analysis

The purpose of this appendix is to document the evaluation of the fuel bundle lower tie plate and cladding during the RAJ-II hypothetical accident condition (HAC) 9-meter end drop using the finite element analysis code ANSYS. This appendix specifically addresses the following:

- Demonstrate the performance of the LTP during regulatory end impact conditions.
- Determine if the bending of the LTP results in excessive flexure of the cladding and its possible breakage.
- Evaluate the performance of the cladding during regulatory fire conditions following the end impact.

This evaluation is a design study to determine the ability of the RAJ-II's containment boundary (fuel bundle), while packaged in the RAJ-II to meet the hypothetical accident conditions free drop test requirements specified in 10 CFR 71 and IAEA TS-R-1.

2.12.6.1 LS-DYNA Finite Element Model – Lower Tie Plate

The solid model of the lower tie plate was created using Autodesk Inventor. The Inventor model was developed from the existing solid model. Figure 2-69 shows the Inventor solid model. To reduce the run time, quarter symmetry was utilized. The Inventor model was meshed using the ANSYS Workbench meshing controls. From Workbench, the model was saved as an LS-DYNA explicit model. Figure 2-70 shows the finite element model. To constrain the quarter model, symmetry boundary conditions were applied.

2.12.6.2 Material Properties

The GNF2 LTP is made from ASTM A351-CF3 cast stainless steel. The material properties at 100ºF (38°C) are:

Table 2-23 LTP Stainless Steel Properties

Property	CF3 Casting
Young's Modulus, E, psi	2.82E+07
Poisson's ratio, ν	0.2656
Yield strength, S_y, psi	30000
Ultimate tensile strength, S_u, psi	70000

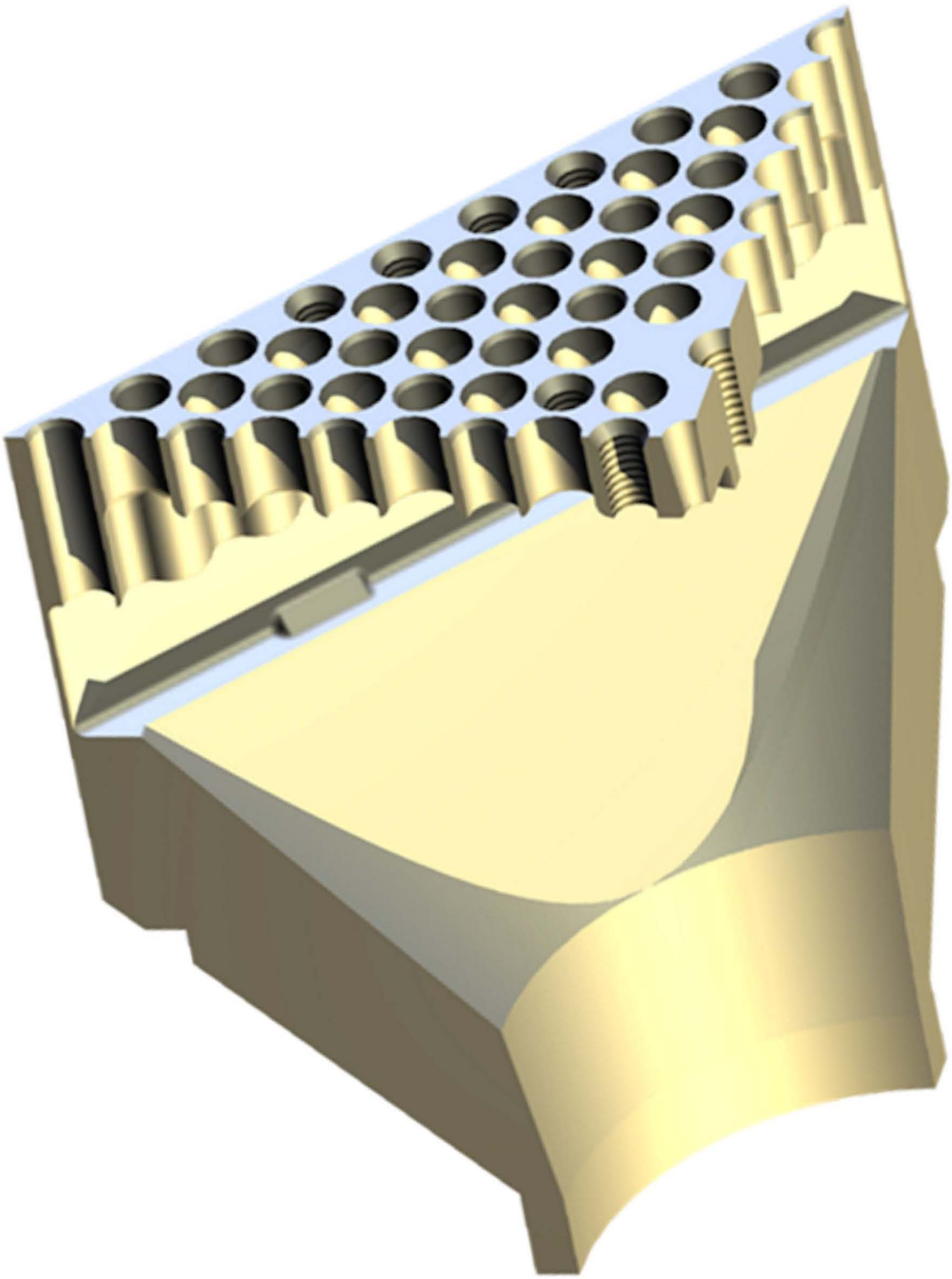

Figure 2-69 LTP Solid Model

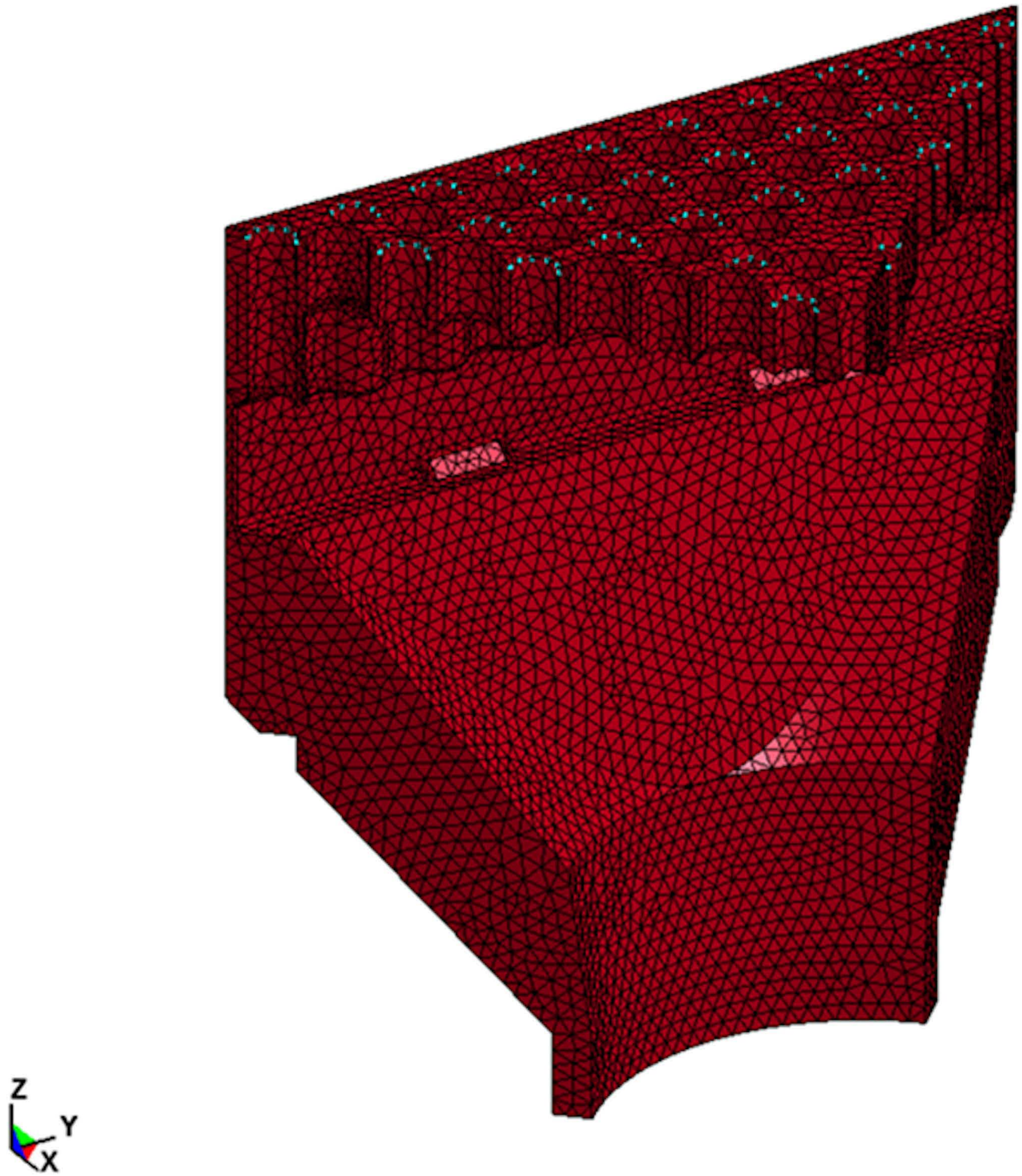

Figure 2-70 LTP Finite Element Model

ASTM A351-CF3 falls within the 304/304L specification. Therefore, the stress-strain properties for 304 stainless steel at 100ºF and a static strain rate were used [Ref. 10]. The stress-strain properties are presented in Table 2-24 are used in this analysis are:

Table 2-24 LTP Stainless Steel Stress-Strain Properties

Total True Stress (psi)	Plastic True Strain (in/in)
30060	**0.0000**
49971	**0.0933**
65829	**0.1803**
79114	**0.2604**
91800	**0.3345**
99913	**0.3799**
103950	**0.4035**
105944	**0.4167**
112000	**0.4680**
114750	**0.5286**

2.12.6.3 Boundary Conditions

Loads were applied to the model in the form of mass elements at the edge of each hole in the LTP casting to represent the weight of each fuel rod, water rod and tie rod. The weight of the entire bundle was supported by the lower nozzle, where all degrees of freedom were fixed. The weight of the upper tie plate (UTP) and channel were distributed equally into all of the full-length fuel rods and water rods. The grid spacer weights were proportionally divided to the rods, which each spacer interacted with for both load cases. The mass elements were divided into five load groups to account for the total bundle weight as shown in Table 2-25:

Table 2-25 LTP Stainless Steel Properties

Property	1/4 Model Load at 203g (lbf)	Number of Nodes	Mass Per Element
Force-Fuel rods	29580.00	162	182.5926
Force-Water rods	842.63	5	168.5263
Force-Tie rods	1409.79	16	88.1117
Force-Long PL Fuel rods	1824.23	16	114.0146
Force-Short PL Fuel rods	724.88	13	55.7599
Total	34381.53		

The maximum acceleration applied to the LTP occurred in the axial direction that translated to the vertical drop orientation of the RAJ-II package. Two cases were identified from the Japanese drop tests that would impose an axial load on the LTP. As Table 2-26 shows, the accelerations measured at the LTP during the end and corner drops (Section 2.12.2).

Table 2-26 End Drop and Corner Drop Test Acceleration Summary

Package	Test Location	Drop Orientation	Impact During (ms)	Acceleration (g)	Sensor Location
RAJ-II	Japan	Vertical end drop	30	58	Lower tie plate
RAJ-II	Japan	Vertical CG over corner	30	203	Lower tie plate

As Table 2-26 shows, the CG over corner test produced higher accelerations at the LTP. To simulate impact on the LTP, the corner drop acceleration of 203g was applied to the LTP model as an instantaneous acceleration. The run termination time was set based on the measured drop duration during the drop test [Refs. 9, 19]. The impact load was conservatively applied to the model for 70 ms then returned to 1g loading conditions for 30ms.

2.12.6.4 Results of LTP Analysis

The resulting displacement calculated by LS-DYNA was 0.036 inches (0.91 mm) which is equivalent to a deflection of approximately 1°. Additional analyses were performed to determine the effect of time. It was noted that the displacement equivalent to the previous static analysis occurred at a time of approximately 0.5 seconds. Therefore, the previous static analysis bounded the dynamic analysis results.

2.12.6.5 ANSYS Finite Element Model – Fuel Cladding

The fuel cladding was modeled based on the parameters defined in Table 3-5 and conservative fuel assembly temperature shown in Figure 3-12. They are summarized in Table 2-27 below.

Table 2-27 Fuel Cladding Parameters

Parameter	Units	10x10 Fuel
Initial pressure	MPa absolute	1.1145
Fill temperature	°C	20
Temperature during HAC (see Fig. 3-12)	°C	300
Outside diameter maximum	mm	10.52
	inches	0.4142
Nominal allowable cladding thickness excluding zirconium liner	inches	0.0201
	mm	0.511
Cladding Inside Diameter Maximum	mm	9.48
	inches	0.373
Pressure @ HAC	MPa(absolute)	3.50
	Psia	508
Applied Pressure @ HAC	MPa	3.40
	Psig	493
Max allowed cladding	Inside Radius/Thickness, mm	9.14

The rod length was assumed as 17.4 inches (442 mm). The finite element model was created in the ANSYS Workbench GUI and exported to an ANSYS APDL input file.

The finite element model used the ANSYS SHELL181 4-node finite strain shell element to mesh the solid model. Surface loads were applied to the model using the ANSYS SURF154 structural surface effect element. Material properties, loads and boundary conditions were defined in the APDL input file. The final results were obtained on an ANSYS 11.0 SP1 Level 2 HPC computer. Figure 2-71shows the finite element model and applied boundary conditions.

The cladding material was ASTM Zircaloy-2. To evaluate worst-case thermal stresses in the cladding, a temperature range of -40°F (-40°C) to 572°F (300°C) was considered to simulate a hypothetical accident, where the cladding was exposed to extreme cold conditions followed immediately by the predicted fire temperatures. The material properties used in this evaluation are presented in Table 2-28.

Table 2-28 Zircaloy-2 Cladding Properties

Property	-40ºF (-40ºC)	572ºF (300ºC)
Yield Strength, σ, psi	62,130	26,059
Young's modulus, E, psi	1.48E+07	1.25E+07
Poisson's ratio,	0.358	0.352
Density, lb/in³	0.237	0.237
Coefficient of thermal expansion X (radial), α, in/in-°F	3.12E-06	4.63E-06
Coefficient of thermal expansion Y (transverse), α, in/in-°F	2.84E-06	3.92E-06
Coefficient of thermal expansion Z (longitudinal), α, in/in-°F	2.61E-06	3.32E-06

Stress-strain properties for Zircaloy-2 at -40°C and 300°C were conservatively used to evaluate the low and high temperature performance of the cladding. To determine the properties of Zircaloy-2 at temperature, the properties at temperature for Zirconium were used to scale the Zircaloy-2 properties [Ref. 1]. The stress-strain properties are:

Table 2-29 LTP Stainless Steel Properties

	Total True Stress (ksi)		
Plastic True Strain (in/in)	-40ºC	21ºC	300ºC
0.000	29.70	28.87	25.07
0.002	62.38	60.21	26.16
0.003	66.05	63.14	27.27
0.004	68.65	65.31	28.22
0.006	72.12	68.48	29.79
0.008	74.68	70.82	31.08
0.018	82.17	77.83	35.60
0.132	106.95	98.51	56.33

The Zircaloy-2 stress-strain curves were input into ANSYS using the multi-linear kinematic hardening material model.

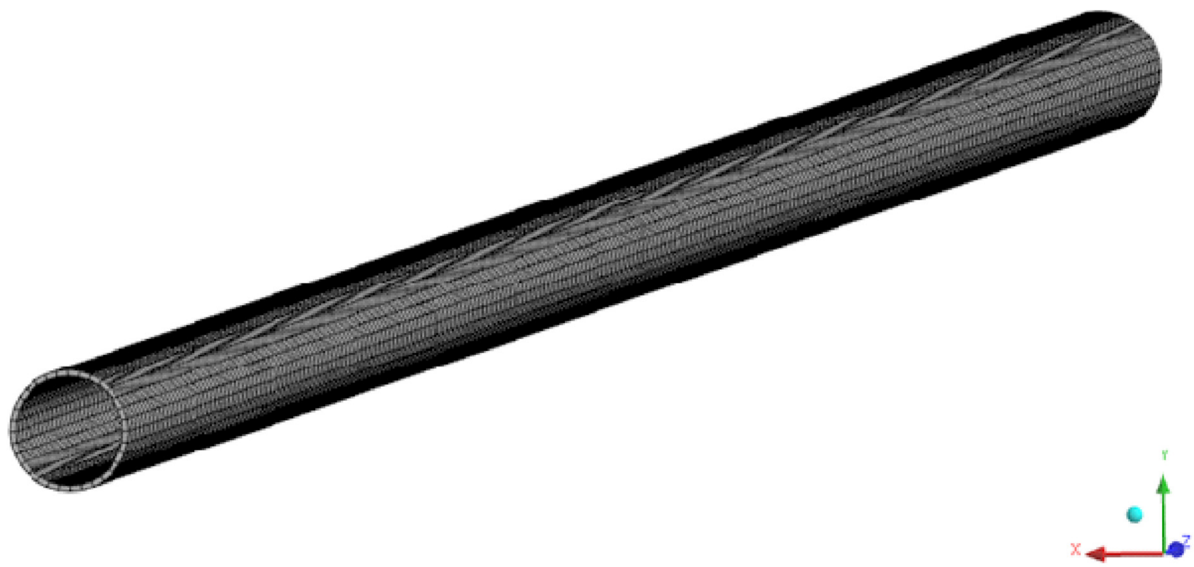

Applied Boundary Conditions

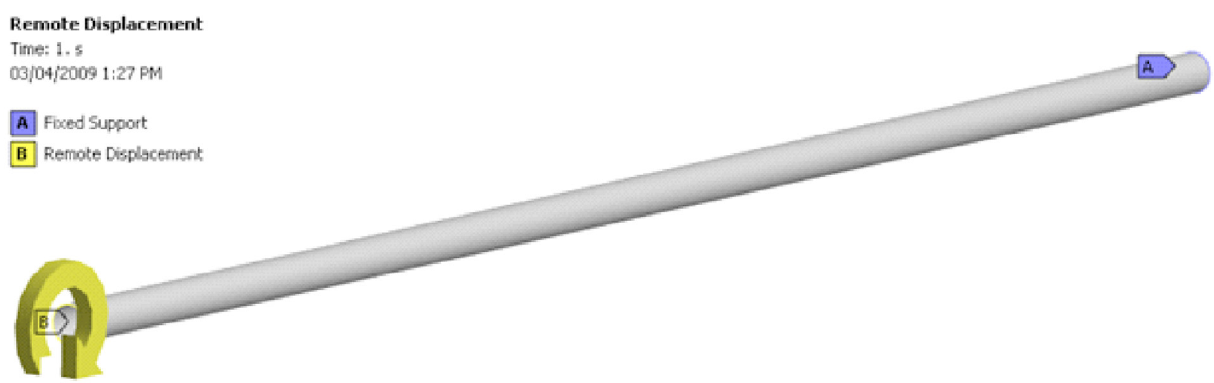

Internal Pressure

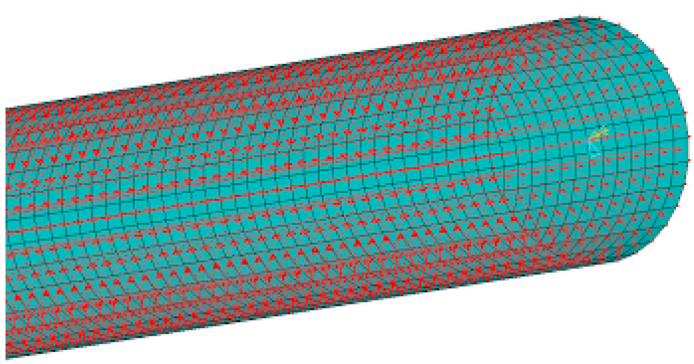

Figure 2-71 Fuel Cladding Finite Element Model and Boundary Conditions

2.12.6.6 Boundary Conditions

The fuel cladding analysis involves a series of steps to simulate the deflection of the cladding that occurs during the end drop of the RAJ-II, and the pressure/thermal stresses that result from the sequential fire.

The first load step applies an angular displacement ranging from 1° to 3° (91° to 93° as measured from the base of the LTP) and normal pressure of 161.6 psi (1.1145 MPa) with material properties at -40°F (-40°C). The angular displacement is applied to the cladding using the remote displacement boundary condition available in ANSYS. In addition to maintaining the cladding displacement, the second load step applies the accident pressure of 508 psi (3.5 MPa) and changes the material properties to reflect the 572°F (300°C) peak cladding temperature (see Figure 3-12). During the third load step the boundary conditions and materials are changed back to the first load step 1 properties, i.e. -40°F (-40°C), to evaluate the cladding stress during the cool down phase.

2.12.6.7 Results of Fuel Cladding Analysis

To evaluate the effects of angular displacement, five cases are considered in half-degree increments. Table 2-30 provides the results for the five cases for each of the three load steps. The first case starts at the angular displacement of 1° predicted by the LTP impact analysis. The progression of increasing stresses shown in load step two best demonstrates the effects of angular displacement on the cladding. For the 1° and 1.5° cases, the combination of pressure/thermal stresses in the cladding shell during the fire is greater than the end effect associated with the angular displacement. Therefore, the stress remains relatively constant. However, as the angle increases the stresses resulting from the angular displacement becomes dominant. This behavior is first seen at 2° during the second load step. Between 2.5° and 3° the stresses in the cladding exceeds the yield stress during the fire. Further evaluation shows that the maximum plastic strain is less than 0.003 that occurs during the fire (second load step). Therefore, failure of the cladding is not predicted. However, stresses in the range of the angular displacement (1°) predicted by LTP impact analysis shows that the pressure/thermal stresses dominated.

Table 2-30 Cladding Analysis Results

Load Step	Stress at Angular Displacement, psi (MPa)					Yield Stress at Temperature, psi (MPa)
	1°	1.5°	2°	2.5°	3°	
1	12015 (83)	17618 (121)	23257 (160)	28925 (199)	33540 (231)	62130 (428)
2	11653 (80)	15797 (109)	20039 (138)	24330 (168)	26120 (180)	26059 (180)
3	12433 (86)	18380 (127)	23234 (160)	28890 (199)	31466 (217)	62130 (428)

2.12.6.8 Conclusions

The LTP and fuel cladding evaluations conclude:

1. LS-DYNA analysis of the LTP design shows that there is local yielding in the body of the LTP but no failure is predicted. Therefore, the LTP will not fail during an end drop event.

2. The cladding evaluation shows that when exposed to extreme cold conditions followed by fire temperatures with the addition of mechanical loads experienced during the 30-foot end drop of the RAJ-II, the fuel cladding will not rupture. The maximum stresses predicted during the end drop, fire event and cool down period are 12015 psi (83 MPa), 11653 psi (80 MPa), and 12433 psi (86 MPa), respectively. In each case, the maximum stress is less than the yield stress.

3. The requirements of IAEA TS-R-1 paragraph 725 and 10 CFR 71.73 are met.

2.12.7 Comparison of RAJ-II and RA-3D Shipping Containers

The RA series of containers were developed from a common design. The first generation design, known in the United States as the RA-3, consisted of a metal inner container and wooden outer container with honeycomb blocks and Ethafoam to line the inner container providing protection against impact and vibration. Each country adopted the design with minor changes. The Japanese container was named the RAJ, and the German equivalent is named the RA-3D. The RAJ is essentially the same design as the RA-3 with a carbon steel inner container, no thermal insulation, and a wooden outer container. The RA-3D is design an exact copy of the RA-3 with the exceptions of a stainless steel inner container, the addition of lifting trunnions and latches used in place of bolts to secure the inner container lid.

In the early 1990's the Japanese developed the second-generation BWR container based on the lessons learned from the previous design. Because of concerns about decontamination and maintenance the wooden outer container was replaced with stainless steel. An additional improvement to the outer container included the addition of a vibration isolation frame to reduce the amount of high cycle vibrations to the fuel bundles during normal transportation.

Because of limitations at the customer facility, the RAJ-II inner container design is little changed from the original RA-3. Like the RA-3D, the RAJ-II inner container is constructed of stainless steel. Unlike the RA-3D, the RAJ-II inner container includes Alumina-Silicate insulation to protect the fuel bundles during the regulatory fire event. Figures A-1 and A-2 show the design features of the RAJ-II and RA-3D, respectively.

2.12.7.1 Detailed Comparison

The following compares the design features of the RAJ-II and RA-3D inner containers:

1. Dimensionally, the RA-3D is almost identical to the RAJ-II inner container in length, width, and height.
2. Testing shows that the bundles act as lumped masses supporting first principle basics that the impact is mass driven. Since both RAJ-II and RA-3D containers ship the same fuel designs, the same lump mass principle applies to both designs.
3. Both containers are designed for the same fuel bundle designs.
4. The RA-3D and RAJ-II inner containers are constructed of 300 series stainless steel.
5. The overall construction of the RA-3D and the RAJ-II is very similar. Both containers are formed and welded of similar sheet metal construction containing an inner and outer skin of similar thicknesses.
6. Both containers use Ethafoam to protect the fuel bundles.
7. Both containers are designed to carry 2 fuel bundles.
8. Both outer containers use honeycomb blocks for impact resistance.
9. The bending resistance about the inner container weak axis is nearly the same. The area moments of inertia for the RAJ-II and RA-3D are 8,909 cm^4 and 9,313 cm^4, respectively. See Figures 2-72 and 2-73.
10. The RAJ-II has a vibration isolation frame that prevents the inner container from shifting during handling and transportation. The RA-3D inner container is free to shift inside of the outer container.
11. The RAJ-II uses Alumina-Silicate as thermal insulation.
12. The RAJ-II has a stainless steel outer container to protect the fuel during accident conditions. The RA-3D outer container is constructed of wood.
13. The RAJ-II all stainless steel construction allows easy decontamination with minimal maintenance.

2.12.7.2 Conclusion

Because of the many similarities between the RA-3D and RAJ-II designs, and since both containers ship the same BWR fuel types, the RA-3D test results are acceptable for use in bounding the performance of the RAJ-II during impact events.

Security Related Information
Figure Withheld Under 10 CFR 2.390

Figure 2-72 Cross-Section RAJ-II Package (dimensions in mm)

Security Related Information
Figure Withheld Under 10 CFR 2.390

Figure 2-73 Cross-Section RA-3D Package (dimensions in mm)

3.0 THERMAL EVALUATION

Provides an evaluation of the package to protect the fuel during varying thermal conditions.

3.1 DESCRIPTION OF THERMAL DESIGN

The RAJ-II package is designed to provide thermal protection as described in Subpart F of 10 CFR 71 for transport of two BWR fuel assemblies with negligible decay heat. Compliance is demonstrated with 10 CFR 71 subpart F in the following subsections. The RAJ-II protects the fuel through the use of an inner and outer container that restricts the exposure of the fuel to external heat loads. The insulated inner container further restricts the heat input to the fuel through its insulation. The fuel requires very little thermal protection since similar fuel has been tested to the 800ºC temperature without rupture.

Given negligible decay heat, the thermal loads on the package come solely from the environment in the form of solar radiation for Normal Conditions of Transport (NCT), as described in Section 3.4 or a half-hour, 800ºC (1,475°F) fire for Hypothetical Accident Conditions (HAC), described in Section 3.5.

Specific ambient temperatures and solar heat loads are considered in the package thermal evaluations. Ambient temperatures ranging from -40ºC to 38ºC (-40ºF to 100ºF) are considered for NCT. The HAC fire event considers an ambient temperature of 38ºC (100ºF), with solar heat loading (insulation) before and after the HAC half-hour fire event.

Details and assumptions used in the analytical thermal models are described with the thermal evaluations.

3.1.1 Design Features

The primary features that affect the thermal performance of the package are 1) the materials of construction, 2) the inner and outer containers and 3) the thermal insulation of the inner container. The stainless sheet metal construction of the structural components of the inner and outer containers influences the maximum temperatures under normal conditions. The material also ensures structural stability under the hypothetical accident conditions as well as provides some protection to the fuel. Likewise the zirconium alloy cladding has also been proven to be stabile at the high temperatures potentially seen during the Hypothetical Accident Conditions (HAC).

The multi walled construction of the single walled outer container and the double walled inner container reduces the heat transfer as well as provides additional stability. The multi walled construction also reduces the opportunity for the fire in the accident conditions to impinge directly on the fuel.

The thermal insulation also greatly reduces the heat transfer to the fuel from external sources. The insulation consists of alumina silicate around most of the package plus the use of wood on the ends that both provide some insulation as well as shock absorbing capabilities.

3.1.2 Content's Decay Heat

Since the contents are unirradiated fuel, the decay heat is insignificant.

3.1.3 Summary Tables of Temperatures

Since the decay heat load is negligible, the maximum NCT temperature of 171ºF (77ºC, 350 K) occurs on the package exterior, and the maximum HAC temperature of 1198ºF (648ºC, 921 K) occurs at the inner surface of the inner container at the end of the fire. These analyses demonstrate that the RAJ-II package provides adequate thermal protection for the fuel assembly and will maintain the maximum fuel rod temperature well below the fuel rod rupture temperature of 800+ºC under all transportation conditions.

3.1.4 Summary Tables of Maximum Pressures

The maximum pressure within the containment, the fuel rods during normal conditions of transport is 1.33 MPa (192.9 psia).

The maximum pressure during the hypothetical accident conditions is 3.50 MPa (508 psia).

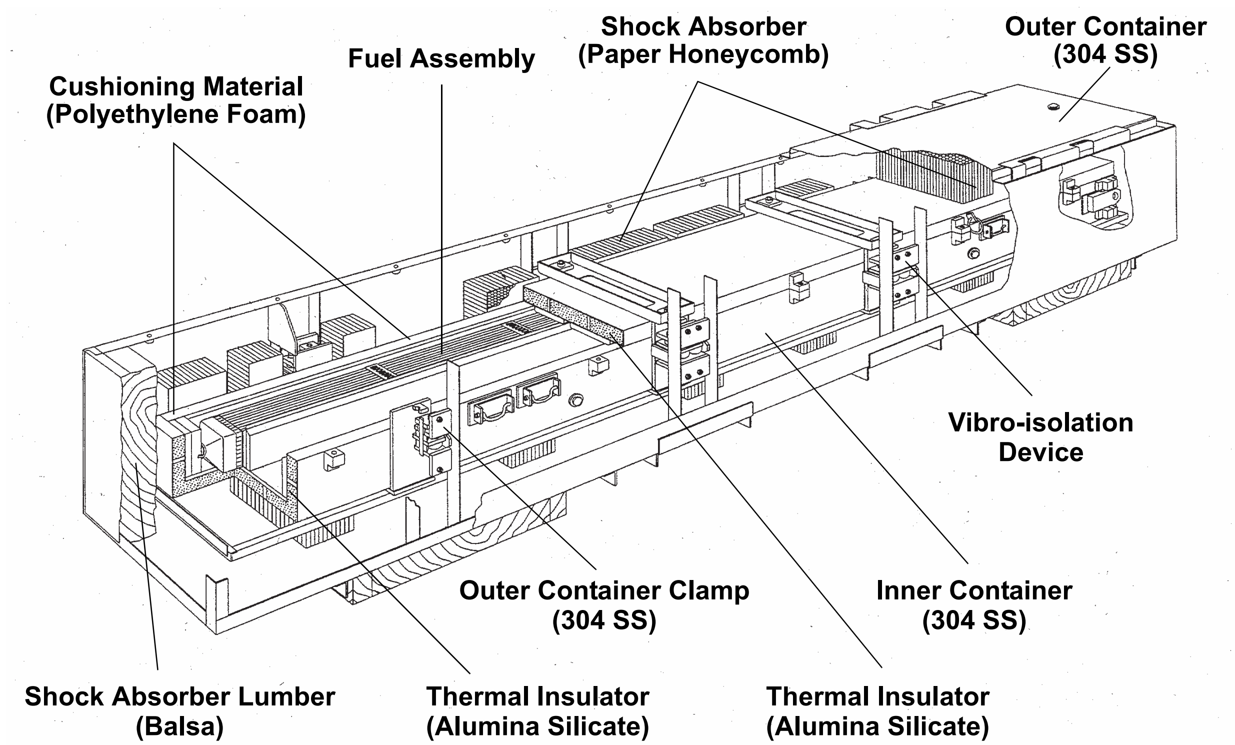

Figure 3-1 Overall View of RAJ-II Package

Security Related Information
Figure Withheld Under 10 CFR 2.390

Figure 3-2 Transverse Cross-Sectional View of the Inner Container

3.2 MATERIAL PROPERTIES AND COMPONENT SPECIFICATIONS

3.2.1 Material Properties

The RAJ-II inner container is constructed primarily of Series 300 stainless steel, wood, and alumina silicate insulation. The void spaces within the inner container are filled with air at atmospheric pressure. The outer container is constructed of series 300 stainless steel, wood, and resin impregnated paper honeycomb. The thermal properties of the principal materials used in the thermal evaluations are presented in Table 3-1 and Table 3-2. Where necessary, the properties are presented as functions of temperature. Note that only properties for materials that constitute a significant heat transfer path are defined. A general view of the package is depicted in Figure 3-1. A sketch of the inner container transversal cross-section with the dimensions used in the calculation is presented in Figure 3-2.

For the Alumina Silicate**,** maximum values are specified because the maximum conductivity is the controlling parameter. This is because there is no decay heat in the payload and the only consideration is the material's ability to block of heat transfer to the fuel during the fire event.

Table 3-1 Material Properties for Principal Structural/Thermal Components

Material	Temperature, K	Thermal Conductivity, W/m-K	Specific Heat, J/kg-K	Density, kg/m^3	Notes
Wood	300	0.240	2,800	500	(1)
Series 300 Stainless Steel	300	15	477	7,900	(2)
	400	17	515		
	500	18	539		
	600	20	557		
	800	23	582		
	1,000	25	611		
Alumina Silicate Insulation	673	≤ 0.105	1,046 (Nominal)	250 (Nominal)	(3)
	873	≤ 0.151			
	1,073	≤ 0.198			(4)
	1,273	≤ 0.267			(4)

Notes:
(1) The material specified for the wood spacers. The properties have been placed with typical values for generic softwood.
(2) [Reference 2. p. 809, 811, 812, and 820]
(3 The values shown are based on published data for Unifrax Duraboard LD [Ref. 11] and include compensation for the possible variation in test data (see discussion in Section 3.2.1).
(4) Values at higher temperatures than 1,000 K are linearly extrapolated.

Table 3-2 Material Properties for Air

Temperature (K)	Thermal Conductivity (W/m·K)	Density (kg/m^3)	Specific Heat (J/kg·K)	Coefficient of Kinematic Viscosity ν(m^2/s)	Prandtl Pr
300	0.0267	1.177	1005	15.66 E-06	0.69
310	0.0274	1.141	1005	16.54 E-06	0.69
320	0.0281	1.106	1006	17.44 E-06	0.69
330	0.0287	1.073	1006	18.37 E-06	0.69
340	0.0294	1.042	1007	19.32 E-06	0.69
350	0.030	1.012	1007	20.30 E-06	0.69
360	0.0306	0.983	1007	21.30 E-06	0.69
370	0.0313	0.956	1008	22.32 E-06	0.69
380	0.0319	0.931	1008	23.36 E-06	0.69
390	0.0325	0.906	1009	24.42 E-06	0.69
400	0.0331	0.883	1009	25.50 E-06	0.69
500	0.0389	0.706	1017	37.30 E-06	0.69
600	0.0447	0.589	1038	50.50 E-06	0.69
700	0.0503	0.507	1065	65.15 E-06	0.70
800	0.0559	0.442	1089	81.20 E-06	0.70
900	0.0616	0.392	1111	98.60 E-06	0.70
1000	0.0672	0.354	1130	117.3 E-06	0.70

Source: Reference 2, p. 824

3.2.2 Component Specifications

None of the materials used in the construction of RAJ-II package, such as series 300 stainless steel and alumina silicate insulation, are sensitive to temperatures within the range of -40°C to 800°C (-40°F to 1,475°F) that spans the NCT and HAC environment. Stainless steel has a melting point above 1,400°C (2,550°F), and maximum service temperature of 427°C (800°F). Similarly, the ceramic fiber insulation has a maximum operating temperature of 1,300°C (2,372°F). Wood is used as dunnage and as part of the inner package wall in the RAJ-II package. Before being consumed in the HAC fire, the wood would insulate portions of the inner container from exposure to the flames. However, the HAC transient thermal analyses presented herein conservatively neglects the wood's insulating effect, and assumes that all of the wood is consumed in the fire generating heat for all of its total mass.

The temperature limit for the fuel assembly's rods is greater than 800°C (1,472°F), based on the pressure evaluation provided in Section 3.5.3.2.

3.3 GENERAL CONSIDERATIONS

3.3.1 Evaluation by Analysis

The normal conditions of transport thermal conditions are evaluated by closed form calculations. The details of this analysis and supporting assumptions are found in that evaluation. The evaluation finds the maximum temperature for the outside of the package due to the insulation and uses that temperature for the contents of the package.

The transient hypothetical accident conditions are evaluated using an ANSYS finite element model. The model does not take credit for the outer container or the wood used in the inner container. Details of the model and the supporting assumptions maybe found in Section 3.5.

3.3.2 Evaluation by Test

Thermal testing was performed on fuel rods to determine the ability of the cladding (primary containment) to withstand temperatures greater than 800°C. The testing was performed for a range of fuel rods of different diameters, clad thickness and internal pressure. Since some of the current fuel designs for use in the RAJ-II are outside the range of parameters tested, additional thermal analyses have been performed to demonstrate the fuel rod's ability to withstand the HAC fire. In these tests, the fuel rods were heated to various temperatures from 700°C to 900°C for periods over one hour to determine the rupture temperature and pressure of the fuel. It was found that the fuel cladding did not fail at 800°C the temperature of the hypothetical accident conditions. This temperature associated pressure and resulting stress were used to provide the allowable conditions of the fuel which is used for containment.

3.3.3 Margins of Safety

For the normal condition evaluation the margins of safety are qualitative, based on comparisons to the much higher temperatures the fuel is designed for when it is in service in the reactors. There is no thermal deterioration of the packaging components at normal condition temperatures therefore no margins for the package components are calculated.

The margins of safety for the accident conditions are evaluated in Section 3.5 and are based on the testing discussed in Section 3.3.2.

3.4 THERMAL EVALUATION UNDER NORMAL CONDITIONS OF TRANSPORT

This section presents the results of thermal analysis of the RAJ-II package for the Normal Conditions of Transport (NCT) specified in 10 CFR 71.71. The maximum temperature for the normal conditions of transport is used as input (initial conditions) in the Hypothetical Accident Condition (fire event) analysis.

3.4.1 Heat and Cold

Per 10 CFR 71.71(c)(1), the maximum environmental temperature is 100°F (311 K), and per 10 CFR 71.71(c)(2), the minimum environmental temperature is -40°F (233 K).

Given the negligible decay heat of the fuel assembly, the thermal loads on the RAJ-II package come solely from the environment in the form of solar radiation for NCT as prescribed by 10 CFR 71.71(c)(1). As such, the solar heat input into the package is 800 g·cal/cm^2 for horizontal surfaces and 200 g·cal/cm^2 for vertical surfaces for a varying insolation over a 24-hour period).

3.4.1.1 Maximum Temperatures

For the analysis, the applied insolation is modeled transiently as sinusoidal over a 24-hour period, except when the sine function is negative (the insolation level is set to zero). The timing of the sine wave is set to achieve its peak at 12:00 PM and peak value of the curve is adjusted to ensure that the total energy delivered matched the regulatory values (800 g·cal/cm^2 for horizontal surfaces, 200 g·cal/cm^2 for vertical surfaces). As such, the total energy delivered in one day by the sine wave model is given by:

$$\int_{6\cdot hr}^{18\cdot hr} Q_{peak} \cdot \sin\left(\frac{\pi t}{12 \cdot hr} - \frac{\pi}{2}\right) dt = \left(\frac{24 \cdot hr}{\pi}\right) \times Q_{peak}$$

Using the expression above for the peak rate of insolation, the peak rates for top and side insolation may be calculated as follows:

Based on these inputs, the maximum NCT temperature on the inside surface of the inner container, as calculated in Section 3.6.3, is 350 K (77ºC, 171ºF).

Given negligible decay heat, the maximum accessible surface temperature of the RAJ-II package in the shade is the maximum environment temperature of 38°C (100°F), which is less than the 50°C (122°F) limit established in 10 CFR 71.43(g) for a non-exclusive use shipment.

3.4.1.2 Minimum Temperatures

The minimum environmental temperature that the RAJ-II package will be subjected to is -40°F, per 10 CFR 71.71(c)(2). Given the negligible decay heat load, the minimum temperature of the RAJ-II package is -40°F.

3.4.2 Maximum Normal Operating Pressure

The fuel rods are pressurized with helium to a maximum pressure of 1.145 MPa (absolute pressure (161.7 psia) helium at ambient temperature prior to sealing. Hence, the Maximum Normal Operating Pressure (MNOP) at the maximum normal temperature is:

$$\mathrm{MNOP} = (P_1)\frac{T_{max}}{T_{ambient}} = 1.1145 \times \frac{350}{293} = 1.33\ \mathrm{MPa} = 192.9\ \mathrm{psia}$$

Since there is no significant decay heat and the fuel composition is stable, MNOP calculated above would not be expected to change over a one year time period.

3.4.3 Maximum Thermal Stresses

Due to the construction of the RAJ-II, light sheet metal constructed primarily of the same material, 304 SS, there are no significant thermal stresses. The package is constructed so that there is no significant constraint on any component as it heats up and cools down. The fuel cladding which provides containment is likewise designed for thermal transients, greater than what is found in the normal conditions of transport. The fuel rod is allowed to expand in the package. The fuel within the cladding is also designed to expand without interfering with the cladding.

3.5 THERMAL EVALUATION UNDER HYPOTHETICAL ACCIDENT CONDITIONS

This section presents the results of the thermal analysis of the RAJ-II package for the Hypothetical Accident Condition (HAC) specified in 10 CFR 71.73(c) (4).

For the purposes of the Hypothetical Accident Conditions fire analysis, the outer container of the RAJ-II package is conservatively assumed to be not present during the fire. This allows the outer surface of the inner container to be fully exposed to the fire event. The wood used in the inner container is conservatively assumed to combust completely. By ignoring the outer container and applying the fire environment directly to the inner container, the predicted temperature of the fuel rods is bounded. To provide a conservative estimate of the worst-case fuel rod temperature, the fuel assembly and its corresponding thermal mass are not explicitly modeled as well as the polyethylene foam shock absorber. The maximum fuel rod temperature is conservatively derived from the maximum temperature of the inside surface of the inner stainless steel wall. The analysis considering the insulation and multi-layers of packaging is very conservative because as discussed in Section 3.3.2 the bare fuel has been demonstrated to maintain integrity when exposed to temperatures that equal those found in the hypothetical accident conditions.

Thermal performance of the RAJ-II package is evaluated analytically using a 2-D model that represents a transversal cross-section of the inner container (Figure 3-2) in the region containing the metallic and wood spacers. The 2-D inner container finite element model was developed using the ANSYS computer code [Ref. 3]. ANSYS is a comprehensive thermal, structural and fluid flow analysis package. It is a finite element analysis code capable of solving steady state and transient thermal analysis problems in one, two or three dimensions. Heat transfer via a combination of conduction, radiation and convection can be modeled.

The solid entities were modeled in the present analysis with PLANE55 two-dimensional elements and the radiation was modeled using the AUX12 Radiation Matrix method. The developed ANSYS input file is included as Section 3.6.2.

The initial temperature distribution in the inner container prior to the HAC fire event is a uniform 375 K conservatively corresponding to the outer surface temperature of the inner container per the normal condition calculations presented in Section 3.6.3.

3.5.1 Initial Conditions

The environmental conditions preceding and succeeding the fire consist of an ambient temperature of 38ºC (311 K) and insulation per the normal condition thermal analysis. The solar absorptivity coefficient of the outer surface has been increased for the post-fire period to 1 to include changes due to charring of the surfaces during the fire event.

3.5.2 Fire Test Conditions

The Hypothetical Accident Condition fire event is specified per 10 CFR 71.73(c) (4) as a half-hour, 800ºC (1,073 K) fire with forced convection. For the purpose of calculation, the value of the package surface absorptivity coefficient (0.8) is selected as the highest value between the actual value of the surface (0.42) and a value of 0.8 as specified in 10 CFR 71.73(c) (4).

A value of 1.0 for the emissivity of the flame for the fire condition is used in the calculation. The rationale for this is that 1.0 maximizes the heating of the package. This value exceeds the minimum value of 0.9 specified in 10 CFR 71.73(c) (4). The Hypothetical Accident Condition (HAC) fire event is specified per 10 CFR 71.73(c)(3) as a half-hour, 800ºC (1,475°F) fire with forced convection and an emissivity of 0.9. The environmental conditions preceding and succeeding the fire consist of an ambient temperature of 100ºF and insulation per the NCT thermal analyses.

To model the combustion of the wood, the wood elements of the model are given a heat generation rate based on the high heat value of Western Hemlock of 3630 Btu/lb (8.442×10^6 J/kg) from Reference 8, Section 7, Table 9. It is conservatively assumed that the entire mass of the wood will burn. Moreover, the wood will burn across its thinnest section from opposite faces. Using data burn rate data for redwood which has approximately the same density as hemlock [Ref. 8], each face will burn 5 mm at a minimum rate of 0.543 mm/min [Ref. 10] resulting in a 9.2 minute time of combustion. This conservatively results in the longest burn time for the hemlock, and the greatest effect on temperature. The resulting heat generation rate in the wood spacers is equal to:

$$\dot{Q} = (8.42\times10^6) \times (500 \text{ kg} / \text{m}^3) / (9.2 \text{ sec} \times 60) = 7.63\times10^6 \text{ W/m}^3\text{/sec.}$$

3.5.2.1 Heat Transfer Coefficient during the Fire Event

During a HAC hydrocarbon fire, the heating gases surrounding the package will achieve velocities sufficient to induce forced convection on the surface of the package. Peak velocities measured in the vicinity of the surfaces were under 10 m/s [Ref. 4].

The heat transfer coefficient takes the form [Reference 4, p. 369]:

$$h = k/D \cdot C \cdot (u \cdot D/\upsilon:)^m \cdot Pr^{1/3} \tag{8}$$

Where:

- D: average width of the cross-section of the inner container (0.373 m)
- k: thermal conductivity of the fluid
- υ: kinematic viscosity of the fluid
- u: free stream velocity
- C, m: constants that depend on the Reynolds number ($Re=u\cdot D/\upsilon$)
- Pr: Prandtl number for the fluid

The property values of k, υ and Pr are evaluated at the film temperature, which is defined as the mean of the wall and free stream fluid temperatures. At the start of the fire the wall temperature is 375 K (101.7ºC, 215ºF) and the stream fluid temperature is 1,073 K (1,475ºF). The film temperature is therefore 710.5 K, and the property values for air at this temperature (interpolated from Table 3-2) are k=0.0509 W/m·K, υ=66.84E-06 m^2/s and Pr= 0.70. Assuming a maximum stream velocity of 10 m/s this yields a Reynolds number of 55.8E03. At this value of Re, the constants C and n are 0.102 and 0.675 respectively [Reference 4, Table 7.3].

$$h = \frac{0.0509 \cdot 0.102 \cdot (10 \cdot 0.373/66.84 \cdot 10^{-6})^{0.675} \cdot (0.70)^{1/3}}{0.373}$$

$$h = 19.8 \text{ W/m}^2 \cdot \text{K}$$

A value of 19.8 $W/m^2 \cdot K$ was conservatively used in the analysis of the regulatory fire.

3.5.2.2 Heat Transfer Coefficient during Post-Fire Period

During the post-fire period of the HAC, it is conservatively assumed that there is negligible wind and that heat is transferred from the inner container to the environment via natural convection. Natural heat transfer coefficients from the outer surface of the square inner container are calculated as follows.

Reference 4 recommends the following correlations for the Nusselt number (Nu) describing natural convection heat transfer to air from heated vertical and horizontal surfaces:

Vertical heated surfaces [Reference 4, p. 493]:

$$Nu = \left(0.825 + \frac{0.387 \cdot (Gr \cdot Pr)^{1/6}}{(1 + (0.492/Pr)^{9/16})^{8/27}}\right)^2 \text{ For entire range of } Ra = Gr \cdot Pr \quad (9)$$

Where:

Nu: Nusselt number

Gr: Grashof number

Pr: Prandtl number

Horizontal heated surfaces facing upward [Reference 4, p. 498]:

$$Nu = 0.54 \cdot (Gr \cdot Pr)^{1/4} \text{ for } (10^4 < Gr \cdot Pr < 10^7) \quad (10)$$

$$Nu = 0.15 \cdot (Gr \cdot Pr)^{1/3} \text{ for } (10^7 < Gr \cdot Pr < 10^{11}) \quad (11)$$

and, for horizontal heated surfaces facing downward:

$$Nu = 0.27 \cdot (Gr \cdot Pr)^{1/4} \text{ for } (10^5 < Gr \cdot Pr < 10^{10}) \quad (12)$$

The correlations for the horizontal surfaces are calculated using a characteristic length defined by the relation L=A/P, where A is the horizontal surface area and P is the perimeter [Reference 4, p. 498]. The calculated characteristic length for the horizontal surfaces of the inner container is L=0.209 m (A=2.14812 m^2 and P=10.278 m).

The following convective heat transfer coefficients (Table 3-1) have been calculated using Eq. (5), (6), (9), (10), (11) and (12). The corresponding characteristic length used in calculating the Nusselt number for each surface is also used in Eq. 5 for calculating the heat transfer coefficient. The thermal properties of air have been evaluated at the mean film temperature (=(T_s+$T_{ambient}$)/2).

The effects of solar radiation are included during the post-fire period by specifying the equivalent heat flow for each node of the surfaces exposed to fire for an additional 3.5 hours, i.e. the fire starts at the time of the peak temperature in the inner container (8 hours after sunrise) and is 0.5 hours in duration. This results in an additional 3.5 hours of solar insolation. Using the peak rates calculated in Section 3.4.1.1, the nodal heat flows at 2:30 PM are equal to:

$$\dot{q}_{top} = \frac{1{,}218 \dfrac{W}{m^2} \left(Sin\left(\dfrac{\pi \times (6+8.5)}{12} - \dfrac{\pi}{2} \right) \right) (0.459\,m)}{(155-1)} = 2.88\,W/m$$

$$\dot{q}_{side} = \frac{305 \dfrac{W}{m^2} \left(Sin\left(\dfrac{\pi \times 14.5}{12} - \dfrac{\pi}{2} \right) \right) (0.281\,m)}{99-1} = 0.69\,W/m$$

where 0.459 m is the width of the inner container, 0.281 m is its height, and the model is 155 nodes in width by 99 nodes in height. For the remaining 3.5 hours of solar insolation, these heat fluxes are conservatively applied as bounding constant values rather than varying with time.

The solar absorptivity coefficient of the outer surface is conservatively assumed to be 1. The duration of the post-fire period has been extended to 12.5 hr to investigate the cool-down of the inner container.

3.5.3 Maximum Temperatures and Pressure

3.5.3.1 Maximum Temperatures

The peak fuel rod temperature, which is conservatively assumed to be the same as the inner wall temperature of the package, response over the course of the HAC fire scenario is illustrated in Figure 3-3. The temperature reaches its maximum point of 921 K or 648ºC (1198ºF) at the end of the fire or 1,800 seconds after the start of the fire. This peak temperature occurs at top corners of the inner wall.

The maximum temperature even when applied to the fuel directly is well below the maximum temperature the fuel can withstand. Similar fuel with no thermal protection has been tested in fire conditions at over 800ºC (1,475ºF) for more than 60 minutes without failures.

3.5.3.2 Maximum Internal Pressure

The maximum pressure for the fuel can be determined by considering that the fuel is pressurized initially with helium. As the fuel is heated, the internal pressure in the cladding increases. By applying the perfect gas law the pressure can be determined and the resulting stresses in the cladding can be determined. Since the temperatures can be well above the normal operating range of the fuel the cladding performance can best be determined by comparison to test data.

Similar fuel with similar initial pressures has been heated in an oven to over 800ºC for over an hour without failures [Ref. 6]. The fuel that was tested in the oven was pressurized with 10 atmospheres of helium. When heated to the 800°C it had an equivalent pressure of:

$$P_{\max} = (P_1)\frac{T_{\max}}{T_{ambient}} = 1.1145 MPa * \frac{1073}{293} = 4.08 MPa = 592\,psia$$

This results in an applied load to the cladding of 3.98 MPa or 577.3 psig. The fuel that was tested had an outer diameter of 0.4054 inch (10.30 mm). Since the fuel when tested to 850°C had some ruptures but did not rupture at 800°C when held at those temperatures for 1 hour, the stresses at 800°C are used as the conservative allowable stress. Both the tested fuel and the fuels to be shipped in the RAJ-II have similar zirconium cladding. The stress generated in the cladding of the test fuel is:

$$\sigma = \frac{\mathrm{pr}}{\mathrm{t}} = \frac{3.98\mathrm{MPa}\mathrm{x}4.56\mathrm{mm}}{0.584\mathrm{mm}} = 31.1\mathrm{MPa} = 4510\mathrm{psi}$$

Recognizing that the properties of the fuel cladding degrade as the temperature increases the above calculated stress is conservatively used as the allowable stress for the fuel cladding for the various fuels to be shipped. The fuel is evaluated at the maximum temperature the inner wall of the inner container sees during the Hypothetical Accident Condition thermal event evaluated above. Table 3-5 shows the maximum pressure for each type of fuel and the resulting stress and margin. The limiting design properties of the fuel, maximum cladding internal diameter, minimum cladding wall thickness and initial pressurization for each type of fuel are considered in determining the margin of safety. Positive margins are conservatively determined for each type of fuel demonstrating that containment would be maintained during the Hypothetical Accident events. The minimum cladding thickness does not include the thickness of the liner if used.

The results of the transient analysis are summarized in Table 3-4. The temperature evolution during the transient in three representative locations on the inner wall and one on the outer wall is included. The maximum temperature on the inner wall is 921 K (648ºC, 1198ºF) and is reached at the upper inner corners of the container, 1,800 seconds after the beginning of the fire. The graphic evolution of the temperatures listed in Table 3-4 is represented in Figure 3-3. Representative plots of the isotherms at various points in time are depicted in Figure 3-4 through Figure 3-7.

The temperatures and resulting pressures are within the capabilities of the fuel cladding as shown by test. Therefore the fuel cladding and closure welds maintain containment during the Hypothetical Accident Conditions.

The temperatures and resulting pressures are within the capabilities of the fuel cladding as shown by test. Therefore the fuel cladding and closure welds maintain containment during the Hypothetical Accident Conditions.

3.5.4 Accident Conditions for Fissile Material Packages for Air Transport

Approval for air transport is not requested for the RAJ-II.

Table 3-3 Convection Coefficients for Post-fire Analysis

T_s (surface temperature)		$T_{ambient}$		H (vertical surface)	h (horizontal surface facing upward)	h (horizontal surface facing downward)
ºF	K	ºF	K	($W/m^2 \cdot K$)	($W/m^2 \cdot K$)	($W/m^2 \cdot K$)
150	338.71	100	311	4.68	5.19	2.34
200	366.48	100	311	5.61	6.34	2.74
250	394.26	100	311	6.18	7.05	2.99
300	422.04	100	311	6.60	7.55	3.17
350	449.82	100	311	6.90	7.92	3.30
400	477.59	100	311	7.13	8.18	3.41
600	588.71	100	311	7.64	8.74	3.67
900	755.37	100	311	8.00	9.07	3.89
1,375	1,019.26	100	311	8.25	9.17	4.09

Table 3-4 Calculated Temperatures for Different Positions on the Walls of the Inner Container Walls

Time (s)	Inner Wall Temperature (top right corner) (K)	Inner Wall Temperature (bottom) (K)	Inner Wall Temperature (top) (K)	Outer Wall Temperature (K)
0.1	375	375	375	377
911	750	667	546	1,062
1,800	921	821	696	1,067
1,900	918	823	710	807
2,000	905	817	723	686
2,200	868	797	742	583
2,600	803	761	760	509
3,268	723	715	758	463
4,280	639	662	727	437
27,973	354	335	369	378
45,000	349	324	358	377

Table 3-5 Maximum Pressure

Parameter	Units	8 × 8 Fuel	9 × 9 Fuel	10 × 10 Fuel
Initial Pressure	MPa absolute	0.608	1.1145	1.1145
Fill temperature	°C	20	20	20
Temperature during HAC	°C	648	648	648
Outside Diameter Maximum	mm	12.5	11.46	10.52
	inches	.492	.4512	.4142
Minimum Allowable Cladding Thickness	inches	0.0268	0.0224	0.0205
	mm	.68	0.570	0.520
Cladding Inside Diameter Maximum	mm	11.14	10.32	9.48
	inches	.439	.406	.373
Pressure @ HAC	MPa (absolute)	1.91	3.50	3.50
	Psia	277	508	508
Applied Pressure @ HAC	MPa	1.81	3.40	3.40
	Psig	262	493	493
Stress Pr/t	MPa	14.82	30.8	31.0
	Psi	2,149	4,467	4,498
Margin	(allowed stress/actual stress)-1	1.10	0.01	0.003
Max allowed cladding	Inside Radius/Thickness	20.20	9.14	9.14

Note: Table values for cladding thickness and diameters are for example purposes and represent current limiting fuel designs. However, all fuel to be shipped must have a maximum pre-pressure times the maximum Inside Radius/Thickness product of 9.14 × 1.1145 MPa = 10.18653 MPa or less. Thus, all products must meet the maximum product of allowed pressure multiplied by Inside Radius/Thickness of 10.18653 MPa.

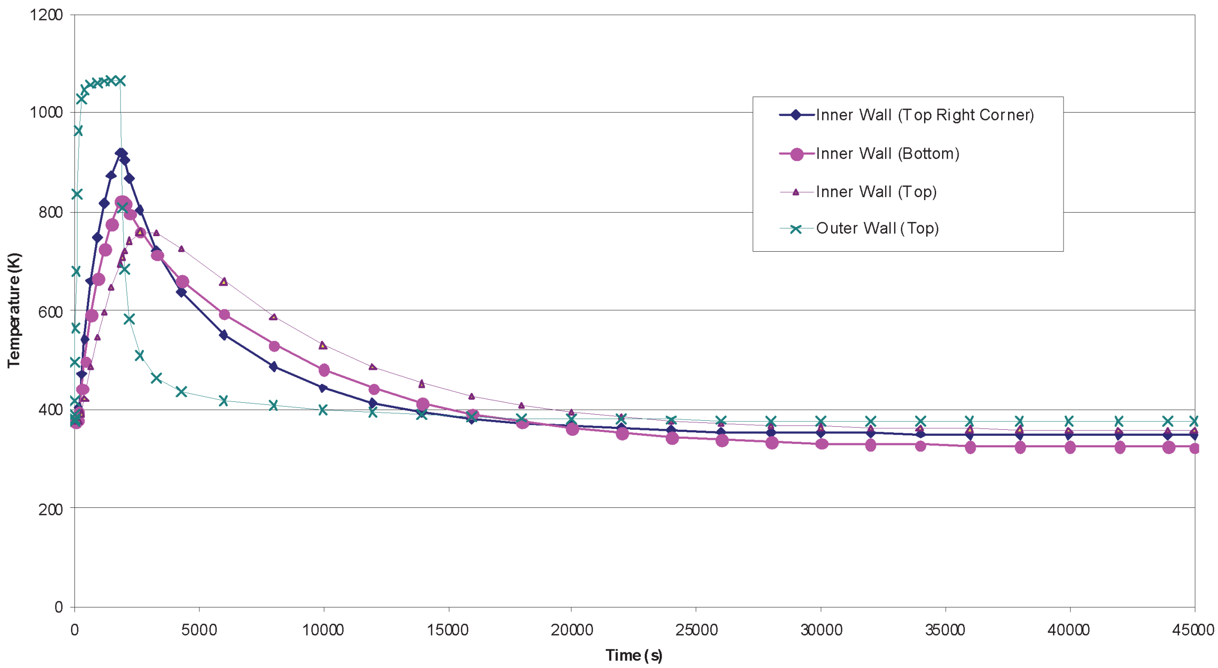

Figure 3-3 Calculated Temperature Evolution During Transient

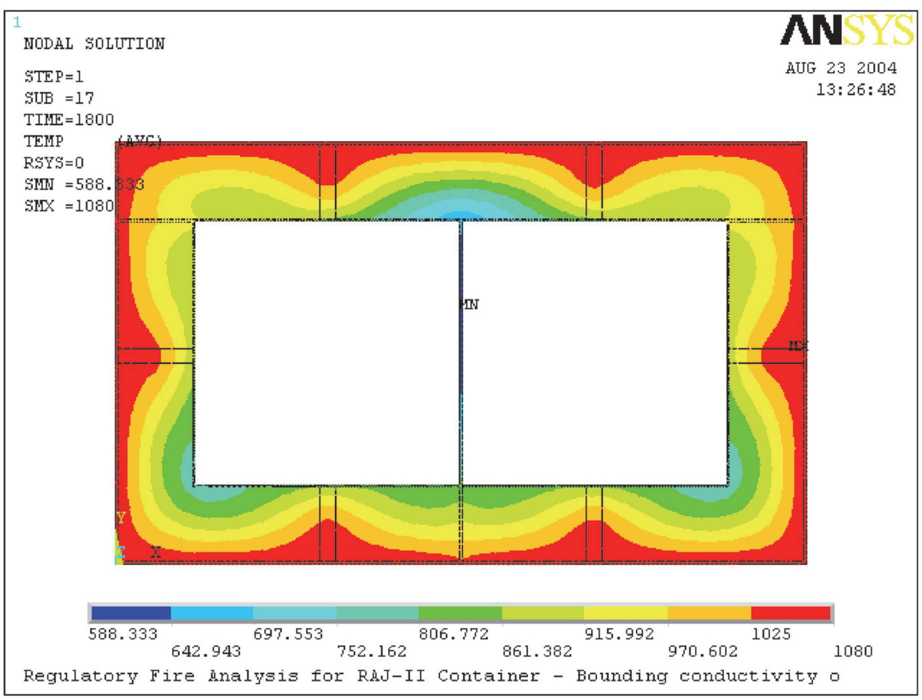

Figure 3-4 Calculated Isotherms at the End of Fire Phase (1,800 s)

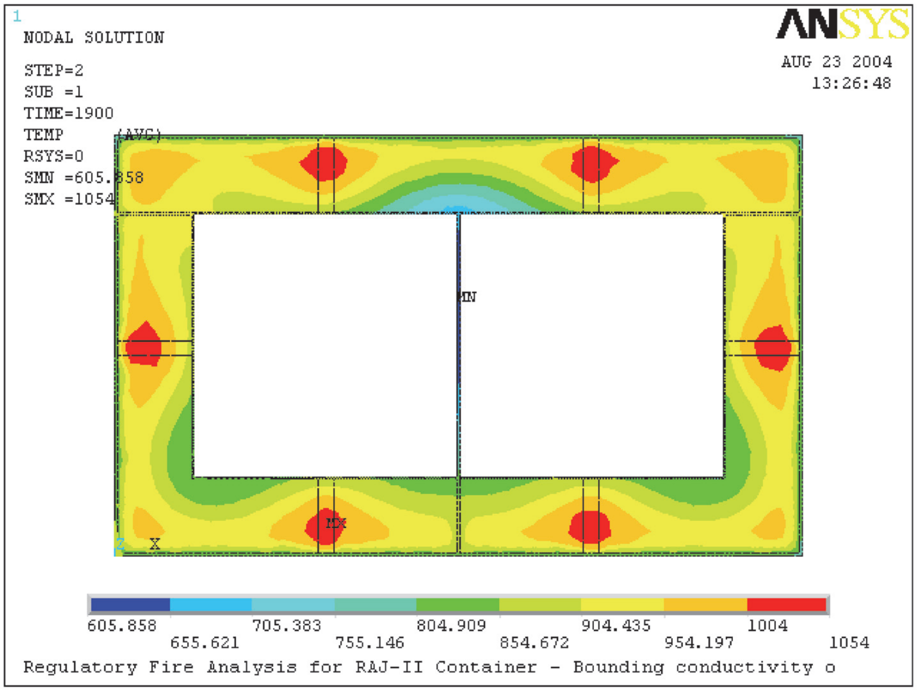

Figure 3-5 Calculated Isotherms at 100s After the End of Fire

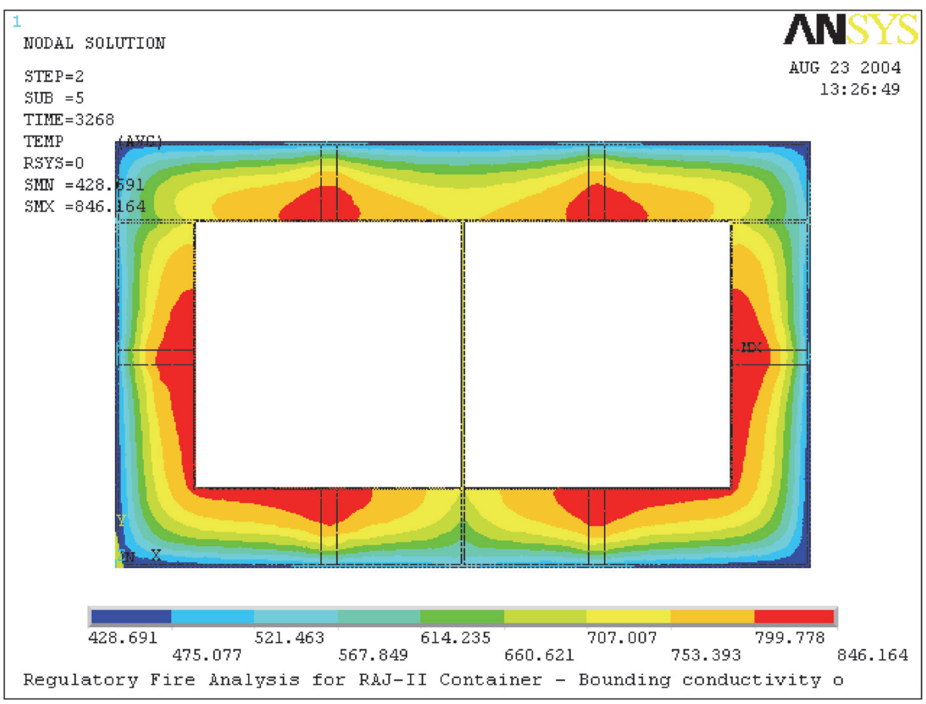

Figure 3-6 Calculated Isotherms at 1,468s After the End of Fire

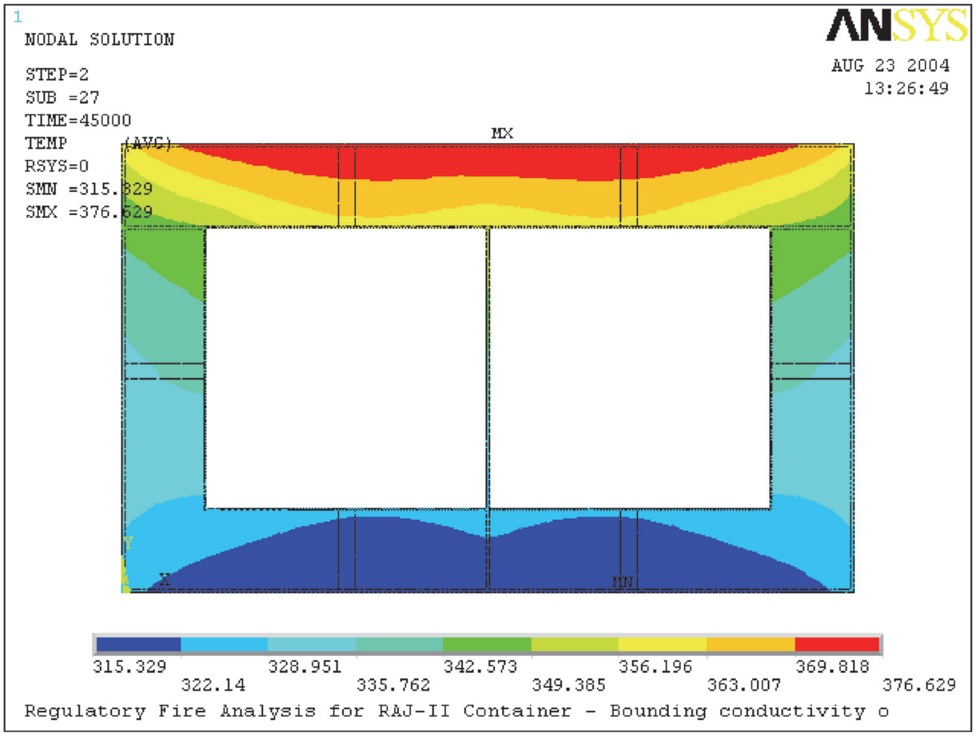

Figure 3-7 Calculated Isotherms at 12 hr After the End of Fire

3.6 APPENDIX

3.6.1 References

1. 10 CFR 71, Packaging and Transportation of Radioactive Material

2. Mills, A.F., Heat Transfer, Irwin, Inc., Homewood, Illinois, 1992

3. ANSYS Finite Element Computer Code, Version 5.6, ANSYS, Inc., 2000

4. McCaffery, B.J., Purely Buoyant Diffusion Flames – Some Experimental Results, Report PB80-112113, U.S. National Bureau of Standards, Washington, D.C., 1979

5. Incropera, F.P., Dewitt, D.P., Fundamentals of Heat and Mass Transfer, John Wiley and Sons, Inc., New York, New York, 1996.

6. GNF-2 Fuel Rod Response to An Abnormal Transportation Event (proprietary) (30 Minute Fire)

7. Handbook of Heat Transfer, Warren M. Rohsenow, James P. Hartnett, McGraw Hill book company.

8. Standard Handbook for Mechanical Engineers, Baumeister, Marks, McGraw Hill book company, Seventh edition.

9. Thermal Properties of Paper, PTN149, Charles Green, Webster New York, 2002 (http://www.frontiernet.net/~charmar/).

10. Tran, H.C., and White, R. H., Burning Rate of Solid Wood Measured in a Heat Release Calrimeter, Fire and Materials, Vol. 16, pp 197-206,1992.

11. "Pactec Specification: Regarding Global Nuclear Fuel Specification for Alumina Silicate for use in the RAJ-II Shipping container," Unifrax Corporation, 6/3/04.

12. Ragland, Aerts, "Properties of Wood for Combustion Analysis," Department of Mechanical Engineering, University of Wisconsin-Madison.

13. EthaFoam 220", Dow Chemical Company.

14. Gaur, Wunderlich, "Heat Capacity and Other Thermodynamic Properties of Linear Macromolecules. II. Polyethylene," Department of Chemistry, Renssalaer Polytechnic Institute.

15. Walters, Hackett, and Lyon, "Heats of Combustion of High Temperature Polymers," Federal Aviation Administration.

16. Hopkins, “Predicting the Ignition Time and Burning Rate of Themoplastics in the Cone Calorimeter,” Department of Fire Protection Engineering, University of Maryland.

17. “Delrin Acetal Resin,” Dow Chemical Company.

18. “EU-Material Safety Data Sheet: Delrin. Issue 250/05,” Dow Chemical Company.

19. Steinberg, Newton, and Beeson, ed, “Flammability and Sensitivity of Materials in Oxygen-Enriched Atmospheres,” ASTM STP 1395, p. 98.

20. Perry, R.H. and Green, D.W., Perry’s Chemical Engineers’ Handbook, 7th Edition, McGraw-Hill, 1997, Table 27-4.

3.6.2 ANSYS Input File Listing

Listing of the ANSYS input file (file: model_fl_heat.inp)

```
fini
/clear
/filnam,model_f1_heat,
/outp, model_f1_heatout,out
/PREP7
/TITLE, Regulatory Fire Analysis for RAJ-II Container -
Bounding conductivity of Alumina
/UNITS,SI
/SHOW,JPEG
!*
!*set element types
!*
ET,1, PLANE55,1
ET,2,LINK32
ET,3,MATRIX50,1
!*
!* define keypoints
!*
K,1,0,0,0,
K,2,0.459,0,0,
K,3,0,0.0015,0,
K,4,0.0015,0.0015,0,
K,5,0.136,0.0015,0,
K,6,0.146,0.0015,0,
K,7,0.2285,0.0015,0,
K,8,0.2305,0.0015,0,
K,9,0.313,0.0015,0,
K,10,0.323,0.0015,0,
K,11,0.4575,0.0015,0,
K,12,0.459, 0.0015, 0,
K,13,0.0015,0.0515 0,
K,14,0.0515,0.0515,0,
K,15,0.136,0.0515,0,
K,16.0.146,0.0515,0,
K,17,0.2285,0.0515,0,
K,18,0.2305,0.0515,0,
K,19,0.313,0.0515,0,
K,20, 0.323,0.0515, 0,
K,21,0.4075,0.0515,0,
K,22,0.4575,0.0515,0,
K,23,0.0515,0.0525,0,
K,24,0.0525,0.0525,0,
K,25,0.2285,0.0525,0,
K,26,0.2305,0.0525,0,
K, 27,0.4065,0.0525,0,
K,28,0.4075,0.0525,0,
K,29,0.0525,0.0705,0,
K,30,0.0705,0.0705,0,
K,31,0.2105,0.0705,0,
K,32,0.2285,0.0705,0,
K,33,0.2305,0.0705,0,
K,34,0.2485,0.0705,0,
```

K,35,0.3885 0.0705,0,

K,36,0.4065,0.0705,0,

K,37,0.0015,0.1335,0,

K,38,0.0515,0.1335,0,

K,39,0.4075, 0.1335,0,

K,40,0.4575,0.1335,0,

K,41,0.0015,0.1435,0,

K,42,0.0515,0.1435,0,

K,43,0.4075,0.1435,0,

K,44,0.4575,0.1435,0,

K,45,0.0705,0.1975,0,

K,46,0.2105,0.1975,0,

K,47,0.2485,0.1975, 0,

K,48,0.3885,0.1975,0,

K,49,0.0525,0.2155,0,

K,50,0.060,0.2115,0,

K,51,0.066,0.2055,0,

K,52,0.2175,0.2055,0,

K,53,0.2235 0.2115,0,

K,54,0.2285,0.2155,0,

K,55,0.2305,0.2155,0,

K,56,0.2355,0.2115,0,

K,57,0.2415,0.2 055,0,

K,58,0.393,0.2055,0,

K,59,0.399,0.2115,0,

K,60,0.4065,0.2155,0,

K,61,0.,0.2275,0,

K,62,.0.0015,0.2275,0,

K,63,0.0515,0.2275,0,

K,64,0.0525,0.2275,0,

K,65,0.4065,0.2275,0,

K,66,0.4075,0.2275,0,

K,67,0.4575,0.2275,0,

K,68,0.459,0.22 75,0,

K,69,0.,0.2285,0,

K,70,0.0525,0.2285,0,

K,71,0.06,0.2285,0,

K,72,0.2235,0.2285,0,

K,73,0.2285,0.2285,0,

K,74,0.2305,0.2285,0,

K,75,0.2355,0.2285,0,

K,76,0.399,0.2285,0,

K,77,0.4065,0.2285,0,

K,78,0.459,0.2285,0,

K,79,0.,0.2295,0,

K,80,0.0015,0.2295,0,

K,81,0.136,0.2295,0,

K,82,0.146,0.2295,0,

K,83,0.313,0.22 95,0,

K,84,0.323,0.2295,0,

K,85,0.4575,0.2295,0,

K,86,0.459,0.22 95,0,

K,87,0.,0.2795,0,

K,88,0.0015,0.2795,0,

K,89,0.136,0.2795,0,

K,90,0.146,0.2795,0,

K,91,0.313,0.2795,0,

K,92,0.323, 0.2795, 0,

```
K,93,0.4575,0.2 795,0,
K,94,0.459,0.2795,0,
K,95,0.,0.281,0,
K,96,0.459,0.281,0,
SAVE
!*
!* define material properties
!*
!*
!* STAINLESS STEEL (SS304)
!*
MP,DENS,1,7900
MPTEMP,1,300,400,500,600,800,1000
MPDATA,kxx,1,1,15,17,18,20,23,25
MPDATA,c,1,1,477,515,539,557,582,611
!*
!* THERMAL INSULATOR
!*
MP,DENS,2,260
MP,C,2,1046
MPTEMP
MPTEMP,1,673,873,1073,1273
MPDATA,KXX,2,1,0.105,0.151,0.198,0.267 !MAX VALUES
!*
!*
!* WOOD (generic softwood)
!*
UIMP,3,EX, , , ,
UIMP,3,NUXY, , , ,
UIMP,3,ALPX, , , ,
 UIMP,3,REFT, , , ,
UIMP,3,MU, , , ,
UIMP,3,DAMP, , , ,
UIMP,3,DENS , , , 500,
UIMP,3,KXX , , , 0.24,
UIMP,3,C , , , 2800,
UIMP,3,ENTH, , , ,
UIMP,3,HF, , , ,
UIMP,3,EMIS, , , ,
UIMP,3,QRATE, , , ,
UIMP,3,VISC, , , ,
UIMP,3,SONC, , , ,
UIMP,3,MURX, , , ,
UIMP,3,MGXX, , , ,
UIMP,3,RSVX, , , ,
UIMP,3,PERX, , , ,
!*
!* define areas
!*
FLST,2,12,3
FITEM,2,1
FITEM,2,2
FITEM,2,12
FITEM,2,11
FITEM,2,10
FITEM,2,9
FITEM,2,8
FITEM,2,7
```

```
FITEM,2,6
FITEM,2,5
FITEM,2,4
FITEM,2,3
A,P51X
FLST,2,7,3
FITEM,2,3
FITEM,2,4
FITEM,2,13
FITEM,2,37
FITEM,2,41
FITEM,2,62
FITEM,2,61
A,P51X
FLST,2,5,3
FITEM,2,4
FITEM,2,5
FITEM,2,15
FITEM,2,14
FITEM,2,13
A,P51X
FLST,2,4,3
FITEM,2,5
FITEM,2,6
FITEM,2,16
FITEM,2,15
A,P51X
FLST,2,4,3
FITEM,2,6
```

```
FITEM,2,7
FITEM,2,17
FITEM,2,16
A,P51X
FLST,2,4,3
FITEM,2,7
FITEM,2,8
FITEM,2,18
FITEM,2,17
A,P51X
FLST,2,4,3
FITEM,2,8
FITEM,2,9
FITEM,2,19
FITEM,2,18
A,P51X
FLST,2,4,3
FITEM,2,9
FITEM,2,10
FITEM,2,20
FITEM,2,19
A,P51X
FLST,2,5,3
FITEM,2,10
FITEM,2,11
FITEM,2,22
FITEM,2,21
FITEM,2,20
A,P51X
```

```
FLST,2,7,3
FITEM,2,11
FITEM,2,12
FITEM,2,68
FITEM,2,67
FITEM,2,44
FITEM,2,40
FITEM,2,22
A,P51X
FLST,2,5,3
FITEM,2,13
FITEM,2,14
FITEM,2,23
FITEM,2,38
FITEM,2,37
A,P51X
FLST,2,8,3
FITEM,2,23
FITEM,2,24
FITEM,2,29
FITEM,2,49
FITEM,2,64
FITEM,2,63
FITEM,2,42
FITEM,2,38
A,P51X
FLST,2,14,3
FITEM,2,14
FITEM,2,15
FITEM,2,16
FITEM,2,17
FITEM,2,18
FITEM,2,19
FITEM,2,20
FITEM,2,21
FITEM,2,28
FITEM,2,27
FITEM,2,26
FITEM,2,25
FITEM,2,24
FITEM,2,23
A,P51X
FLST,2,8,3
FITEM,2,25
FITEM,2,26
FITEM,2,33
FITEM,2,55
FITEM,2,74
FITEM,2,73
FITEM,2,54
FITEM,2,32
A,P51X
FLST,2,8,3
FITEM,2,27
FITEM,2,28
FITEM,2,39
FITEM,2,43
FITEM,2,66
```

```
FITEM,2,65
FITEM,2,60
FITEM,2,36
A,P51X
FLST,2,5,3
FITEM,2,21
FITEM,2,22
FITEM,2,40
FITEM,2,39
FITEM,2,28
A,P51X
FLST,2,4,3
FITEM,2,37
FITEM,2,38
FITEM,2,42
FITEM,2,41
A,P51X
FLST,2,4,3
FITEM,2,39
FITEM,2,40
FITEM,2,44
FITEM,2,43
A,P51X
FLST,2,4,3
FITEM,2,41
FITEM,2,42
FITEM,2,63
FITEM,2,62
A,P51X
FLST,2,4,3
FITEM,2,43
FITEM,2,44
FITEM,2,67
FITEM,2,66
A,P51X
SAVE
FLST,2,6,3
FITEM,2,61
FITEM,2,62
FITEM,2,63
FITEM,2,64
FITEM,2,70
FITEM,2,69
A,P51X
FLST,2,6,3
FITEM,2,65
FITEM,2,66
FITEM,2,67
FITEM,2,68
FITEM,2,78
FITEM,2,77
A,P51X
FLST,2,18,3
FITEM,2,69
FITEM,2,70
FITEM,2,71
FITEM,2,72
FITEM,2,73
```

```
FITEM,2,74
FITEM,2,75
FITEM,2,76
FITEM,2,77
FITEM,2,78
FITEM,2,86
FITEM,2,85
FITEM,2,84
FITEM,2,83
FITEM,2,82
FITEM,2,81
FITEM,2,80
FITEM,2,79
A,P51X
FLST,2,4,3
FITEM,2,79
FITEM,2,80
FITEM,2,88
FITEM,2,87
A,P51X
FLST,2,4,3
FITEM,2,80
FITEM,2,81
FITEM,2,89
FITEM,2,88
A,P51X
FLST,2,4,3
FITEM,2,81
FITEM,2,82
FITEM,2,90
FITEM,2,89
A,P51X
FLST,2,4,3
FITEM,2,82
FITEM,2,83
FITEM,2,91
FITEM,2,90
A,P51X
FLST,2,4,3
FITEM,2,83
FITEM,2,84
FITEM,2,92
FITEM,2,91
A,P51X
FLST,2,4,3
FITEM,2,84
FITEM,2,85
FITEM,2,93
FITEM,2,92
A,P51X
FLST,2,4,3
FITEM,2,85
FITEM,2,86
FITEM,2,94
FITEM,2,93
A,P51X
SAVE
FLST,2,10,3
```

```
FITEM,2,87
FITEM,2,88
FITEM,2,89
FITEM,2,90
FITEM,2,91
FITEM,2,92
FITEM,2,93
FITEM,2,94
FITEM,2,96
FITEM,2,95
A,P51X
SAVE
!*
!* glue all areas
!*
FLST,2,31,5,ORDE,2
FITEM,2,1
FITEM,2,-31
AGLUE,P51X
!*
/PNUM,KP,0
/PNUM,LINE,0
/PNUM,AREA,1
/PNUM,VOLU,0
/PNUM,NODE,0
/PNUM,TABN,0
/PNUM,SVAL,0
/NUMBER,0
!*
/PNUM,ELEM,0
/REPLOT
!*
APLOT
FLST,5,14,5,ORDE,10
FITEM,5,1
FITEM,5,-2
FITEM,5,6
FITEM,5,10
FITEM,5,12
FITEM,5,-15
FITEM,5,21
FITEM,5,-24
FITEM,5,30
FITEM,5,-31
ASEL,S , , , P51X
/REPLOT
FLST,5,14,5,ORDE,10
FITEM,5,1
FITEM,5,-2
FITEM,5,6
FITEM,5,10
FITEM,5,12
FITEM,5,-15
FITEM,5,21
FITEM,5,-24
FITEM,5,30
FITEM,5,-31
CM,_Y,AREA
```

```
ASEL, , , ,P51X
CM,_Y1,AREA
CMSEL,S,_Y
!*
CMSEL,S,_Y1
AATT,     1, ,   1,     0
CMSEL,S,_Y
CMDELE,_Y
CMDELE,_Y1
!*
ALLSEL,ALL
FLST,5,11,5,ORDE,11
FITEM,5,3
FITEM,5,5
FITEM,5,7
FITEM,5,9
FITEM,5,11
 FITEM,5,16
FITEM,5,19
FITEM,5,-20
FITEM,5,25
FITEM,5,27
FITEM,5,29
ASEL,S , , , P51X
FLST,5,11,5,ORDE,11
FITEM,5,3
FITEM,5,5
FITEM,5,7
FITEM,5,9
FITEM,5,11
FITEM,5,16
FITEM,5,19
FITEM,5,-20
FITEM,5,25
FITEM,5,27
FITEM,5,29
CM,_Y,AREA
ASEL, , , ,P51X
CM,_Y1,AREA
CMSEL,S,_Y
!*
CMSEL,S,_Y1
AATT,     2, ,   1,     0
CMSEL,S,_Y
CMDELE,_Y
CMDELE,_Y1
!*
ALLSEL,ALL
FLST,5,6,5,ORDE,6
FITEM,5,4
FITEM,5,8
FITEM,5,17
FITEM,5,-18
FITEM,5,26
FITEM,5,28
ASEL,S , , , P51X
FLST,5,6,5,ORDE,6
FITEM,5,4
```

```
FITEM,5,8
FITEM,5,17
FITEM,5,-18
FITEM,5,26
FITEM,5,28
CM,_Y,AREA
ASEL, , , ,P51X
CM,_Y1,AREA
CMSEL,S,_Y
!*
CMSEL,S,_Y1
AATT,     3, ,   1,     0
CMSEL,S,_Y
CMDELE,_Y
CMDELE,_Y1
!*
ALLSEL,ALL
SAVE
!*
!* mesh the areas
!*
ALLSEL,ALL
APLOT
SMRT,10
FLST,5,31,5,ORDE,2
FITEM,5,1
FITEM,5,-31
CM,_Y,AREA
ASEL, , , ,P51X
CM,_Y1,AREA
CHKMSH,'AREA'
CMSEL,S,_Y
!*
AMESH,_Y1
!*
CMDELE,_Y
CMDELE,_Y1
CMDELE,_Y2
!*
/PNUM,KP,0
/PNUM,LINE,0
/PNUM,AREA,0
/PNUM,VOLU,0
/PNUM,NODE,0
/PNUM,TABN,0
/PNUM,SVAL,0
/NUMBER,0
!*
/PNUM, MAT,1
/REPLOT
ALLSEL,ALL
!* select nodes on the outer sufaces
NSEL, S, LOC,X,0.,0.0001
NSEL,A, LOC,X,0.4589,0.459
NSEL,A, LOC,Y,0.,0.0001
NSEL,A, LOC,Y,0.2809,0.281
!* define element for outer surface
!*
```

```
TYPE,   2
MAT,        1
NPLOT
esurf
!*
!* create space node
N, 50000, 0.3, 0.5, 0, , , ,
!* select the nodes and elements that
!* make up the radiation surfaces
ESEL,S,TYPE,, 2
NSLE,R
NSEL, S, LOC,X, 0., 0.0001
NSEL,A, LOC,X, 0.4589, 0.459
NSEL,A, LOC,Y,0.,0.0001
NSEL,A, LOC,Y,0.2809,0.281
ESLN,R
NSEL,a,node,,50000
FINISH
!* define radiation matrix
/AUX12
EMIS,1,0.8,
STEF,5.67e-08,
GEOM,1,0,
SPACE,50000,
!*
VTYPE,0,20,
MPRINT,0
WRITE,rad
!*
ALLSEL,ALL
FINISH
/PREP7
!*
!*
TYPE, 3
MAT,        1
REAL,
ESYS,        0
SECNUM,
TSHAP,LINE
!*
SE,rad, , ,0.0001,
ESEL,S,TYPE,, 2
EDELE,ALL
SAVE
!* Define effective heat transfer coeficients for
!* post-fire (vert-20,horiz-up-25, horiz-down-35)
MPTEMP
M PTEMP,1,338.71,366.48,394.26,422.04,449.82,477.59,
M PTEMP,7,588.71,755.37,1019.26,
MPDATA,HF,20,1,4.68,5.61,6.18,6.60,6.90,7.13,
MPDATA, HF, 20, 7, 7.64, 8.00, 8.25,
MPDATA,HF,25,1,5.19,6.34,7.05,7.55,7.92,8.18,
MPDATA,HF,25,7,8.74,9.07, 9.17,
MPDATA,HF,35,1,2.34,2.74,2.99,3.17,3.30,3.41,
MPDATA, HF, 35, 7, 3.67, 3.89, 4.09,
MPLIST
SAVE
```

```
FINISH

/SOLU

!* setup convection coefficients for fire case

ALLSEL,ALL

NSEL,S,LOC,X, 0., 0.0001

NSEL,A,LOC,X, 0.4589, 0.459

NSEL,A,LOC,Y,0.,0.0001

NSEL,A,LOC,Y,0.2809,0.281

SF,ALL,CONV,19.8,1073

NSEL,ALL

!*****************************************************************

******

!* Test Heat Generation modelling wood burning

ASEL,S,MAT,,3

ESLA,S

/GO

!*

*DIM,burning,TABLE,5,1,0,TIME

!*

BFE,ALL,HGEN, , %burning%

!*

!*********BFA,ALL,HGEN, %burning%

*SET,BURNING(1,0,1), 0.0

*SET,BURNING(2,0,1), 0.1

*SET,BURNING(3,0,1), 0.2

*SET,BURNING(4,0,1), 552.2

*SET,BURNING(5,0,1), 552.3

*SET,BURNING(1,1,1), 0.0

*SET,BURNING(2,1,1), 0.0

*SET,BURNING(3,1,1), 7.63e6

*SET,BURNING(4,1,1), 7.63e6

*SET,BURNING(5,1,1), 0.0

ALLSEL,ALL

SAVE

!*****************************************************************

******

D,50000,TEMP, 1073

!*****************************************************************

******

TUNIF,375,!REVISED FOR NEW NCT

NUMBER (IC OUTER SHELL)

!*****************************************************************

******

SAVE

!*

!* set up run parameters for fire case

!*

ANTYPE,4

!*

TRNOPT,FULL

LUMPM,0

!*

TIME,1800

AUTOTS,-1

DELTIM,0.1,0.1,600,1

KBC,1

!*

TSRES,ERASE
```

```
!*
OUTRES,ALL,ALL,
!*
LSWRITE,2,
!*
!* change boundary conditions for post fire case
!*
ALLSEL,ALL
NSEL,S, LOC,X,0.000,0.0001
NSEL,A, LOC,X, 0.4589, 0.459
SF,ALL,CONV,-20, 311
ALLSEL,ALL
NSEL,S, LOC,Y,0.0,0.0001
SF,ALL,CONV,-35, 311
ALLSEL,ALL
NSEL,S, LOC,Y,0.2809,0.281
SF,ALL,CONV,-25, 311
ALLSEL,ALL
D,50000,TEMP,311
!*
!* apply solar heat flux
!*
ALLSEL,ALL
!* select vertical lines and nodes on the left side
nsel,s,loc,x,0
!FLST,5,4,4,ORDE,4
!FITEM,5,18
!FITEM,5,76
!FITEM,5,94
!FITEM,5,97
!LSEL,S , , , P51X
!NSLL,S,1
! FLST,2,97,1,ORDE,9
!FITEM,2,12
!FITEM,2,17
!FITEM,2,56
!FITEM,2,70
!FITEM,2,72
!FITEM,2,447
!FITEM,2,-521
!FITEM,2,2039
!FITEM,2,-2055
/GO
!*
F,all,HEAT,0.69

ALLSEL,ALL
!* select lines and nodes on the right side
nsel,s,loc,x,.459,.460
!FLST,5,4,4,ORDE,4
!FITEM,5,35
!FITEM,5,77
!FITEM,5,86
!FITEM,5,108
!LSEL,S , , , P51X
!NSLL,S,1
!FLST,2,97,1,ORDE,9
!FITEM,2,3
```

```
!FITEM,2,27
!FITEM,2,57
!FITEM,2,63
!FITEM,2,78
!FITEM,2,795
!FITEM,2,-869
!FITEM,2,2240
!FITEM,2,-2256
!/GO
!*
F,all,HEAT,0.69

!* select nodes on upper surface
ALLSEL,ALL
NSEL,S, LOC,Y,0.2809,0.281
!FLST,2,155,1,ORDE,4
!FITEM,2,79
!FITEM,2,-80
!FITEM,2,2257
!FITEM,2,-2409
!/GO
!*
F,all,HEAT,2.88
ALLSEL,ALL
!* set up run parameters for post fire
TIME,14400 !was 9000
AUTOTS,-1
DELTIM,0.5,0.1,2000,1
KBC,1
!*
TSRE S,ERASE
!*
TINTP,0.005, , ,-1,0.5,-1
!*
OUTRES,ALL,ALL,
TIME,45000
DELTIM,100,10,2000,1
LSWRITE,3,
SAVE
FINISH
/SOLU
/STATUS,SOLU
LSSOLVE,2,3,1
FINISH
SAVE
/POST26
!*
!* plot temperature evolution at specified nodes
!*
!*
!* inner wall, top right corner
NSOL,2,58,TEMP, ,inn_wtr
!*
!*
!* inner wall, bottom mid position
NSOL,3,1185,TEMP, ,inn_wbm
!*
!*
```

```
!* inner wall, top mid position
NSOL,4,1720,TEMP, ,inn_wtm
!*
!*
!* outer wall, top mid position
NSOL,5,2333,TEMP, ,out_wtm
!*
!*
PLVAR,2,3,4,5,,, , , , ,
PRVAR,2,3,4,5,,,
FINISH
!* plot isothermes at certain moments in time
/POST1
SET,LIST,2
SET, , , 1 , , , , 17,
/EFACE,1
!*
PLNSOL,TEMP, ,0,
FINISH
/POST1
SET, , , 1 , , , , 18,
/EFACE,1
!*
PLNSOL,TEMP, ,0,
SET, , , 1 , , , , 20,
/EFACE,1
!*
PLNSOL,TEMP, ,0,
SET, , , 1 , , , , 22,
/EFACE,1
!*
PLNSOL,TEMP, ,0,
SET, , , 1 , , , , 30,
/EFACE,1
!*
PLNSOL,TEMP, ,0,
SET, , , 1 , , , , 43,
/EFACE,1
!*
PLNSOL,TEMP, ,0,
SET,PREVIOUS
FINISH


! ********************************NEW
allsel
/post1


Tmax=0
TimeMAX=0
nmax=0


nsel ,s,loc, x, 0.0525, .4065,
nsel, r,loc,y,0.0525,.2285,
!nsel, u, loc,y,0.053, .2280


nplot
*GET, ncount, NODE, 0, count
cm,icnodes,node
```

```
set, 1,1


*do,t,1,46
tmaxn=0
cmsel,s,icnodes


*do, i,1, ncount
nodei=node(0,0,0)
*get,tempi,node, nodei,temp
*if,tempi, gt,tmaxn,then
tmaxn=tempi
nmaxn=nodei
*endif
nsel,u ,,, nodei
*enddo
*if,tmaxn, gt,tmax,then
tmax=tmaxn
nmax=nmaxn
*GET,timemax, ACTIVE, 0, set, time
*endif
set,next
*enddo


tmax=tmax
nmax=nmax
timemax=timemax


allsel
/show,term
/post1,
! Reverse Video
/rgb, index,100,100,100,0
/rgb, index,80,80,80,13
/rgb, index,60,60,60,14
/rgb,index,0,0,0,15
set, 1,17
plnsol,temp
/image, save,fig3-4(1800),wmf
set,2,1
/replot
/image, save,fig3-5(1900),wmf
set,2,5
/replot
/image, save,fig3-6(3268),wmf
set,last
/replot
/image, save,fig3-7(45000),wmf
!********************************NEW
! /EXIT,ALL
```

3.6.3 NCT Transient Analysis

The transient analysis uses a one dimensional model of the vertical face of the packaging (thinner part of the packaging) as described in the figure below:

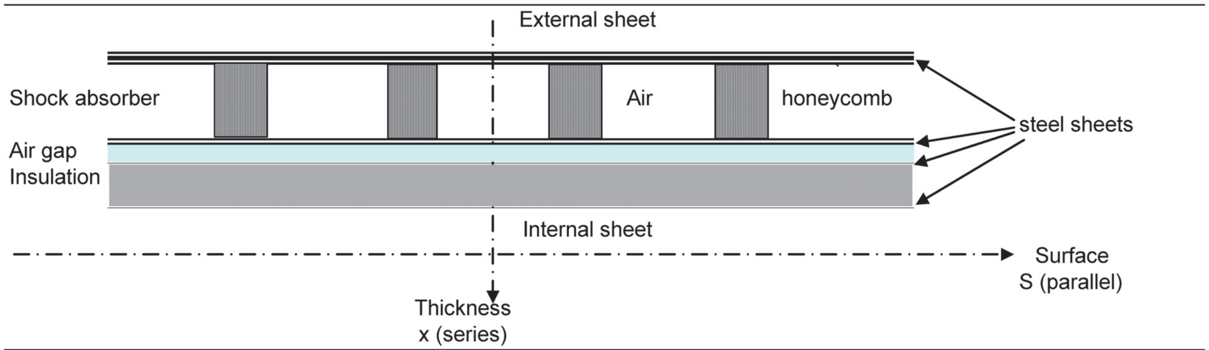

Figure 3-8 Vertical Face Model

The heat flux is set as a sine wave function:

$Q = \pi/2 \times 800 \sin(\omega\ \theta)$ $\quad\quad 0 < (\omega\ \theta) < \pi$

$Q = 0$ $\quad\quad \pi < (\omega\ \theta) < 2\pi$

With:

Q = heat energy in g-cal/cm^2

ω = $2\pi / 24$ pulsation

θ = time in hour

Note that the peak value of $(\pi/2 \times 800)$ complies with 10 CFR 71.71(c)(1), conservatively assuming the highest value of 800 g-cal/cm^2 for the insolation.

$$\int_0^{24\text{hours}} Q\, d\theta = 800 \text{ g-cal/cm}^2$$

Assuming that at each time step, the external surface of the package achieves steady state conditions, the energy balance between the solar heat load, and the convection and radiation exchanges (see Section 3.4.1.1), results time dependant solution for the external surface temperature.

The result is plotted on the Figure 3-9 (blue curve) and is close to a sine wave function. Indeed, when calculating the energy balance equation, it appears that the convention term represents 65%

of the exchange, and the radiation term 35%. As the convection term is linearly proportional to the external temperature, this curve is nearly proportional to the solar heat load.

Assume that the external temperature is a sine function with respect to time as follows (and as plotted on Figure 3-9):

$$Ts = T_{avg} + T^{+} \sin(\omega\ \theta)$$

With:

$T_{avg} = 420$ K (maximum value of the blue curve)

$T^{+} = (420\text{-}311) = 109$ K

The system is thus modeled as a one dimensional model of conduction, with a sinusoidal wave temperature on the external surface as a boundary condition.

Using equation 4-22 of the "Handbook of Heat Transfer," [Ref. 7], the heat equation through a layer of material leads to a temperature of:

$$T(x,\theta) = T_{avg} + T^{+} \exp(-L\ x/d) \sin[L(2\ L\ Fo - x/d)]$$

Using the reference's notation, it becomes:

$$T(x,\theta) = T_{avg} + T^{+} \exp[-(\omega/2\alpha)^{1/2}\ x] \sin[\omega\ \theta - (\omega/2\alpha)^{1/2} x]$$

With:

$\alpha = K / \rho\ C$ = thermal diffusivity,

K = conductivity if material,

ρ = density of material,

C = specific heat of the material,

x = thickness thru the material.

Through each layer of material "i" in the RAJ-II packaging, the temperature of the external surface is so decreased by a factor η and lagged by a factor ϕ:

$$\eta_i = \exp[-(\omega/2\alpha_i)^{1/2}\ x_i]$$
$$\phi_i = (\omega/2\alpha_i)^{1/2} x_i$$

Table 3-6 summarizes the material properties for each component layer through the thickness of the model.

Equivalent Properties of Material

The thermal properties (K, ρ, C) of a material equivalent to materials of a system are following the rules:

Materials in series $K = \dfrac{e_T}{\sum_i \dfrac{e_i}{K_i}}$ Materials in parallel $K = \dfrac{1}{S_T}\sum_i S_i K_i$

Materials in series $\rho\, C = \dfrac{\sum_i \rho_i C_i e_i}{e_T}$ Materials in parallel $\rho\, C = \dfrac{\sum_i \rho_i C_i S_i}{S_T}$

The maximum temperature of the cavity surface of the packaging resulting from solving the one dimensional model occurs at ten hours into the cycle and is equal to 350 K. The maximum temperature on the outer surface of the inner container occurs at 8 hours and is equal to 375K. Temperatures are summarized on Figure 3-7.

Table 3-6 Material Properties

Component	Material	Thickness x (m)	Surface S (m)	Conductivity K (W/m-K)	Density r (kg/m^3)	Specific heat C (J/kg-K)	Diffusivity a (m^2/s)
OC outer sheet	steel	0.004	–	15	7900	477	3.981E-06
Honeycomb①	paper	–	0.084①	0.13595	700①	1531①	3.932E-07
	air	–	0.916①	0.0267	1.177	1005	
Shock absorbers	honeycomb	0.108	0.64	0.0359	60	1522	1.737E-06
	air		3.186	0.0267	1.177	1005	
OC inner sheet	steel	0.001	–	15	7900	477	3.981E-06
Air gap	air	0.01	–	0.0267	1.177	1005	2.257E-05
IC outer sheet	steel	0.0015	–	15	7900	477	3.981E-06
IC insulation	Alumina	0.048	–	0.09	250	1046	3.442E-07
IC inner sheet	steel	0.001	–	15	7900	477	3.981E-06

Note:
① The honeycomb is assumed to be a combination of paper and air in a parallel system (see below). The proportion of paper and air is determined by the ratio of the densities:

Honeycomb density = 60 kg/m^3	
Paper density = 700 kg/m^3	8.4%
Air density = 1.177 kg/m^3	91.6%

Thermal properties of resin impregnated kraft paper (density, conductivity, specific heat) are conservatively assumed to correspond to that of ordinary paper. [Ref. 9]

Table 3-7 NCT Temperatures through the Package Thickness

Time (hour)	Surface temp sin wave Ts (K)	T thru OC Outer Shell	T thru Honeycomb and Air	T thru OC Inner Steel	T thru Air Gap	T thru IC Inner Shell	T thru Alumina Silicate
0	311	311	311	311	311	311	311
0.5	325	324	311	311	311	311	311
1	339	338	311	311	311	311	311
1.5	353	351	311	311	311	311	311
2	366	364	312	312	311	311	311
2.5	377	376	321	320	320	319	311
3	388	386	329	329	328	327	311
3.5	397	396	337	337	336	335	311
4	405	404	345	345	343	343	312
4.5	412	410	352	352	350	350	317
5	416	415	358	358	357	356	322
5.5	419	418	364	364	362	362	327
6	420	419	368	368	367	367	332
6.5	419	418	372	372	371	370	336
7	416	415	375	375	373	373	340
7.5	412	411	376	376	375	375	343
8	405	405	377	376	376	**375**	346
8.5	397	397	376	376	375	375	348
9	388	388	374	374	373	373	349
9.5	377	378	371	371	371	371	**350**
10	366	366	367	367	367	367	350
10.5	353	353	362	362	362	362	350
11	339	340	357	357	357	357	349
11.5	325	326	350	350	350	350	347
12	311	312	343	343	343	343	344
12.5	311	311	335	335	336	336	342
13	311	311	327	327	328	328	338
13.5	311	311	318	319	319	320	334
14	311	311	311	311	311	311	330
14.5	311	311	311	311	311	311	325
15	311	311	311	311	311	311	320
15.5	311	311	311	311	311	311	315
16	311	311	311	311	311	311	311
16.5	311	311	311	311	311	311	311

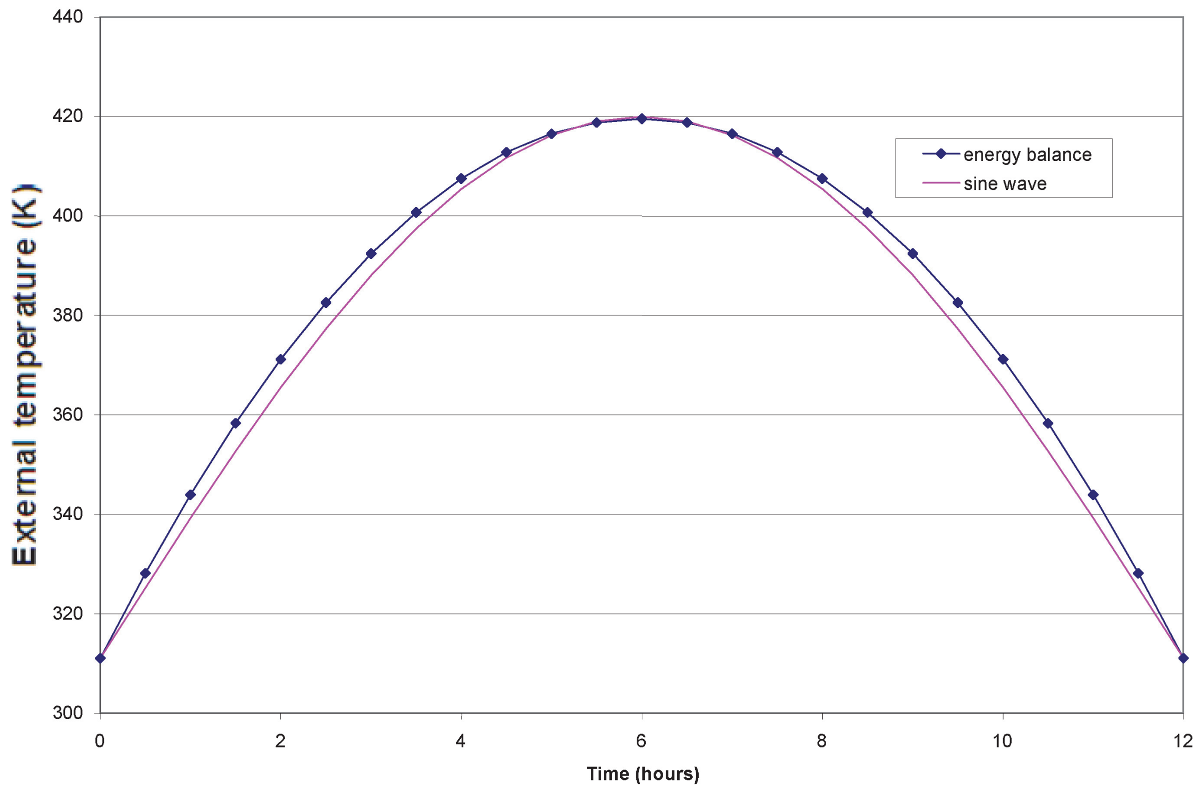

Figure 3-9 Comparison between Energy Equation Solution with a Sine Wave Equation

3.6.4 HAC 3D Transient Fire Analysis

A new 3-D finite element model is used to evaluate the performance of the RAJ-II when exposed to the NRC/IAEA regulatory fire conditions. The new model includes the complete geometry of the RAJ-II outer and inner containers. Boundary conditions include preheating of the container, combustion of the honeycomb paper, charring of the balsawood, charring of hemlock and the phase change of the polyethylene foam (both melting and vaporizing) within the inner container. Also included are the combustible materials located at the ends of the RAJ-II package.

3.6.4.1 Finite Element Model Description

The 3-D finite element model includes both transverse and longitudinal heat transfer and end effects, e.g., burning of Delrin® (polyacetal). In order to decrease computing time, geometric symmetries were used, requiring only one-half of the transverse cross section to be modeled. Similarly, only a portion of the overall length was required. The finite element model is shown in Figure 3-10.

All solid components within the RAJ-II container, as well as the air encased between the inner and outer container walls, are modeled with 81,216 nodes and 75,578 ANSYS Type 70 Thermal Solid elements.

The fuel assembly is modeled as a single monolith of appropriate envelope. The "law of mixtures" is used to estimate the material properties of this monolith.

For purposes of analysis, an equivalent volume of honeycomb shock absorber is calculated. This equivalent volume shock absorber is located at the centeroid of the summed volumes. The equivalent volume is 0.0848 m^3 with a centroid at 477 mm from the end of the internal package.

Radiation heat transfer between the outer container wall and the surrounding environment is modeled with a Matrix 50 element utilizing the 7,064 surface nodes on the outer container and a single environment node.

Radiation heat transfer between the outer container wall and the inner container wall is modeled using the radiosity solver capability of ANSYS. This method allows for symmetries to be used to reduce the overall model size, and superimposes thermal surface elements over existing solid elements. The parameters used in the modeling create 15,988 ANSYS Type 252 3D Thermal Surface elements and 8,404 nodes.

3.6.4.2 Assumptions

The following are the assumptions made for the 3-D model:

- Combustion is simulated by heat generation rates in the appropriate combusting elements.

- Paper honeycomb shock absorbers in the outer compartment are exposed to enough oxygen to fully combust. The combustion rate of the honeycomb is based on the rate of consumption of wood in free air modified by the flame front propagation rate in the model when loaded only by external sources. The resulting flame front propagation rate is 0.785 mm per minute. The resin impregnating the honeycomb is assumed to contribute negligibly to the heat of combustion of the honeycomb.

- Delrin® (polyacetal) guides in the outer compartment are exposed to enough oxygen to fully combust. The Delrin® material is assumed to burn for one hour with resulting flame front propagation rate of 0.582 mm per minute.

- The end compartment houseing the balsawood impact absorber are oxygen starved, resulting in pyrolysis (charring) of the balsa wood components only. Thermal experiments documented in Section 3.6.5 support this assumption.

- The volume between the inner container shell walls is oxygen starved, resulting in pyrolysis (charring) of the hemlock wood components only. The drop testing result support this assumption.

- If any polyethylene foam reaches ignition temperature, it is allowed to fully combust.

- The system is conservatively assumed to be to be essentially closed, with the only method of heat escaping the package being through the outer compartment wall radiating to the environment, or by the free convection cooling modeled on the outer wall, both of which are included in the model. No accounting was made for “chimney effects” where hot gasses are evacuated from the enclosure through any enclosure opening.

3.6.4.3 Boundary Conditions

For the initial state, the bulk temperature is fixed at 311 K (38°C). The surface heat flux for horizontal surfaces is 387.4 W/m^2, while the surface heat flux for vertical surfaces is 96.9 W/m^2, as shown in Table 3-8.

Combustion is simulated by applying heat generation rates in the appropriate combusting elements. Elements that were allowed to combust include the paper honeycomb, polyacetal inserts, and polyethylene foam.

For the transient state time t=0 was considered the start of the external fire. To simulate the external fire, the environment node was fixed at 1073 K (800°C) for thirty minutes. The paper honeycomb material was calculated to begin burning 30 seconds after the start of the external fire, continuing for 200 minutes. The polyacetal was calculated to begin burning 21 minutes after the start of the external fire, continuing for 60 minutes. After the end of the external fire, the bulk temperature was fixed at 311 K (38°C) and a temperature dependent heat transfer coefficient, as calculated in Section 3.5, was applied to the outer container. An external heat flux, representing solar radiation was applied to the package for 3.5 hours after the HAC fire, then removed for the duration of the transient analysis. The boundary conditions are summarized in Table 3-8.

Radiation heat transfer is modeled between the outer container wall and the surrounding environment and between the outer container wall and the inner container. The ANSYS program internally calculates view factors between components. Emissivity in all radiation cases is conservatively chosen as 1.

The convection heat transfer from the outer container wall to the environment is also modeled. The mixing effects of convection are included in the enclosure between the outer container wall and the inner container wall, equalizing temperature in all air elements.

3.6.4.4 Material Properties

The RAJ-II inner container is constructed primarily of Series 300 stainless steel, wood, and alumina silicate insulation. The void spaces within the inner container are filled with air at atmospheric pressure. The outer container is constructed of series 300 stainless steel, wood, and resin impregnated paper honeycomb. The thermal properties of the principal materials used in the thermal evaluations are presented in Table 3-1 and Table 3-2. Where necessary, the properties are presented as functions of temperature. Note that only properties for materials that constitute a significant heat transfer path are defined. A general view of the package is depicted in Figure 3-1. A sketch of the inner container transversal cross-section with the dimensions used in the calculation is presented in Figure 3-2.

For the Alumina Silicate, maximum values are specified because the maximum conductivity is the controlling parameter. This is because there is no decay heat in the payload and the only consideration is the material's ability to block of heat transfer to the fuel during the fire event.

The possible ignition of polyethylene foam is of primary concern due to the relatively great heat energy potentially released during combustion. Somewhat associated with this capacity are relatively high latent heats, both fusion and in particular vaporization. In order to better predict the behavior of the polyethylene foam, this latent heat was considered as part of the transient problem. The ANSYS FEA package allows this phase change, but requires the use of enthalpy change when doing so, rather than the typical simplification of using specific heat. There is no restriction on using enthalpy with one material and specific heat with a second material within the same analysis. Therefore, the RAJ-II material properties are specific heat based except for the polyethylene foam, which is enthalpy based as required to account for the phase changes. The material properties for the Fuel Assembly are defined in Table 3-10. The material properties for the RAJ-II packaging is presented in Table 3-11.

The heat of combustion for polyacetal is 20.05 MJ/kg [Ref. 19] and ignition temperature is 595 K (322°C) [Ref. 17] [Ref. 18]. The heat of combustion for the paper honeycomb is 17.6125 MJ/kg [Ref. 20] and ignition temperature is assumed the same as ignition for paper, 505 K (232°C). The heat of combustion for the polyethylene form is 44.6 kJ/g [Ref. 15], and ignition temperature is 573 K (300°C) [Ref. 16].

3.6.4.5 Evaluation

3.6.4.5.1 Steady State Analysis

The transport normal steady-state condition for ambient exposure was calculated by hand in Section 3.5. In the type of transient problem that exists with consideration of this Hypothetical Accident Condition, where steady state conditions exist before some upset condition, the analyst establishes initial conditions for the transient upset by judicious use of the load stepping capabilities of the ANSYS program. By doing so, an additional measure of accuracy in the transient case is ensured, as the initial temperature gradients are also necessarily calculated.

3.6.4.5.2 Transient Analysis

Heat generation rates in ANSYS are on a volumetric basis, and the program internally creates a heat energy transfer out of the nodes loaded. In the case of an interface where a single node is shared by elements of two substantially differing materials, the potential to artificially transfer too much heat energy across the interface to the material with the lower capacity exists. This leads to artificially high indications of temperature. As such, when combustion is simulated in this analysis, only the nodes and elements completely internal to the volume of interest are loaded with a heat generation rate. The total energy released by this generation is, however, calculated on the basis of the total volume.

The transient conditions for heat generation rates were calculated as follows:

The equivalent paper honeycomb volume is 0.0848 m^3. The heat of combustion of the paper honeycomb is 17.6125 MJ/kg. The density is 18 kg/m^3. The combustion rate of the honeycomb was assumed 200 minutes, based on the propagation speed of the ignition temperature front through the honeycomb paper in the model with only external loads. The heat generation rate (W/m^3) was then calculated from:

$(17.6125 \text{ MJ/kg})(18 \text{ kg/m}^3)(84.84 \times 10^{-3} \text{ m}^3) = 26.90 \text{ MJ}$ (total energy released)

$(26.90 \text{ MJ}) / (84.84 \times 10^{-3} \text{ m}^3) / (12000 \text{ s}) = 26.4 \times 10^3 \text{ W/m}^3$ (heat generation rate for paper honeycomb)

The Delrin® (polyacetal) insert volume is 2.2×10^{-3} m^3. The heat of combustion of polyacetal is 20.05 MJ/kg [Ref. 19]. The density of polyacetal is 1420 kg/m^3 [Ref. 17]. The combustion of the polyacetal was assumed to require one hour, based on the propagation of the temperature front with no internal heat generation of the polyacetal. The heat generation rate (W/m^3) was then calculated from:

$(20.05 \text{ MJ/kg})(1420 \text{ kg/m}^3)(1.1 \times 10^{-3} \text{m}^3) = 62.64 \text{ MJ}$ (total energy released)

$(62.64 \text{ MJ}) / (2.2 \times 10^{-3} \text{ m}^3) / (3600 \text{ s}) = 7.91 \times 10^6 \text{ W/m}^3$ (heat generation rate for polyacetal)

From Section 3.5, the polyethylene (EthaFoam®) heat of combustion of is 46.4 MJ/kg. The density of polyethylene is 35 kg/m^3. Based on data from hydrocarbon combustibles, a combustion rate of 0.5mm per minute for the polyethylene is used. For a typical element size of (0.01m × 0.01m × 0.01m) used in this analysis, the heat generation rate (W/m^3) is estimated from:

$(44.6 \text{ MJ/kg})(35 \text{ kg/m}^3)(1.0\text{x}10^{-6} \text{ m}^3) = 1561 \text{ J}$ (total energy released per element)

$(1561 \text{ J}) / (1.0\text{x}10^{-6} \text{ m}^3) / (1200 \text{ s}) = 1.3\text{x}10^6 \text{ W/m}^3$ (typical heat generation rate for polyethylene)

Beginning with the initial steady-state analysis followed by the fire transient, it was determined that the onset of combustion in the honeycomb paper occurs at approximately 30 seconds and the propagation of the ignition temperature front through the thickness of the honeycomb takes 200 minutes. Following the combustion progression of the paper honeycomb, it was determined that the Delrin® (polyacetal) ignited at approximately 21 minutes thus inputting addition heat into the inner container. However, no polyethylene reached ignition temperature over the span of the thermal transient. Therefore, and it is concluded that this material did not ignite or combust.

3.6.4.5.3 Results

Temperature time-history plots of the transient analysis are presented in Figure 3-11 and Figure 3-12. Figure 3-13 shows the post fire thermal response of the RAJ-II package at 4 hours and 9 minutes. For comparison Figure 3-14 shows the temperatures in the inner container at the 4 hour and 9 minute time. Figure 3-15 shows the temperatures in the inner container at 1 hour and 21 minutes, the time at which the maximum temperatures occur and at the end of the polyacetal fire.

Results of the transient analysis shows that the temperatures inside of the inner container reached the melting point of the polyethylene foam but not the combustion temperature. Therefore, only the melting and vaporization of the polyethylene foam contributes to the internal temperature of the fuel bundle. The analysis shows that the peak temperature of the polyethylene is ~225°C below the combustion temperature that occurs at 300°C and the fuel assembly is ~200°C.

Based on these results, the fuel cladding temperature is below the mechanical limit for the material and the pressure stresses are below the values previously presented in this safety analysis report. Therefore, the existing 2-D thermal analysis presented in Section 3.5 bounds the worst-case thermal conditions and no further analysis is required.

Table 3-8 Summary of Transient Boundary Conditions

	Time Regime	Environment*	Force Convection on External Surface	Heat Flux on External Surface	Internal Heat Generation
Initial Conditions		311 K (38° C)	4.8 W/m²-K	387.4 W/m²(h) 96.9 W/m² (v)	—
HAC	0–30 min	1073 K (800°C)	19.8 W/m²-K	—	(see specific items)
Immed. Post HAC	30 min–4 hr	311 K (38° C)	Table 3-3	966.27 W/m²(h) 260.64 W/m² (v)	(see specific items)
Post HAC	4 hr–18 hr	311 K (38° C)	Table 3-3	—	(see specific items)
Honeycomb Burn	30 sec– ~200min	HAC	HAC	HAC	18.762×10³ W/m³
Polyacetal Burn	~21 in– 1 hr 21 min	HAC	HAC	HAC	7.91×10³ W/m³

*Bulk temperatures for radiative and convective loads.

Table 3-9 Ignition Temperatures and Heat Generation Rates

Material	Ignition Temperature	Typical Heat Generation Rate
Paper Honeycomb	505 K (232°C)	26.4×10^3
Polyacetal	595 K (322°C)	7.91×10^6
Polyethylene	573 K (300°C)	1.30×10^6

Table 3-10 Fuel Assembly Material Properties

Material	Density (g/m^3)	Mass (kg)	Thermal Conductivity (W/m-K)	Specific Heat (J/kg-K)
Zirconium	6,550	105.5	—	335
UO_2	11,200	189.0	—	243
Fuel Assembly	$= (M_{Zr}+M_{UO2})$ / Cavity Volume = (105.5+189.0) / (140×140×4580) = (294.5) / (0.090) = 3280	—	16.8	$= [(CP_{UO2})\times(M_{UO2}) + (CP_{Zr})\times(M_{Zr})]/(M_{UO2} + M_{Zr})$ = [(243)×(189) + (335)×(105.5)]/(189 + 105.5) = 276

Table 3-11 RAJ-II Thermal Properties Summary

Material	Temperature (K)	Density (kg/m^3)	Thermal Conductivity (W/m-K)	Specific Heat (J/kg-K)	Reference
Stainless Steel	300	7900	15	477	Table 3-1
	400		17	525	
	500		18	539	
	600		20	557	
	800		23	582	
	1000		25	611	
Alumina Silicate	673	250	0.0697	1046	Table 3-1
	873		0.1046		
	1073		0.1512		
	1273		0.2092		
Wood	300	500	0.12	2800	Table 3-1
	500		0.12	2800	
Char	550		0.26	1588	[Ref. 12]
	600		0.26	1606	
	800		0.26	1678	
	1000		0.26	1750	
	1073		0.26	1776	
	1273		0.26	1848	
Polyacetal (Delrin)	(all)	1420	0.40	1465	[Ref. 17]
Paper Honeycomb	(all)	18	0.24	2800	
Air	300	1.177	0.0267	1005	Table 3-2
	400	0.883	0.0331	1009	
	500	0.706	0.0389	1017	
	600	0.589	0.0447	1038	
	800	0.442	0.0559	1089	
	1000	0.354	0.0672	1130	
	1073	0.354	0.0672	1130	
	1273	0.354	0.0672	1130	
Polyethylene Foam	200	35	0.33	11.1	Section 3.5
	250			14.6	[Ref. 13]
	300			18.3	[Ref. 14]
	350			22.3	
	400			26.5	
	410			27.4	
	415			(melt temp)	
	420			38.5	
	450			41.3	
	500			46.1	
	550			51.1	
	560			53.3	
	575			(vaporization temp)	
	590			186.5	
	600			188.7	
	620			190.9	
	660			195.4	

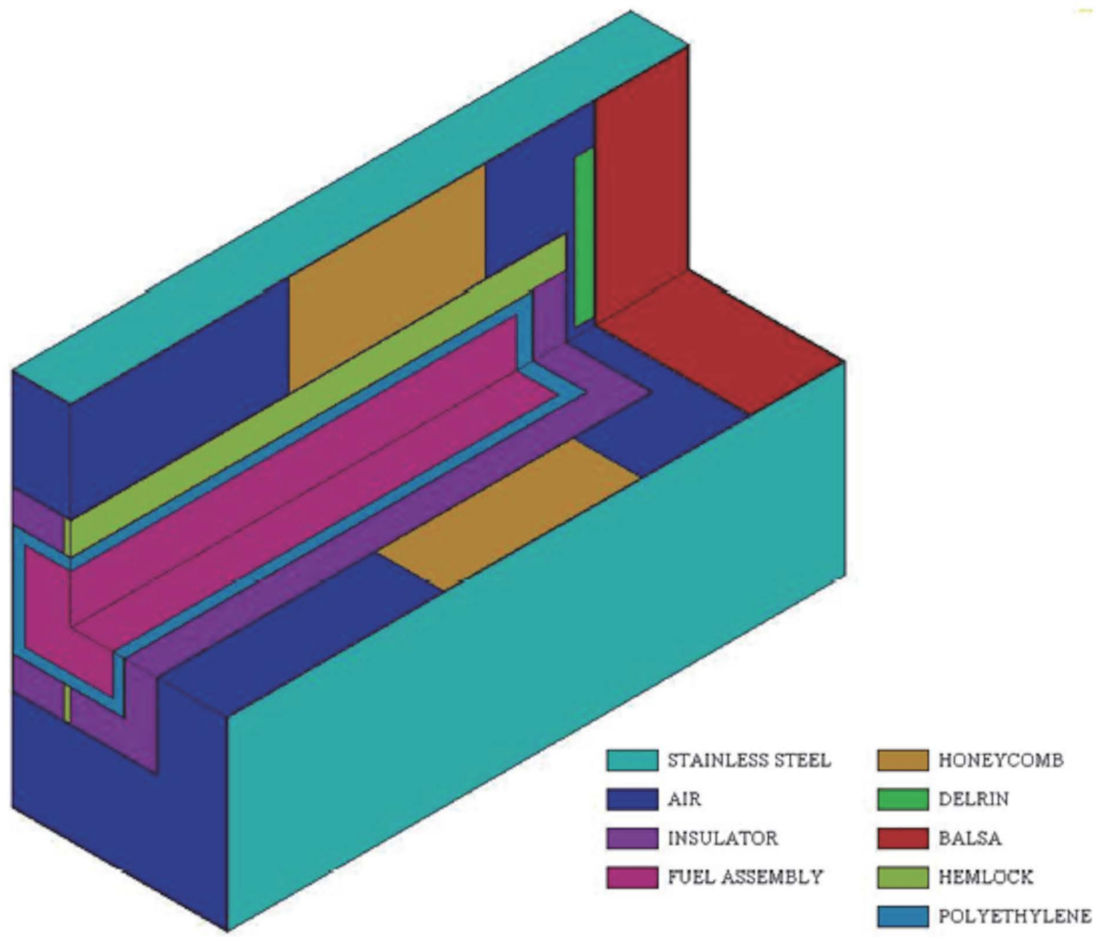

Figure 3-10 ANSYS Model with Cutaway

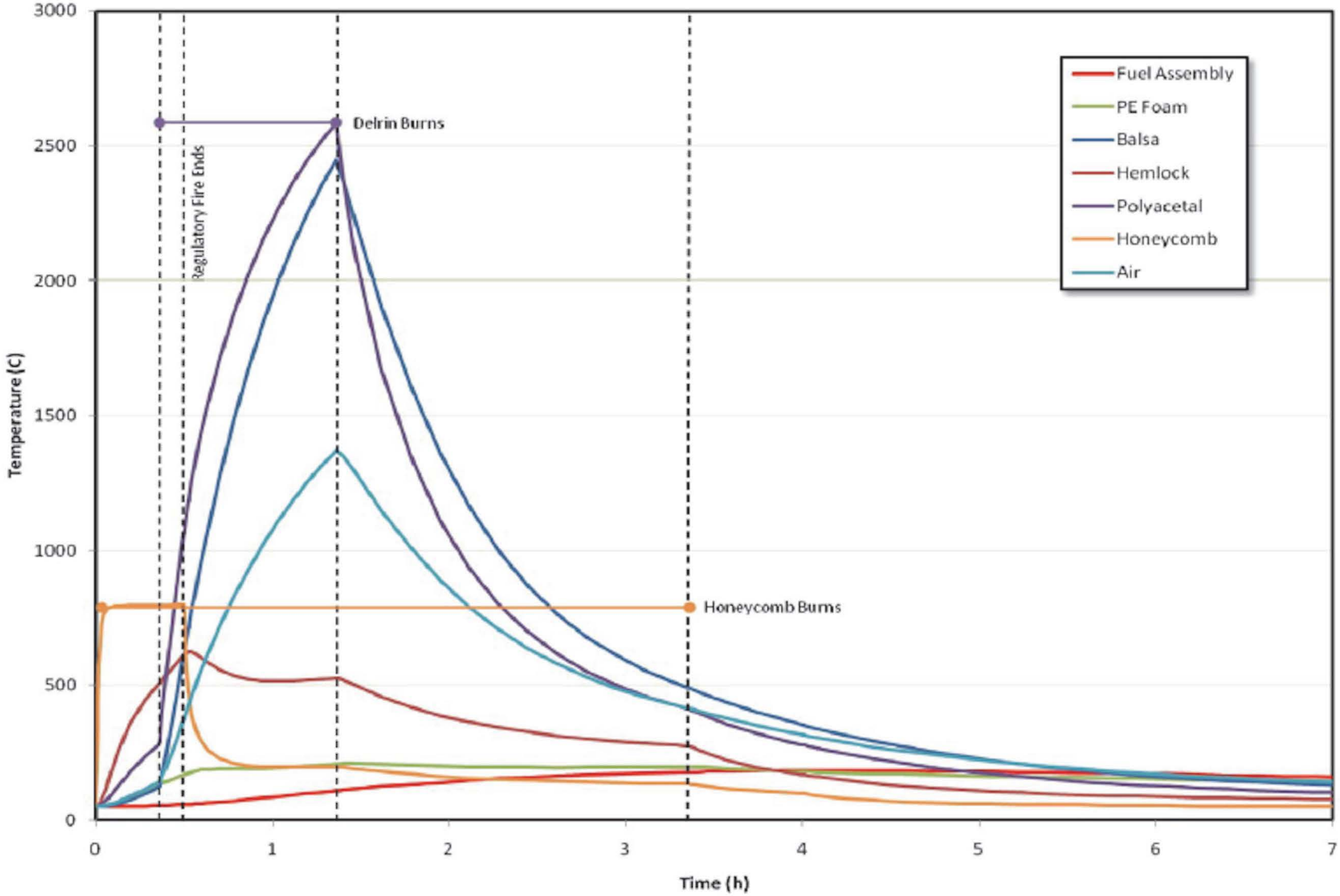

Figure 3-11 Fire Analysis Transient Response RAJ-II Inner and Outer Container Components

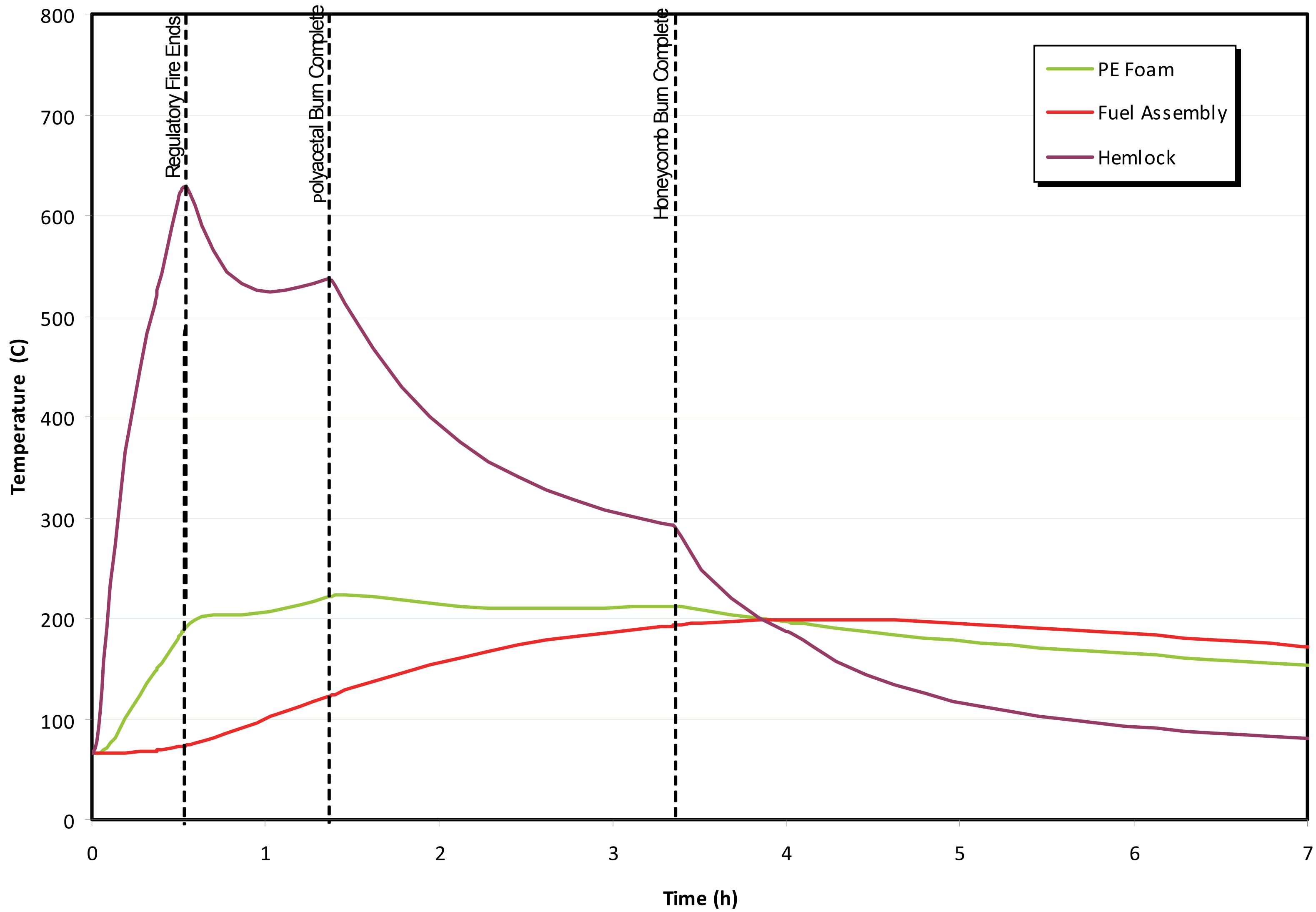

Figure 3-12 Fire Analysis Transient Response RAJ-II Inner Container Components

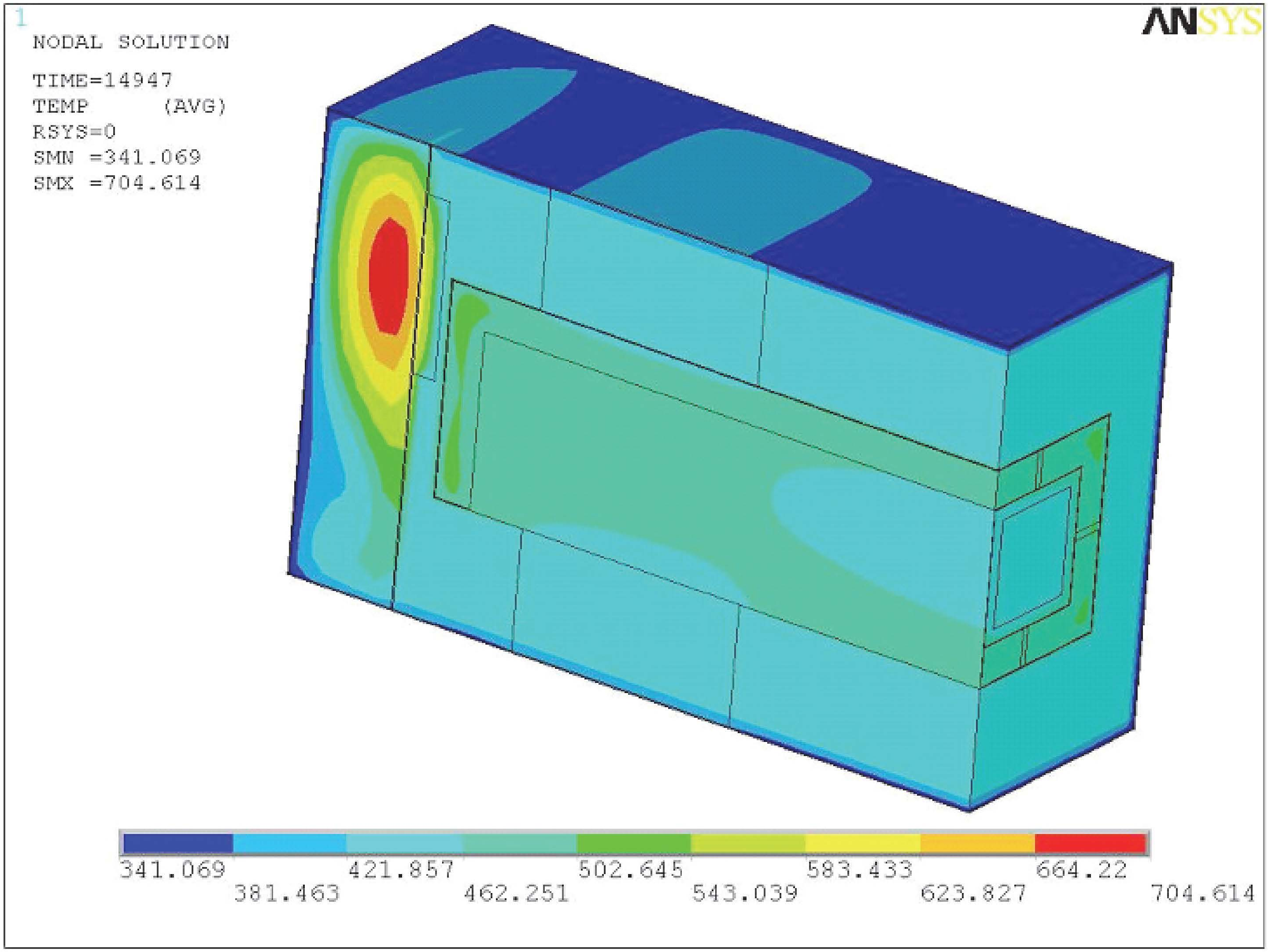

Figure 3-13 Package Temperature (°K) Distribution, t = 4 hr 9 min

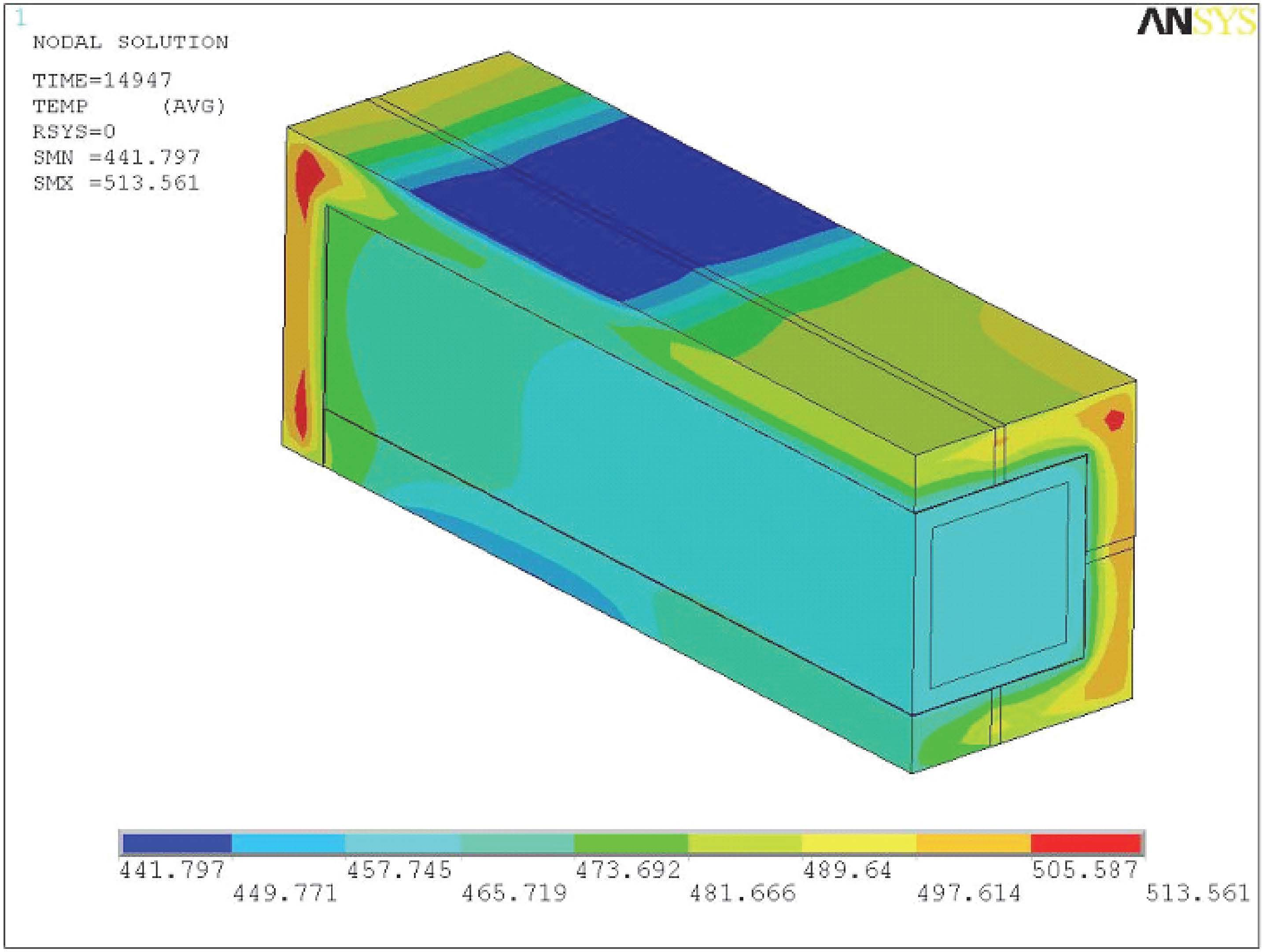

Figure 3-14 Inner Container Temperature (°K) Distribution, t = 4 hr 9 min

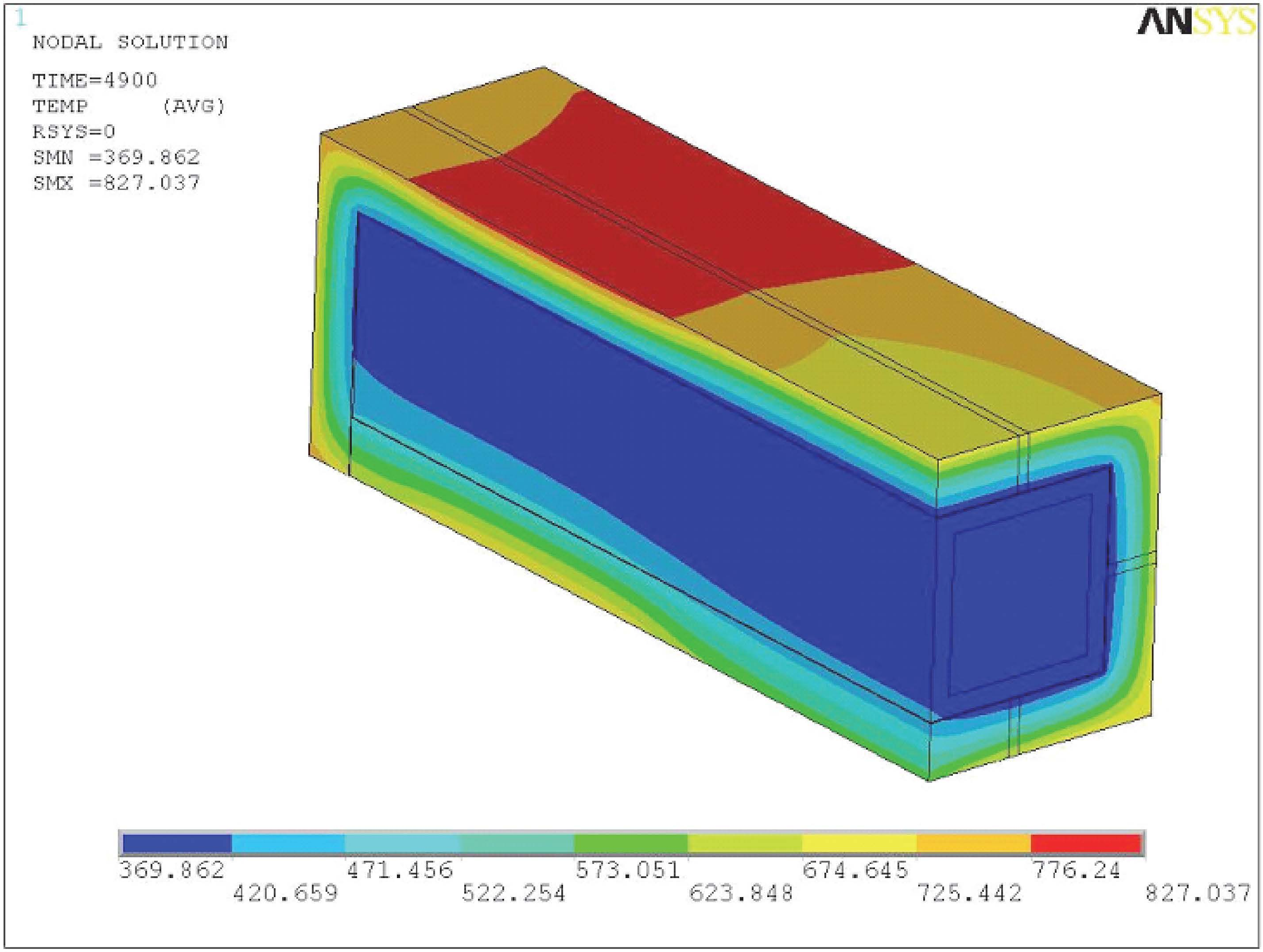

Figure 3-15 Inner Container Temperature (°K) Distribution, t = 1 hr 21 min

3.6.5 Thermal Test of Balsa Wood

Reference No.AT793016
P.No.NNH21141

Attention to:
Transnuclear,LTD.
Engineering Dept.

TEST REPORT

Thermal Test of Balsa Wood

(Translation)

April 2009

KOBELCO RESEARCH INSTITUTE, INC.
Applied Chemistry Division
Technology Dept.

1-5-5 Takatsukadai, Nishi-ku Kobe, 651-2271 JAPAN
TEL: 81-78-992-5193
FAX: 81-78-993-4403

Approved	Prepared

Thermal test of Balsa Wood

Kobelco Research Institute, Inc.
Applied Chemistry Division
Technology Dept.

1. Subject: Thermal test of Balsa Wood

2. Purpose
   In order to demonstrate the behavior of Balsa wood under thermal test conditions.

3. Specimen
   Balsa wood covered by stainless steel plate (an extremity is opened)
   2 lateral surfaces of stainless steel are cut off as the following figures.

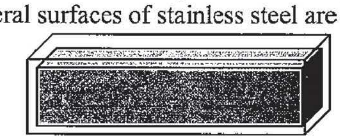

Dimensions: 58 x 58 x 150 mm

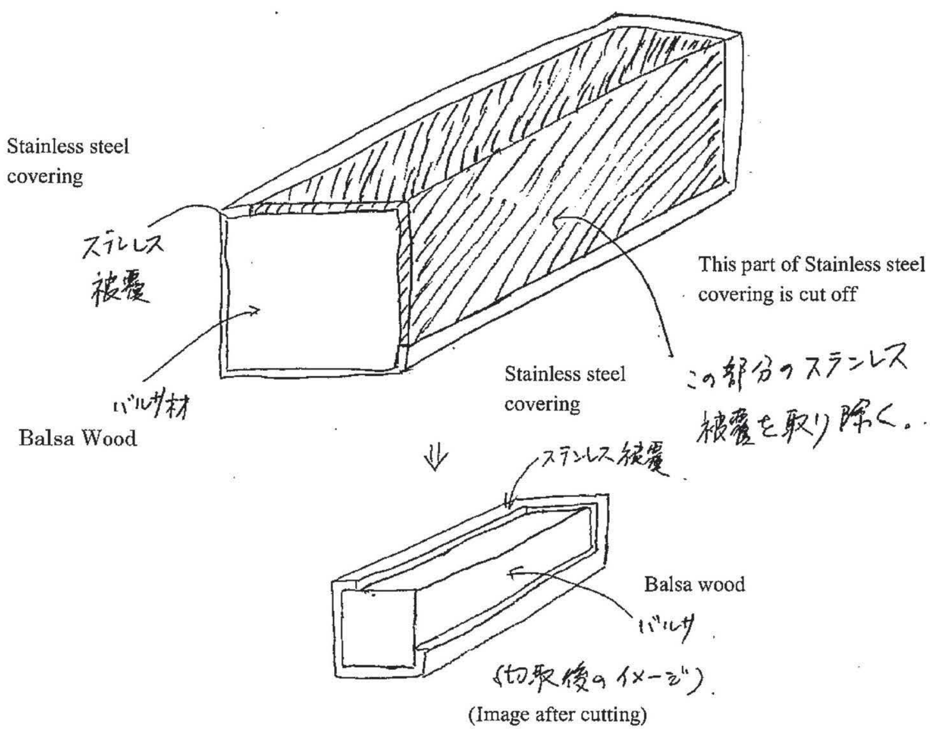

Fig. 1 Procedure of cutting for stainless steel covering

4. Test method
   An oven (Dimensions: 800x800x800 mm) is used in Kakogawa plant.
   Ambient temperature in the oven is set at 800 °C.
   After specimen is loaded in the oven and the ambient temperature is reached at 800 °C, thermal test is started and maintained during 30minutes. And then, specimen is

taken out of the oven, and is left for cooling.
After cooling, the specimen is observed.

①Heating: Ambient temperature in the oven is set at 800 °C. The specimen is heated during 30 minutes after the temperature in the oven reach at 800 °C.
Temperatures near the specimen and itself are measured.
Oxygen rate in the oven is measured continuously.

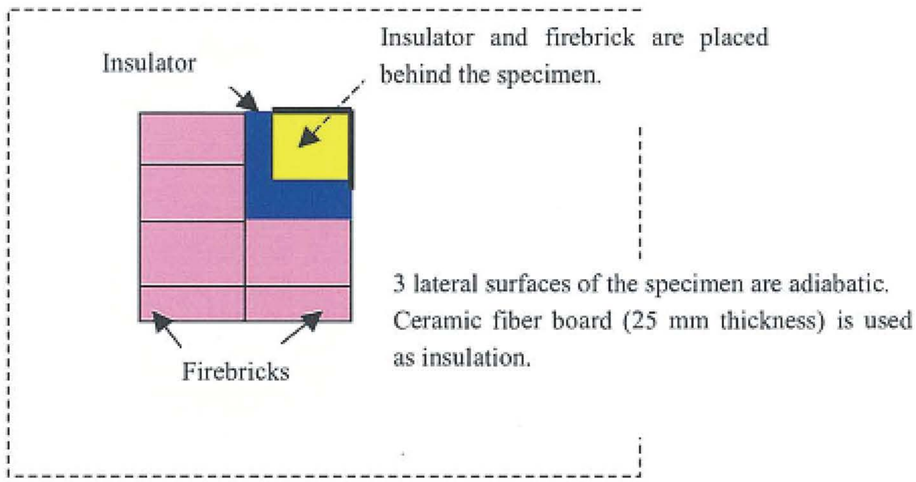

(Oven)

②Cooling: The specimen is cooled outside the oven.
Measurement of specimen temperature during cooling

③Observation: Balsa wood is taken out of stainless steel covering, and is observed

5. Date of testing

13:00 to 16:00 of March 19, 2009

6. Results

Just after the specimen is loaded in the oven, it looks combustion. Oxygen rate decrease down to 17% temporarily.
And then, oxygen rate recover to around 20%.
After the specimen is hold under 800 °C during 30 minutes, it is taken out the oven, cooled, and observed.
As the results, the Balsa wood is carbonized, but almost its shape is maintained. All Balsa wood is not burned to ashes.
Refer to the attachment-1 as the detail of the test results.

<Attachment-1>

Thermal Test of Balsa Wood

1. Subject: Thermal test of Balsa Wood
2. Purpose: In order to demonstrate the behavior of Balsa wood under thermal test conditions
3. Specimen:
   Balsa wood covered by stainless steel plate (an extremity is opened)
   2 lateral surfaces of stainless steel are cut off as the following figures.

Specimen (58 × 58 × 150)

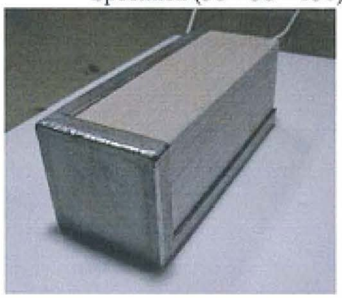

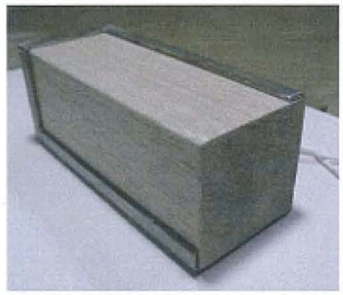

4. Test Method
   An oven (Dimensions: 800x800x800 mm) is used in Kakogawa plant.
   Ambient temperature in the oven is set at 800 °C.
   After specimen is loaded in the oven and the ambient temperature is reached at 800 °C, thermal test is started and maintained during 30minutes. And then, specimen is taken out of the oven, and is left for cooling.
   After cooling, the specimen is observed.
   ① Heating: Ambient temperature in the oven is set at 800 °C. The specimen is heated during 30 minutes after the temperature in the oven reach at 800 °C.
   Temperatures near the specimen and itself is measured.
   Oxygen rate in the oven is measured continuously.

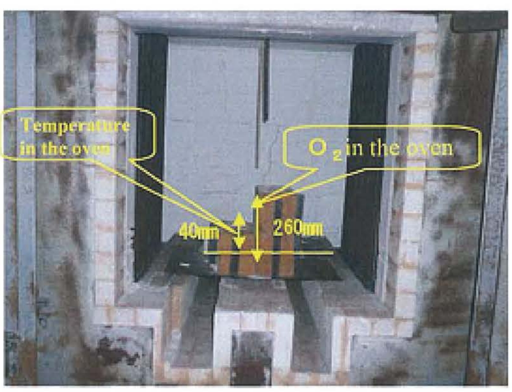

Electric oven (Mizukami Electric Works)
RT～1300℃、60kw

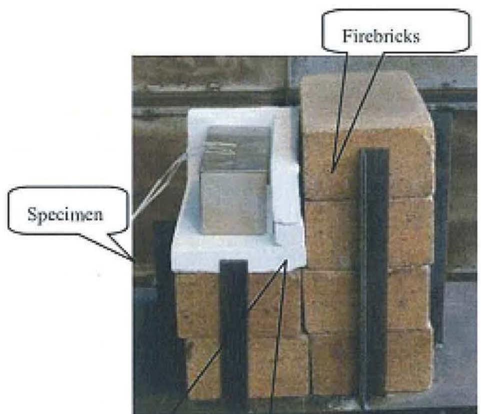

Insulation material (Ceramic fiber board)
MAX=1700°C

②Photos of specimen before and after test

Before test	After test
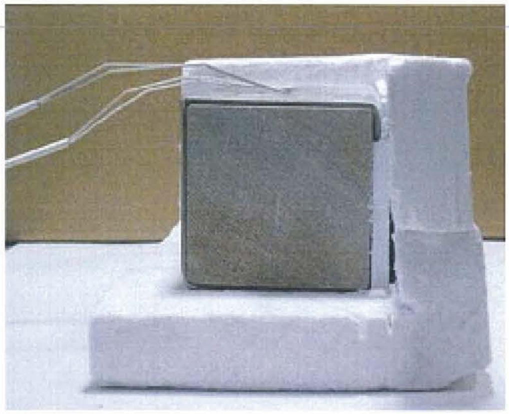	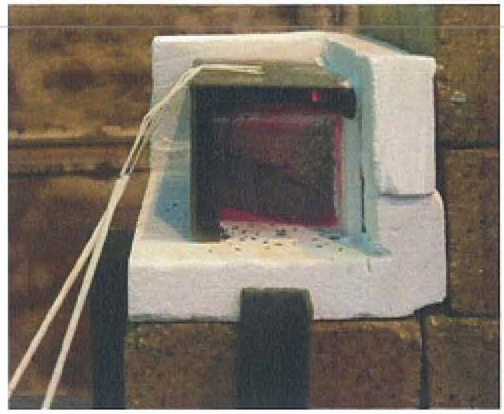

5. Test results

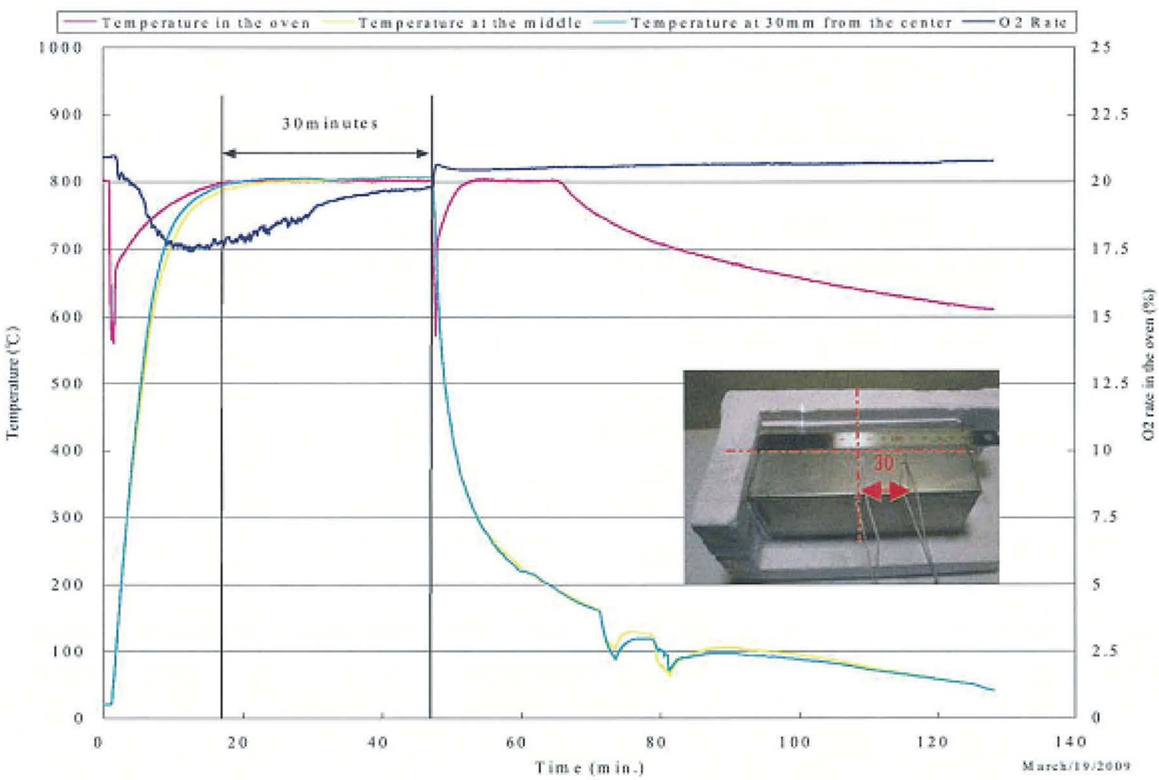

6. Items of data recorded

① Temperature in the oven : R-Thermo couples (Yamari Industries, Limited)

② Temperature of specimen (Center, 30 mm from the center) : K (ϕ 0.3) Thermo couples (Asahi Pyro Industrial Co. Ltd.) JIS C1602−1995 Grade 2 (±2.5℃) adapted

③ Environment in the oven : O_2 Analyzer (POT−101)

④ Data collection and processing : Data logger (GL800, GRAPHTEC) Interval: Every 0.5 sec

6. Observation after test

Balsa wood and stainless steel covering after test

Stainless steel covering after test

Adiabatic side (lateral surface)

Direction of an open extremity

Adiabatic side (Rear)

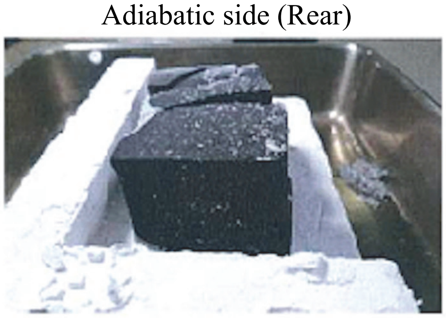

Side of cutting covering

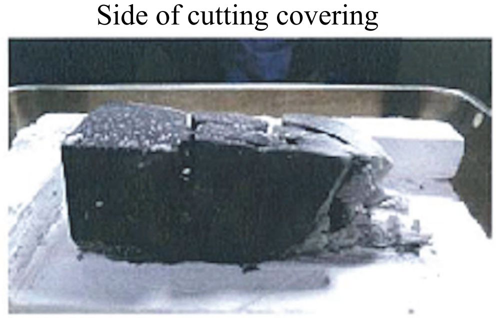

Photos after thermal test

4.0 CONTAINMENT

4.1 DESCRIPTION OF THE CONTAINMENT SYSTEM

Fuel rod cladding and welded end plugs form the containment vessel for the containment of radioactive material in the contents that is transported in the RAJ-II package. Design and fabrication details for fuel rod are described in Section 1.0. Compliance with the containment requirements does not rely upon either filters or mechanical cooling systems. The RAJ-II package does not incorporate a feature intended to allow continuous venting of the containment vessel under normal conditions of transport.

4.2 CONTAINMENT UNDER NORMAL CONDITIONS OF TRANSPORT

The RAJ-II package is constructed, and prepared for shipment so that there is no loss or dispersal of the radioactive contents and no substantial reduction in the effectiveness of the packaging during normal conditions of transport. The nature of the contained radioactive material and the structural integrity of the fuel rod cladding including the closure welds are such that there will be no loss or dispersal of radioactive material under normal conditions of transport. Each rod is pressurized with helium gas to a nominal internal pressure of approximately 1.1 MPa (160 psi) and undergoes a leak check during fabrication. A helium leak test is done during the fabrication of each fuel rod to demonstrates that the fuel rod is leak tight ($<1 \times 10^{-7}$ std-cm^3/s). The release rate limit for normal transport condition is less than 10^{-6}A2 in a period of one week. Details for the calculation of the release rate limit are in Section 4.5.2.

4.3 CONTAINMENT UNDER HYPOTHETICAL ACCIDENT CONDITIONS

The containment requirement of 10 CFR 71.51(a)(2) requires that no escape of other radioactive material exceeding a total amount A_2 in 1 week. [Ref. 1] Following the drop test, a fuel bundle was leak tested and shown to have a leak rate of He equivalent to a rate of 5.5×10^{-6} atm cm^3/s. Fuel rods were also heated to 800°C for over 30 minutes and remained leaktight. The release rate limit for the accident condition is less than an A2 in the period of one week following the accident transport conditions. Details for the calculation of the release rate limit are in Section 4.5.2.

4.4 LEAKAGE RATE TESTS FOR TYPE B PACKAGES

During manufacturing each fuel rod is He leak tested to demonstrate that it is leak tight ($<1 \times 10^{-7}$atm-cm^3/s). The fabrication leakage rate test for each fuel rod satisfies the requirement for the pre-shipment leakage rate test. There are no maintenance or periodic leakage rate tests for the fuel rods.

4.5 APPENDIX

4.5.1 References

1. 10 CFR 71, Packaging and Transport of Radioactive Materials

2. NUREG/CR-6487 Containment Analysis for Type B Packages Used to Transport Various Contents

3. ASTM C 1295-05 Standard Test Method for Gamma Energy Emission from Fission products in Uranium Hexafluoride and Uranyl Nitrate Solution

4. ANSI N14.5-1997 American National Standard for Radioactive Materials – Leakage Tests on Packages for Shipment

5. Petersen, Helge, Riso Report No. 224, The properties of Helium: Density, Specific Heats, Viscosity, and Thermal Conductivity at Pressures from 1 to 100 bar and from Room Temperature to about 1800 K, Danish Atomic Energy Commission, September, 1970

4.5.2 Determination of Allowable Release Rates

Allowable release rates are determined for both normal conditions of transport and hypothetical accident conditions as follows:

Step 1: Identify the radioactive contents.

The radioactive contents is limited to commercial grade or reprocessed uranium in solid form as ceramic uranium oxide that is enriched to no more than 5.00 wt%. The uranium and other nuclides are considered to be dispersible solids that have a homogeneous distribution.

The total activity contained in the radioactive material contents is calculated for a maximum allowed payload of two fuel assemblies containing 550 kg UO_2 (484 kg U) with nuclide specification for enriched reprocessed uranium.

The basic radionuclide values from 10 CFR 71, Appendix A [Ref. 1], (A_2 and specific activity) for the enriched reprocessed uranium contents described in Section 1.2.2 are summarized in Table 4-1.

Table 4-1 Basic Radionuclide Values

Symbol of Radionuclide	Element and Atomic Number	A_2(TBq)	A_2(Ci)	Specific Activity (TBq/g)	Specific Activity (Ci/g)
U-232 (slow lung absorption)	Uranium (92)	1.0×10^{-3}	2.7×10^{-2}	8.3×10^{-1}	2.2×10^{-1}
U-234 (slow lung absorption)		6.0×10^{-3}	1.6×10^{-1}	2.3×10^{-4}	6.2×10^{-5}
U-235 (all lung absorption types)		Unlimited	Unlimited	8.0×10^{-8}	2.2×10^{-6}
U-236 (slow lung absorption)		6.0×10^{-3}	1.6×10^{-1}	2.4×10^{-6}	6.5×10^{-5}
U-238 (all lung absorption types)		Unlimited	Unlimited	1.2×10^{-8}	3.4×10^{-7}
Tc-99	Technetium(43)	9.0×10^{-1}	2.4×10^{1}	6.3×10^{-4}	1.7×10^{-2}
Alpha emitting	Neptunium(93) Plutonium(94)	9.0×10^{-5}	2.4×10^{-3}		
Gamma emitting	Fission Products	2.0×10^{-2}	5.4×10^{-1}		

Step 2: Determine the total releasable activity.

Releasable airborne materials can originate from the radionuclides within the individual fuel rods. The contribution of the fuel to the overall release rate largely depends on its initial pre-transport condition and on subsequent fuel rod response to transportation events. Loose radioactive particles may originate from spallation of material from the surface of the pellets during normal transport conditions. The uranium oxide pellets may fracture and crumble due to handling, vibration, or accident conditions. These conditions will tend to cause the fuel pellets inside the fuel rod to produce a powder aerosol in the helium fill gas. To estimate the source terms under normal and accident conditions, an assumption is made that of the total fuel rod inventory is fine fuel particles. A reasonable bounding value for the mass density of a powder aerosol is 9×10^{-6}g/cm^3. [Ref. 2]

The activity of the radioactive material in the contents is summarized in Table 4-2.

Table 4-2 Activity of Radioactive Material

			Activity	
Nuclide	**Maximum Content**	**Mass (g)**	**TBq**	**Ci**
U-232	0.050 μg/gU	2.42×10^{-2}	2.01×10^{-2}	5.32×10^{-1}
U-234	2000 μg/gU	$9.68\times10^{+2}$	2.23×10^{-1}	6.00
U-235	50000 μg/gU	$2.42\times10^{+4}$	1.94×10^{-3}	5.32×10^{-2}
U-236	25000 μg/gU	$1.21\times10^{+3}$	2.90×10^{-3}	7.78×10^{-2}
U-238	9.23×10^5 μg/gU	$4.47\times10^{+5}$	5.36×10^{-3}	2.47×10^{-1}
Tc-99	5 μg/gU	2.42	1.52×10^{-3}	4.11×10^{-2}
Np/Pu	3300 Bq/kgU	---------	1.60×10^{-6}	4.31×10^{-5}
Gamma Emitters[1]	4.4 X 10^5 MeV Bq/kgU	---------	3.45×10^{-2}	9.30×10^{-2}
Total activity			**2.58×10^{-1}**	**6.95**

Note:
1. The mean gamma energy per disintegration for the gamma emitting measured by the standard test method for gamma energy emission from fission products ranges from 0.0618 to 0.766 [Ref. 3]. The gamma energy production specification for reprocessed uranium (4.4 X 105 MeV Bq/kg) is divided by the lowest mean gamma energy (0.0618 MeV) to conservatively estimate the activity of the gamma emitters.

The specific activity of the solid uranium oxide pellets is

$$S_A = 6.95 \text{ Ci} / 550 \text{ kg } UO_2 = 1.27\ 10^{-5} \text{ Ci/g } UO_2$$

The total releasable activity inside an individual fuel rod is

$$C = S_A \times \rho$$

where:

C is the releasable activity concentration inside the fuel rod [Ci/cm^3],

S_A is the specific activity of the fines in fuel rods [Ci/g UO_2],

ρ is the aerosol mass density [g/cm^3].

The release activity for the reprocessed enriched uranium for both normal and accident conditions is

$$C_N = C_A = (1.27 \times 10^{-5}\ \mathrm{Ci/g\ UO_2})\ (9{\times}10^{-6}\mathrm{g/cm^3}) = 1.14 \times 10^{-11}\mathrm{Ci/\ cm^3}$$

Step 3: Determine an A2 value for the releasable activity.

Table 4-3 A_2 for Mixture

Nuclide	Fraction of Activity f(i)	f(i)/A2(i) A2/TBq	A2/Ci
U-232	$7.66{\times}10^{-2}$	$7.79{\times}10^{+1}$	2.84
U-234	$8.64{\times}10^{-1}$	$1.44{\times}10^{+2}$	5.40
U-235	$7.66{\times}10^{-3}$	0	0
U-236	$1.13{\times}10^{-2}$	1.88	$7.08{\times}10^{-2}$
U-238	$2.12{\times}10^{-2}$	0	0
Tc-99	$5.92{\times}10^{-3}$	$6.57{\times}10^{-3}$	$2.47{\times}10^{-4}$
Np/Pu	$6.21{\times}10^{-6}$	$6.88{\times}10^{-2}$	$2.59{\times}10^{-3}$
Gamma Emitters	$1.34{\times}10^{-2}$	$6.68{\times}10^{-1}$	$2.48{\times}10^{-2}$
Totals	**1.0**	**224**	**8.34**

The release fraction of the individual radionuclide is assumed to be the same for all nuclides. The A2 value for a mixture of releasable radionuclides can be derived using 10 CFR Part 71, Appendix A from the expression.

$$A_2 \text{ for mixture} = \frac{1}{\sum_i \frac{f(i)}{A2(i)}}$$

where f(i) is the releasable activity fraction of radionuclide (i). The A_2 for mixture is 0.12 Ci ($4.46{\times}10^{-3}$ TBq).

Step 4: Determine the release rate for normal conditions of transport, R_N, and for hypothetical accident conditions, R_A.

Standard methods described in ANSI N14.5 [Ref. 4] are used to determine the package release limits. Leaktightness is the specified containment criterion for the design, fabrication, and preshipment leakage rate of the fuel rod containment. Leaktightness is defined as 10^{-7} $\mathrm{cm^3/s}$, based on dry air at 1 atm abs and 298 K leaking to a 0.01 atm abs ambient. The maximum fuel rod conditions are 350 K (77ºC, 171ºF) and 1.33 MPa (192.9 psia, 13.1 atm abs) for normal conditions, and 1073 K (800ºC, 1472ºF) and 4.08 MPa (592 psia, 40.3 atm abs) assuming no rod deformation for accident conditions.

The volume leakage rate at the upstream conditions is estimated by the following equation:

$$L_u = (F_c + F_m)(P_u - P_d)(P_a / P_u)\,cm^3 / s$$

$$F_c = [2.49\times10^6\ D^4]/(a\times\mu)\ cm^3/atm\times s$$

$$F_m = [3.81\times10^3\ D^3\ (T/M)^{0.5}]/(a\times P_a)\ cm^3/atm\times s$$

where

a	is leakage hole length, cm
D	is leakage hole diameter, cm
F_c	is coefficient of continuum flow conductance per unit pressure, cm^3/atm s,
F_m	is coefficient of free molecular flow conductance per unit pressure, cm^3/atm s,
M	is molecular weight, g/mol
P_u	is fluid upstream pressure, atm abs,
P_d	is fluid downstream pressure, atm abs,
P_a	is average stream pressure = 1/2 (Pu+Pa), atm abs
T	is fluid absolute temperature, K, and
μ	is fluid viscosity, cP (centipoises).

The correlation for the coefficient of dynamic viscosity [Ref. 5] for helium is

$$\mu = 3.674\times10^{-7}\ T^{0.7}\ kg/m\times s = 3.674\times 10^{-4}T^{0.7}\ cP$$

Normal Transport

A reference air leakage rate corresponding to normal transport conditions is $L_{R,N}=1\times10^{-7}$ std cm^3/s (air at 25°C and 1.0 atm abs leaking to a 0.01 ambient). A 1.0-cm path length is assumed. The corresponding leakage rate for helium, $L_{u,He}$, at 77ºC and 13.1 atm abs leaking to 1.0 atm abs ambient is calculated to determine the allowable leak rate for helium.

For the air flow, a = 1.0 cm, T = 298 K, u(air, 298 K) = 0.0198 cP, Pu = 1 atm, Pd = 0.01 atm, M=29 g/mol, and Pa = 0.505 atm,

$$F_c = [2.49\times10^6\ D^4]/(1.0\times0.0185) = 1.34\times10^8\ D^4\ cm^3/atm\times s$$

$$F_m = [3.81\times10^3\ D^3\ (298/29)^{0.5}]/(1.0\times0.505) = 2.41\times10^4\ D^3\ cm^3/atms$$

$$L_u = (F_c + F_m)(P_u - P_d)(P_a / P_u)\,cm^3 / s$$

$L_{R,N} = L_{u} = 1\times10^{-7}$ atm cm^3/s

1×10^{-7} atm $\times$ cm^3/s = $[1.34\times10^8 D+2.41\times10^4](D^3)(0.99)(0.505)$

Solving implicitly for D gives,

$D = 1.63\times10^{-4}$ cm

For the helium leak flow conditions: Pu = 13.1 atm, Pd = 1.0 atm, T = 350 K, μ(helium, 350 K) =0.02218 cP, Pu – Pd = 12.1 atm, Pa = 7.1 atm, a (fuel rod cladding thickness) = 0.2 cm, M=4.0 g/mol, and

Pa/Pu = 0.525.

$F_c = [2.49\times10^6 (1.63\times10^{-4})^4]/(0.2\times0.02218) = 3.96\times10^{-7}$ cm^3/atm×s

$F_m = [3.81\times10^3 (1.63\times10^{-4})^3 (350/4)^{0.5}]/(0.2\times7.1) = 1.09\times10^{-7}$ cm^3/atm×s

Then, the helium flow rate equivalent to the leaktightness criteria 10^{-7} cm^3/s based on air is:

$L_{u,He} = (3.96\times10^{-7}+1.09\times10^{-7})(13.1-1.0)(0.542) = 3.31\times10^{-6}$ cm^3/s

The helium flow rate for the package contents based on 2 fuel bundles with 92 fuel rods per fuel bundle is:

$\mathbf{L_N} = 2\times92\times(3.31\times10^{-6}$ cm^3/s) = 6.09×10^{-4} cm^3/s

The release rate for normal transport conditions based on the contents of 2 fuel bundles is:

$\mathbf{R_N} = \mathbf{L_N C_N} = (6.09\times10^{-4}$ cm^3/s) $\times$ (1.14×10^{-11}Ci/ cm^3) = 6.94×10^{-15} Ci/s

where:

L_N is the time-averaged volumetric gas flow rate for normal transport conditions [cm^3/s], and

C_N is the curies per unit volume of the releasable radioactive material within the containment vessel normal transport conditions [Ci/cm^3].

The maximum allowed release rate for normal conditions in units of curies per second assuming a time-averaged constant flow rate is:

$A_2\times10^{-6}$/hour = ($A_2\times10^{-6}$/hour)/3600 seconds/hour) =A_2 2.78×10^{-10}/second

$A_2\times2.78 \times10^{-10}$/second = (0.12 Ci)($2.78 \times 10^{-10}$/second) = 3.34×10^{-11} Ci/s

The release rate for normal transport conditions, **R_N** is less than $A_2\times10^{-6}$/hour.

Accident Conditions

The reference air leakage rate corresponding to accident conditions for a single fuel bundle subject is $L_{R,A}$=5.5×10^{-6} atm cm^3/s (air at 25°C and 1.0 atm abs leaking to a 0.01 ambient). The corresponding leakage rate for helium at 25ºC and 36 atm abs leaking to 1.0 atm abs ambient is calculated to determine the allowable leak rate for helium.

For the air flow, a = 1.0 cm, T = 298 K, u(air, 298 K) = 0.0198 cP, Pu = 1 atm, Pd = 0.01 atm, M=29 g/mol, and Pa = 0.505 atm,

$$F_c = [2.49\times10^6\ D^4]/(1.0\times0.0185) = 1.34\times10^8\ D^4\ cm^3/atm \times s$$

$$F_m = [3.81\times10^3\ D^3\ (298/29)^{0.5}]/(1.0\times0.505) = 2.41\times10^4\ D^3\ cm^3/atms$$

$$L_u = (F_c + F_m)(P_u - P_d)(P_a / P_u)\, cm^3 / s$$

$$L_{R,A} = L_u = 5.5\times10^{-6}\ atm\ cm^3/s$$

$$5.5\times10^{-6}\ atm \times cm^3/s = [1.34\times10^8\ D + 2.41\times10^4](D^3)(0.99)(0.505)$$

Solving implicitly for D gives,

$$D = 4.95\times10^{-4}\ cm$$

For the helium leak flow conditions: Pu = 40.3 atm, Pd = 1.0 atm, T = 1073 K, μ(helium, 1073 K) = 0.0486 cP, Pu – Pd = 39.3 atm, Pa = 20.2 atm, a (fuel rod cladding thickness) = 0.2 cm, M=4.0 g/mol, and Pa/Pu = 0.501.

$$F_c = [2.49\times10^6\ (4.95\times10^{-4})^4]/(0.2\times0.0486) = 1.54\times10^{-5}\ cm^3/atm \times s$$

$$F_m = [3.81\times10^3\ (4.95\times10^{-4})^3\ (1073/4)^{0.5}]/(0.2\times20.2) = 1.87\times10^{-6}\ cm^3/atm \times s$$

Then, the helium flow rate equivalent to the measured leak rate 5.5x10^{-6} cm^3/s based on air is:

$$L_{u,He} = (1.54\times10^{-5} + 1.87\times10^{-6})(40.3-1.0)(0.501) = 3.40\times10^{-4}\ cm^3/s$$

The helium flow rate for the package contents based on 2 fuel bundles with 92 fuel rods per fuel bundle is:

$$\mathbf{L_A} = 2\times(3.40\times10^{-4}) = 6.80\times10^{-4}\ cm^3/s$$

$$\mathbf{R_A} = \mathbf{L_A C_A} = (6.80\times10^{-4}\ cm^3/s) \times (1.14 \times 10^{-11} Ci/cm^3) = 7.75\times10^{-15}\ Ci/s$$

where:

L_A is the time-averaged volumetric gas flow rate for accident transport conditions [cm^3/s], and

C_A is the curies per unit volume of the releasable radioactive material within the containment vessel accident transport conditions [Ci/cm^3].

The maximum allowed release rate for accident conditions in units of curies per second assuming a time-averaged constant flow rate is:

A_2 /week = (A_2 /week)/6.048 seconds/week) =A_2 1.65×10^{-6}/second

A_2 1.65×10^{-6}/second = (0.12 Ci)(1.65×10^{-6}/second)=1.98×10^{-6} Ci/s

The release rate for accident conditions, **R_A,** is less than A_2 /week.

5.0 SHIELDING EVALUATION

The contents of the RAJ-II require no shielding since unirradiated fuel gives off no significant radiation either gamma or neutron. Hence the RAJ-II provides no shielding. The minimal shielding provided by the stainless steel sheet is not required. The dose rate limits established by 10 CFR 71.47(a) for normal conditions of transport (NCT) are verified prior to shipping by direct measurement.

Since there is no shielding provided by the package, there is no shielding change during the Hypothetical Accident Conditions (HAC). Therefore, the higher dose rate allowed by 10 CFR 71.51(a)(2) will be met.

6.0 CRITICALITY EVALUATION

6.1 DESCRIPTION OF CRITICALITY DESIGN

6.1.1 Design Features

A principle safety function of the RAJ-II is to provide criticality control. The inner and outer containers retain the contents within a fixed geometry relative to other such packages in an array. The fuel assembly structure or fuel rod container retains the fuel rods within a fixed geometry. Individual fuel rods retain the fuel pellets within a fixed geometry of the fuel rod tube. The *confinement system* consists of the inner and outer containers, fuel assembly structure or fuel rod container, and the fuel rod tube. Neutron absorption is provided by packaging structural materials and gadolinium oxide in the uranium oxide fuel mixture. Neutron moderation is provided from external sources consistent with the normal or accident transport conditions. Packaging materials, such as paper honeycomb, wood, and polyethylene, also provides neutron moderation, but none of these materials is intended to provide the neutron moderation required for effective neutron absorption. Dimensions and tolerances of the confinement system for fissile material, floodable void spaces, and overall package that affect the physical separation of fissile contents in package arrays are described in Section 1.

6.1.2 Summary Table of Criticality Evaluation

A criticality evaluation is done for each of the type and form of contents that includes fuel rods, fuel bundles, and fuel assemblies. Each fuel rod, fuel bundle, and fuel assembly design as described in Section 1 is considered in the evaluation of the package. A demonstration of maximum reactivity determined the most reactive package configuration for each type and form of contents.

The criteria to establish subcriticality of the package includes an allowance for uncertainties in the calculated multiplication factor k_{eff} of the package or array of packages and margin for uncertainty in the mean k_{eff} that results from calculation of the benchmark criticality experiments [Ref. 1].

$$k_p + \Delta k_p \leq k_c - \Delta k_c - \Delta k_m$$

where:

k_p is the calculated multiplication factor k_{eff} of the individual package or package array for normal and accident transport conditions;

k_c is the mean k_{eff} that results from the calculation of the benchmark criticality experiments;

Δk_p is an allowance for statistical uncertainty in the calculation of k_p, material and fabrication tolerances, and uncertainties due to limitation in the geometric or material representations used in the computational method;

Δk_c is a margin for uncertainty in k_c that includes allowances for uncertainties in the critical experiments, statistical uncertainties in the computation of k_c, uncertainties due to extrapolation of k_c outside the range of experimental data, and uncertainties due to limitation in the geometric or material representations used in the computational method;

Δk_m is an administrative margin to ensure the subcriticality of k_p.

The maximum multiplication factor (*Maximum* k_{eff}) is the maximum value of $k_p + \Delta k_p$ for the contents and transport condition that is used to demonstrate that criteria for subcriticality is satisfied. The statistical uncertainty for k_p is 2 times the standard deviation for the calculation method ($2\sigma_p$). The total uncertainty Δk_p also includes allowances for other uncertainties (Δk_u) that depend on package assessment such that $\Delta k_p = 2\sigma_p + \Delta k_u$. The upper subcritical limit (USL) is defined as the value for $k_c - \Delta k_c - \Delta k_m$, where Δk_m is 0.05. Table 6-1 provides a summary of the USL for the package configurations. The criterion for all package configurations is as follows:

Maximum $k_{eff} \leq$ USL

where:

Maximum $k_{eff} = k_p + 2\sigma_p + \Delta k_u$, and

USL= $k_c - \Delta k_c - \Delta k_m$

Table 6-1 Summary of Upper Subcritical Limits

Package Configuration	USL = $k_c - \Delta k_c - \Delta k_m$
Individual Package, Fuel Bundle or Fuel Assembly, no BA Rods	0.9448
Package Array, Fuel Bundle or Fuel Assembly, with BA Rods	0.9434
Package Array, Fuel Bundle or Fuel Assembly, no BA Rods	0.9449
Individual Package, Fuel Rods or Fuel Rod Container	0.9405
Package Array, Fuel Rods or Fuel Rod Container	0.9441

6.1.2.1 Fuel Bundle or Fuel Assembly

A criticality evaluation is done for fuel bundles that have no BA rods and fuel bundles that have a minimum number of BA rods. A fuel assembly is the fuel bundle with the fuel channel installed. The credible rearrangement of the fuel bundle due to accident conditions of transport is limited by the fuel channel for a fuel assembly, whereas, the inner container limits the fuel rod rearrangement for a fuel bundle. Polyethylene packing materials are permitted for protection during transport. A minimum of eight (8) BA rods meeting the following constraints is assumed in the criticality evaluation of the fuel bundles and fuel assembly contents:

1. BA rods shall be in positions that are symmetric across the major geometric diagonal (defined from the control blade of position A1)

2. No BA rod shall be in the outermost edge or corner locations

3. Partial length fuel rods shall not be BA rods

4. At least one BA rod shall be in three of the four fuel bundle quadrants

5. At least eight (8) BA rods must be located in each fuel lattice (the bundle design defines the axial lattices in a bundle)

6. No BA rods are required in fuel lattices (i.e., axial zones) that do not have fissile material or have uranium enriched in ^{235}U to a maximum of 1.0% by weight.

7. Blanket zones at top, bottom, and combine top and bottom without BA present are permitted to a maximum length of 8 in. and ^{235}U enrichments up to 5 wt%.

Table 6-2 Individual Package, Fuel Bundle or Fuel Assembly, no Gad Rod (USL=0.9448)

Condition of Transport	Contents	Maximum k_{eff}	Reference
Normal	Fuel Assembly or Fuel Bundle	0.8198	Table 6-31
Accident	Fuel Assembly	0.8322	Table 6-31
	Fuel Bundle	0.9324	Table 6-31

Table 6-3 Package Array, Fuel Bundle or Fuel Assembly, with BA Rods (USL=0.9434)

Condition of Transport	Contents	Array Size	Maximum k_{eff}	Reference
Normal	Fuel Assembly	5N=529	0.6240	Table 6-40
	Fuel Bundle	5N=361	0.6086	Table 6-40
Accident	Fuel Assembly	2N=144	0.9076	Table 6-59
	Fuel Bundle	2N=132	0.9405	Table 6-59

Table 6-4 Package Array, Fuel Bundle or Fuel Assembly, no BA Rods (USL=0.9449)

Condition of Transport	Contents	Array Size	Maximum k_{eff}	Reference
Normal	Fuel Assembly	5N=169	0.6087	Table 6-40
	Fuel Bundle	5N=100	0.5751	Table 6-40
Accident	Fuel Assembly	2N=49	0.9291	Table 6-59
	Fuel Bundle	2N=25	0.9268	Table 6-59

6.1.2.2 Fuel Rods

Fuel rods may be transported either packaged in a rod container or as a cluster of fuel rods without a rod container. Each individual fuel rod may be protected by a polyethylene sleeve. The routine and normal condition of transport is for the fuel rods to be close packed. During accident conditions the rod container confines the fuel rods to fixed geometry whereas a cluster of fuel rods are confined only by the inner container. For fuel rod shipment without a rod container, a maximum of 25 fuel rods in each compartment of the inner container is permissible. For a rod container, the number of fuel rods is limited by the capacity of the rod container (protective case, rod pipe, or rod box).

Table 6-5 Individual Package, Fuel Rods or Fuel Rod Container (USL=0.9405)

Condition of Transport	Contents	Maximum k_{eff}	Reference
Normal	Fuel Rods without Rod Container	0.4308	Table 6-31
	Fuel Rod with Rod Container	0.6300	Table 6-31
Accident	Fuel Rods without Rod Container	0.7152	Table 6-31
	Fuel Rod with Rod Container	0.6828	Table 6-31

Table 6-6 Package Array, Fuel Rods or Fuel Rod Container (USL=0.9441)

Condition of Transport	Contents	Array Size	Maximum k_{eff}	Reference
Normal	Fuel Rods without Rod Container	5N=361	0.4670	Table 6-40
	Fuel Rod with Rod Container	5N=361	0.8747	Table 6-40
Accident	Fuel Rods without Rod Container	2N=144	0.8423	Table 6-59
	Fuel Rod with Rod Container	2N=144	0.9239	Table 6-59

6.1.3 Criticality Safety Index

CSI = 50/N where the number of undamaged packages in an array is 5N and number of damaged packages in an array is 2N. The CSI is rounded up to the nearest tenth decimal place. BA Rods refers to a minimum number and positions of BA Rods assumed in the evaluation. If a minimum number of eight BA rods meeting the constraints is not satisfied by the actual fuel bundle design, the CSI for a fuel assembly or fuel bundle without BA rods must be used. For fuel rod shipment without a rod container, a maximum of 25 fuel rods in each compartment of the inner container is permissible. For a rod container, the number of fuel rods is limited by the capacity of the rod container (protective case, rod pipe, or rod box).

Table 6-7 Summary of Criticality Safety Index

Contents	Transport Conditions Normal 5N	Transport Conditions Accident 2N	CSI
Fuel Assembly, no BA Rods	169	49	2.1
Fuel Assembly, with BA Rods	529	144	0.7
Fuel Bundle, no BA Rods	100	25	4.0
Fuel Bundle, with BA Rods	361	132	0.8
Fuel Rods or Fuel Rod Container	361	144	0.7

6.2 FISSILE MATERIAL CONTENTS

The contents are evaluated using nominal mass, density and dimensions described in Section 1.0 with the following exceptions to the uranium enrichment, fuel pellet density, and gadolinium oxide content in the BA rods.

1. The fissile material in fuel pellets is assumed to be uranium enriched up to a maximum of 5.0 wt% uranium-235 in all fuel rods.

2. Theoretical density for uranium dioxide (10.96 g/cm^3), and

3. A minimum number of eight (8) burnable absorber fuel rods with a minimum 2.0 wt% Gd_2O_3 is assumed for the BA rods in every axial lattice zone of the fuel bundle.

6.3 GENERAL CONSIDERATIONS

6.3.1 Model Configuration

Figure 6-1 and Figure 6-2 show a comparison between actual packaging and model configuration used for the k_{eff} calculations. The actual packaging configurations shown in Figure 6-1 and Figure 6-2 are a summary of dimensions from the engineering drawings in Section 1.0. The model configuration represents the actual packaging with the following exception:

Gasket gap of about 5 to 8 mm, between the inner container upper lid and inner container box is not included in the model. Omitting the gap results in the height dimension of the inner wall of the inner container and the overall height of the inner container in the model that is less than the dimensions shown on engineering drawings. The inner container lid deformation during accident condition impacts results in an increase in the inner container height dimension. The inner wall of the inner container is a confinement feature that limits fuel rearrangement, and increase in the inner wall height due to gasket gap and other impacts is considered in the assessment of the contents for accident transport conditions.

Thermal insulator replaced with water for the individual package or void for package arrays. The replacement increases either neutron reflectivity for the individual package or package interaction for arrays, both resulting to the most reactive packaging configuration, as seen Section 6.9.6.

Container stainless steel structure is partially omitted (outer container 50 mm stainless steel angles that make the framework angle, inner and outer container tightening blocks and closure bolts, inner container hold down bar boss, partition plate angle). Structural stainless steel is a criticality feature that provides neutron absorption. Stainless steel sheet in the inner container and outer container provides significant neutron absorption for package array configurations. The effect of omitting angles that make the framework and other components results is less neutron absorption in the model.

Figure 6-3 shows typical configurations for the fuel bundle contents. There are four groups of fuel bundles 1) GE11 and GE13, 2) GE12B, GE14C, and GE14G, 3) GNF2, and 4)SVEA. The GE11 and GE13 fuel bundles are 9x9 lattice of fuel rods, and all other fuel bundles are 10x10 lattice of fuel rods. Detailed description of the fuel bundle configurations is found in Section 1.0. Fuel bundles are modeled explicitly in three-dimensions including the partial length fuel rods and water rods. The fuel bundle spacers, finger springs, upper tie plate, lower tie plate, lower fuel support piece, transition nosepiece, fuel channel and other hardware (i.e., springs, nuts, etc.) are not included in the model. These components are either stainless steel or a zirconium alloy that would insert additional neutron absorption, displace water moderation from the fuel lattice, or displace water reflector from the fuel bundle envelope in the model. The net effect of omitting the fuel assembly components has no significant effect of the neutron multiplication factor.

Although loose rods are in reality unconstrained by spacers or other fixtures when loaded into the product containers for storage or shipment, they have been conservatively modeled in fixed lattices with constant spacings between individual rods for optimum moderation.

6.3.1.1 Protective Case

Square and triangular lattices have been considered with the intent of identifying the most reactive arrangement and determining the maximum allowable number of loose rods inside the product protective case that can be transported within the RAJ-II package. Figure 6-4 shows the SCALE model of the protective case. This approach to modeling the fuel rods is conservative, since it permits the rods to be spaced in optimally moderated configurations within the rectangular box and eliminates any restriction on the number of rods that can be transported in a rod container. Actual shipments will utilize the full rod container capacity such that the rods will be nearly close-packed in the rod container; however, there a partially loaded rod container is credible.

The protective case is a SS body holding the fuel rods, surrounded by a poly urethane cushioning material. The length of the body has exterior dimensions of 9.7 cm wide by 8.9 cm tall by 418.6 cm long, composed of 0.4 cm thick SS. The top lid is installed on top of the body and run the length of the case, composed of 0.5 cm thick SS. The end plates are 0.5 cm thick SS, with a resultant modeled case length of 418.6 cm. Assembly pieces such as the lumber shock absorbers, exterior cushioning materials, and structural steel components are conservatively neglected.

6.3.1.2 Rod Pipe

Triangular and square lattices have been considered with the intent of identifying the most reactive arrangement and determining the maximum allowable number of loose rods that can be transported within the RAJ-II package inside the product container of a 5 in. rod pipe. Figure 6-5 shows the SCALE model of the rod pipe. This approach to modeling the fuel rods is conservative, since it permits the rods to be spaced in optimally moderated configurations within the cylindrical pipe and eliminates any restriction on the number of rods that can be transported in a rod container. Actual shipments will utilize the full rod container capacity such that the rods will be nearly close-packed in the rod container; however, there a partially loaded rod container is credible.

The 5 inch schedule 40 pipe container, composed of 304 SS, has an outer diameter of 5.563 in. (14.13 cm) with a 0.258 in. (0.65532 cm) thickness. The pipe has a length 424.18 cm plus the end caps, which are 0.5 in. (1.27 cm) thick and modeled with the same exterior dimensions of the pipe body.

6.3.1.3 Rod Box

Square and triangular lattices have been considered with the intent of identifying the most reactive arrangement and determining the maximum allowable number of loose rods inside the rod box that can be transported within the RAJ-II package. Figure 6-6 shows the SCALE model of the rod box. This approach to modeling the fuel rods is conservative, since it permits the rods to be spaced in optimally moderated configurations within the cuboid and eliminates any restriction on the number of rods that can be transported in a rod container. Actual shipments will utilize the full rod container capacity such that the rods will be nearly close-packed in the rod container; however, there a partially loaded rod container is credible.

The rod box is a rectangular box, composed of an external shell and internal steel bars limiting the contents spacing. Conservatively, internal steel bars of the rod box are not modeled, although the internal spacing is maintained and fully moderated for hypothetical accident transport conditions. The outer shell is a 0.15 cm thick box 13.5 cm wide by 13.0 cm tall, modeled at a length of 429 cm. The shell has large punched holes with 5.0 cm diameter on three sides to avoid water moderation buildup within the container. The seven holes have a 5.0 cm diameter with an approximate center-to-center spacing of 60 cm and the end holes located 15.5 cm from the ends of the container; each hole is filled with moderation similar to the fuel envelop.

Security Related Information
Figure Withheld Under 10 CFR 2.390

Figure 6-1 End View Cross Section Comparison of Actual Packaging (Top) and Model Geometry (Bottom), (Units in mm)

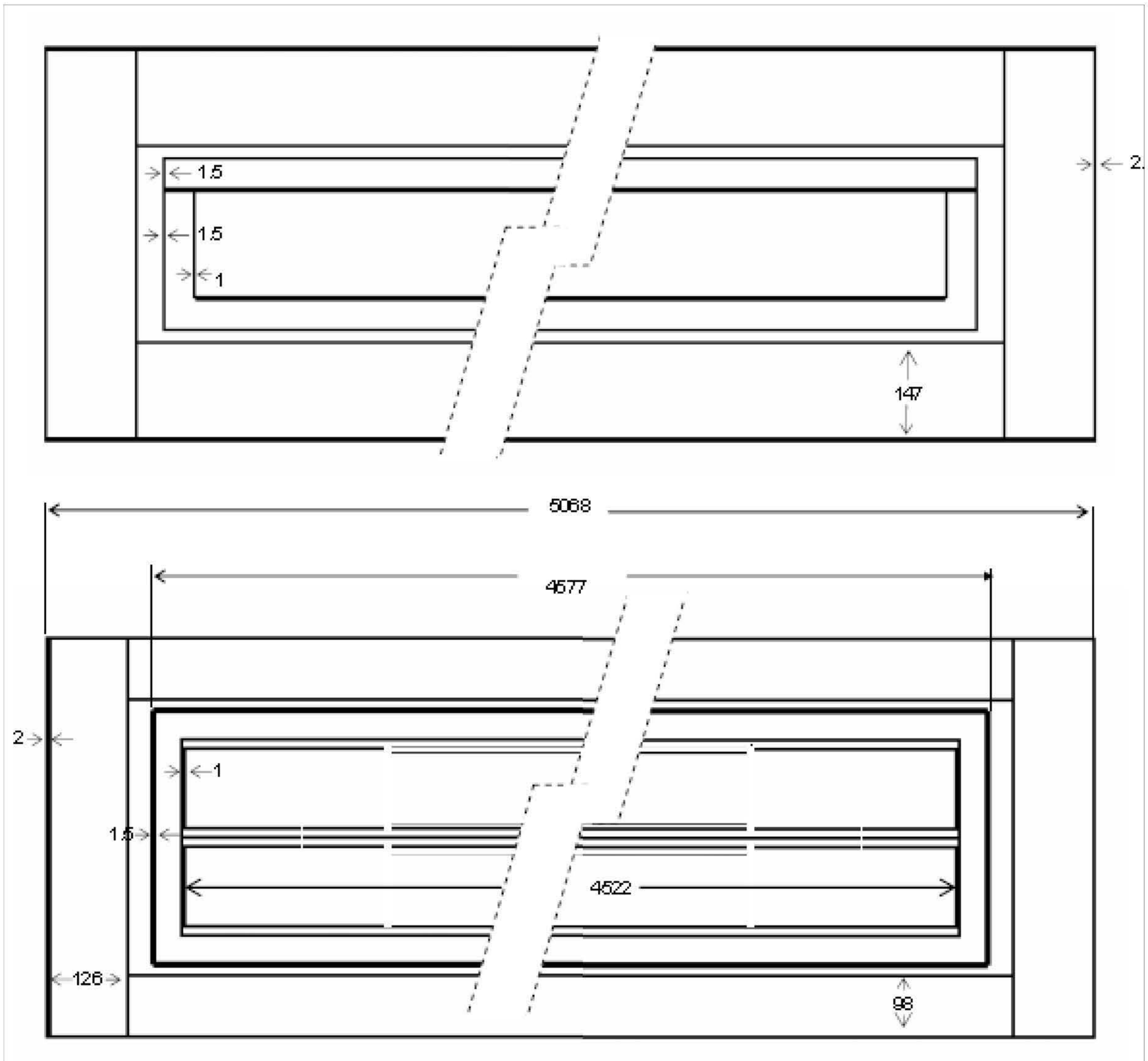

Figure 6-2 Side View (Top) and Top View (Bottom) Cross Section of Model Geometry, (Units in mm)

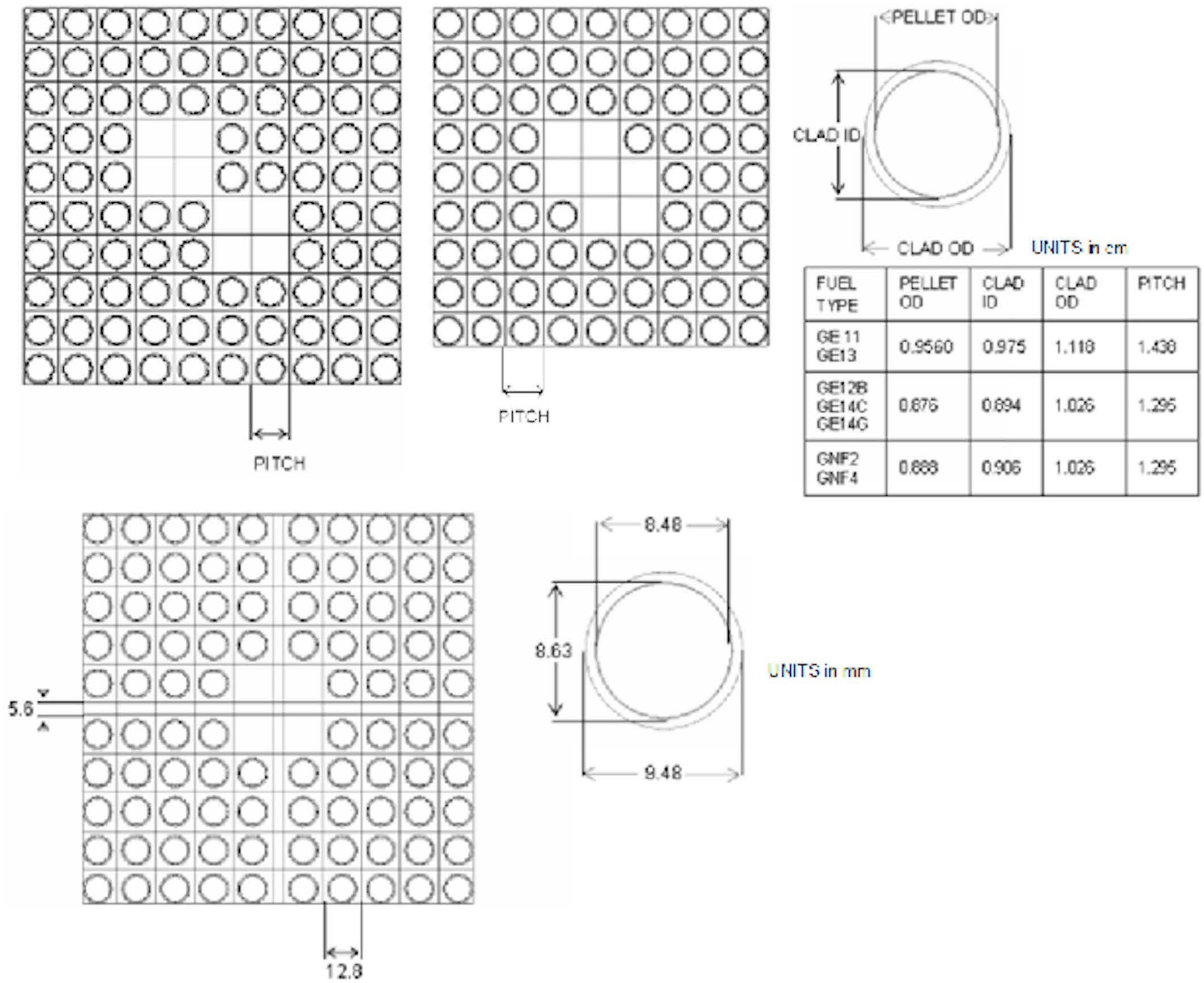

FUEL TYPE	PELLET OD	CLAD ID	CLAD OD	PITCH
GE 11 GE13	0.9560	0.975	1.118	1.438
GE12B GE14C GE14G	0.876	0.894	1.026	1.295
GNF2 GNF4	0.888	0.906	1.026	1.295

Figure 6-3 Fuel Bundle Model – GNF 10X10 and 9X9 (Top) and Westinghouse 10X10 (Bottom)

Security Related Information
Figure Withheld Under 10 CFR 2.390

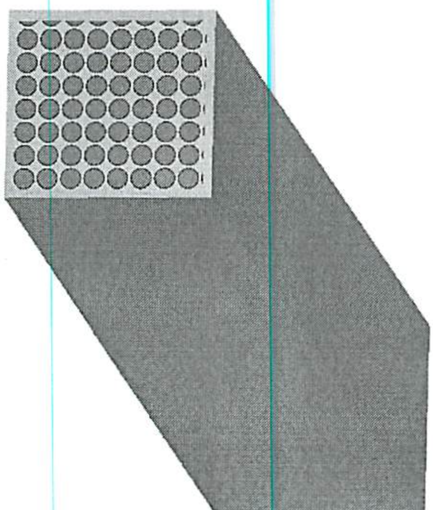

Figure 6-4 Protective Case: SCALE Model Slice (left), Licensing Drawing (right)

Security Related Information
Figure Withheld Under 10 CFR 2.390

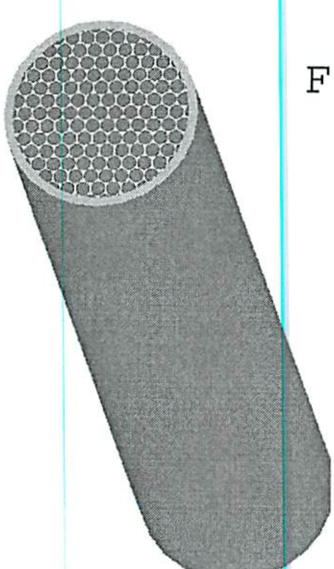

Figure 6-5 Rod Pipe: SCALE Model Slice (left), Licensing Drawing (right)

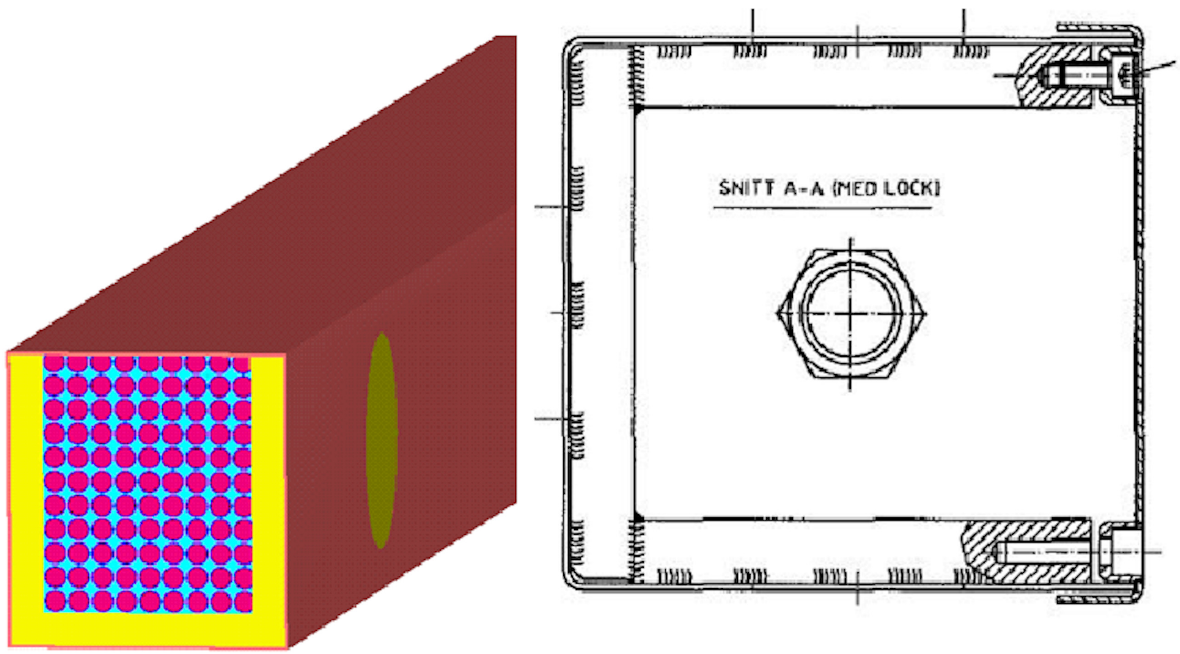

Figure 6-6 WEC Rod Box: SCALE Model Slice (left), Licensing Drawing (right)

6.3.2 Material Properties

6.3.2.1 UO_2

A mixture defining UO_2 has a density of 10.96 g/cm^3 that is the theoretical density for the compound. Actual density of UO_2 fuel pellets is between 95% and 97% of theoretical density to provide porosity for fuel performance in the reactor. The uranium is 5 wt% ^{235}U and 95 wt% ^{238}U. Reprocessed enriched uranium specification [Ref. 2] allows 5.0E-06 wt% ^{232}U, 0.2 wt% ^{234}U, and 0.25 wt% ^{236}U. Any ^{232}U, ^{234}U, or ^{236}U is assumed to be ^{238}U since these uranium isotopes are not fissile, present in small amounts and have total neutron cross sections that tend to be greater than the total neutron cross section for ^{238}U (Figure 6-7). The maximum actual nominal enrichment is 4.95 wt% ^{235}U. The density is incorporated into the density multiplier, VF, rather than using the DEN=keyword. The generic input specification for this standard composition is

SC MX VF TEMP (IZAi WTPi) END

where

SC	is the standard composition component name (UO2).
MX	is the mixture number (1).
VF	is the density multiplier (the density multiplier is the ratio of actual to theoretical density (10.96/10.96 = 1).
TEMP	is the temperature in Kelvin (300).
IZA	is the isotope ID number (92235 for ^{235}U and 92238 for ^{238}U).
WTP	is the weight percent of the isotope in the material (5 for ^{235}U and 95 for ^{238}U).

The input data for the UO_2 are given below.

```
UO2      1 1 300  92235 5  92238 95  end
```

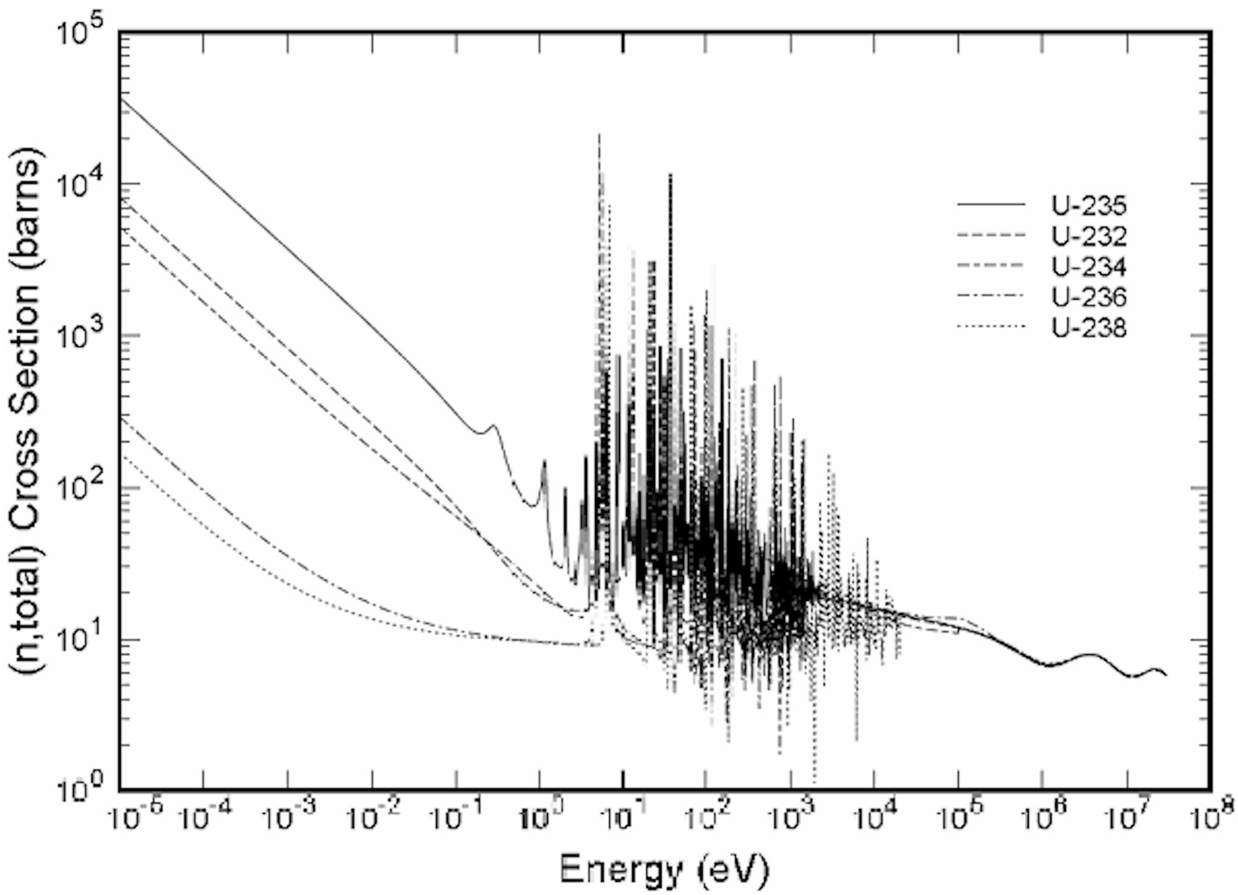

Figure 6-7 Uranium (n, total) Cross Section [Ref. 9]

6.3.2.2 UO_2 - Gd_2O_3

The design objective for gadolinia oxide is to suppress reactivity during the beginning of a reactor cycle. A uniform distribution of burnable absorber (BA) contents allow for depletion from the outer surface of the pellet inward as the exposure increases. The number density for the elements in Gd_2O_3 is calculated using 75 percent of Gd for a nominal 2.0 wt% Gd_2O_3 content and an actual BA pellet density of 10.53 ± 0.015 g/cm^3. The theoretical density is used for the UO_2 in the urania-gadolinia mixture.

$$10.53\ g/cm^3 \times 0.02 = 0.1827\ g/cm^3\ Gd_2O_3$$
$$\mathrm{M(Gd2O3)} = 362.504$$
$$\mathrm{A(Gd\text{-}NAT)} = 157.256$$
$$2\ \mathrm{Gd/mole\ Gd2O3} \times \frac{157.256\ \mathrm{g/mole\ Gd\text{-}NAT}}{362.504\ \mathrm{g/mole\ Gd2O3}} \times 0.1827\ g/cm^3\ Gd_2O_3 \times 0.75 = 0.1370\ g/cm^3\ Gd$$
$$0.2106\ g/cm^3\ Gd_2O_3 - 0.1370\ g/cm^3\ Gd = 0.0736\ g/cm^3\ O$$

$$N = \frac{\rho \cdot N_A}{M}$$
$$N_{Gd} = \frac{0.1370\ g/cm^3\ Gd \cdot 0.6022 \times 10^{24}\ atoms/mole \cdot 10^{-24}\ cm^3/b}{157.256\ g/mole} = 5.2463 \times 10^{-4}\ atoms/b \cdot cm$$
$$N_O = \frac{0.0736\ g/cm^3\ O \cdot 0.6022 \times 10^{24}\ atoms/mole \cdot 10^{-24}\ cm^3/b}{16.000\ g/mole} = 2.7701 \times 10^{-3}\ atoms/b \cdot cm$$

The generic standard composition specification is

SC MX VF ADEN END

where

SC is the standard composition component name (GD and O).

MX is the mixture number (6).

VF is the density multiplier (enter 0 because the number density is to be used).

ADEN is the number density of the standard composition (GD 5.2463E-04, O 2.7701E-03).

The input data for the Gd_2O_3 are given below:

```
GD    6 0 5.2463E-04 end
O     6 0 2.7701E-03 end
```

The input data for UO_2 component of the mixture is the same as for the UO_2 and is given below:

```
UO2    6 1 300  92235 5  92238 95  end
```

6.3.2.3 Zircaloy

Zircaloy is the material of the fuel rod cladding represented by Zr-2 for BWR rods and Zr-4 for PWR rods.

Zircaloy-2

Standard composition of ZIRC2 is used to represent the Zircaloy-2 for the fuel rod cladding material. The standard density is 6.56 g/cm^3 and composition is as follows:

98.250 wt% zirconium
1.45 wt% tin
0.100 wt% chromium
0.135 wt% iron
0.055 wt% nickel
0.01 wt% hafnium

Zircaloy-4

Standard composition of ZIRC4 is used to represent the Zircaloy-4 for the fuel rod cladding material. The standard density is 6.56 g/cm^3 and composition is as follows:

98.23 wt% zirconium
1.45 wt% tin
0.100 wt% chromium
0.210 wt% iron
0.01 wt% hafnium

6.3.2.4 Stainless Steel-304

Several specifications of stainless steel as apply to Grade 304/304L are provided in Section 1.3.4. The stainless steel 304 (SS304) composition from the SCALE standard composition library is used to represent all specifications for stainless steel. The standard density is 7.94 g/cm^3 and composition is as follows:

68.375 wt % iron
19 wt % chromium
9.5 wt % nickel
2 wt % manganese
1 wt % silicon
0.08 wt % carbon
0.045 wt % phosphorus

6.3.2.5 Polyethylene

Standard material POLY(H2O) is used to represent all polyethylene packing and packaging materials in normal and accident transport conditions (i.e., plastic sheathing, cluster separators, foam cushions, and melted foam). The POLY(H2O) composition is CH_2, standard density is 0.92 g/cm^3, and uses hydrogen in the water with a S(α,β) thermal kernel.

The densities of the polyethylene packing and packaging materials are as follows:

Cluster separator fingers (LDPE)	0.925 g/cm^3
Cluster separator holders (HDPE)	0.959 g/cm^3
Protective sheath	0.919 g/cm^3
Foam cushion	0.080 g/cm^3

The polyethylene material is represented by a mixture of the components (i.e., cluster separator assembly units), the following equation are used to calculate the weighted average density:

$$\frac{1}{\rho_T} = \sum_i \frac{\omega_i}{\rho_i}$$

where,

ω_i is the weight fraction of material/component *i,*

ρ_i is the density of the material/component *i*, and

ρ_T is the density of the mixture.

For modeling fuel packing materials (i.e., plastic sheathing and cluster separators), instead of representing the individual material components within the contents, an equivalent mass of material is distributed uniformly around each of the fuel rods as a wrap. The uniform poly wrap on each rod is conservative, as compared to nominal positioning between fuel rod rows (See Section 6.9.6.3 for comparison). Additionally, several melting stages of the polyethylene were evaluated for HAC; any positive reactivity from melting stages based on transport condition is included as additional uncertainty to k_u.

The evaluation of polyethylene in the package sets limits for the total polyethylene mass based on the component and its corresponding maximum average density as shown in Table 6-8. Ethafoam packaging/packing materials are the inner container wall foam and the additional cushioning foam. The polyethylene packing materials are the sheathing bag and cluster separators, dependent of fuel design. The total polyethylene mass limit per inner container compartment (2 per package) is a combination of Ethafoam packaging/packing materials and polyethylene packing materials. Other types of inserts or polyethylene packing materials are acceptable provided that their polyethylene inventory is within the limits established using Table 6-8. Fuel assemblies and WEC SVEA fuel do not utilize cluster separators as they are channeled, hence only the protective sheath bag at its nominal density (0.919 g/cm^3) is modeled as a uniform wrap around each rod. The polyethylene mass per fuel rod is calculated as a multiple of the total volume of packing material per fuel rod and the higher polyethylene density. The mass limits represent the routine packing materials for the fuel rod contents (i.e., plastic sheath).

Table 6-8 Polyethylene Mass and Density Limits per IC Compartment (2 per package)

Material	Mass (kg)	Maximum Volume Weighted Average Density
Ethafoam packaging/packing	11.21	0.08 g/cm^3
Polyethylene packing (i.e., sheathing bag & cluster separators), Fuel Bundle/Assembly		
GNF Fuels	8.11	0.947 g/cm^3
WEC Fuels (SVEA only)	0.65	0.919 cm^3
Polyethylene packing (i.e., sheathing bag), Fuel Rods		
Rod Box with maximum 118 rods	5.29	0.925 g/cm^3
Rod Pipe with maximum 142 rods	6.37	0.925 g/cm^3
Protective Case with maximum 84 rods	3.77	0.925 g/cm^3
No rod container with maximum 25 rods	1.12	0.925 g/cm^3

6.3.2.5.1 Cluster Separator and Protective Sheath

When fuel assemblies are shipped without a channel as a fuel bundle, polyethylene inserts or polyethylene cluster separators are positioned between fuel rods at various locations along the axis of the fuel bundle to avoid stressing the axial grids during transportation. The cluster separators, as shown in Figure 6-8, provide a higher volume average density polyethylene inventory, hence are chosen for the RAJ-II criticality analysis. The cluster separator is composed of Low Density Polyethylene (LDPE, 0.925 g/cm^3) fingers and a High Density Polyethylene (HDPE, 0.959 g/cm^3) holder. For a 10X10 cluster separator assembly unit, the LDPE fingers occupy an approximate volume of 38 cm^3 while the HDPE holder has an approximate volume of 85 cm^3. A weight average density of 0.949 g/cm^3 is calculated for the polyethylene cluster assembly as a mixture of the actual densities since the cluster separator assembly is modeled as a single unit. The calculation is as follows:

$$\omega_{LDPE} = \frac{V_{LPDE}\rho_{LPDE}}{V_{LPDE}\rho_{LPDE} + V_{HPDE}\rho_{HPDE}} = \frac{38\,cm^3 \times 0.925\,g/cm^3}{38\,cm^3 \times 0.925\,g/cm^3 + 85\,cm^3 \times 0.959\,g/cm^3} = 0.30$$

$$\omega_{HDPE} = 1 - \omega_{LDPE} = 1 - 0.30 = 0.70$$

$$\frac{1}{\rho_T} = \frac{\omega_{LDPE}}{\rho_{LDPE}} + \frac{\omega_{HDPE}}{\rho_{HDPE}} = \frac{0.30}{0.925} + \frac{0.70}{0.959} = 1.054$$

$$\rho_T = 0.949\,g/cm^3$$

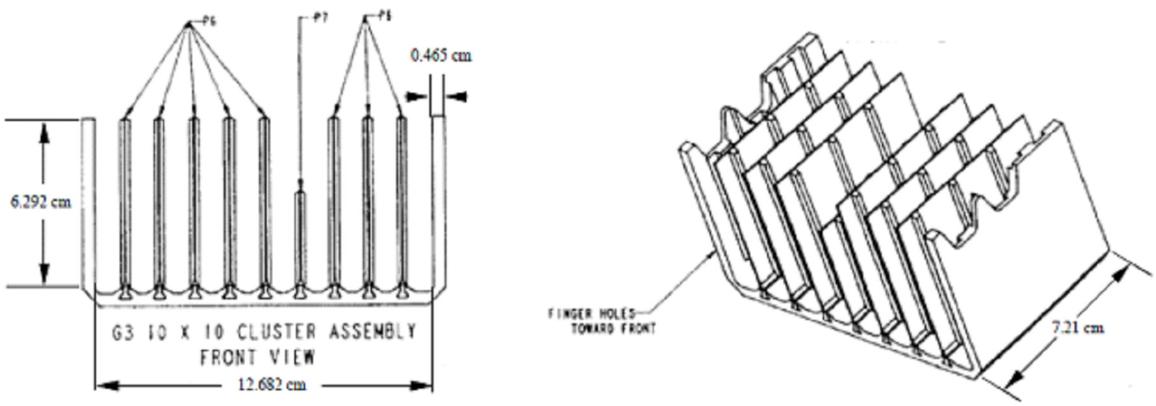

Figure 6-8 Polyethylene Cluster Separator

The fuel bundle and fuel assembly is also wrapped in a polyethylene protective sheathing. The mass of sheath varies with the fuel design, within the range of 582 g to 672 g, based on a 10 mil bag wrapped around the assembly with a length of the assembly plus 12 in.

The cluster separator assembly and protective sheath make up the normal packing materials, and are conservatively modeled as a uniform polyethylene wrap around each rod in the bundle. Modeled as a single material wrapped around each rod, a combined weight average density of 0.947 g/cm^3 is calculated, as shown below, for the polyethylene normal packing material. Additional information regarding modeling is provided in Section 6.3.4.1.2. The poly wrap composed of normal packing materials is present for NCT and HAC models, as conservative modeling of polyethylene presence.

Fuel assemblies and WEC SVEA fuel do not utilize cluster separators as they are channeled, hence only the protective sheath bag at its nominal density (0.919 g/cm^3) is modeled as a uniform wrap around each rod.

$$\omega_{CLUSTER\,SEP} = \frac{V_{CLUSTER\,SEP}\,\rho_{CLUSTER\,SEP}}{V_{CLUSTER\,SEP}\,\rho_{CLUSTER\,SEP} + V_{SHEATH}\,\rho_{SHEATH}} =$$

$$\frac{8000\,cm^3 \times 0.949\,g/cm^3}{8000\,cm^3 \times 0.949\,g/cm^3 + 700\,cm^3 \times 0.919\,g/cm^3} = 0.92$$

$$\omega_{SHEATH} = 1 - \omega_{CLUSTER\,SEP} = 1 - 0.93 = 0.08$$

$$\frac{1}{\rho_T} = \frac{\omega_{CLUSTER\,SEP}}{\rho_{CLUSTER\,SEP}} + \frac{\omega_{SHEATH}}{\rho_{SHEATH}} = \frac{0.92}{0.949} + \frac{0.08}{0.919} = 1.056$$

$$\rho_T = 0.947\,g/cm^3$$

To model fuel packing materials (i.e., plastic sheathing), for fuel rod transport, an equivalent mass of material is distributed uniformly around each of the fuel rods. This plastic sheathing has been conservatively included in the model as 0.015 inch (0.0381 cm) thick polyethylene material wrapped around the cladding at a 0.925 g/cm^3 density, representing a higher density polyethylene than typical protective sheathing. The density is applied in the model as a density multiplier of 1.00543, which is the multiplication of the standard SCALE material input for POLY(H2O).

The packing material is represented in the model as a polyethylene wrapped uniformly thick (POLYRN minus CLADR) around each fuel rod over the active fuel length. The volume of packing material assumed to be distributed within the fuel rod configuration is used to determine the total mass of polyethylene evaluated. The uniform poly thickness (POLYRN minus CLADR) around each fuel rod is determined as the fuel rod outer diameter (CLADR) plus the thickness of the polyethylene material (0.0381 cm).]

V_T is total volume of packaging material wrapped uniformly on each fuel rod

$$V_T = [\pi(POLYR_N)^2 - \pi(CLADR)^2]H, \text{ where}$$

H is fuel rod category height

$POLYR_N$ is the fuel rod outer diameter with polyethylene wrap

CLADR is the fuel rod outer diameter

6.3.2.5.2 Foam Cushion

Ethafoam packaging/packing materials are the inner container wall foam and the additional cushioning foam. The range of nominal densities includes Ethafoam 400 (0.058 g/cm^3), Ethafoam HS-45 (0.062 g/cm^3), and Suntec <15> (0.068 g/cm^3). A maximum density of 0.080 g/cm^3 is used to evaluate moderating effect of packaging materials. Specifications for the foam material are provided in Section 1.3.4. Presence of moderating material in the inner container is evaluated in Section 6.9.6.

6.3.2.6 Alumina Silicate

Fiberfrax® Duraboard® products are a family of rigid, high temperature ceramic fiber boards manufactured in a wet forming process using Fiberfrax alumina-silica fibers and binders. Board type LD is a higher quality surface finish and tighter dimensional tolerances make this board suitable for use in situations where aesthetic quality, as well as performance, is important with a nominal density of 258 kg/m^3 (16 lb/ft^3) consisting of 100% Fiberfrax, which is Unifrax's patented 2300°F/1260°C amorphous alumina-silica fiber. Specifications for Fiberfrax® Durabond® are provided in Section 1.3.4.

The arbitrary chemical compound specification is used to create a mixture that is a alumina silicate, Al_2O_3(49%) -SiO_2(51%) where density and chemical equation are known.

ATOM MX ROTH NEL ($NCZA_i$ $ATPM_i$) VF TEMP END

where

ATOM	is the standard composition component name (ATOMAL2O3SIO2).
MX	is the mixture number (26).
ROTH	is the theoretical density of the compound in g/cm^3 (3.247).
NCZA	is the element ID number. (13000 for aluminum, 8016 for oxygen, and 14000 for silicon)
ATPM	is the number of atoms of this element per molecule of user-defined compound. (2 for aluminum, 5 for oxygen, and 1 for silicon)
VF	is the fraction of this user-defined compound in the mixture (0.077). (The actual density is RHO=ROTH × VF, RHO=3.247 × 0.077=0.250)
TEMP	is the temperature in Kelvin (300).

The input data for Alumina Silicate are given below:

```
atomal2o3sio2   26  3.247  3 13000 2 8016 5 14000 1 0.077 300   end
```

6.3.2.7 Paper Honeycomb

Standard composition BALSA is used to represent the paper honeycomb for the shock absorber on the sides, bottom and top of the outer container. A density 0.08 g/cm^3 is specified for the material $C_6H_{10}O_5$.

6.3.2.8 Balsa Wood

Standard composition BALSA is used to represent the balsa wood for the shock absorber material on the ends of the outer container. The standard density is 0.125 g/cm^3 and composition is $C_6H_{10}O_5$.

6.3.2.9 Char

Char is material resulting from thermal decomposition of paper honeycomb or balsa wood. Char is produced in the absence of oxygen by the slow pyrolysis of organic material. Charring is a chemical process of incomplete combustion of a solid when subjected to high heat. The resulting residue matter is called char. By the action of heat, charring removes hydrogen and oxygen from the solid, so that the remaining char is composed primarily of carbon. The resulting char is 85% to 90% carbon with the remainder consisting of volatile chemicals and ash. Char composition evaluated from the incomplete combustion of paper honeycomb or balsa wood is assumed to be 100% of the carbon content in the nominal material composition defined in Table 6-9. Atomic density of char is assumed to be to be the carbon number densities used in the evaluation are the same that for the material prior to thermal decomposition.

6.3.2.10 Full Density Water

Standard composition H2O is used to represent the water moderator and reflector. The standard density is 0.9982 g/cm^3 and uses hydrogen in the water $S(\alpha,B)$ thermal kernel.

Table 6-9 Summary of Material Compositions

Material	Density (g/cm^3)	Constituent	Atomic Density (atoms/b-cm)
UO_2	10.96	U-235	1.23762E-03
5 wt% uranium 235		U-238	2.32178E-02
		O-16	4.89109E-02
UO_2-Gd_2O_3	11.17	U-235	1.23762E-03
	(Note: Density is	U-238	2.32178E-02
5 wt% uranium 235	greater than UO2	O-16	5.16810E-02
1.5 wt% Gd_2O_3	due to assumption	Gd-152	1.04926E-06
	that Gd_2O_3 in the	Gd-154	1.14369E-05
	mixture does not	Gd-155	7.76452E-05
	reduce UO2	Gd-156	1.07392E-04
	density)	Gd-157	8.21046E-05
		Gd-158	1.30318E-04
		Gd-160	1.14684E-04
Zircaloy-2	6.56	Zr-90	2.18914E-02
		Zr-91	4.77399E-03
98.250 wt% zirconium		Zr-92	7.29714E-03
1.45 wt% tin		Zr-94	7.39501E-03
0.135 wt% iron		Zr-96	1.19137E-03
0.100 wt% chromium		Sn-112	4.68066E-06
0.055 wt% nickel		Sn-114	3.13652E-06
0.01 wt% hafnium		Sn-115	1.73715E-06
		Sn-116	7.01133E-05
		Sn-117	3.70592E-05
		Sn-118	1.16872E-04
		Sn-119	4.14021E-05
		Sn-120	1.57260E-04
		Sn-122	2.23417E-05
		Sn-124	2.79392E-05
		Fe-54	5.63467E-06
		Fe-56	8.75953E-05
		Fe-57	2.00556E-06
		Fe-58	2.67408E-07
		Cr-50	3.30123E-06
		Cr-52	6.36617E-05
		Cr-53	7.21788E-06
		Cr-54	1.79687E-06

Table 6-9 Summary of Material Compositions (Cont)

Zircaloy-2 (continued)		Ni-58	2.52754E-05
		Ni-60	9.66291E-06
		Ni-61	4.18356E-07
		Ni-62	1.32911E-06
		Ni-64	3.36906E-07
		Hf-174	3.58562E-09
		Hf-176	1.15227E-07
		Hf-177	4.11815E-07
		Hf-178	6.04177E-07
		Hf-179	3.01657E-07
		Hf-180	7.76885E-07
Zircaloy-4	6.56	Zr-90	2.18870E-02
		Zr-91	4.77302E-03
98.230 wt% zirconium		Zr-92	7.29566E-03
1.45 wt% tin		Zr-94	7.39350E-03
0.210 wt% iron		Zr-96	1.19113E-03
0.100 wt% chromium		Sn-112	4.68066E-06
0.01 wt% hafnium		Sn-114	3.13652E-06
		Sn-115	1.73715E-06
		Sn-116	7.01133E-05
		Sn-117	3.70592E-05
		Sn-118	1.16872E-04
		Sn-119	4.14021E-05
		Sn-120	1.57260E-04
		Sn-122	2.23417E-05
		Sn-124	2.79392E-05
		Fe-54	8.76505E-06
		Fe-56	1.36259E-04
		Fe-57	3.11976E-06
		Fe-58	4.15968E-07
		Cr-50	3.30123E-06
		Cr-52	6.36617E-05
		Cr-53	7.21788E-06
		Cr-54	1.79687E-06
		Hf-174	3.58562E-09
		Hf-176	1.15227E-07
		Hf-177	4.11815E-07
		Hf-178	6.04177E-07
		Hf-179	3.01657E-07
		Hf-180	7.76885E-07

Table 6-9 Summary of Material Compositions (Cont)

Stainless steel-304 68.375 wt% iron 19 wt% chromium 9.5 wt% nickel 2 wt% manganese 1 wt% silicon 0.08 wt% carbon 0.045 wt% phosphorus	7.94	Fe-54 Fe-56 Fe-57 Fe-58 Cr-50 Cr-52 Cr-53 Cr-54 Ni-58 Ni-60 Ni-61 Ni-62 Ni-64 Mn-55 Si-28 Si-29 Si-30 P-31 C-12	3.45421E-03 5.36984E-02 1.22947E-03 1.63929E-04 7.59182E-04 1.46402E-02 1.65989E-03 4.13226E-04 5.28415E-03 2.02016E-03 8.74628E-05 2.77869E-04 7.04346E-05 1.74072E-03 1.57022E-03 7.95072E-05 5.27778E-05 6.94681E-05 3.18477E-04
Polyethylene (Sheeting, Melted Foam)	0.92	H-1 C-12	7.89975E-02 3.94988E-02
Polyethylene (Foam Cushion)	0.08	C-12 H-1	3.43467E-03 6.86935E-03
Alumina Silicate Al_2O_3(49%)-SiO_2(51%)	0.25	Al-27 Si-28 Si-29 Si-30 O-16	1.85853E-03 8.57060E-04 4.33966E-05 2.88072E-05 4.64632E-03
Paper Honeycomb $C_6H_{10}O_5$	0.08	C-12 H-1 O-16	1.78300E-03 2.97167E-03 1.48583E-03
Char (Paper Honeycomb)	0.036	C-12	1.78300E-03
Balsa Wood $C_6H_{10}O_5$	0.125	C-12 H-1 O-16	2.78594E-03 4.64323E-03 2.32161E-03
Char (Balsa wood)	0.056	C-12	2.78594E-03
Full Density Water H_2O	0.9982	H-1 O-16	6.67515E-02 3.33757E-02

6.3.3 Computer Codes and Cross-Section Libraries

6.3.3.1 Computer Codes

SCALE Version 6 is used to perform the criticality evaluation [Ref. 3]. Standardized automated procedures process cross sections to provide resonance-corrected library based on the physical characteristics of the RAJ-II package. CSAS6 (Criticality Safety Analysis Sequence with KENO-VI) and TSUNAMI (Tools for Sensitivity and Uncertainty Analysis Methodology Implementation) are used in the evaluation.

6.3.3.1.1 CSAS6 (Criticality Safety Analysis Sequence with KENO-VI)

CSAS6 calls BONAMI, to perform the unresolved resonance processing, CENTRM/PMC/WORKER, to perform the resolved resonance processing for ENDF/B-VII cross-section library, and finally KENO-VI. CENTRM/PMC is used instead of NITAWL to address a limitation in NITAWL for the resonance processing for gadolinium in the urania-gadolinia oxide fuel rods. A major limitation of the analytical model used by the Nordheim integral treatment in NITAWL is a lattice system whose fuel or moderator contains an absorber that has rapidly varying cross sections across the resonance region that may be inadequately treated. The codes utilized in CSAS6 start with an AMPX master format cross-section library and generated a self-shielded, group-averaged library applicable to the RAJ-II package. These cross sections are then used by KENO-VI Monte Carlo code to determine the neutron multiplication factor (k_{eff}). KENO-VI provides a geometry package known as SCALE Generalized Geometry Package (SGGP). This feature simplifies data input for the complex geometry of the RAJ-II package and benchmark experiments.

CSAS6

The CSAS6 sequence calculates the system k_{eff} for 3-D problems. This sequence uses the functional module BONAMI to process the required cross sections in the unresolved resonance region. By default for ENDF/B-V and ENDF/B-VII master libraries the functional modules WORKER, CENTRM, and PMC are used to process the required cross sections in the resolved resonance range.

Table 6-10 CSAS6 Parameter Values

Parameter	Value for KENO in CSAS Sequences or as Stand-Alone Code	Description
CFX	NO (default)	collect fluxes
GEN	550	number of generations to be run
NSK	3 (default)	number of generations to be omitted when collecting results
NPG	10000	number of particles per generation
PNM	0 (default)	highest order of flux moments tallies
SIG	0 (default)	deviation limit
TFM	NO (default)	perform coordinate transform for flux moment and angular flux calculations

6.3.3.1.2 TSUNAMI (Tools for Sensitivity and Uncertainty Analysis Methodology Implementation)

TSUNAMI-3D provides automated, problem-dependent cross sections using the same methods and input as the **C**riticality **S**afety **A**nalysis **S**equences (CSAS). TSUNAMI-3D sequence calls the cross-section processing codes BONAMIST and CENTRM/PMC/WORKER and accesses the SENLIB routines. After the cross sections are processed, the TSUNAMI-3D-K6 sequence performs two KENO-VI criticality calculations, one forward and one adjoint. Finally, the sequence calls the SAMS module to calculate the sensitivity coefficients that indicate the sensitivity of the calculated value of k_{eff} to changes in the cross sections and the uncertainty in the calculated value of k_{eff} due to uncertainties in the basic nuclear data. SAMS prints energy-integrated sensitivity coefficients and their statistical uncertainties to the SCALE output file and generates a separate data file containing the energy-dependent sensitivity coefficients. TSUNAMI-3D-K6 is used to generate sensitivity data to study the relative worth of urania-gadolinia rods in the fuel assembly lattice and evaluate the applicability of benchmark experiments.

TSUNAMI-3D-K6

This sequence is used for sensitivity and uncertainty calculations with KENO-VI. By default, resonance self-shielding calculations are performed with BONAMIST and CENTRM/PMC/WORKER with input to these codes generated with routines from SENLIB. The TSUNAMI-3D-K6 sequence can also be abbreviated as or TS3DK6.

Table 6-11 Tsunami Parameter Values

Parameter	Value for TSUNAMI-3D	Corresponding KENO Parameter	Description
ABK	APG x 2 (default)	NBK = NPG+25 (default)	number of positions in the neutron bank for the adjoint calculation
AGN	GEN = NSK + ASK = 550	GEN = 550	number of generations to be run for the adjoint calculation-default value produces the same number of active generations as the forward calculation
APG	NPG x 3	NPG = 10000	number of particles per generation
ASG	SIG (default SIG = 0)	SIG	if > 0.0, this is the standard deviation at which the adjoint problem will terminate
ASK	NSK x 3 (default)	NSK = 3 (default)	number of generations to be omitted when collecting results for the adjoint calculation
CFX	YES (default)	NO (default)	collect fluxes
PNM	3 (default)	0 (default)	highest order of flux moments tallies
NSK	50 (default)	3 (default)	number of generations to be omitted when collecting results
MFX	YES	NO (default)	compute mesh fluxes

Table 6-11 Tsunami Parameter Values (Cont)

Parameter	Value for TSUNAMI-3D	Corresponding KENO Parameter	Description
MSH	15	0 (default)	size of flux mesh
TFM	YES	NO (default)	coordinate transform

Sensitivity data generated by TSUNAMI-3D is used to evaluate the relative importance of materials in the package. The sensitivity coefficient for the material is the percentage change in k_{eff} for a 1% increase in the total cross section of all nuclides applied to all energy groups and regions for the mixture.

TSUNAMI-IP (**T**ools for **S**ensitivity and **U**ncertainty **A**nalysis **M**ethodology **I**mplementation – **I**ndices and **P**arameters) uses sensitivity data generated by TSUNAMI-3D and cross section-covariance data to generate several relational parameters and indices that can be used to determine the degree of similarity between benchmark experiments and RAJ-II package evaluations.

6.3.3.2 Cross-Section Libraries

A 238-group ENDF/B-VII Release 0 library is used for general-purpose criticality analyses. The 238-group and continuous-energy ENDF/B-VII.0 libraries have 417 nuclides that include 19 thermal-scattering moderators. The ENDF/B-VII.0 library cannot be used with the NITAWL module for resonance self-shielding calculations in the resolved range. The CENTRM/PMC modules must be used for resonance self-shielding calculations in the resolved region with the ENDF/B-VII.0 library [Ref. 4].

Both the LATTICECELL and MULTIREGION unit cell options are used to process the cross section data to account for the effects of energy self shielding and rod shadowing on resonance escape probabilities. The resonance correction techniques treat the fuel rods as a single fuel lump in an infinite moderator. To account for the heterogeneous effects of the lattice of fuel rods, a correction known as the Dancoff factor is applied to the leakage probability from the fuel rod. The algorithms in SCALE for LATTICECELL and MULTIREGION calculations are analytical methods used to determine the Dancoff factor for the fuel rods. The LATTICECELL and MULTIREGION calculations represent the fuel rod lattice in one dimension and account for the effects of neighboring fuel rods. The MULTIREGION treatment allows for a more general representation of the fuel to include an additional region of polyethylene on the outside of the cladding. A white outer boundary condition is used in the unit cell description for the MULTIREGION calculation to approximate an infinite array of fuel rods. Both the LATTICECELL and MULTIREGION representations are an approximation of an infinite lattice of uniformly spaced fuel rods with negligible leakage out the axial ends of the fuel.

Two dimensional effects of non-uniform fuel rod pitch as result of the fuel lattice design features such as partial length rods and water channels are not accounted for by the analytic methods for calculating Dancoff factors and one dimension methods used to calculate unit cell fluxes. Monte Carlo methods can be used to calculate a Monte Carlo Dancoff factor that accounts for two and three dimensional effects of non-uniform fuel lattice design features (i.e., non-uniform fuel rod pitch, partial length rods, and water rod/channel placement).

A secondary evaluation calculated the Dancoff factors for each fuel pin in the lattice using MC-DANCOFF module in SCALE6 [Ref. 3]. The individual Dancoff factors are applied to the unit cell calculations to account for the two dimensional rod shadowing effect for either the LATTICECELL or MULTIREGION. The Monte Carlo Dancoff factors were calculated for two cases of the SVEA pitch lattice: 1) assuming a uniform average fuel rod pitch of 12.8 mm and 2) using actual fuel rod spacing/positions described in Section 1 of the safety report. Array geometry is used to represent the uniform average fuel rod pitch and holes are used to represent the actual fuel rod positions in the lattice geometry. The reference case (CSAS6) uses the Dancoff factor calculated for the average rod pitch of 12.8 mm using the analytical Dancoff factor calculation for the lattice cell. Then Dancoff values were calculated for each rod for both the average pitch cell (FIXED PITCH) and the actual rod pitches (VARIABLE PITCH). The Monte Carlo Dancoff values were applied to the KENO-VI calculation by entering a DAN2PITCH value in the CENTRM DATA block for a LATTICECELL calculation for each fuel rod. These calculations of k_{eff} were done for both the single fuel assembly reflected with 30 cm water, and an infinite array of fuel assemblies represented by a mirror boundary condition.

Dancoff values calculated using the MC-Dancoff method show the main effect is caused by the increased moderation of the water channel. The effect of the partial length rods and non-uniform pitch within the mini-bundle quadrant are minor compared to the water channels. Increased moderation in the fuel cell results in less rod shadowing relative to the reference value (CSAS), that is, there is greater probability resonance escape with the effect of increasing the k_{eff} value. This result was consistent with the lower MC-Dancoff values being associated with rod positions near the water channels for both the single and infinite fuel assemblies, and edges of the fuel assembly for the water reflected single fuel assembly.

There is no significant effect due to the cross-section methodology. No significant effect is apparent for representation of fuel rod pitch. For a water reflected single bundle, k_{eff} varies less than 0.5% between pitch representation and methodology. For a mirror reflected infinite bundle array, k_{eff} varies less than 0.9% between pitch representation and methodology. The effects are similar for both the single and infinite fuel bundle arrangements and results are typically with two sigma. Hence LATTICECELL and MULTIREGION unit cell options are used to process the cross section data.

6.3.4 Demonstration of Maximum Reactivity

The configuration of the contents and packaging are considered to demonstrate the most reactive configuration for the package. Configurations of the contents that are consistent with each transportation case (single package, arrays of undamaged packages, and arrays of damaged packages) are evaluated. A most reactive configuration for the types of contents (fuel bundle, fuel assembly, fuel rods) is determined. The most reactive contents will be evaluated in the packaging to identify the optimum combination of internal moderation and interspersed moderation. This most reactive package configuration will be used to evaluate the individual package and package arrays.

6.3.4.1 Contents

The contents may be a fuel bundle, fuel assembly, or fuel rods. The most reactive configuration for each type of contents takes into consideration partial length fuel rods in a fuel bundle and fuel assembly, neutron absorbing BA rods in the fuel bundle and fuel assembly, rearrangement of the fuel contents in the form of lattice expansion during accident transport conditions, and partial loadings of fuel rods. Fuel rearrangement is limited by the fuel bundle and fuel assembly structure, inner container body inner wall, or fuel rod container depending on the contents category. Table 6-12 defines the confinement boundary for each of the contents categories.

Table 6-12 Confinement Boundary

Contents Category	Confinement Boundary
Fuel Assembly	Distance between two spacer grids and fuel channel
Fuel Bundle	Distance between two spacer grids and inner wall of inner container
Fuel Rods without Rod Container	Inner wall of inner container
Fuel Rods with Rod Container	Rod box, rod pipe or protective case

Three confinement boundaries are defined by the contents and packaging. First, the fuel bundle structure (tie plates, spacer grids) confines fuel rods to a nominal pitch during normal transport conditions. Second, rearrangement of the bundle lattice resulting from an impact consistent with accident transport conditions is confined by the fuel channel for fuel assembly contents. Third, the inner wall of the inner container provides confinement for fuel bundle contents or fuel rods without the rod container. Figure 6-9 shows the three confinement boundaries and the fuel rod pitch associated with each confinement dimension for each of the fuel types. An additional confinement boundary is provided by the rod container (rod box, rod pipe, or protective case) for the fuel rod contents.

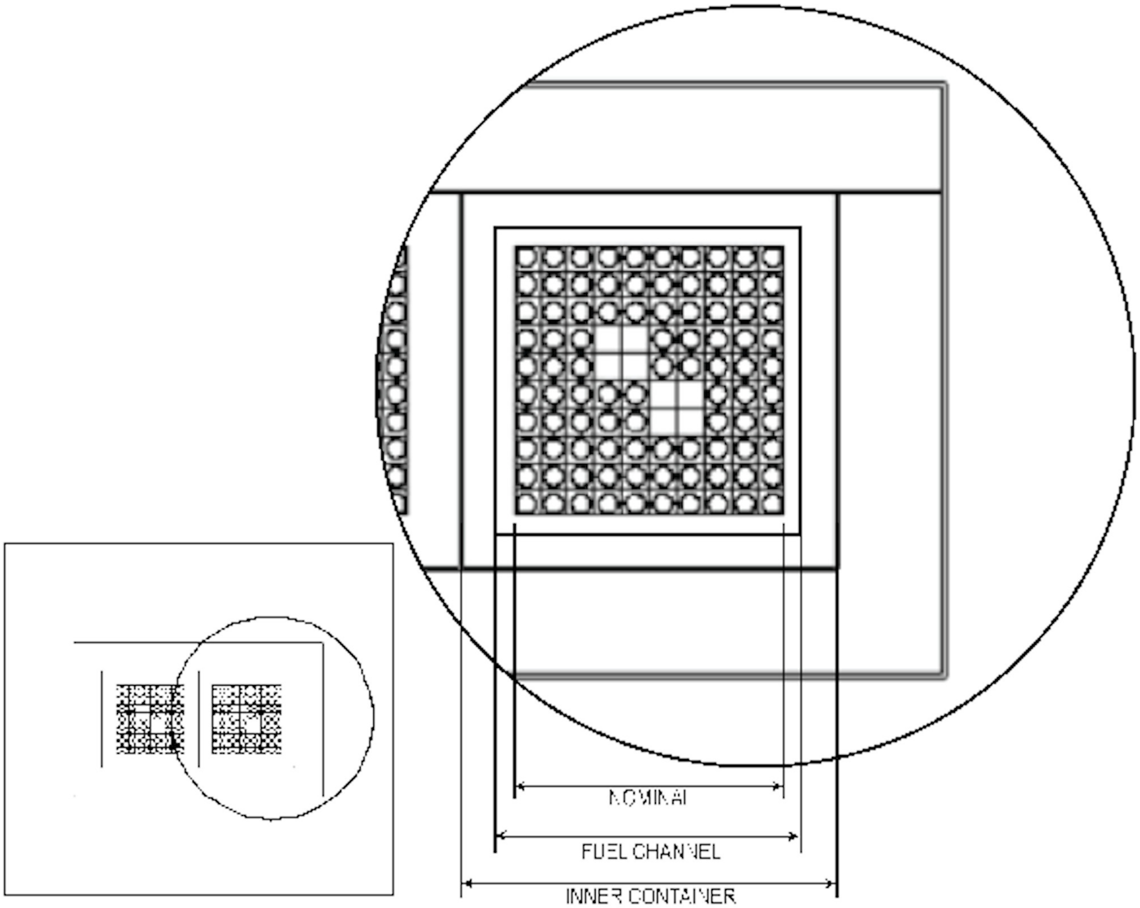

	Fuel Rod Pitch (cm)		
Fuel Type	Nominal	Fuel Channel	Inner Container
GE11, GE13	1.438	1.5378	2.0603
GE12B, GE14C, GE14G, GNF2, GNF4	1.295	1.3771	1.8416
SVEA	1.280	1.3796	1.8018

Figure 6-9 Fuel Rod Confinement Boundaries

6.3.4.1.1 Burnable Absorber Rods (Gd_2O_3)

Burnable absorber (BA) rods that are used to extend the life of the fuel bundle during the power generation cycle also provide neutron absorption for transport conditions that may result in moderation of the fuel bundle. Moderation of the fuel bundle is consistent with transport conditions for the single package, arrays of undamaged packages and arrays of damaged packages. Packaging materials, such as polyethylene foam, and packing materials, such as protective polyethylene spacers, cluster separators, and sheathing, or water from external environment are credible sources of moderation for the fuel bundle. The effectiveness of the BA rods as a neutron absorber is significant in a moderated fuel bundle, but the relative efficacy as a neutron absorber varies sensitively with the location of the BA rod within the fuel bundle lattice. In order to evaluate the relative efficacy of BA rods, neutron absorption in the gadolinium must be assessed at each location within a fuel bundle lattice.

A direct perturbation method could be used to evaluate the effectiveness of each possible arrangement for a fixed number of BA rods in the fuel bundle lattice. The rod worth of each combination would be determined by evaluating the multiplication factor with BA rods inserted and removed as $\rho_{\omega} = \frac{k_{in} - k_{out}}{k_{in}}$. The direct perturbation approach requires an exhaustive evaluation of every combination of BA rods for a specified number of BA rods. A more efficient methodology is to use analytical perturbation methods to calculate sensitivity coefficients, dk/k /ΔΣ/Σ, of the absorber nuclides for each credible BA rod locations in the bundle lattice. This evaluation can be completed for all possible BA rod locations in a single calculation sequence. Analytical perturbation methods require calculating the forward and adjoint fluxes that are then used to calculate of sensitivity coefficients for each isotope in the system. The nuclide of interest for BA rods is the gadolinium, Gd, in the Gd_2O_3. The nuclide abundance, thermal neutron cross section, and resonance integral for each of the nuclides in natural gadolinium are shown in Table 6-13.

Table 6-13 Natural Gadolinium Isotope Specifications [Ref. 9]

Nuclide	Atom Percent Abundance	Thermal Neutron Capture Cross Section (barns)	Resonance Integral (barns)
Gd-152	0.20	7.0E2	7.0E2
Gd-154	2.18	6.0E1	2.3E2
Gd-155	14.80	6.1E4	1.54E3
Gd-156	20.47	2.0	1.0E2
Gd-157	15.65	2.53E5	8.0E2
Gd-158	24.84	2.4	7.0E1
Gd-160	21.86	1.0	8.0

Thermal neutron cross sections correspond to neutron energy of 0.0253 eV. In the intermediate energy range each of the Gd nuclides have similar resonance structure. The resonance integral (RI) represents the probability of neutron reactions in the energy range above thermal energies. ^{155}Gd and ^{157}Gd have the largest thermal neutron capture cross sections. Total neutron cross section of the Gd nuclides as a function of the neutron energy in shown in Figure 6-10.

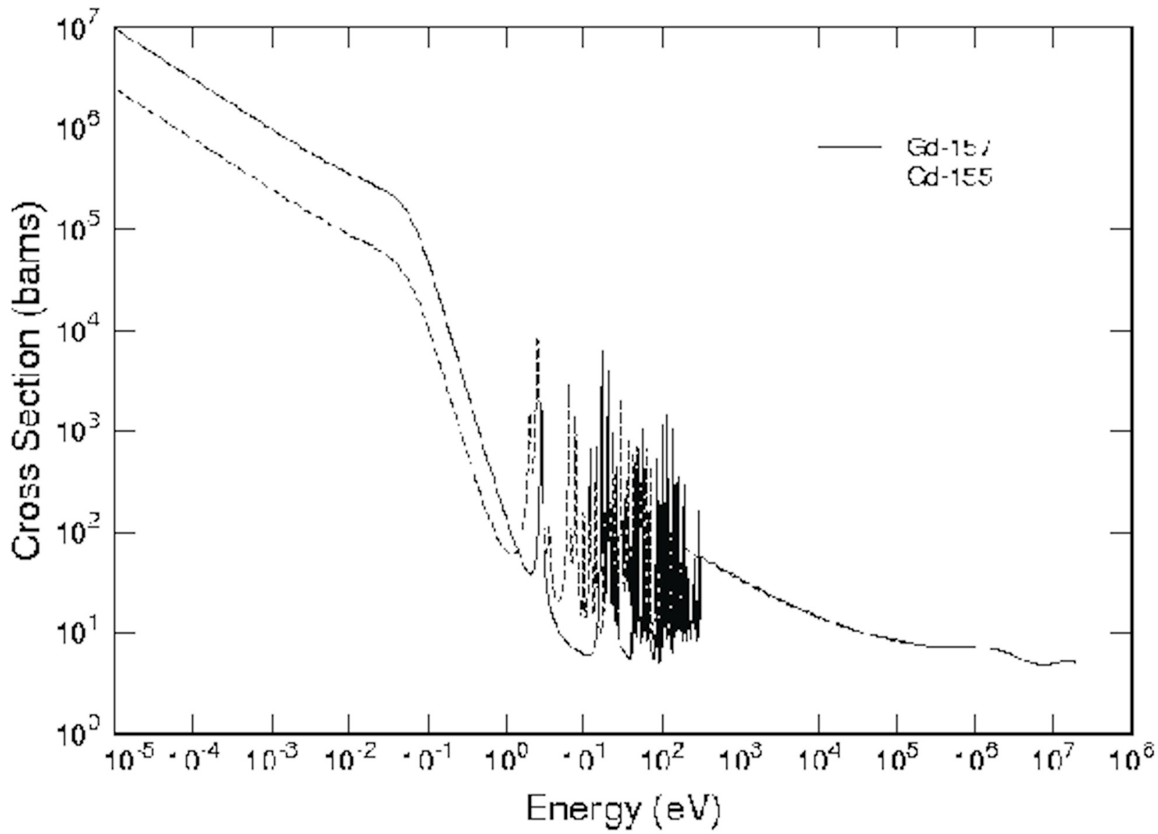

Figure 6-10 Gadolinium (n, total) Cross Section [Ref. 9]

A small quantity of Gd_2O_3 is included in the fuel mixture for each fuel rod and a unique material identifier is assigned for each fuel rod. The sensitivity coefficient for ^{157}Gd that is calculated by TSUNAMI is used to compare the worth of the BA rod in each lattice location. ^{157}Gd is used to trace the sensitivity coefficients because of its large abundance in natural gadolinium and large thermal neutron cross section.

A set of BA rod locations is chosen by considering the BA rod worth and constraints placed by design on BA rod locations. Details of the BA rod selection process are provided in Section 6.9.3. In general, the lower worth BA rods are found in lattice locations furthest from moderated regions (water hole, water channel or edge of lattice). The locations are determined for an infinite array of fuel bundles such as to represent the package array. There is no evaluation of BA rod positions for an isolated fuel bundle because the individual package is not evaluated with BA rods. An additional uncertainty exists for deviations in the methodology of the BA rod pattern selection process. Development of the uncertainty value is documented in Section 6.9.3. The single largest uncertainty of 0.015 is applied to the total uncertainty, Δk_u, for fuel bundle/assembly with BA rods.

The positions are described using a convention of letters and numbers for the purpose of this evaluation where the positions are referenced to a lattice pattern as shown in Figure 6-11. The eight BA rods are in lattice positions such that three of the four fuel lattice quadrants contain at least one

BA rod and the BA rod positions are in symmetric locations around the geometric diagonal. The BA rod locations determined for each fuel bundle design with associated water rod and partial rod arrangements as described in Section 1.3.3 are summarized in Table 6-14. The evaluated Gd_2O_3 content in a BA rod is 1.5 wt%.

	A	B	C	D	E	F	G	H	I	J
1										
2		P		P			P		P	
3			B	B	B			B		
4		P	B	B		W	W		P	
5			B		P	W	W			
6				W	W	P				
7		P		W	W				P	
8			B							
9		P		P			P		P	
10										

GE12B, GE14C, GE14G

	A	B	C	D	E	F	G	H	I	J
1	P									P
2		B								
3			B	B			B	B		
4			B		P	P				
5				P	W	W	P			
6				P	W	W	P			
7			B		P	P				
8			B							
9										
10	P									P

SVEA

	A	B	C	D	E	F	G	H	I
1									
2		P			P			P	
3							B		
4					W	W			
5		P		W	W	W		P	
6				W	W		B	B	
7			B			B		B	
8		P			P	B	B	P	
9									

GE13

	A	B	C	D	E	F	G	H	I	J
1					P	P				
2		B	B							
3		B	B	B				B		
4			B		P	W	W			
5	P			P	P	W	W			P
6	P			W	W	P	P			P
7				W	W	P				
8			B							
9										
10					P	P				

GNF2

Key: P Part length rod; B BA rod; W Water rod; (blank) Full length UO2 rod

Figure 6-11 Examples of the Most Reactive Credible Fuel Lattice Configurations

Table 6-14 Summary of BA Rod Locations for Fuel Bundle Configurations

Fuel Design	BA Rods			Water Rod			Partial Length Fuel Rod					
							Short		Long			
GE11	C-2	D-2	B-3	E-4	F-4	D-5			B-2	E-2	H-2	B-5
	D-3	G-3	B-4	E-5	F-5	D-6			H-5	B-8	E-8	H-8
	C-4	C-7		E-6								
GE12B	C-3	D-3	E-3	F-4	G-4	F-5			B-2	D-2	G-2	I-2
	H-3	C-4	D-4	G-5	D-6	E-6			B-4	I-4	E-5	F-6
	C-5	C-8		D-7	E-7				B-7	I-7	B-9	D-9
									G-9	I-9		
GE13	G-3	G-6	H-6	E-4	F-4	D-5			B-2	E-2	H-2	B-5
	C-7	F-7	H-7	E-5	F-5	D-6			H-5	B-8	E-8	H-8
	F-8	G-8		E-6								
GE14C	C-3	D-3	E-3	F-4	G-4	F-5			B-2	D-2	G-2	I-2
	H-3	C-4	D-4	G-5	D-6	E-6			B-4	I-4	E-5	F-6
	C-5	C-8		D-7	E-7				B-7	I-7	B-9	D-9
									G-9	I-9		
GE14G	C-3	D-3	E-3	F-4	G-4	F-5			B-2	D-2	G-2	I-2
	H-3	C-4	D-4	G-5	D-6	E-6			B-4	I-4	E-5	F-6
	C-5	C-8		D-7	E-7				B-7	I-7	B-9	D-9
									G-9	I-9		
GNF2	B-2	C-2	B-3	F-4	G-4	F-5	E-4	D-5	E-1	F-1	A-5	J-5
	C-3	D-3	H-3	G-5	D-6	E-6	E-5	F-6	A-6	J-6	E-10	F-10
	C-4	C-8		D-7	E-7		G-6	F-7				
SVEA	B-2	C-3	D-3	E-5	F-5	E-6	E-4	F-4	A-1	J-1	A-10	J-10
	G-3	H-4	C-4	F-6			D-5	G-5				
	C-7	C-8					D-6	G-6				
							E-7	F-7				

6.3.4.1.2 Lattice Expansion

Fuel Bundles

Tests demonstrate that virtually all fuel rod deformations induced from an axial impact are due to interactions between the end of the fuel rod and the deformed nozzles. BWR fuels are designed to be under moderated, hence an impact event which increases the pin pitch can result in a general increase in reactivity. It has been observed that for end impacts on BWR designs of fuel, the lattice may contract near the impacted end but expand slightly in the adjacent intra-grid length, as shown in Figure 6-12. A mean lattice pitch change of less than 5 mm is predicted by static analysis methods between the second and third spacer grids from the bottom of the fuel assembly. Nominal dimension between the second and third grid is less than 50 cm for BWR fuel assemblies. Analyzed performance of the lower tie plate and cladding during an end impact as evaluated in Section 2.12.6 of the structural analysis, and predicts responses that are consistent with the testing. The analysis concludes that the lower tie plate will not fail during an end drop and the cladding will not rupture due to the rod bowing. The testing and analytical results justify the assumptions that the individual fuel pellets will be contained in the cladding and no water can lead into the void space between fuel pellet and cladding.

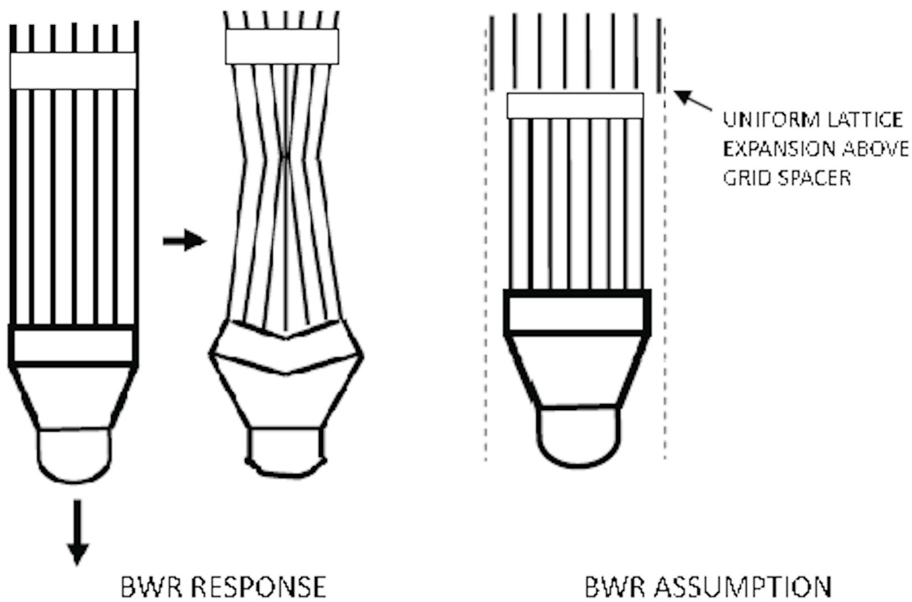

Figure 6-12 Effect of End Impact of BWR Fuel Bundle

The criticality analysis ignores lattice contraction near the end but does consider the uniform lattice expansion. Each BWR fuel assembly type is evaluated to determine the maximum reactivity due to an increase in lattice pitch that is confined to a length of 50 cm at the end of the fuel bundle with 20 cm of close fitting, full density water. Each fuel assembly type is evaluated using the spacing provided by the structure of the packaging, but not including the packaging materials. The individual package is assessed using fuel bundles with no BA rods, with all void space filled with water and the package closely reflected by 20 cm of water. The package array is assessed as an infinite array using fuel bundles with the BA rod configuration determined previously in Section 6.3.4.1.1 and filling only the void space within the fuel bundle with water. This assessment is done for a range of fuel rod pitch that includes the dimension that is associated with each confinement boundary (nominal, fuel channel, inner container) for the fuel bundle.

In addition to the water moderation, polyethylene packing materials provide moderation of the contents consistent with the transport condition. Cluster separators, spacers, and wrap are considered for all transport conditions. The effect of moderation by packing materials that are part of the contents is evaluated by assuming that these materials are uniformly distributed on the fuel rod outer surface regardless of the condition of transport. The additional effect of foam cushion that may melt during accident conditions and provide moderation within the fuel bundle is considered in the evaluation of packaging materials. The lattice expansion is evaluated with and without packing materials (cluster separators, fuel rod spacers and wrap) to determine if there is any interaction for the effect on reactivity.

Polyethylene inserts or cluster separators, as utilized by GNF only, are positioned between fuel rods at various locations along the axis of the fuel bundle to avoid stressing the axial grids during transportation. Since the polyethylene cluster separators provide a higher volume average density polyethylene inventory than the inserts/spacers, they are chosen for the RAJ-II criticality analysis. Other types of inserts are acceptable provided that their polyethylene inventory is within the limits established using the cluster separators.

As a maximum limit, 64 separator cluster pieces (32 separator cluster units) are inserted into the bundle. The packing material is represented in the model as a polyethylene wrapped uniformly thick ($POLYR_N$ minus *CLADR*) around each fuel rod (*FUELR*) over the active fuel length. The volume of packing material assumed to be distributed within the fuel bundle is used to determine the uniform poly outer radius ($POLYR_N$) around each fuel rod. This volume of material consists of the cluster separators (GNF fuel bundles only) and protective sheath for all transport conditions.

The density specified in the material composition is an apparent density of the polyethylene that is a volume weighted average of the cluster separator and plastic sheath. The apparent density is determined as follows:

$$\textit{Apparent polyethylene density for } POLYR_N$$

$$\rho_{POLYR\ N} = \frac{\rho_{CLUSTER\ SEPARATOR} V_{CLUSTER\ SEPARATOR} + \rho_{PLASTIC\ SHEATH} V_{PLASTIC\ SHEATH}}{V_{POLYR_N}}, \textit{ where}$$

$$V_{POLYR_N} \textit{ is total volume of packing material wrapped uniformly on each fuel rod}$$

The volume of packing material is used to determine a uniform poly outer radius ($POLYR_N$) around each fuel rod is calculated as follows:

$$Area\ of\ fuel\,rod\ with\ polyethylene = Area\ of\ polyethylene + Area\ of\ fuel\,rod$$

$$\pi(POLYR_N)^2 = \frac{V_{POLYN}}{\sum_i N_i H_i} + \pi(FUELR)^2,\ where$$

N is number of fuel rods with active fuel height H

V_{POLYN} is total volume of packing material wrapped uniformly on each fuel rod

$$POLYR_N = \sqrt{\frac{V_{POLYN}}{\pi \sum_i N_i H_i} + (FUELR)^2}$$

The outer radius for the polyethylene ($POLYR_N$) used to represent the routine packing material for the contents (cluster separators and plastic sheath) and apparent densities are summarized in Table 6-15.

Table 6-15 Polyethylene for Routine and Normal Transport Conditions

Fuel Type	Cluster Separator Volume ρ=0.949 g/cm^3 (cm^3)	Plastic Sheath Volume ρ=0.919 g/cm^3 (cm^3)	Total $V_{POLY\text{-}N}$ (cm^3)	$\sum_i N_i H_i$	Apparent Polyethylene Density, $\rho_{POLYR\text{-}N}$ (g/ cm^3)	$POLYR_N$ (cm)
GE12B	7872	730.88	8602.88	35263.4	0.947	0.5838
GE14C		689.81	8561.81	33131.2	0.947	0.5877
GE14G		672.71	8544.71	32297.8	0.947	0.5894
GNF2		689.81	8561.81	32614	0.947	0.5888
SVEA	0	704.89	704.89	34840	0.919	0.4985

In addition to the geometry representation in the model, the effect of polyethylene packing materials on resonance self shielding is accounted for in the cross-section processing by specifying a cylindrical MULTIREGION unit cell as shown in Figure 6-13. The lattice effects are approximated by applying a white boundary condition to the cylindrical MULTIREGION unit to represent a uniform lattice (See Section 6.3.3.2 for further discussion of lattice cell cross section processing).

Although the geometric lattice cell (pitch type) may be hexagonal or square (e.g., loose rod stacking or fuel bundle spacing), the moderator region of the lattice cell is converted to a cylindrical geometry for cross-section processing by the MULTIREGION unit celldata. The moderator cylindrical radius is calculated preserving area by setting the moderator lattice cell area (i.e., square or hexagonal region) equal to the cylindrical area and solving for the radius (MODR). Conversion equations are shown below for a square and hexagonal geometry, respectively

$$\pi R^2 = P^2$$

$$\pi R^2 = 2\sqrt{3}\,(P/2)^2$$

where

R is the radius of the equivalent circle (MODR)

P is the pitch of the cell (i.e., square or hexagonal)

This technique is always applied when polyethylene packing materials are present to ensure the additional hydrogen content is accounted for in the cross-section processing of the model. The corrected radius preserves the Dancoff factor calculations. Hence the nominal lattice and expanded lattice regions both incorporate the polyethylene packing materials. The NCT and HAC models utilize the maximum allowable polyethylene mass of normal packing materials, including cluster separators and sheathing, and applies the mass uniformly over the full axial length of the fuel.

The results for the lattice expansion evaluation are in Section 6.9.4.

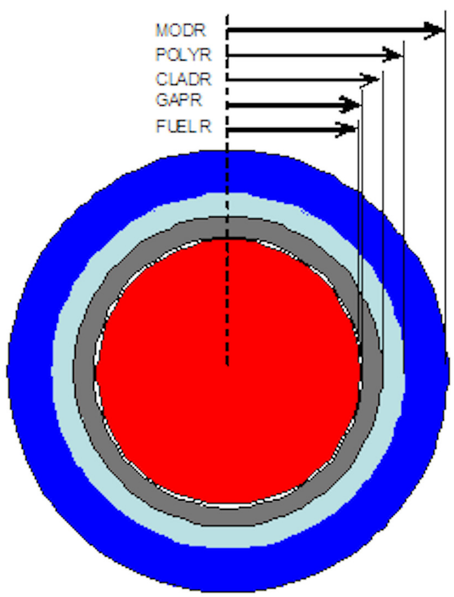


```
CELLTYPE    CS          RIGHT_BDY          FUELR     GAPR     CLADR      POLYR      MODR
multiregion cylindrical right_bdy=white end  1 0.444  0 0.453  3 0.513  21 0.5888  4 0.7306  end zone
```

Figure 6-13 SCALE Unit Cell Demonstration for Re-distribution of Polyethylene

Fuel Rods

The evaluation for fuel rods determines a pitch for the maximum k_{eff} for each fuel rod category, as defined in Section 6.9.5. The detailed evaluation used to determine the optimum pitch is in Section 6.9.5.

The optimum fuel rod configuration is most sensitive to the pitch and the maximum k_{eff} value is not as sensitive to differences in the dimensions for fuel rod parameters characterized by the fuel designs as shown in Table 6-16. The k_{eff} values for the optimum pitch of the fuel rod configurations are not significantly different.

As shown in Table 6-16, the BWR_G3 fuel rod category at a pitch of 0.9 cm is the most reactive fuel rod configuration. Hence, the BWR_G3 rod configuration is evaluated in the package with confinement provided by the inner container (without rod container) or the rod container (rod pipe, rod box, or protective case) for the package transport evaluations. Additionally the minimum (PWR_W5) and maximum (PWR_W3) fuel rod categories as based on fuel pellet diameter are evaluated for the fuel rod contents.

The pitch type is typically modeled to fit the container shape (i.e., square pitch in square containers and hexagonal pitch for the cylindrical container). For comparison, both pitch types (i.e., hexagonal pitch and square pitch) were modeled for varying pitches to encompass the peak reactivity point and ±0.5 cm half-pitch steps. The package array model is used to compare pitch types, as the package array for fuel rods is a more reactive case than the individual package for fuel rods. The resultant more reactive pitch type is applied to the individual package analysis.

Although the geometric lattice cell (pitch type) may be hexagonal or square (e.g., loose rod stacking or fuel bundle spacing), the moderator region of the lattice cell is converted to a cylindrical geometry for cross-section processing by the MULTIREGION unit celldata. The moderator cylindrical radius is calculated preserving area by setting the moderator lattice cell area (i.e., square or hexagonal region) equal to the cylindrical area and solving for the radius (MODR). Conversion equations are shown below for a square and hexagonal geometry, respectively:

$$\pi R^2 = P^2$$

$$\pi R^2 = 2\sqrt{3}\,(P/2)^2$$

where

R is the radius of the equivalent circle (MODR)

P is the pitch of the cell (i.e., square or hexagonal).

Table 6-16 Optimum Pitch for Fuel Rod Configurations

Fuel Category	Half-Pitch	Moderator/Fuel	k_{inf}
BWR_W1	0.85	3.0850	1.52685
BWR_G1	0.95	2.7851	1.52663
BWR_G2	0.90	3.2838	1.52616
BWR_G3	0.90	3.1957	1.52738
PWR_W1	0.90	3.3195	1.52656
PWR_W2	0.95	3.2784	1.52689
PWR_W3	0.95	2.9164	1.52731
PWR_W4	0.85	3.4037	1.52624
PWR_W5	0.85	3.2942	1.52641
PWR_W6	0.85	3.2942	1.52604
PWR_W7	0.85	3.2847	1.52608

In addition to the water moderation, polyethylene packing materials provide moderation of the contents consistent with the transport condition. For fuel rod transport polyethylene sheathing is considered for all transport conditions. The effect of moderation by packing materials that are part of the contents is evaluated by assuming that an equivalent mass of material is distributed uniformly around each of the fuel rods. This plastic sheathing has been conservatively included in the model as 0.015 inch (0.0381 cm) thick high density (0.925 g/cm^3) polyethylene wrapped around the cladding. This results in a maximum of 38.5 g of polyethylene per rod for the minimum fuel category of PWR_W5.

The MULTIREGION technique is always applied when polyethylene packing materials are present to ensure the additional hydrogen content is accounted for in the cross-section processing of the model (See Section 6.3.3.2 for further discussion of lattice cell cross section processing). The corrected radius preserves the Dancoff factor calculations. The NCT and HAC models utilize the maximum allowable polyethylene mass of normal packing materials, and applies the mass uniformly over the full axial length of the fuel even as the lattice size expands.

6.3.4.1.3 Summary of Most Reactive Configuration for Contents

Fuel Bundle or Fuel Assembly

Structural features of the fuel bundle (grids, tie plates, handle) are considered to limit the lattice expansion, but only materials in the active length of the fuel rod (fuel pellet and cladding) are considered in the evaluation of reactivity. The other fuel bundle components are fabricated from materials (stainless steel, inconel, and zircalloy) that absorb neutrons by radiative capture and the volume of the structure displaces moderator in the fuel lattice. Representing the fuel bundle components as water results in an increase in reactivity; this is due to both a decrease in neutron absorption and an increase in fuel rod lattice moderation. Partial length rods are a feature of the fuel bundle design, and as such are considered specific to the fuel bundle design in the demonstration of the most reactive configuration.

The most reactive configuration for the fuel bundle and fuel assembly takes into consideration the Gd_2O_3 content in the BA rods, position of neutron absorbing BA rods in the fuel bundle, position of partial length rods, moderation by packing materials and lattice expansion as result of fuel bundle rearrangement during accident transport conditions.

The fuel rod lattice moderation is less than optimum for the extent of lattice expansion that is considered as limited by the confinement system. The 10X10 fuel lattice is the most reactive configuration for the fuel bundle within the range of fuel rod pitch limited by the confinement system for lattice expansion within a maximum credible fuel length of 50 cm. Lattice expansion is uniform along a 50 cm axial length at one end of the fuel bundle. The maximum lattice pitch is a value that depends on the condition of transport and confinement boundary. The lattice pitch for an undamaged package is the nominal fuel rod pitch. For a damaged package the maximum fuel rod pitch is limited to the fuel channel for a fuel assembly or the inner container for a fuel bundle.

Although the reactivity of the 10X10 fuel bundle configurations are similar, three of the fuel bundle configurations that represent design differences are used in the package evaluation. These differences are characterized by partial length rod and water rod arrangements as follows:

GE14 is a GNF fuel design with only long partial length rods and central water rods.

GNF2 is a GNF fuel design with long and short partial length rods and central water rods.

SVEA is a Westinghouse fuel design with water cross and central water channel.

The GE14G, GNF2, and SVEA fuel bundle configurations are used for the evaluations without BA rods (i.e., individual package and small array sizes) and GE14C, GNF2, and SVEA fuel bundle configurations are used for the evaluations with BA rods (i.e., large array sizes). The selection of these fuels is based on the bundle lattice expansion comparison in Section 6.9.4. The GNF fuel designs represent the two most reactive fuel designs at nominal and peak reactivity for expanded lattice pitches. While, the Westinghouse fuel design represents a major design difference in water rods/channel and not a most reactive configuration. The GE14 designs have similar fuel assembly dimensions except fuel rod heights, as defined in Table 1-10.

Fuel Rods

The BWR_G3 fuel rod category is used to represent the most reactive fuel rod configuration for the evaluation of the package transport conditions. Additionally, the minimum (PWR_W5) and maximum (PWR_W3) fuel rod categories as based on fuel pellet diameter are evaluated for the fuel rod contents. The selection of these fuel rod categories are based on the lattice expansion comparison in Section 6.9.5. These rod configurations are evaluated in the package with lattice expansion confinement provided by only the inner container (without rod container) or the rod container (rod pipe, rod box, or protective case).

The most reactive configuration for loose fuel rods takes into consideration moderation by packing materials and lattice expansion as result of rearrangement during accident transport conditions. For fuel rod transport polyethylene sheathing is considered present for all transport conditions. For evaluating rearrangement, the package array model is used to compare pitch types, as the package array for fuel rods is a more reactive case than the individual package for fuel rods. The resultant more reactive pitch type is applied to the individual package analysis.

6.3.4.2 Packaging Materials

Interspersed moderation (moderation between packages) is limited to moderators no more effective than water from sources external to the package. There are packaging materials that are internal moderators (within the package) that may be more effective than water either in their normal condition or as degraded by combustion or melting in a thermal event such as a fire. Water can leak into all void spaces of the package, including those within the containment system. Four regions of the package, as shown in Figure 6-14, are considered to assess the effect of packaging materials inside the containment system and surrounding the confinement system.

The reference case for the individual package is to fill all regions that are normally void space or occupied by packaging material with full density water. The reference case for the package array is void in all space normally occupied by packaging material. In both the individual package and package array the void space within the fuel bundle is filled with full density water. Void space within the fuel bundle contents is assumed to always contain water, because the low enriched uranium requires moderation to have any significant neutron multiplication. Additional moderation from the redistribution of the normal packing materials (polyethylene sleeves and cluster separators) are present for all transport conditions.

Accident transport conditions (impact, fire, or water submersion) may degrade the packaging material or damage the package resulting in water filling the void space or saturating the packaging material. Water or void is replaced by nominal packaging material (AlSi insulation, polyethylene foam cushion, paper honeycomb and balsa wood impact limiter) to assess the effect on neutron multiplication.

Two regions (2 and 3) are within the boundary of the confinement system. The polyethylene foam cushion, represented as region 2 for normal transport conditions, may redistribute from region 2 to the fuel bundle due to melting at elevated temperature during a fire event. Region 3 defines polyethylene material from the normal package configuration of the polyethylene foam cushion material that is redistributed from region 2. Polyethylene material in the fuel bundle has the greatest effect on neutron multiplication when distributed uniformly as a full density, close fitting layer on each fuel rod [Ref. 10].

The remaining two regions (1 and 4) are outside the boundary of the confinement system. Decomposition of the impact absorber material, region 4, is assessed by either assuming formation of char at elevated temperatures during a fire event or assuming complete combustion. The effect of material in region 1 is assessed as present or by assuming saturation of the thermal insulation during water immersion. Although decomposition of the impact absorber or saturation of thermal insulation is possible during accident transport conditions, it is important to assess package configuration assuming that a fire or water immersion does not have any effect on nominal packaging materials inside the containment or surrounding the confinement system.

A packaging configuration consistent with the transport condition that results in the maximum neutron multiplication is identified for further use in the package evaluation. The details of the packaging material evaluation are in Section 6.9.6.

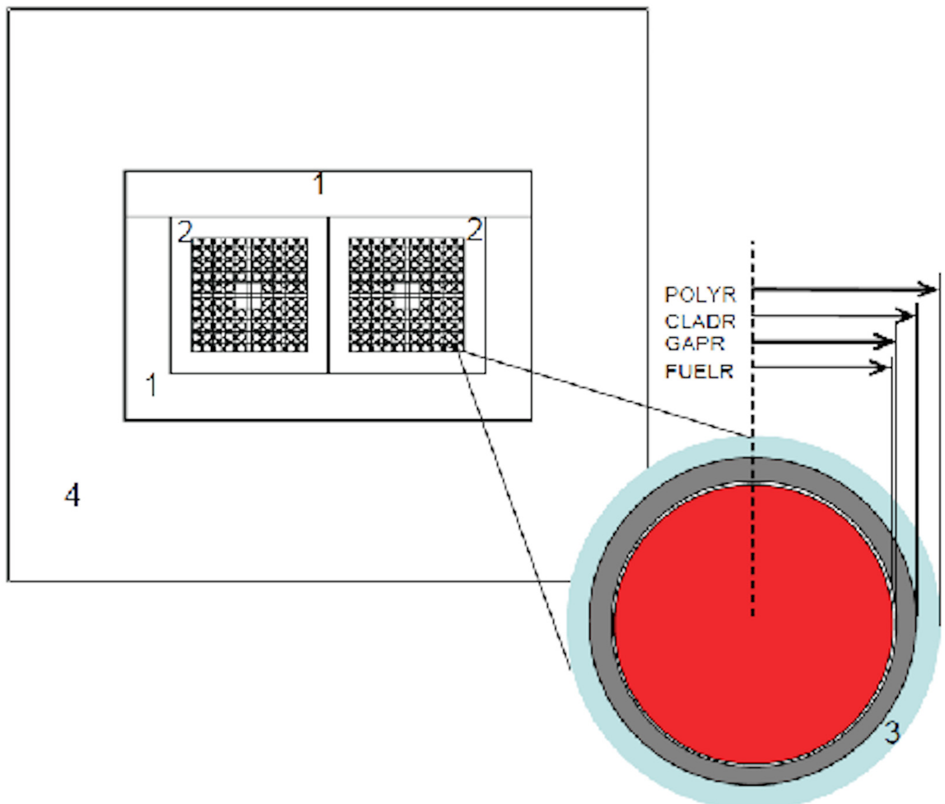

Region	Nominal Packaging Material
1	Alumina Silica (AlSi)
2	Polyethylene foam cushion
3	Redistributed polyethylene foam cushion
4	Impact absorber (paper honeycomb, balsa wood, char)

Figure 6-14 Packaging Material Regions

6.3.4.2.1 Impact Absorber

Thermal testing and analysis demonstrate that the impact absorber material (paper honeycomb, balsa wood) may undergo complete or partial combustion during a fire. The chemical composition of impact absorber material is carbon (C), hydrogen (H), and oxygen (O). Char is produced in the absence of oxygen by the slow pyrolysis of the impact absorber material. Charring is a chemical process of incomplete combustion a solid when subjected to high heat. The resulting residue matter is called char. By the action of heat, charring removes hydrogen and oxygen from the solid, so that the remaining char is composed primarily of carbon. The resulting char is 85% to 90% carbon with the remainder consisting of volatile chemicals and ash.

A void space with some residual ash would result in the volume normally occupied by impact absorber when complete combustion occurs, but in the absence of oxygen a char may form. Water or void is assumed to fill the void space left by the complete combustion of impact absorber material. Carbon at the density of the original material is assumed to remain if incomplete combustion of the impact absorber material were to occur.

The number of scattering collisions necessary to slow a neutron to thermal energies is inversely proportional to ξ, the average logarithmic energy decrement. Better moderators are characterized by large values ξ, large scattering cross sections, Σ_s, and small absorption cross section, Σ_a. A measure of the moderating power of a material is the moderating ration,

$$\text{Moderating ratio} = \xi\Sigma_s/\Sigma_a$$

Carbon is a better moderator than the water because moderating ratio for carbon almost 3 times larger than for water (H_2O).

The effect on neutron multiplication would depend on the ratio of scattering to absorption in the packaging material and interspersed moderation. The presence of materials with a moderating ratio larger than water, such as carbon, will cause the slowing down of neutrons to be more effective due to a higher moderating ratio. Therefore, more neutrons are available to be absorbed by stainless steel packaging structure because of higher absorption cross sections of elements in stainless steel. Stainless steel in the packaging structure is assumed to remain intact for transport conditions. As a result, k_{eff} is decreased for the HAC array.

The neutron multiplication increases for a single package for normal and accident transport conditions where the package is subject to moderation and close reflection with full density water. The damaged package array multiplication factor decreases when carbon or water is an interspersed moderator or internal moderator.

6.3.4.2.2 Polyethylene Foam

Polyethylene foam that may melt and provide moderation within the fuel bundle is considered for accident transport conditions. The effect of moderation by packing materials that are part of the contents is evaluated by assuming that these materials are uniformly distributed on the fuel rod outer surface regardless of the condition of transport.

Thermal evaluation demonstrates that temperatures for a fire during the accident transport condition in the inner container is above the melting point range of 120-130°C (248 to 266°F) and ignition temperature of 349°C (660°F) for polyethylene materials. The polyethylene foam either remains in place, melts, or combusts depending on the duration of the fire. Melting polyethylene may slump into the void space in between fuel rods in a fuel bundle, and water may fill the remaining void space during immersion in water. The effect of polyethylene is considered in the demonstration of maximum reactivity for the contents. If temperatures in the inner container do not exceed the melt temperature of polyethylene either due to a short duration fire or absence of a fire in the accident condition, the foam would remain intact.

The assessment of the fuel types for an accident transport condition is done assuming the thermal input is sufficient to melt the polyethylene. An increase in the dimension for the polyethylene radius ($\Delta POLYR$) from normal packing material ($POLYR_N$) is determined assuming that all the foam cushion material redistributes uniformly onto the fuel rods. The nominal volume of packaging foam cushion is 53,190 cm^3 ($V_{FOAM\ CUSHION}$) with a maximum density assumed to be 0.08 g/ cm^3. Assuming an apparent density that is the same as for the normal packing materials ($\rho_{POLYR-N}$), the volume of polyethylene for the accident condition ($V_{POLYR-A}$) is determined as follows:

$$Equivalent\ volume\ of\ polyethylene\ foam\ cushion$$

$$V_{POLYR} = \frac{\rho_{POLY\ FOAM} V_{POLY\ FOAM}}{\rho_{POLYR}},\ where$$

$$V_{POLY\ FOAM} = 53190\ cm^3\ is\ total\ volume\ of\ packaging\ foam\ material$$

$$\rho_{POLY\ FOAM} = 0.080\ g/cm^3$$

$$V_{POLYR}\ is\ total\ volume\ of\ packaging\ foam\ cushion\ wrapped\ uniformly\ on\ each\ fuel\ rod$$

The volume of packing material is used to determine a uniform poly thickness (equals $\boldsymbol{POLYR_A}$ minus clad outer radius) around each fuel rod is calculated as follows:

$$Area\ of\ fuel\ rod\ with\ polyethylene = Area\ of\ polyethylene + Area\ of\ fuel\ rod$$

$$\pi(POLYR_A)^2 = \frac{V_{POLYR_A}}{\sum_i N_i H_i} + \pi(FUELR)^2,\ where$$

$$N\ is\ number\ of\ fuel\ rods\ with\ active\ fuel\ height\ H$$

$$POLYR_A = \sqrt{\frac{V_{POLYR_A}}{\pi \sum_i N_i H_i} + (FUELR)^2}$$

The outer radius for the polyethylene ($POLYR_A$) used to represent the packaging and packing materials for an accident condition is summarized in Table 6-17. The outer radius for the polyethylene ($POLYR_N$) used to represent the routine packing material for the contents (cluster separators and plastic sheath) and apparent densities are summarized in Table 6-15.

Table 6-17 Polyethylene for Accident Transport Conditions

Fuel Type	Foam Cushion $V_{FOAM\ CUSHION}$ (cm^3)	Normal Condition (from Table 6-15) $V_{POLY\text{-}N}$ (cm^3)	Accident Condition $V_{POLYR\text{-}A}$ (cm^3)	$\sum_i N_i H_i$	$POLYR_A$ (cm)	$\Delta POLYR$[1] (cm)
GE12B	4495.92	8602.88	13098.80	35263.4	0.6175	0.0337
GE14C	4495.29	8561.81	13057.10	33131.2	0.6233	0.0356
GE14G	4495.03	8544.71	13039.74	32297.8	0.6257	0.0363
GNF2	4495.29	8561.81	13057.10	32614	0.6249	0.0360
SVEA	4630.22	704.89	5335.11	34840	0.5391	0.0406

Note 1: ΔPOLYR is the increase in polyethylene radius from normal packing materials ($POLYR_A$ - $POLYR_N$) that is attributed to the melting of the polyethylene foam cushion packing material.

6.3.4.2.3 Structural Stainless Steel

Stainless steel is present in large quantities as the main structural packaging material. A significant amount of neutron elastic scatter occurs due to the iron and neutron absorption occurs due to chromium and nickel content. Only the sheet stainless steel is included in the model and all other structural stainless steel (angle, channel, and inner container support) is omitted.

6.3.4.2.4 Summary of Most Reactive Configuration for Packaging Materials

The packaging configurations are evaluated using the most reactive of the GNF fuel types and SVEA fuel bundle in the packaging configurations for the individual package and package array. The evaluation of effect of packaging materials is in Section 6.9.6 and the effects are summarized in Table 6-18 as an average Δk_u for the fuel types and confinement boundaries (nominal, fuel channel, and inner container). The effects show no significant dependence on the fuel type, but there is a small dependence on the pitch associated with the confinement boundary. However, the effect of the packaging configuration on Δk_u differs significantly between the individual package and package array.

Table 6-18 Summary of Effects of Packaging Materials

Packaging Configuration	Individual Package	Δk_u	Package Array	Δk_u
Reference	Water (1,2,3,4)	–	Void (1,2,4)	–
Thermal Insulator	AlSi (1) Water (2,3,4)	-0.0419	AlSi (1) Void (2,4)	-0.0032
Normal Condition Polyethylene	Poly (2), Water (1,3,4)	-0.0762	Poly (2), Void (1,4)	-0.0141
Accident Condition Polyethylene	Pack Material (3), Water (1,2,4)	+0.0042	Pack Material (3), Void (1,2,4)	+0.0031
Accident Condition Impact Limiter	Char (4), Water (1,2,3)	-0.0025	Char (4), Void (1,2)	-0.0065

The *Reference* packaging configuration is used for the package evaluations are *Water (1,2,3,4)* for the individual package and *Void (1,2,4)* for the package array. With exception of the *Accident Condition Polyethylene* packaging configuration, the effect of the packaging materials relative to water or void is to decrease k_{eff}.

Evaluating the effects of package materials shows that the presence of polyethylene has the largest material impact on the k_{eff} of the system. Section 6.9.6.3 further evaluates the modeling techniques of realistic representations of the package through NCT and HAC time varied phases. Summarized maximum reactivity results are shown in Table 6-19 for the polyethylene redistribution analysis.

Instead of including the polyethylene redistribution explicitly in the model, an uncertainty, Δk_u, listed in Table 6-19 will be added to k_u for the NCT package evaluations and HAC package evaluations.

Table 6-19 Polyethylene Redistribution Summary Results

Analysis Condition	Analysis Model	Fuel Bundle		
		k_{eff}	σ	Δk_u
NCT package array	Stage 1: nominal - plates + ethafoam Horizontal / vertical	0.84605	0.00033	0.01862
NCT individual package Void	Stage 1: nominal - plates + ethafoam Horizontal / vertical	0.54980	0.00034	0.01142
HAC package array (Intermediate state)	Stage 3: full melt Vertical	0.90206	0.00034	0.02789
HAC individual package (Intermediate state)	Stage 3: full melt Vertical	0.8366	0.0004	-0.07762

6.3.4.3 Uncertainty Evaluation for Material and Fabrication Tolerances

Uncertainties are represented by material and fabrication tolerances and geometric or material representations in the models. The combination of these uncertainties represents the total uncertainty, Δk_u, for the individual or package array analysis. Models chosen for uncertainty analyses represent the most reactive contents configuration for the package analysis, whether individual or package array.

For the tolerance values being studied in this system, the reactivity effect on the system must be determined based on a change in the total amount of the material of interest present. This can be accomplished by the study of an explicit change in material volume due to tolerance value. Tolerances for each parameter evaluated are displayed in Table 6-20.

Direct perturbations of each parameter are calculated individually to determine the conservative uncertainty for a particular parameter tolerance. Any positive reactivity from the parameter variation is statistically combined to the total uncertainty Δk_u. The total absolute uncertainty, Δku, is the combined uncertainty of material tolerances and material and geometric representation evaluations.

Uncertainty values are the positive reactivity changes from variations of material and fabrication tolerances and geometric or material representations, as compared to the representative package case used for determining the most reactive case per transport condition. The uncertainty in k_{eff}, $\Delta k_u (x_i)$, for each parameter is calculated based on a statistical error propagation method, as follows:

$$\Delta k_u(x_i) = k_{pert} - k_{base} + \sqrt{\sigma_{pert}^2 + \sigma_{base}^2}$$

where

$\Delta k_u (x_i)$ is the uncertainty in k_{eff} for each parameter x

k_{pert} is the k_{eff} for each perturbed parameter x

σ_{pert} is the σ, standard deviation, for each perturbed parameter x

k_{base} is the k_{eff} for each base case parameter x

σ_{base} is the σ, standard deviation, for each base case parameter x

The statistical combination of the uncertainties results in the Δk_u value used to define the maximum k_{eff}. The total uncertainty is calculated as the square root of the sum of the constituent uncertainties squared; this assumes the parameters accounting for uncertainty in k_{eff} are independent. Hence, the Δk_u value is simply the root-sum-square (rss) combination of system uncertainties, as expressed in the following equation.

$$\Delta k_u^2 = \sum_{i=1}^{N} \Delta k_u(x_i)^2$$

where

$\Delta k_u\ (x_i)$ is the uncertainty in k_{eff} for each parameter x

Δk_u is the total combined uncertainty

The total uncertainty in k_{eff} is the square root of the sum of the constituent uncertainties. The latter quantity is simply the root sum square or rss of the constituent uncertainties.

Table 6-20 Tolerance Specifications

Parameter	Tolerance	Reference
Fuel pellet diameter	0.20%	AA284999
Clad thickness (fuel tube)	1%	AA294145
Fuel rod pitch (fuel bundle water moderator)	1%	AA273878
Packaging steel sheet	10%	ASTM A480 / A480M-10
Polyethylene (annulus around fuel rod)	1%	Note 1

Note 1: There is no reference for the uncertainty in the quantity of polyethylene available in the packaging. The polyethylene thickness is assumed to vary the same as the clad thickness.

6.4 INDIVIDUAL PACKAGE IN ISOLATION

6.4.1 Configuration

For the individual package, inner space of the packaging including the volume for the alumina silica thermal insulator, balsa wood and paper honeycomb is assumed to be filled with water. The individual package is reflected with 20 cm of full density water.

6.4.2 Results

6.4.2.1 Contents

6.4.2.1.1 Fuel Bundle or Fuel Assembly

The most reactive type of fuel bundle and fuel assembly contents without BA rods (GE14C, GNF2, and SVEA) are assessed in the individual package. Fuel assembly and fuel bundle contents are assessed without BA rods as the neutron absorption provided by the gadolinia is not needed to ensure that an individual package is subcritical under conditions consistent with normal and accident transport conditions. Normal packing materials (cluster separators and sheathing) are present as polyethylene around each rod for all transport conditions, as they provide additional moderation in the fuel. Water in the package void space provides greater reflection than that provided by the packaging materials.

Table 6-21 Individual Package, Normal Conditions of Transport

Contents	GE14C		GNF2		SVEA	
	k_p	σ_p	k_p	σ_p	k_p	σ_p
Fuel assembly or Fuel bundle						
Full density water in void space	0.80397	0.00041	0.80009	0.00032	0.80053	0.00038
No water in void space	0.54336	0.00032	0.53882	0.00028	0.53680	0.00034

Table 6-22 Individual Package, Accident Conditions of Transport

Contents	GE14C		GNF2		SVEA	
	k_p	σ_p	k_p	σ_p	k_p	σ_p
Fuel assembly						
Full density water in void space	0.80825	0.00035	0.81203	0.00040	0.82325	0.00043
No water in void space	0.54611	0.00031	0.54402	0.00032	0.54591	0.00038
Fuel bundle						
Full density water in void space	0.92011	0.00039	0.92442	0.00047	0.91885	0.00034
No water in void space	0.74882	0.00048	0.75328	0.00039	0.74274	0.00035

6.4.2.1.2 Fuel Rods

Fuel rods may be transported either packaged in a rod container or as a cluster of fuel rods without a rod container. The individual package with fuel rod contents is evaluated using the BWR_G3 fuel rod category, determined as the most reactive category in the infinite rod array comparison (See Section 6.9.5). Additionally the minimum (PWR_W5) and maximum (PWR_W3) fuel rod categories as based on fuel pellet diameter are evaluated for the fuel rod contents. Three fuel rod containers are evaluated: rod pipe, rod box, and protective case. For fuel rod shipment without a rod container, a maximum of 25 fuel rods in each compartment of the inner container is permissible. For a rod container, the number of fuel rods is limited by the capacity of the rod container. The contents are evaluated through the optimum rod pitch within a fuel rod container and for a cluster of 25 fuel rods to the maximum pitch of the IC. Normal packing materials (polyethylene sleeve) are present for all transport conditions, and wrap each individual fuel rod.

The routine and normal condition of transport is for the fuel rods to be close packed, represented by a pitch of the nominal fuel rod outer diameter with normal packing materials included. Accident conditions of transport are representative of the fuel lattice expansion of the active fuel length to the confinement boundaries of either the rod container for fuel rods in a rod container or the IC for clustered rods without a rod container.

For fuel rod shipment without a rod container, the contents are evaluated through the optimum rod pitch for a cluster of 25 fuel rods to the maximum full pitch of the IC, which is equivalent to

1.76 cm half-pitch for square pitch and 1.6 half-pitch for hexagonal pitch. Additionally for the fuel rod contents without a rod container, fewer than 25 rods in each inner container compartment are evaluated at pitches optimized to the IC size. Results for individual package, NCT and HAC fuel rod shipment without a rod container are displayed in Table 6-23.

Table 6-23 Individual Package, No Rod Container, Fuel Category Comparison

No. of Rods per IC Side	Fuel Category Half-Pitch (cm)		BWR_G3		PWR_W5 Minimum		PWR_W3 Maximum	
			k_p	σ_p	k_p	σ_p	k_p	σ_p
25	Rod OR (with NPM)[b]		0.38902	0.00026	0.3588	0.00026	0.41117	0.00027
25	1.3[b]		0.63284	0.00031	0.58417	0.00028	0.6653[a]	0.00033
25	1.6[b]		0.6465	0.00029	0.58769	0.00029	0.68554	0.00029
25	1.60-hex	1.76-sq[a]	0.6336	0.00031	0.57736	0.00028	0.68264	0.0003
22	1.60-hex	1.76-sq[a]	0.60896	0.0003	0.55323	0.00027	0.64747	0.00028
20	1.91-hex	1.76,2.2-sq[a]	0.55844	0.00027	0.49965	0.0003	0.60048	0.00029

Note: *hex* is hexagonal pitch shape; *sq* is square pitch shape; maximum k_{eff} is represented in table independent of pitch shape; pitch type result shown as [a] hexagonal pitch or [b] square pitch,

For fuel rods in a rod container, comparison of pitch types is evaluated with the package array model and applied to the individual package, as the package array for fuel rods is a more reactive case than the individual package. The pitch type is modeled as a square and hexagonal for varying pitches to encompass the normal and accident conditions of transport. The resultant more reactive pitch type is applied to the individual package analysis.

The individual package with fuel rods in a container is analyzed for each of the three fuel categories in each of the three rod containers; however Table 6-24 shows only the most reactive fuel category per transport condition. NCT is represented by a close packed pitch, while HAC is represented by expansion of the lattice to the confinement boundary.

Table 6-24 Individual Package, Fuel Rods with Rod Container

Half-Pitch (cm)	5 in. Rod Pipe [a]		Rod Box [b]		Protective Case [c]	
	k_p	σ_p	k_p	σ_p	k_p	σ_p
Close packed	0.60941	0.00026	0.59382	0.00031	0.44570	0.00029
0.5	–	–	–	–	0.44959	0.00025
0.6	–	–	–	–	0.47464	0.00029
0.65	–	–	–	–	0.45932	0.00027
0.7	–	–	0.63113	0.00033	0.47097	0.00028

Table 6-24 Individual Package, Fuel Rods with Rod Container (Cont)

Half-Pitch (cm)	5 in. Rod Pipe [a]		Rod Box [b]		Protective Case [c]	
	k_p	σ_p	k_p	σ_p	k_p	σ_p
0.75	–	–	0.63618	0.0003	0.45507	0.00028
0.8	0.59841	0.00031	0.65309	0.00034	–	–
0.85	0.61146	0.00031	0.64308	0.00033	–	–
0.9	0.60266	0.00035	0.62495	0.0003	–	–
0.95	0.57231	0.00029	–	–	–	–

Note: [a] NCT fuel PWR_W5, HAC fuel BWR_G3; [b] NCT and HAC fuel BWR_G3; [c] NCT fuel PWR_W3, HAC fuel PWR_W5

6.4.2.2 Uncertainties

To determine uncertainty, fuel bundle evaluations use the GNF2 and GE14C fuels without BA rods as reference models. The GNF2 and GE14C fuel types are determined to represent the most reactive NCT and HAC individual package configuration for fuel assembly and fuel bundle confinements. The PWR_W3 fuel category without a rod container is the reference model used for individual package uncertainty evaluations, as it represents the most reactive HAC individual package configuration. The NCT uncertainties are the material and fabrication tolerances. The HAC uncertainty evaluation accounts for shifting components and package material effects, as well as material and fabrication tolerances. Per uncertainty parameter, only the largest positive reactivity is statistically combined in the uncertainty total. The statistical combination of the uncertainties results in the Δk_u value used to define the maximum k_{eff}. The total uncertainty is calculated as the square root of the sum of the constituent uncertainties squared; this assumes the uncertainties are independent of one another.

6.4.2.2.1 Material and Fabrication Tolerances

For the tolerance values being studied in this system, the reactivity affect on the system must be determined based on a change in the total amount of the material of interest present. This can be accomplished by the study of an explicit change in material volume due to tolerance value. Tolerances for each parameter evaluated are displayed in Section 6.3.4.3. Direct perturbations of each parameter are calculated individually to determine the conservative uncertainty for a particular parameter tolerance. Any positive reactivity from the parameter variation is added to the total uncertainty Δk_u.

Material and fabrication tolerances apply to NCT and HAC. The uncertainty values represent the statistical error propagation of k_p and σ_p for the configuration as compared to the representative package base case used for determining the most reactive case per transport condition.

Table 6-25 Material and Fabrication Uncertainties, Individual Package, Fuel Bundle

Parameter	NCT w/o BA Δk_u	HAC w/o BA Δk_u
Fuel pellet diameter	0.00145	0.00136
Clad thickness	0.00459	0.00233
Fuel rod pitch	0.00702	0.00114
Packaging steel	0.00323	0.00307
Polyethylene (annulus on fuel rod)	0.00199	0.0019

Table 6-26 Material and Fabrication Uncertainties, Individual Package, Loose Fuel Rods

Parameter	Δk_u
Fuel pellet diameter	0.00104
Clad thickness	0.00067
Fuel rod pitch	–
Packaging steel	0.00173
Polyethylene (annulus on fuel rod)	0.00013

6.4.2.2.2 Geometric or Material Representations

The uncertainty associated with geometric or material representations is evaluated for the HAC case, which accounts for shifting components and package material effects. Per uncertainty parameter, only the largest positive reactivity is statistically combined to the uncertainty total, Δk_u.

6.4.2.2.2.1 Spacing within Outer Container

The rubber vibro-isolating devices are also assumed to degrade or melt when exposed to an external fire, allowing the inner container to shift downward about 2.54 cm. Maximum temperature inside the outer container is 800°C and the ignition temperature for rubber is between 260° – 316°C. The inner container horizontal position within the outer container remains the same as the normal condition model, since the stainless steel fixture assemblies remained intact following the 9-meter drop.

The effect of shifting the position of the inner container is assessed by positioning the inner container in a corner of the outer container and evaluating k_{eff} for the single package. Table 6-27 below demonstrates that the effect of position of the inner container within the outer container is to decrease k_{eff} for the single package configuration.

Table 6-27 Single Package, Spacing of Inner Container within Outer Container

Fuel Type		Confinement Boundary: Fuel Assembly k_p	Fuel Assembly Δk_u	Fuel Bundle k_p	Fuel Bundle Δk_u
GE14C	Centered	0.80825	-0.00044	0.92011	-0.00094
	Shifted	0.80734		0.9186	
SVEA	Centered	0.81203	-0.00119	0.92442	-0.00054
	Shifted	0.81032		0.92331	

Note: Statistical uncertainty, σ_p, in the calculation of k_p is less than 0.00050.

6.4.2.2.2.2 Orientation in Inner Container

The ethafoam cushioning within the IC is assumed to degrade or melt when exposed to an external fire, allowing the assembly to shift within the inner container. A following drop, may also allow the assembly to shift within the inner container.

The effect of orientation of the fuel within the inner container is assessed by positioning the fuel in the four corners of the inner container and evaluating k_{eff} for the infinite array, independently. Table 6-28 below demonstrates that the effect of orientation of the fuel within the inner container for the individual package configuration.

Table 6-28 Individual Package, Fuel Bundle, Orientation in IC

Fuel Type Position	GNF2 k_p	GNF2 σ_p	GNF2 Δk_u	GE14C k_p	GE14C σ_p	GE14C Δk_u
Center	0.92442	0.00047	0	0.92056	0.00037	0
Outer-bottom	0.92101	0.00038	-0.00281	0.91713	0.0004	-0.00289
Inner-bottom	0.92507	0.00034	0.000123	0.92151	0.00044	0.00152
Outer-top	0.92038	0.00035	-0.00345	0.91621	0.00042	-0.00379
Inner-top	0.92581	0.00039	0.00200	0.92154	0.00038	0.00151

6.4.2.3 Summary

The total uncertainty, Δk_u, for the individual package is a statistical combination of applicable uncertainties. The NCT uncertainties are the material and fabrication tolerances. The HAC uncertainty evaluation accounts for shifting components and package material effects, as well as material and fabrication tolerances. Package material effect uncertainties are those associated with melting polyethylene, including, the assembly orientation shift in the inner container (Section 6.4.2.2.2) and the re-distribution of polyethylene (Section 6.3.4.2.4).

Table 6-29 Uncertainties for Individual Package, Fuel Assembly or Bundle

Parameter	NCT w/o BA	HAC w/o BA	HAC w/o BA
		Individual Package	
Package lattice size	Nominal	Fuel Assembly	Fuel Bundle
Material and Geometric Representations assembly shift in IC	--	0.002	0.002
IC shift in OC	--	0	0
Container deformation	--	0	0
Polyethylene modeling	0.01142	0.00504	0.00375
Moderation	--	0	0
Manufacturing Tolerances			
Fuel pellet diameter	0.00145	0.00136	0.00136
Clad thickness	0.00459	0.00233	0.00233
Fuel rod pitch	0.00702	0.00114	0.00114
Material Tolerance			
Packaging steel	0.00323	0.00307	0.00307
Polyethylene (annulus on fuel rod)	0.00199	0.0019	0.0019
Additional Uncertainties			
Blanket zones without BA rods	--	--	--
BA rod reactivity worth verification	--	--	--
Total Uncertainty, Δk_u (rss value)	0.015	0.008	0.007

Table 6-30 Uncertainties for Individual Package, Fuel Rods

Parameter Package Configuration	NCT Individual Package No Container	HAC Individual Package No Container
Material and Geometric Representations assembly shift in IC	–	0.002
IC shift in OC	–	0
Container deformation	–	0
Polyethylene modeling	0.01862	0.02789
Moderation	–	0
Manufacturing Tolerances		
Fuel pellet diameter	0.00104	0.00104
Clad thickness	0.00067	0.00067
Fuel rod pitch	–	–
Material Tolerance		
Packaging steel	0.00173	0.00173
Polyethylene (annulus on fuel rod)	0.00013	0.0013
Total Uncertainty Δk_u (rss value)	0.019	0.029

Table 6-31 Individual Package, Normal and Accident Conditions of Transport, Summary

Contents Description	k_p	σ_p	Δk_u	Maximum k_p
Normal Conditions of Transport				
Fuel Assembly or Fuel bundle without BA Rods (Table 6-21, Full density water in void space, GE14C)	0.80397	0.00041	0.015	0.8198
Fuel Rods with Rod Container (Table 6-24, close packed, 5 inch Rod Pipe, PWR_W5)	0.60941	0.00026	0.019	0.6300
Fuel Rods without Rod Container (Table 6-23, close packed, PWR_W3)	0.41117	0.00027	0.029	0.4308
Hypothetical accident conditions of transport				
Fuel Assembly without BA Rods (Table 6-22, Full density water in void space, SVEA)	0.82325	0.00043	0.008	0.8322
Fuel Bundle without BA Rods (Table 6-22, Full density water in void space, GNF2)	0.92442	0.00047	0.007	0.9324
Fuel Rods with Rod Container (Table 6-24, 0.8 pitch, rod box, BWR_G3)	0.65309	0.00034	0.029	0.6828
Fuel Rods without Rod Container (Table 6-23, 1.6 cm pitch, PWR_W3)	0.68554	0.00029	0.029	0.7152

6.5 PACKAGE ARRAYS UNDER NORMAL CONDITIONS OF TRANSPORT

6.5.1 Configuration

The demonstration of maximum reactivity showed void in the inner space of the packaging including the volume for the normal packaging materials (alumina thermal insulator, balsa wood and paper honeycomb) results in the highest k_{eff} for an infinite array. A number N is derived from the evaluation of packages under accident conditions of transport. At least five times N packages is shown to be subcritical without the normal packaging materials, with no moderation between the packages and the package arrangement reflected on all sides by 20 cm of water.

6.5.2 Results

6.5.2.1 Contents

6.5.2.1.1 Fuel Bundle or Fuel Assembly without BA Rods

The most reactive type of fuel bundle and fuel assembly contents without BA rods are GE14C, GNF2, and SVEA. Fuel assembly and fuel bundle contents assessed without BA rods is evaluated since the neutron absorption provided by the gadolinia is not needed to ensure that a small package array is subcritical under conditions consistent with normal and accident transport conditions. Normal packing materials (cluster separators and sheathing) are present as redistributed polyethylene around each rod for all transport conditions, as they provide additional moderation in the fuel.

Table 6-32 NCT Package Array (without BA Rods)

		GE14C		GNF2		SVEA	
Array Size	**5N**	k_p	σ_p	k_p	σ_p	k_p	σ_p
Fuel Bundle without BA Rods	100	0.54045	0.00029	0.53970	0.00025	0.35710	0.00020
Fuel Assembly without BA	169	0.57419	0.00025	–	–	–	–

6.5.2.1.2 Fuel Bundle or Fuel Assembly with BA Rods

The most reactive type of fuel bundle and fuel assembly contents with BA rods are GE14G, GNF2, and SVEA. Normal packing materials (cluster separators and sheathing) are present as redistributed polyethylene around each rod for all transport conditions, as they provide additional moderation in the fuel.

Table 6-33 NCT Package Array (with BA Rods)

		GE14G		GNF2		SVEA	
Array Size	5N	k_p	σ_p	k_p	σ_p	k_p	σ_p
Fuel Bundle with 8 BA Rods	361	0.57334	0.00027	0.57509	0.00025	0.36130	0.00019
Fuel Assembly with 8 BA Rods	529	–	–	0.59044	0.00027	–	–

6.5.2.1.3 Fuel Rods

Fuel rods may be transported either packaged in a rod container or as a cluster of fuel rods without a rod container. The package array with fuel rod contents is evaluated using the BWR_G3 fuel rod category, determined as the most reactive category in the infinite rod array comparison (See Section 6.9.5). Additionally the minimum (PWR_W5) and maximum (PWR_W3) fuel rod categories as based on fuel pellet diameter are evaluated for the fuel rod contents. For fuel rod shipment without a rod container, a maximum of 25 fuel rods in each compartment of the inner container is permissible. For a rod container, the number of fuel rods is limited by the capacity of the rod container.

The routine and normal condition of transport is for the fuel rods to be close packed, represented by a pitch of the nominal fuel rod outer diameter with normal packing materials included. The rod container generating the peak reactivity along with the fuel rod cluster without a rod container are evaluated for the normal transport conditions.

The HAC package array fuel rod transport model is used to compare pitch types, as the package array is a more reactive case for fuel rods. The resultant more reactive pitch type is applied to the normal package analysis. For NCT, where rods are tightly packed, square pitches allow more moderator present, which in an undermoderated system increases k_{eff}.

Table 6-34 Package Array (Fuel Rods)

Array Size	5N	k_p	σ_p
Fuel Rods with Rod Container rod box, BWR_G3, square pitch	361	0.85193	0.00034
Fuel Rods without Rod Container PWR_W3, hex pitch	361	0.44442	0.00027

6.5.2.2 Uncertainties

To determine uncertainty, evaluations use the GNF2 fuel bundle with and GNF2 and GE14C fuel bundles without BA rods as reference models. The GNF2 fuel is determined to represent the most reactive NCT and HAC package array configuration for fuel assembly and fuel bundle confinements. As for fuel rod transport, the BWR_G3 fuel category represents the most reactive NCT fuel rod package array configuration; the model is a WEC rod box shown as the most reactive HAC configuration. The NCT uncertainties are the material and fabrication tolerances. Per uncertainty parameter, only the largest positive reactivity is combined in the uncertainty total. The statistical combination of the uncertainties results in the Δk_u value used to define the maximum k_{eff}. The total uncertainty is calculated as the square root of the sum of the constituent uncertainties squared; this assumes the uncertainties are independent.

6.5.2.2.1 Material and Fabrication Tolerances

For the tolerance values being studied in this system, the reactivity affect on the system must be determined based on a change in the total amount of the material of interest present. This can be accomplished by the study of an explicit change in material volume due to tolerance value. Tolerances for each parameter evaluated are displayed in Section 6.3.4.3. Direct perturbations of each parameter are calculated individually to determine the conservative uncertainty for a particular parameter tolerance. Any positive reactivity from the parameter variation is statistically combined to the total uncertainty Δk_u.

Material and fabrication tolerances apply to NCT and HAC. The uncertainty values represent the statistical error propagation of k_p and σ_p for the configuration as compared to the representative package case used for determining the most reactive case per transport condition.

Tolerances for the package array of fuel rods are based on HAC model of the most reactive configuration.

Table 6-35 NCT Material and Fabrication Uncertainties, Package Array, Fuel Assembly or Bundle

Parameter	NCT w/o BA rods Δk_u	NCT w/o BA rods Δk_u
Fuel pellet diameter	0.00098	0.00073
Clad thickness	0.01489	0.01075
Fuel rod pitch	0.0011	0.00098
Packaging steel	0.01466	0.01316
Polyethylene (annulus on fuel rod)	0.01808	0.01287

Table 6-36 NCT Material and Fabrication Uncertainties, Package Array, Fuel Rods

Parameter	Δk_u
Fuel pellet diameter	0.00047
Clad thickness	0.00252
Fuel rod pitch	–
Packaging steel	0.01064
Polyethylene (annulus on fuel rod)	0.00097

6.5.2.2.2 Blanket Zones without BA Rods

BA rods are modeled the entire active fuel length. A case is evaluated with the BA removed from the blanket length of the active fuel length; therefore the blanket may be enriched without any BA present. The effect of blanket zones without BA is assessed for top, bottom, and combine top and bottom blanket zones with various lengths up to 8 in. and ^{235}U enrichments up to 5 wt% in a 6x6 array. Table 6-37 demonstrate the impact of k_{eff} for the fuel bundle at the nominal pitch for NCT.

The maximum k_{eff} value evaluated is resultant of an 8 in. blanket at the top and bottom of the active fuel height with a ^{235}U enrichment of 5 wt% and no BA present.

Table 6-37 Package Array (6x6) Summary, GNF2 w/BA Rods, Blanket(s) w/o BA

Blanket Configuration Material (Region)	Nominal Δk_u
Bottom Only, 5wt% U-235	0.00093
Bottom and Top, 5wt% U-235	0.00122
Top Only. 5wt% U-235	0.00107

6.5.2.3 Summary

The total uncertainty, Δk_u, for the package array is a statistical combination of applicable uncertainties. The NCT uncertainties are the material and fabrication tolerances and the modeling of polyethylene (Section 6.3.4.2.4).

Table 6-38 NCT Total Uncertainties for Package Array, Fuel Assembly or Bundle

Uncertainty	NCT w/o BA rods Δk_u	NCT w/BA rods Δk_u
Material and fabrication tolerances		
Fuel pellet diameter	0.00098	0.00073
Clad thickness	0.01489	0.01075
Fuel rod pitch	0.0011	0.00098
Packaging steel	0.01466	0.01316
Polyethylene (annulus on fuel rod)	0.01808	0.01287
Geometric and material representation (total)		
Polyethylene redistribution	0.01862	0.01862
Blanket Zones without BA rods	–	0.0013
BA rod reactivity worth verification	–	0.015
Total Uncertainty, Δk_u (rss value)	0.034	0.033

Table 6-39 NCT Total Uncertainties for Package Array, Fuel Rods

Uncertainty	NC Δk_u
Material and fabrication tolerances	
Fuel pellet diameter	0.00047
Clad thickness	0.00252
Fuel rod pitch	–
Packaging steel	0.01064
Polyethylene (annulus on fuel rod)	0.00097
Geometric and material representation (total)	
Polyethylene redistribution	0.01862
Blanket Zones without BA rods	–
BA rod reactivity worth verification	–
Total Uncertainty, Δk_u (rss value)	0.0022

Table 6-40 Package Array under Normal Transport, Summary

Contents	5N	k_p	σ_p	Δk_u	Maximum k_p
Fuel Bundle without BA Rods Table 6-32, GE14C	100	0.54045	0.00029	0.034	0.5751
Fuel Bundle with 8 BA Rods Table 6-33, GNF2	361	0.57509	0.00025	0.033	0.6086
Fuel Assembly without BA Rods Table 6-32, GE14C	169	0.57419	0.00025	0.034	0.6087
Fuel Assembly with 8 BA Rods Table 6-33, GNF2	529	0.59044	0.00027	0.033	0.6240
Fuel Rods with Rod Container Table 6-34, rod box, BWR_G3	361	0.85193	0.00034	0.022	0.8747
Fuel Rods without Rod Container Table 6-34, PWR_W3	361	0.44442	0.00027	0.022	0.4670

6.6 PACKAGE ARRAYS UNDER ACCIDENT CONDITIONS OF TRANSPORT

6.6.1 Configuration

A number N is derived, such that two times N packages is subcritical with no moderation between packages and the package arrangement reflected on all sides by 20 cm of water.

6.6.2 Results

6.6.2.1 Contents

6.6.2.1.1 Fuel Assembly or Fuel Bundle

The most reactive type of fuel bundle and fuel assembly contents without BA rods (GE14C, GNF2, and SVEA) and contents with BA rods (GE14G, GNF2, and SVEA) are assessed in the package array. Fuel assembly and fuel bundle contents are assessed with and without BA rods with expansion of 50 cm of the active fuel length. Normal packing materials (cluster separators and sheathing) are present as redistributed polyethylene around each rod, as they provide additional moderation in the fuel. An array size of 2N is determined for the fuel assembly with and without the BA rods and likewise for the fuel bundle. The confinement boundary for the fuel assembly is the dimension of the fuel channel where as the fuel bundle may expand to the extent of the inside of the inner container. The fuel rod pitch resulting from expansion to the inside dimension of the inner container is near the optimum pitch as shown in the demonstration of maximum reactivity.

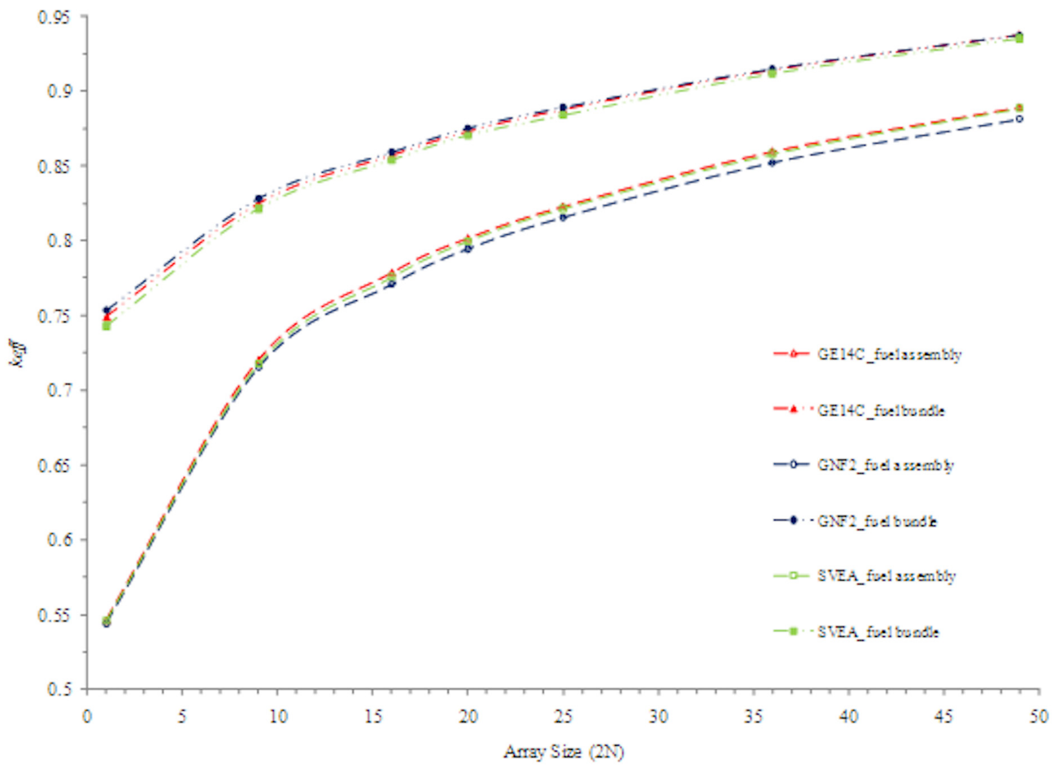

Figure 6-15 Fuel Assembly and Fuel Bundle w/o BA Rods

Table 6-41 Fuel Bundle w/o BA Rods

	GE14C		GNF2		SVEA	
Array Size	k_p	σ	k_p	σ_p	k_p	σ_p
1x1	0.74882	0.00048	0.75328	0.00039	0.74274	0.00035
3x3	0.82482	0.0004	0.82820	0.00049	0.82146	0.00035
4x4	0.85698	0.00038	0.85913	0.00044	0.85384	0.00038
4x5	0.87295	0.00042	0.87503	0.00036	0.87039	0.00041
5x5	0.88767	0.00035	0.88900	0.00040	0.88375	0.00038
6x6	0.91429	0.00035	0.91476	0.00037	0.91155	0.00039
7x7	0.93771	0.00033	0.93743	0.00038	0.93507	0.00045

Table 6-42 Fuel Assembly w/o BA Rods

	GE14C		GNF2		SVEA	
Array Size	k_p	σ	k_p	σ	k_p	σ
1x1	0.54611	0.00031	0.54402	0.00032	0.54591	0.00038
3x3	0.72028	0.00038	0.71527	0.00034	0.71764	0.00038
4x4	0.77855	0.00034	0.77078	0.00035	0.77556	0.00036
4x5	0.08017	0.00037	.07946	0.00039	0.79972	0.00033
5x5	0.82299	0.00033	0.81568	0.00036	0.82139	0.00033
6x6	0.85982	0.00038	0.85237	0.00033	0.85798	0.00032
7x7	0.88940	0.00033	0.88135	0.00036	0.88845	0.00038

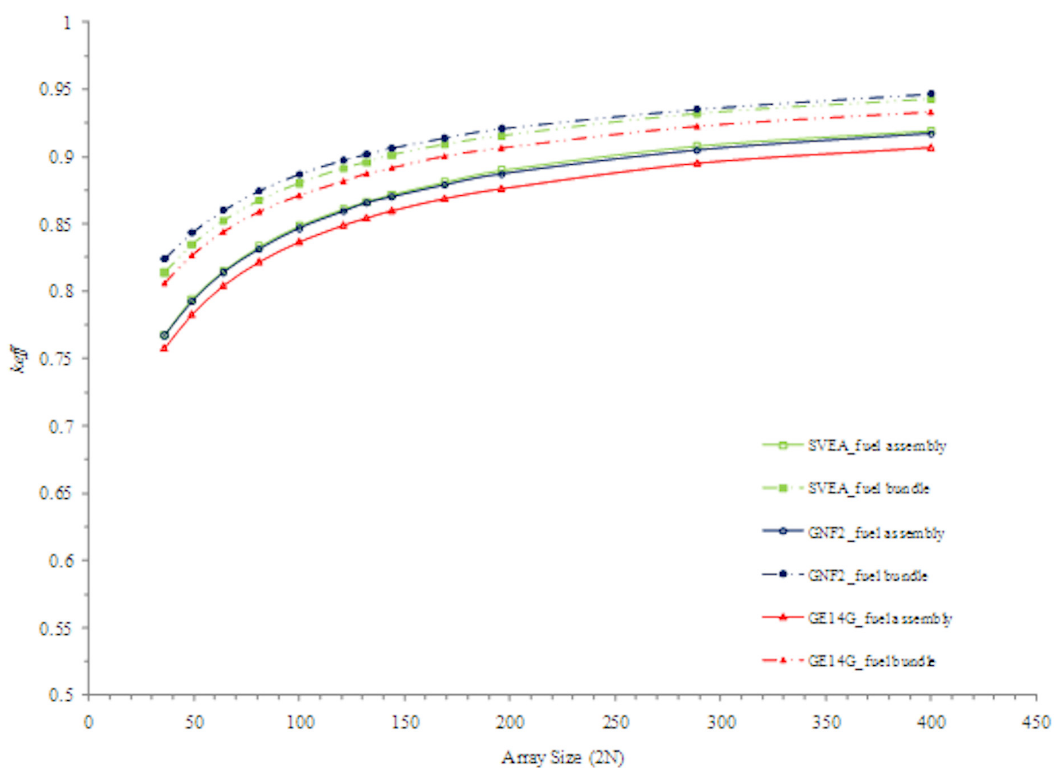

Figure 6-16 Fuel Assembly and Fuel Bundle w/ BA Rods

Table 6-43 Fuel Assembly w/ BA Rods

	GE14G		GNF2		SVEA	
Array Size	k_{eff}	σ	k_{eff}	σ	k_{eff}	σ
6x6	0.75771	0.00031	0.76716	0.00035	0.76755	0.00034
7x7	0.78282	0.00037	0.79228	0.00033	0.7943	0.00031
8x8	0.80426	0.0003	0.81398	0.00036	0.8153	0.00032
9x9	0.822	0.00033	0.83129	0.00034	0.82518	0.00036
10x10	0.83676	0.00034	0.84677	0.00033	0.84075	0.00032
11x11	0.84923	0.00037	0.85930	0.00034	0.85351	0.00034
11x12	0.85456	0.00039	0.86559	0.00032	0.85819	0.00040
12x12	0.86000	0.00034	0.86997	0.0003	0.86311	0.00033
13x13	0.86899	0.00035	0.87873	0.00032	0.87244	0.00032
14x14	0.87633	0.0004	0.88698	0.00032	0.88056	0.00036
17x17	0.89530	0.0003	0.90458	0.00032	0.89869	0.00035
20x20	0.90699	0.00035	0.91695	0.00034	0.91105	0.00045

Table 6-44 Fuel Bundle w/ BA Rods

	GE14G		GNF2		SVEA	
Array Size	k_{eff}	σ	k_{eff}	σ	k_{eff}	σ
6x6	0.80634	0.00034	0.82385	0.00035	0.81381	0.00037
7x7	0.82707	0.00033	0.84352	0.00036	0.83455	0.00046
8x8	0.84443	0.00036	0.86008	0.00036	0.85234	0.00034
9x9	0.85925	0.00035	0.87473	0.00044	0.85892	0.00039
10x10	0.87118	0.00040	0.88708	0.00035	0.87151	0.00036
11x11	0.88182	0.00031	0.89753	0.00037	0.88250	0.00032
11x12	0.88741	0.00032	0.90176	0.00035	0.88805	0.00030
12x12	0.89156	0.00033	0.90647	0.00035	0.89250	0.00031
13x13	0.90022	0.00037	0.91382	0.00035	0.90071	0.00030
14x14	0.90635	0.00042	0.92084	0.00039	0.90666	0.00037
17x17	0.92230	0.00035	0.93511	0.00032	0.92320	0.00033
20x20	0.93292	0.00032	0.94662	0.00036	0.93395	0.00033

6.6.2.1.2 Fuel Rods

Fuel rods may be transported either packaged in a rod container or as a cluster of fuel rods without a rod container. The package array with fuel rod contents is evaluated using the BWR_G3 fuel rod category, determined as the most reactive category in the infinite rod array comparison (See Section 6.9.5). Additionally the minimum (PWR_W5) and maximum (PWR_W3) fuel rod categories as based on fuel pellet diameter are evaluated for the fuel rod contents. Three fuel rod containers are evaluated: rod pipe, rod box, and protective case. For fuel rod shipment without a rod container, a maximum of 25 fuel rods in each compartment of the inner container is permissible. For a rod container, the number of fuel rods is limited by the capacity of the rod container. The contents are evaluated through the optimum rod pitch within a fuel rod container and for a cluster of 25 fuel rods to the maximum pitch of the IC.

During accident conditions the rod container confines the fuel rods to fixed geometry, where as a cluster of fuel rods are confined only by the inner container. Accident conditions of transport are representative of the fuel lattice expansion of the active fuel length to the confinement boundaries of either the rod container for fuel rods in a rod container or the IC for clustered rods without a rod container. Normal packing materials (polyethylene sleeve) are present for all transport conditions.

Fuel Rods without a Rod Container

For fuel rod shipment without a rod container, a maximum of 25 fuel rods in each compartment of the inner container is permissible. The contents are evaluated through the optimum rod pitch for a cluster of 25 fuel rods to the maximum full pitch of the IC, which is equivalent to 1.76 cm half-pitch for square pitch and 1.6 half-pitch for hexagonal pitch. Additionally for the fuel rod contents without a rod container, fewer than 25 rods in each inner container compartment are evaluated at pitches optimized to the IC size.

Table 6-45a displays the comparison of the fuel rod categories for a maximum of 25 fuel rods in each compartment of the inner container at several pitches including the limiting maximum full pitch of the IC, and then the increasing pitch and reduction of fuel rods. The maximum k_{eff}, irrespective of pitch type, is used to define the most reactive loose fuel rod case per container.

Table 6-45a 144 Package Array, No Rod Container, Fuel Category Comparison

No. of Rods per IC Side	Fuel Category Half-Pitch (cm) Triangular	Square	BWR_G3 k_p	σ_p	PWR_W5 Minimum k_p	σ_p	PWR_W3 Maximum k_p	σ_p
25 [b]	Rod OR (with NPM)		0.43322	0.00029	0.39644	0.0003	0.45934	0.00027
25	1.3	1.3	0.76709	0.00033	0.67505	0.0003	0.77324	0.00034
25 [a]	1.6	1.6	0.75877	0.00031	0.68578	0.0004	0.80154	0.00034
25 [a]	1.76	1.76	0.74686	0.00029	0.66542	0.00028	0.79549	0.00033
22 [a]	1.6	1.76	0.70655	0.00031	0.63758	0.00037	0.74762	0.00033
20 [a]	1.91	1.76, 2.2 (x, y)	0.65976	0.00028	0.58585	0.00031	0.70517	0.00028

Note: alpha indicates pitch shape represented for maximum keff; [a] triangular pitch; [b] square pitch

The pitch shape is modeled as a hexagonal and square pitch array, maximum k_p is displayed. Table 6-45b displays k_{eff} results for a comparison of the pitch shape for the most reactive fuel rod contents, PWR_W3, for shipment with no rod container (determined in Table 6-45a). The largest variation, an increase in k_{eff} for a square pitch over hexagonal pitch, occurs when rods are tight packed. However, as the pitch is increased and/or the quantity of rods decreases then the hexagonal pitch array becomes more reactive due to optimization of the moderator-to-fuel ratio.

Table 6-45b 144 Package Array, No Rod Container, Pitch Shape Comparison, PWR_W3 Maximum Fuel Category

No. of Rods per IC Side	Fuel Category Half-Pitch (cm)		Hexagonal Pitch		Square Pitch	
	Triangular	Square	k_p	σ_p	k_p	σ_p
25	Rod OR (with NPM)		0.44061	0.00031	0.45934	0.00027
25	1.3	1.3	0.7595	0.00031	0.77324	0.00034
25	1.6	1.6	0.80154	0.00034	0.79852	0.00038
25	1.76	1.76	0.79549	0.00033	0.78663	0.00029
22	1.6	1.76	0.74762	0.00033	0.73784	0.00033
20	1.91	1.76, 2.2 (x, y)	0.70517	0.00028	0.69094	0.00033

Fuel Rods in a Rod Container

The package array model is used to compare pitch types, as the package array for fuel rods is a more reactive case than the individual package for fuel rods. The pitch type is first modeled to fit the container shape (i.e., square pitch in square containers and hexagonal pitch for the cylindrical container). For comparison, the other pitch option (i.e., hexagonal pitch in square containers and square pitch for the cylindrical container) was modeled for varying pitches to encompass the peak reactivity point and ±0.5 cm half-pitch. The resultant more reactive pitch type is applied to the individual package analysis.

The following tables show the pitch type comparison for the three fuel rod categories evaluated in the three fuel rod containers, respectively. Results in Table 6-46a show for the Protective case the BWR_G3 fuel category in a square pitch type is most reactive for the NCT half-pitch size (rod OR) and HAC expanded half-pitch size at 0.80 cm. For the rod box, as shown in Table 6-46b, the BWR_G3 fuel category in a square pitch type is most reactive for the NCT half-pitch size (rod OR), while the hexagonal pitch type is more reactive for the HAC expanded half-pitch size at 0.75 cm. Results in Table 6-46c for the rod pipe show the BWR_G3 fuel category with a square pitch type is most reactive for the NCT half-pitch size (rod OR), while the hexagonal pitch type is more reactive for the HAC expanded half-pitch size at 0.85 cm.

For NCT, where rods are tightly packed, square pitches allow more moderator present, which in an undermoderated system increases k_{eff}. While as the pitch expands the hexagonal pitch type allows more fuel mass present in the container due to the shape and stacking-ability of the pitch type, which may increase k_{eff}. However the shape of the container has a role in the optimization of the moderator-to-fuel ratio, which along with pitch type controls the amount of fuel and moderator present.

Table 6-46a 144 Package Array, Protective Case, Fuel Category and Pitch Comparison

Pitch Size	Fuel Type, Pitch Type (k_{eff} ± sigma)					
	BWR_G3 Square	**BWR_G3 Hexagonal**	**PWR_W5 Square**	**PWR_W5 Hexagonal**	**PWR_W3 Square**	**PWR_W3 Hexagonal**
Rod OR	0.49095 ±0.00024	0.43199 ±0.00027	0.48644 ±0.00029	0.43098 ±0.00023	0.46588 ±0.00027	0.41014 ±0.00022
0.65	–	–	0.59403 ±0.00031	0.58221 ±0.0003	–	–
0.70	0.60148 ±0.00034	0.58299 ±0.00032	0.60557 ±0.00029	0.59939 ±0.0003	–	–
0.75	0.60755 ±0.00033	0.60195 ±0.00031	0.59856 ±0.00032	0.60312 ±0.0003	–	–
0.80	0.61028 ±0.00031	0.60036 ±0.00032	0.58957 ±0.00032	0.5852 ±0.0003	0.58663 ±0.0003	0.57282 ±0.00032
0.85	0.60722 ±0.00033	0.59378 ±0.00033	–	–	0.59145 ±0.00035	0.57568 ±0.00036
0.90	–	–	–	–	0.58983 ±0.00037	0.58375 ±0.00032
0.95	–	–	–	–	–	0.58702 ±0.00029
1.0	–	–	–	–	–	0.58722 ±0.00034
1.10	–	–	–	–	–	0.56607 ±0.00036

Table 6-46b 144 Package Array, Rod Box, Fuel Category and Pitch Comparison

Pitch Size	Fuel Type, Pitch Type (k_{eff} ± sigma)					
	BWR_G3 Square	**BWR_G3 Hexagonal**	**PWR_W5 Square**	**PWR_W5 Hexagonal**	**PWR_W3 Square**	**PWR_W3 Hexagonal**
Rod OR	0.81196 ±0.00034	0.77644 ±0.00032	0.80462 ±0.00033	0.76907 ±0.00036	0.78481 ±0.00034	0.75001 ±0.00029
0.60	0.83621 ±0.00033	–	0.85356 ±0.00038	0.83771 ±0.00035	–	–
0.65	0.86103 ±0.00035	0.85196 0.00032	0.86869 ±0.00042	0.86913 ±0.00034	–	–

Table 6-46b 144 Package Array, Rod Box, Fuel Category and Pitch Comparison (Cont)

Pitch Size	Fuel Type, Pitch Type (k_{eff} ± sigma) BWR_G3 Square	BWR_G3 Hexagonal	PWR_W5 Square	PWR_W5 Hexagonal	PWR_W3 Square	PWR_W3 Hexagonal
0.70	0.87251 ±0.00038	0.86154 ±0.00034	0.86527 ±0.00038	0.85932 ±0.00033	–	0.82585 ±0.00037
0.75	0.88320 ±0.00035	0.86604 ±0.0004	0.86815 ±0.00037	0.85600 ±0.00039	0.86124 0.00033	0.84024 ±0.00034
0.80	0.85915 ±0.00035	0.88320 ±0.00035	0.83241 ±0.00031	0.86599 ±0.0004	0.84918 ±0.00034	0.86398 ±0.00035
0.85		0.86744 ±0.00041	0.82755 ±0.00035	0.83411 ±0.00035	0.86041 ±0.00038	0.86016 ±0.00037
0.90		0.83937 ±0.0035	–	–	0.86888 ±0.00031	0.84001 ±0.00034
0.95		–	–	–	0.81917 ±0.00032	0.83609 0.00033

Table 6-46c 144 Package Array, Pipe, Fuel Category and Pitch Comparison

Pitch Size	Fuel Type, Pitch Type (k_{eff} ± sigma) BWR_G3 Hexagonal	BWR_G3 Square	PWR_W5 Hexagonal	PWR_W5 Square	PWR_W3 Hexagonal	PWR_W3 Square
Rod OR	0.60923 ±0.0003	0.69781 ±0.0003	0.60941 ±0.00026	0.69466 ±0.00031	0.5802 ±0.00026	0.67183 ±0.00029
0.65	–	0.81911 ±0.00033	–	0.84252 ±0.00031	–	–
0.70	–	0.84791 ±0.00035	0.85117 ±0.00038	0.85448 ±0.00034	–	–
0.75	–	0.86077 ±0.00034	0.84822 ±0.0003	0.85105 ±0.0004	–	–
0.80	0.85776 ±0.00032	0.85384 ±0.00032	0.85001 ±0.00039	0.82955 ±0.00032	0.8205 ±0.00034	0.83357 ±0.00034
0.85	0.86587 ±0.00034	0.8486 ±0.00035	0.84757 ±0.00038	–	0.83929 ±0.00032	0.83669 ±0.0003
0.90	0.85738 ±0.00039	0.8426 ±0.00031	0.82633 ±0.00033	–	0.84296 ±0.0004	0.83933 ±0.00032
0.95	0.83027 ±0.00038	–	–	–	0.82667 ±0.00036	0.82991 ±0.00032

6.6.2.2 Uncertainties

To determine uncertainty, evaluations use the GNF2 fuel with and GNF2 and GE14C fuels without BA rods as reference models, respectively. The GNF2 fuel is determined to represent the most reactive NCT and HAC package array configuration for fuel assembly and fuel bundle confinements. For evaluations without BA rods, the fuel which demonstrates the largest uncertainty is shown in the results. The BWR_G3 fuel category in a rod box as the reference model is used for fuel rod package array uncertainty evaluations, as it represents the most reactive HAC package configuration. The HAC uncertainty evaluation accounts for shifting components and package material effects, as well as material and fabrication tolerances. Per uncertainty parameter, only the largest positive reactivity is added to the uncertainty total.

6.6.2.2.1 Material and Fabrication Tolerances

For the tolerance values being studied in this system, the reactivity affect on the system must be determined based on a change in the total amount of the material of interest present. This can be accomplished by the study of an explicit change in material volume due to tolerance value. Tolerances for each parameter evaluated are displayed in Section 6.3.4.3. Direct perturbations of each parameter are calculated individually to determine the conservative uncertainty for a particular parameter tolerance.

Material and fabrication tolerances apply to NCT and HAC. The uncertainty values represent the statistical error propagation of k_p and σ_p for the configuration as compared to the representative package base case used for determining the most reactive case per transport condition. Per uncertainty parameter, only the largest positive reactivity is combined in the uncertainty total. The statistical combination of the uncertainties results in the Δk_u value used to define the maximum k_{eff}. The total uncertainty is calculated as the square root of the sum of the constituent uncertainties squared.

Table 6-47 HAC Material and Fabrication Uncertainties, Package Array, Fuel Assembly or Bundle

Parameter	HAC w/o BA Rods Δk_u	HAC w/ BA Rods Δk_u
Fuel pellet diameter	0.0008	0.00112
Clad thickness	0.00235	0.00235
Fuel rod pitch	0.00294	0.00138
Packaging steel	0.01097	0.00969
Polyethylene (annulus on fuel rod)	0.00071	0.00061

Table 6-48 HAC Material and Fabrication Uncertainties, Package Array, Fuel Rods

Parameter	Δk_u
Fuel pellet diameter	0.00047
Clad thickness	0.00252
Fuel rod pitch	–
Packaging steel	0.01064
Polyethylene (annulus on fuel rod)	0.00097

6.6.2.2.2 Geometric or Material Representations

To determine uncertainty, evaluations for geometric and material representations use the GNF2 fuel with BA rods as a reference model. This reference model, fuel with BA rods, represents the most common configuration for shipment. Additionally, the GNF2 and GE14C without BA rods represents the most reactive HAC package array configuration for fuel without BA rods, and hence are used for uncertainty evaluations; the most limiting case is shown in the following subsections.

6.6.2.2.2.1 Spacing within Outer Container

The rubber vibro-isolating devices are also assumed to degrade or melt when exposed to an external fire, allowing the inner container to shift downward about 2.54 cm. Maximum temperature inside the outer container is 800°C and the ignition temperature for rubber is between 260° - 316°C. The inner container horizontal position within the outer container would be the same as the normal condition model, since the stainless steel fixture assemblies remained intact following the 9-meter drop.

The effect of shifting the position of the inner container is assessed by two repositioning cases of the inner container in the outer container and evaluating k_{eff} for the infinite package array. One case has the inner container positioned in the outer container with a mirror boundary, creating a pattern of the same position. The second case has the inner container positioned in a corner of the outer container, so four adjacent inner containers are positioned near one another with outer container boundaries touching.

Table 6-49 Package Array (Infinite) Uncertainty, Spacing of IC within OC

	Confinement Boundary					
	Fuel Assembly			Fuel Bundle		
Region Position	k_p	σ_p	Δk_u	Δk_p	σ_p	Δk_u
GNF2 with BA Rods				1.13883	0.00026	–
Centered	1.13417	0.00026	–	1.14207	0.00028	0.00359
Corner	1.13689	0.00029	0.00310	1.14098	0.00027	0.000249
Cruciform	1.13592	0.00026	0.00212	1.13883	0.00026	–
GE14C without BA Rods						
Centered	1.2825	0.00029	–	1.2789	0.00025	–
Corner	1.28246	0.00029	0.00394	1.28642	0.00025	0.00430
Cruciform	1.2819	0.00029	0.00338	1.28645	0.00026	0.00434
Fuel Rods, WEC box, BWR_G3					Optimal Pitch	
Centered	–	–	–	1.04593	0.00033	–
Corner	–	–	–	1.05019	0.00031	0.00471
Cruciform	–	–	–	1.0500	0.00031	0.00450

6.6.2.2.2.2 Package Spacing

The container deformation modeled for the package array includes the damage from the 9-meter drop onto an unyielding surface that causes container deformation is considered by varying the outside dimensions of the outer container. The outer container height and width reduction by 2.5 cm is consistent with the damage observed during the 9-meter drop. Table 6-50 below demonstrates the effect of decreasing the spacing by 2.5 cm.

Table 6-50 Package Array (Infinite) Uncertainty, OC Dimensional Variation

Fuel Type	Fuel Bundle, GNF2 w/ BA rods		Fuel Bundle, GE14C w/o BA Rods		Fuel Rods, Rod Box, BWR_G3	
Spacing (cm)	k_p	Δk_u	k_p	Δk_u	k_p	Δk_u
10	0.86034	-0.04615	0.87213	-0.04212	1.0403	-0.00569
5	0.8824	-0.02411	0.89182	-0.02235	1.0427	-0.00333
2.5	0.89368	-0.01281	0.90295	-0.01132	1.0436	-0.00234
0	0.90647	0	0.91429	0	1.0459	0.0
-2.5	0.91982	0.01337	0.9277	0.01341	1.0493	0.00727
-5	0.93409	0.02754	0.94124	0.02703	1.0532	0.01548
-10	0.96431	0.05772	0.97381	0.05962	1.0614	0.01548

Note: Statistical uncertainty, σ_p, in the calculation of k_p is less than 0.00035 for all cases.

6.6.2.2.2.3 Moderation between Packages

The array is slightly undermoderated at zero water density. For evaluations of limited size package arrays, at very low moderator density (0.01 to 0.1) there a small peaking effect on k_{eff}. As the water density increases further, the neutron absorption comes into effect, neutron interaction between packages decreases, and k_{eff} decreases to a minimum and rises again due to increased reflection provided by more interspersed water. The array k_{eff} at full-density moderation is less than the k_{eff} of the flooded and reflected single unit, indicating that the edge-to-edge spacing of the packages is not sufficient to permit full reflection. The fuel design with BA rods is evaluated as a 12x12 package array, while the fuel design without BA rods is evaluated as 6x6 package array similar to the HAC base case.

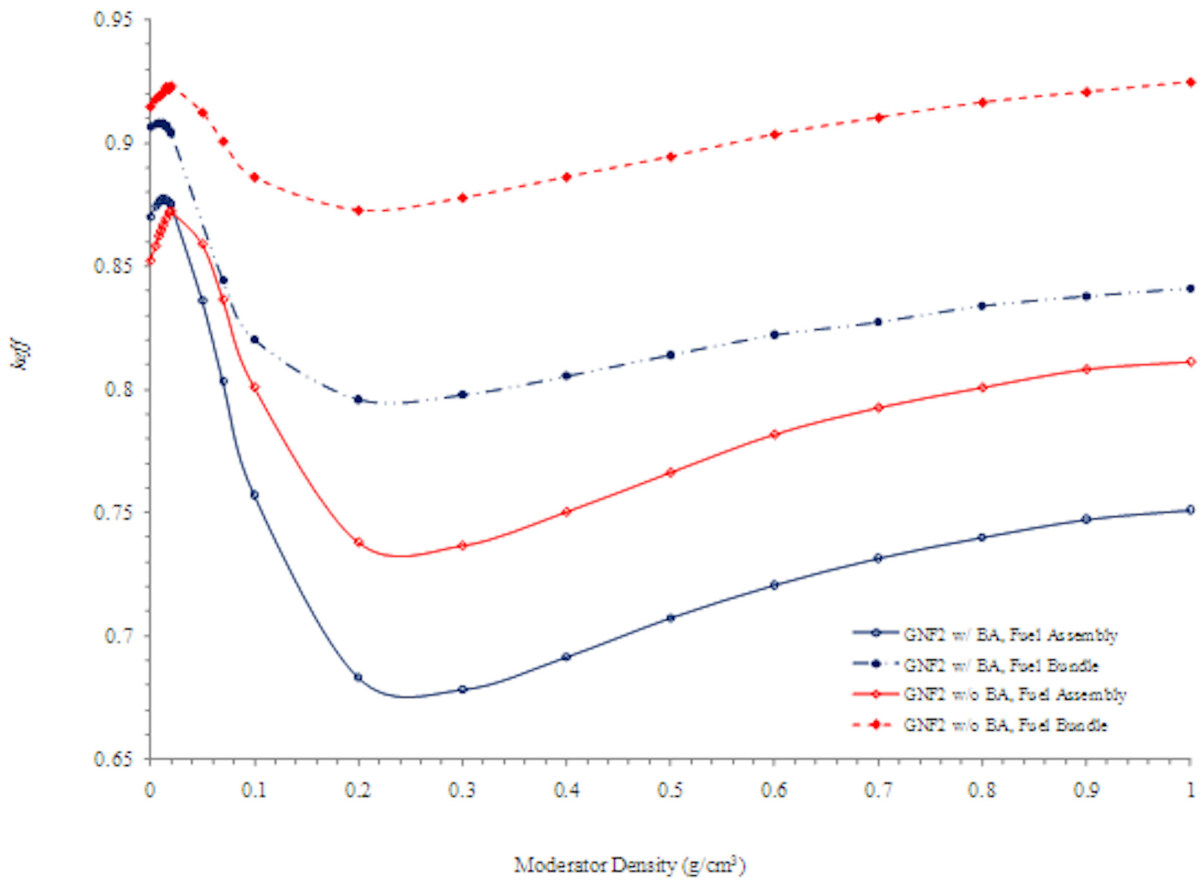

Figure 6-17 Package Array Uncertainty, Moderation Variation

Table 6-51a Package Array Uncertainty, Fuel with BA Rods, Moderation Variation

Moderation Density (g/cm^3)	GNF2 w/ BA Rods					
	Fuel Assembly			Fuel Bundle		
	k_p	σ_p	Δk_u	k_p	σ_p	Δk_u
0	0.86997	0.0003	–	0.90647	0.00035	–
0.005	0.87441	0.00032	0.00488	0.90774	0.0003	0.00173
0.008	0.87588	0.00032	0.00635	0.90826	0.0003	0.00225
0.01	0.87679	0.00031	0.00725	0.90779	0.00034	0.00181
0.012	0.87753	0.0004	0.00806	0.9082	0.00034	0.00222
0.015	0.87689	0.0004	0.00742	0.90692	0.0003	0.00091
0.018	0.87576	0.00032	0.00623	0.90486	0.00036	-0.00111
0.02	0.87518	0.00036	0.00568	0.9042	0.00031	-0.00180
0.05	0.83605	0.00032	-0.03348	–	–	–
0.07	0.80317	0.00038	-0.06632	0.84432	0.00039	-0.06163
0.1	0.75722	0.00036	-0.11228	0.82032	0.00033	-0.08567
0.2	0.68317	0.00034	-0.18635	0.79603	0.00036	-0.10994
0.3	0.67818	0.00033	-0.19134	0.79778	0.00035	-0.10820
0.4	0.69146	0.00043	-0.17799	0.80541	0.00038	-0.10054
0.5	0.7073	0.00035	-0.16221	0.81398	0.00039	-0.09197
0.6	0.72064	0.00033	-0.14888	0.8221	0.00035	-0.08388
0.7	0.73156	0.00035	-0.13795	0.82731	0.00037	-0.07865
0.8	0.73996	0.0004	-0.12951	0.83389	0.00045	-0.07201
0.9	0.74725	0.00038	-0.12224	0.83779	0.00036	-0.06818
1	0.75109	0.00033	-0.11843	0.8411	0.00035	-0.06488

Table 6-51b Package Array Uncertainty, Fuel without BA Rods, Moderation Variation

Moderation Density (g/cm^3)	GNF2 Fuel without BA Rods					
	Fuel Assembly			Fuel Bundle		
	k_p	σ_p	Δk_u	k_p	σ_p	Δk_u
0	0.84717	0.00035	--	0.84717	0.00035	--
0.005	0.85836	0.00036	0.00648	0.91777	0.00039	0.00355
0.008	0.86237	0.00033	0.01047	0.91893	0.00047	0.00477
0.01	0.86447	0.00035	0.01258	0.91947	0.00038	0.00524
0.012	0.86677	0.00036	0.01489	0.92033	0.00048	0.00618
0.015	0.86946	0.00038	0.01759	0.92265	0.00035	0.00840
0.018	0.87202	0.00042	0.02018	0.92176	0.00034	0.00750
0.02	0.87238	0.00034	0.02048	0.92307	0.00041	0.00886
0.05	0.85915	0.00034	0.00725	0.91235	0.00036	-0.00189
0.07	0.83656	0.00036	-0.01532	0.90065	0.0004	-0.01357
0.1	0.80089	0.00033	-0.05101	0.88614	0.00036	-0.02810
0.2	0.73791	0.00039	-0.11395	0.87269	0.00042	-0.04151
0.3	0.73651	0.00034	-0.11539	0.87777	0.00036	-0.03647
0.4	0.75023	0.00034	-0.10167	0.88617	0.00039	-0.02805
0.5	0.76624	0.00041	-0.08560	0.8944	0.00035	-0.01985
0.6	0.78173	0.00036	-0.07015	0.90345	0.00039	-0.01077
0.7	0.79262	0.00035	-0.05927	0.91025	0.00037	-0.00399
0.8	0.80079	0.00046	-0.05101	0.91641	0.00039	0.00219
0.9	0.80822	0.00038	-0.04365	0.92062	0.00036	0.00638
1	0.81127	0.00039	-0.04059	0.92467	0.00043	0.01048

6.6.2.2.2.4 Orientation in Inner Container

The ethafoam cushioning within the IC is assumed to degrade or melt when exposed to an external fire, allowing the assembly to shift within the inner container. A following drop, may also allow the assembly to shift within the inner container.

The effect of orientation of the fuel within the inner container is assessed by positioning the fuel in the four corners of the inner container and evaluating k_{eff} for the infinite array, independently. Table 6-52 below demonstrates that the effect of orientation of the fuel within the inner container.

Table 6-52 Package Array Uncertainty, Bundle/Container Orientation in IC

Fuel Type Position	Fuel Bundle, GNF2 w/ BA Rods		Fuel Bundle, GE14C w/o BA Rods		Fuel Rods, Rod Box, BWR_G3	
	k_p	Δk_u	k_p	Δk_u	k_p	Δk_u
center	0.90647	–	0.91429	–	1.0459	0.0
outer-bottom	0.90252	-0.00344	0.92101	0.00724	1.0396	-0.00588
inner-bottom	0.91336	0.00738	0.92507	0.01127	1.0585	0.01302
outer-top	0.90314	0.00019	0.92038	0.00658	1.0391	-0.00635
inner-top	0.91307	0.00710	0.92581	0.01204	1.0587	0.01318

Note: Statistical uncertainty, σ_p, in the calculation of k_p is less than 0.00040.

6.6.2.2.2.5 Blanket Zones without BA Rods

BA rods are modeled the entire active fuel length. A case is evaluated with the BA removed from the blanket length of the active fuel length; therefore the blanket may be enriched without any BA present. The effect of blanket zones without BA is assessed for top, bottom, and combine top and bottom blanket zones with various lengths up to 8 in. and ^{235}U enrichments up to 5 wt% in a 6x6 array. Table 6-53 demonstrate the impact of k_{eff} for the fuel bundle with lattice expansion for HAC.

The maximum k_{eff} value evaluated is resultant of an 8 in. blanket at the top and bottom of the active fuel height with a ^{235}U enrichment of 5 wt% and no BA present. As compared to a base case 6x6 array evaluation results shows the additional Δk_{eff} margin associated with the blanket evaluation for HAC.

Table 6-53 Package Array (6x6) Summary, GNF2 w/ BA Rods, Blanket(s) w/o BA

Blanket Configuration Material (Region)	Fuel Assembly Δk_u	Fuel Bundle Δk_u
Bottom Only, 5wt% U-235	0.00111	0.00369
Bottom and Top, 5wt% U-235	0.00119	0.00394
Top Only, 5wt% U-235	0.00055	0.00124

Table 6-54 Package Array (6x6) Fuel Bundle, GNF2 w/ BA Rods, Bottom Blanket w/o BA

Blanket Length	U-235 wt%	1.1	2.1	2.6	3.1	3.6	4.1	5.0
3"	k_{eff}	0.82194	0.82295	0.82249	0.82362	0.82379	0.82371	0.82466
	sigma	0.00031	0.00035	0.00035	0.00041	0.00032	0.00039	0.00031
4"	k_{eff}	0.82116	0.82173	0.82271	0.82388	0.82329	0.8239	0.82477
	sigma	0.00036	0.0003	0.00037	0.00032	0.00051	0.00037	0.00039
5"	k_{eff}	0.81915	0.82205	0.8229	0.82333	0.8235	0.82421	0.82546
	sigma	0.00036	0.0004	0.00032	0.0004	0.00035	0.00036	0.00031
6"	k_{eff}	0.81845	0.8215	0.82214	0.82305	0.82325	0.8244	0.82604
	sigma	0.00036	0.00038	0.00038	0.00042	0.00036	0.00039	0.00037
7"	k_{eff}	0.81704	0.82012	0.82102	0.82309	0.82295	0.82467	0.82607
	sigma	0.00034	0.00038	0.00042	0.0004	0.00045	0.00033	0.00043
8"	k_{eff}	0.81657	0.82003	0.821	0.82186	0.82367	0.82519	0.82703
	sigma	0.00033	0.00042	0.00034	0.00034	0.00034	0.00038	0.00037

Table 6-55 Package Array (6x6) Fuel Bundle GNF2 w/ BA Rods, Top and Bottom Blanket w/o BA

Blanket Length	U-235 wt%	1.1	2.1	2.6	3.1	3.6	4.1	5.0
3"	k_{eff}	0.82179	0.82346	0.82231	0.82299	0.82391	0.82402	0.82504
	sigma	0.00032	0.00032	0.00042	0.00033	0.00037	0.00036	0.00037
4"	k_{eff}	0.8211	0.82229	0.8229	0.82319	0.82376	0.82419	0.82433
	sigma	0.00035	0.00043	0.00036	0.00034	0.00037	0.00042	0.00034
5"	k_{eff}	0.81928	0.82095	0.82216	0.82345	0.82359	0.82468	0.82513
	sigma	0.00041	0.00036	0.00034	0.0004	0.00039	0.00038	0.00039
6"	k_{eff}	0.81917	0.82132	0.82188	0.82271	0.82425	0.82433	0.82513
	sigma	0.00043	0.00038	0.00043	0.0004	0.00035	0.00036	0.00035
7"	k_{eff}	0.81619	0.8199	0.82153	0.823	0.82484	0.82517	0.8267
	sigma	0.00035	0.00035	0.00035	0.0004	0.00036	0.00031	0.00036
8"	k_{eff}	0.8157	0.81915	0.82172	0.82284	0.82375	0.82586	0.8273
	sigma	0.00034	0.00035	0.00034	0.00038	0.00038	0.00039	0.00034

Table 6-56 Package Array (6x6) Fuel Bundle GNF2 w/ BA Rods, Top Blanket w/o BA

Blanket Length	U-235 wt%	1.1	2.1	2.6	3.1	3.6	4.1	5.0
3"	k_{eff}	0.82409	0.82326	0.82392	0.82388	0.82353	0.82441	0.82383
	sigma	0.00043	0.00037	0.00034	0.00037	0.00032	0.00054	0.00034
4"	k_{eff}	0.82353	0.82409	0.82455	0.82344	0.82409	0.82359	0.82357
	sigma	0.00035	0.00041	0.00041	0.00032	0.00033	0.00034	0.00035
5"	k_{eff}	0.82305	0.82355	0.82328	0.82363	0.82373	0.82312	0.82367
	sigma	0.00039	0.00037	0.00032	0.00034	0.00043	0.00035	0.00035
6"	k_{eff}	0.82347	0.82386	0.82338	0.82403	0.82338	0.82418	0.82417
	sigma	0.00043	0.00037	0.00036	0.00032	0.00039	0.00042	0.00037
7"	k_{eff}	0.82378	0.82413	0.8241	0.82323	0.82338	0.82379	0.82312
	sigma	0.0004	0.00037	0.00037	0.00037	0.00035	0.00032	0.0004
8"	k_{eff}	0.82377	0.82377	0.82404	0.8241	0.82355	0.82354	0.82383
	sigma	0.00033	0.0004	0.00033	0.00037	0.00035	0.00034	0.00041

6.6.2.3 Summary

The total uncertainty, Δk_u, for the package array is a sum of applicable uncertainties. The HAC uncertainty evaluation accounts for shifting components and package material effects, as well as material and fabrication tolerances. Package material effect uncertainties associated with presence of polyethylene include the assembly orientation shift in the inner container (Section 6.6.2.2.2.4) and the re-distribution of polyethylene (Section 6.3.4.2.4). Uncertainties for the fuel bundle evaluations are applied to the fuel assembly analysis.

Table 6-57 HAC Total Uncertainties for Package Array, Fuel Assembly and Bundle

	HAC Fuel Assembly		HAC Fuel Bundle	
	w/o BA rods	w/ BA rods	w/o BA rods	w/ BA rods
Uncertainty	Δk_u	Δk_u	Δk_u	Δk_u
Material and fabrication tolerances				
Fuel pellet diameter	0.0008	0.00112	0.0008	0.00112
Clad thickness	0.00235	0.00235	0.00235	0.00235
Fuel rod pitch	0.00294	0.00138	0.00294	0.00138
Packaging steel	0.01097	0.00969	0.01097	0.00969
Polyethylene (annulus on fuel rod)	0.00071	0.00061	0.00071	0.00061
Geometric and material representation				
Spacing in outer container	0.00394	0.00310	0.00434	0.00359
Package spacing	0.0159	0.01580	0.01341	0.01385
Moderation	0.02048	0.00806	0.01048	0.00225
Orientation in inner container	0.01204	0.01460	0.01204	0.00738
Polyethylene redistribution	0.02789	0.02789	0.02789	0.02789
Blanket Zones without BA rods	–	0.00118	–	0.00394
BA rod reactivity worth verification	–	0.015	–	0.015
Total Uncertainty, Δk_u(rss value)	0.042	0.041	0.037	0.038

Table 6-58 HAC Total Uncertainties for Package Array, Fuel Rods

Uncertainty	Δk_u
Material and fabrication tolerances	
Fuel pellet diameter	0.00047
Clad thickness	0.00252
Fuel rod pitch	–
Packaging steel	0.01064
Polyethylene (annulus on fuel rod)	0.00094
Geometric and material representation	
Spacing in outer container	0.00471
Package spacing	0.00387
Moderation	0.02048
Orientation in inner container	0.01318
Polyethylene redistribution	0.02789
Blanket Zones without BA rods	–
BA rod reactivity worth verification	–
Total Uncertainty, Δk_u(rss value)	0.040

Table 6-59 Package Array under HAC Transport Summary

Contents	2N	k_p	σ_p	Δk_u	Maximum k_p
Fuel Bundle without BA Rods Table 6-41, GNF2	25	0.88900	0.00040	0.037	0.9268
Fuel Bundle with 8 BA Rods Table 6-44, GNF2	132	0.90176	0.00035	0.038	0.9405
Fuel Assembly without BA Rods Table 6-42, GE14C	49	0.88940	0.00033	0.042	0.9291
Fuel Assembly with 8 BA Rods Table 6-43, GNF2	144	0.86997	0.00030	0.041	0.9076
Fuel Rods with Rod Container Table 6-46b, BWR_G3, rod box, 0.75 half-pitch	144	0.88320	0.00035	0.040	0.9239
Fuel Rods without Rod Container Table 6-45a, PWR_W3, 1.6 half-pitch	144	0.80154	0.00034	0.040	0.8423

6.7 FISSILE MATERIAL PACKAGES FOR AIR TRANSPORT

RAJ-II does not satisfy the requirements for fissile material package designs to be transported by air specified in 10 CFR 71.55(f).

6.7.1 Configuration

Not applicable.

6.7.2 Results

Not applicable.

6.8 BENCHMARK EVALUATIONS

The criticality safety critical experiment benchmarks were computed using SCALE 6 CSAS6 and the 238GROUPNDF7 cross-section library. Critical experiments were selected to represent the materials and geometry of the package. The USLSTATS methodology [Ref. 6] is used to determine an Upper Subcritical Limit (USL).

6.8.1 Applicability of Benchmark Experiments

Critical experiment cases were selected from NUREG/CR-6361 [Ref. 6] to evaluate the performance of the SCALE codes and cross-section libraries for heterogeneous systems with similarity to the package configurations. These experiments include low-enriched light-water-reactor (LWR) lattices and demonstrate the performance of both the cross sections and the SCALE resonance cross-section processing methodology. The critical experiments span a range of moderation and fuel pin arrangements that are applicable in evaluating LWR fuel storage and transport and a BWR reactor core configuration with BA rods. A summary of the critical experiments is provided in Section 6.9.7.

TSUNAMI in SCALE 6 is used to calculate sensitivity and uncertainty data for each of the critical experiments and each of the package configurations. TSUNAMI-IP is used to calculate global indices that assess the similarity of the package and critical experiments on a system wide basis for all nuclides and reactions. The integral index, $c_{k,}$ is calculated for each package configuration (individual package and package array) with contents (fuel bundle or fuel assembly and fuel rods). The interpretation of the correlation coefficient, $c_{k,}$ is as follows: a value of 0.0 represents no correlation between the package configuration and critical experiment and a value of 1.0 represents full correlation between the systems. Each package configuration has different sensitivities that affect the bias determination, and no critical experiments were allowed to qualify for use in determining the USL for a given package configuration unless their c_k value was at least 0.80.

TSUNAMI-IP also calculates a penalty for the application response due to uncovered sensitivity coefficients. The penalty due to noncoverage by the benchmarks (i.e., the penalty due to the application not being in the area of applicability of benchmarks completely) could be used as an additional subcritical margin in licensing calculations. This penalty due to noncoverage of Gd capture cross sections is small, with a maximum total penalty of 0.134 %Δk/k. Therefore, it is concluded that although sufficient benchmark experiments did not exist to provide full coverage for all design scenarios, the potential impact on the noncoverage on the criticality safety of the shipping package was minimal.

6.8.2 Bias Determination

In all cases the distribution of k_{eff} values calculated for the final set of applicable benchmarks could be considered to represent a normal distribution at a confidence level of 0.95. This was determined by running several statistical analyses, each of which took a different approach to the hypothesis that “the sample data are not significantly different than a normal population.” The three quantitative tests chosen were: the Chi-Square goodness of fit test, the Kolmogorov-Smirnov/ Lilliefors test and the Shaprio Wilk normality test. The results of these tests for each of the USL evaluations are given below in Table 6-60, along with the number of critical benchmarks which qualified for each test by meeting or exceeding a c_k value of 0.80.

Table 6-60 Normality Test Results for USL Evaluations

Test Type	Calculated Value	Critical Value	Conclusion (95% Confidence)
Individual Package, Containing Fuel Bundle without BA Rods (n = 41)			
Shaprio-Wilk, *W*	0.94728	≥ 0.05617	Accept Normality
Kolmogoroc-Smirnov/Lilliefor, *D*	0.0744	≤ 0.82211	No evidence against normality
Chi-Square, χ^2	6.6829	≤ 9.49	Accept Normality
Package Array, Containing Fuel Bundles without BA Rods (n = 43)			
Shaprio-Wilk, *W*	0.96038	≥ 0.14314	Accept Normality
Kolmogoroc-Smirnov/Lilliefor, *D*	0.06807	≤ 0.88559	No evidence against normality
Chi-Square, χ^2	4.9048	≤ 9.49	Accept Normality
Package Array, Containing Fuel Bundles with BA Rods (n = 43)			
Shaprio-Wilk, *W*	0.96038	≥ 0.14314	Accept Normality
Kolmogoroc-Smirnov/Lilliefor, *D*	0.06807	≤ 0.88559	No evidence against normality
Chi-Square, χ^2	4.7907	≤ 9.49	Accept Normality
Individual Package, Containing Fuel Rods (n = 43)			
Shaprio-Wilk, *W*	0.96038	≥ 0.14314	Accept Normality
Kolmogoroc-Smirnov/Lilliefor, *D*	0.06807	≤ 0.88559	No evidence against normality
Chi-Square, χ^2	4.7907	≤ 9.49	Accept Normality
Package Array, Containing Fuel Rods (n = 36)			
Shaprio-Wilk, *W*	0.98184	≥ 0.80556	Accept Normality
Kolmogoroc-Smirnov/Lilliefor, *D*	0.06062	≤ 0.98355	No evidence against normality
Chi-Square, χ^2	0.2857	≤ 9.49	Accept Normality

After testing for normal distributions, the USL was calculated for each application using parametric methods consistent with USLSTATS [Ref. 6], using c_k as the trending parameter. In each package configuration evaluation, this produces two non-linear extrapolations towards a trend value of 1.0 for c_k. USL Method 1 (USL1) uses a confidence band with an administrative margin to determine a limit, while USL Method 2 (USL2) develops a single-sided closed-interval with a statistically calculated margin of subcriticality to determine a limit.

In each configuration, the USL2 values calculated exceeded USL1 by a significant margin, indicating that an administrative margin of 0.05 is sufficient. These results are shown in Figures 6-18 through 6-22 below, and both of these USL values as evaluated at c_k = 1.0 are given in Table 6-61.

As the USL1 values were consistently more conservative than the values determined using the USL2 method, the USL1 values at c_k = 1.0 are identified as the upper subcritical limit defined in Section 6.1.2.

Table 6-61 USL Summary for Δk_m=0.05 Evaluated at c_k=1.0

Package Configuration	$USL_1=k_c-\Delta k_c-\Delta k_m$	$USL_2=k_c-\Delta k_c$
Fuel Bundle or Fuel Assembly no BA Rods, Individual Package	0.9448	0.9898
Fuel Bundle or Fuel Assembly with BA Rods, Package Array	0.9434	0.9880
Fuel Bundle or Fuel Assembly no BA Rods, Package Array	0.9449	0.9887
Fuel Rods, Individual Package	0.9405	0.9820
Fuel rods, Package Array	0.9441	0.9900

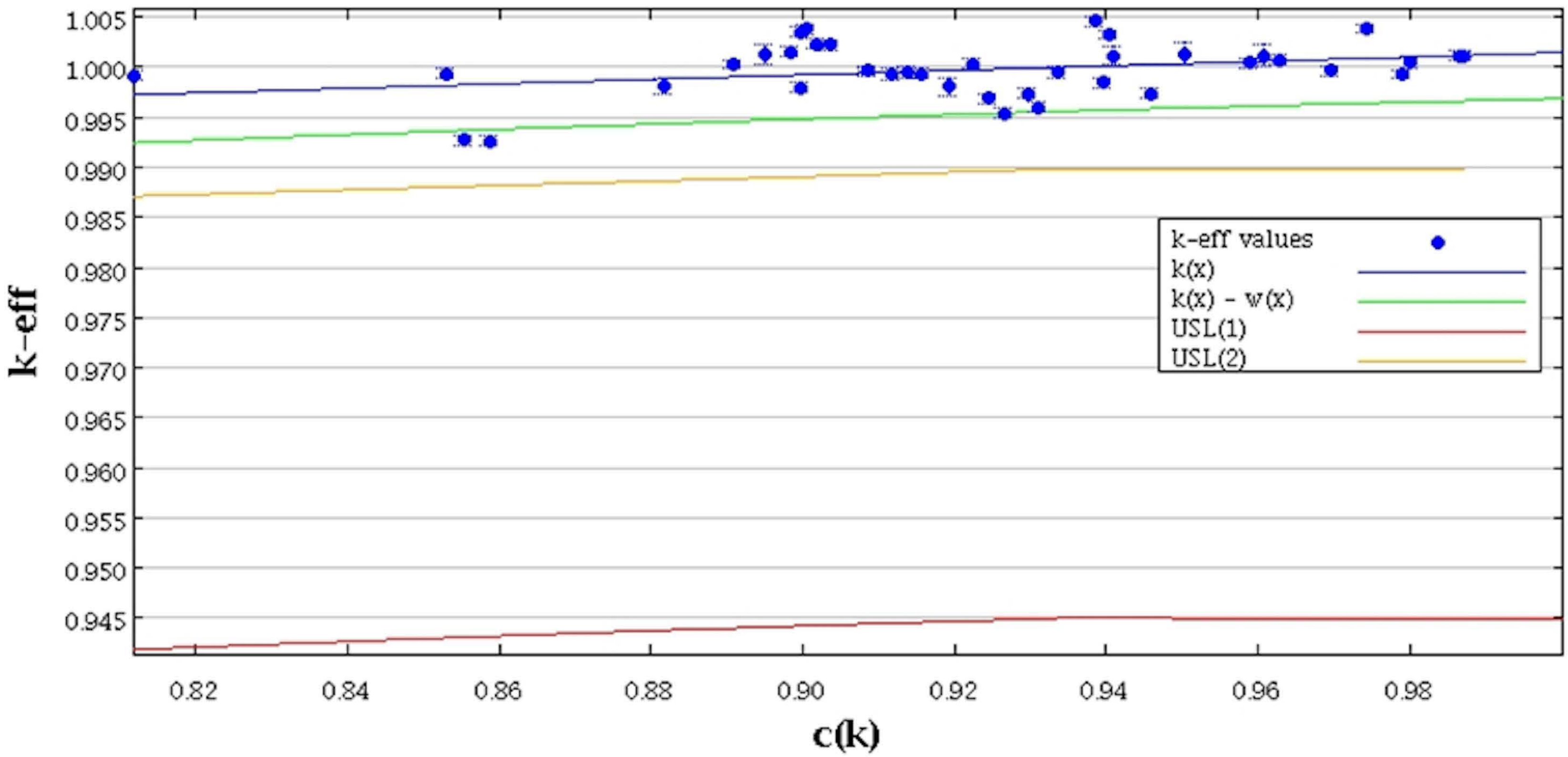

Figure 6-18 USLSTATS Evaluated Limits for an Individual Package, Containing Fuel Bundle without BA Rods

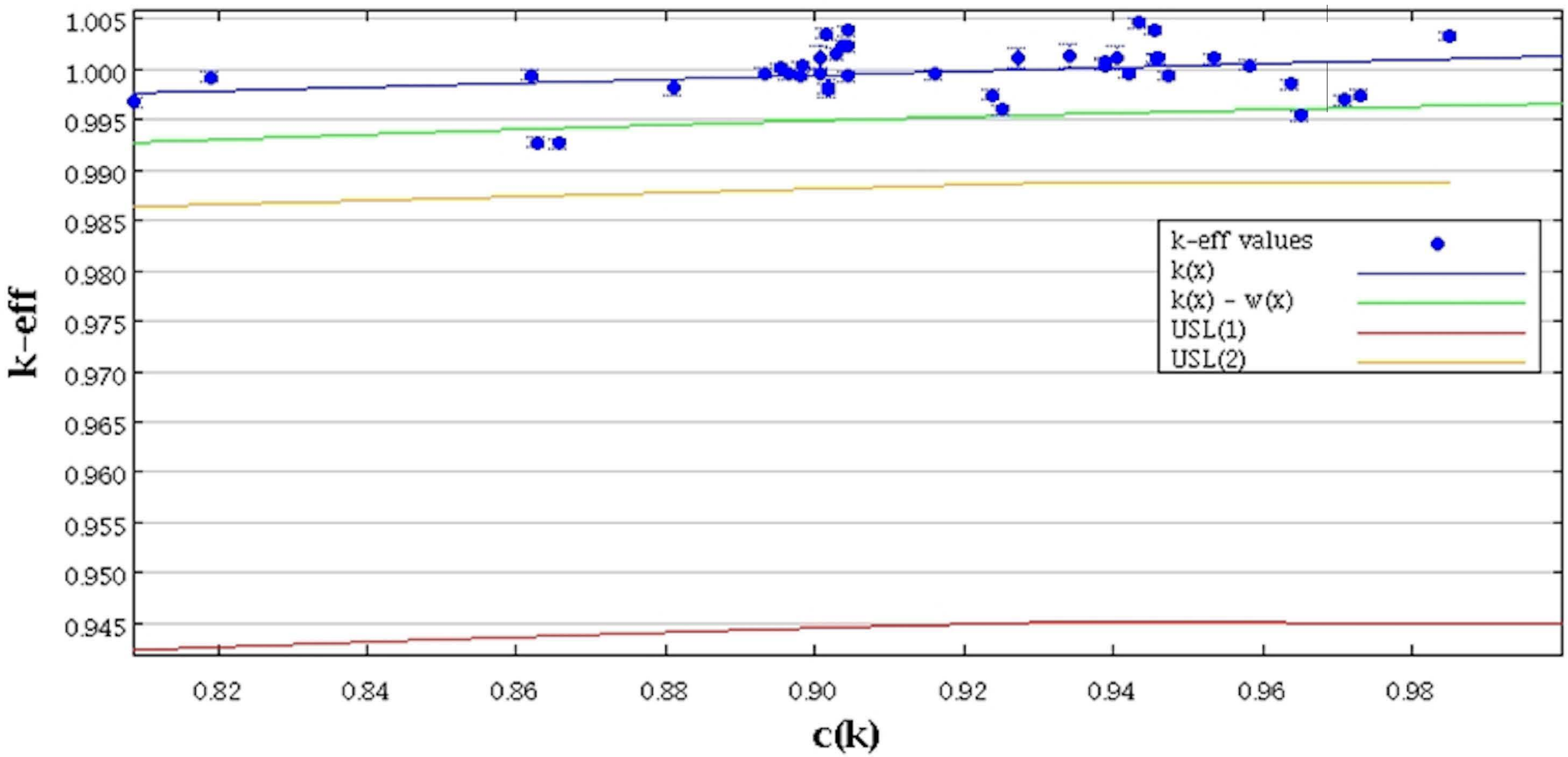

Figure 6-19 USLSTATS Evaluated Limits for a Package Array, Containing Fuel Bundles without BA Rods

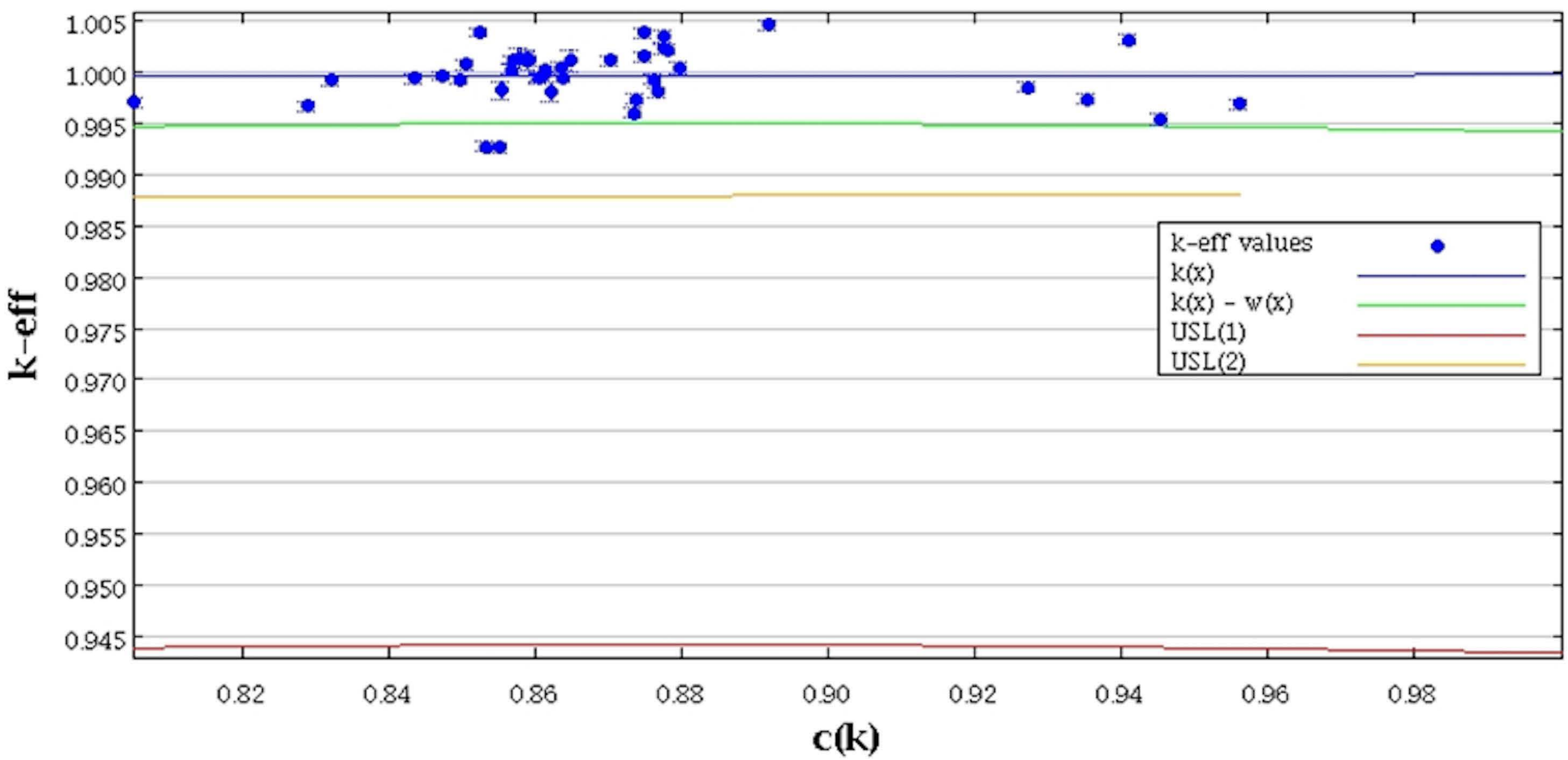

Figure 6-20 USLSTATS Evaluated Limits for a Package Array, Containing Fuel Bundles with BA Rods

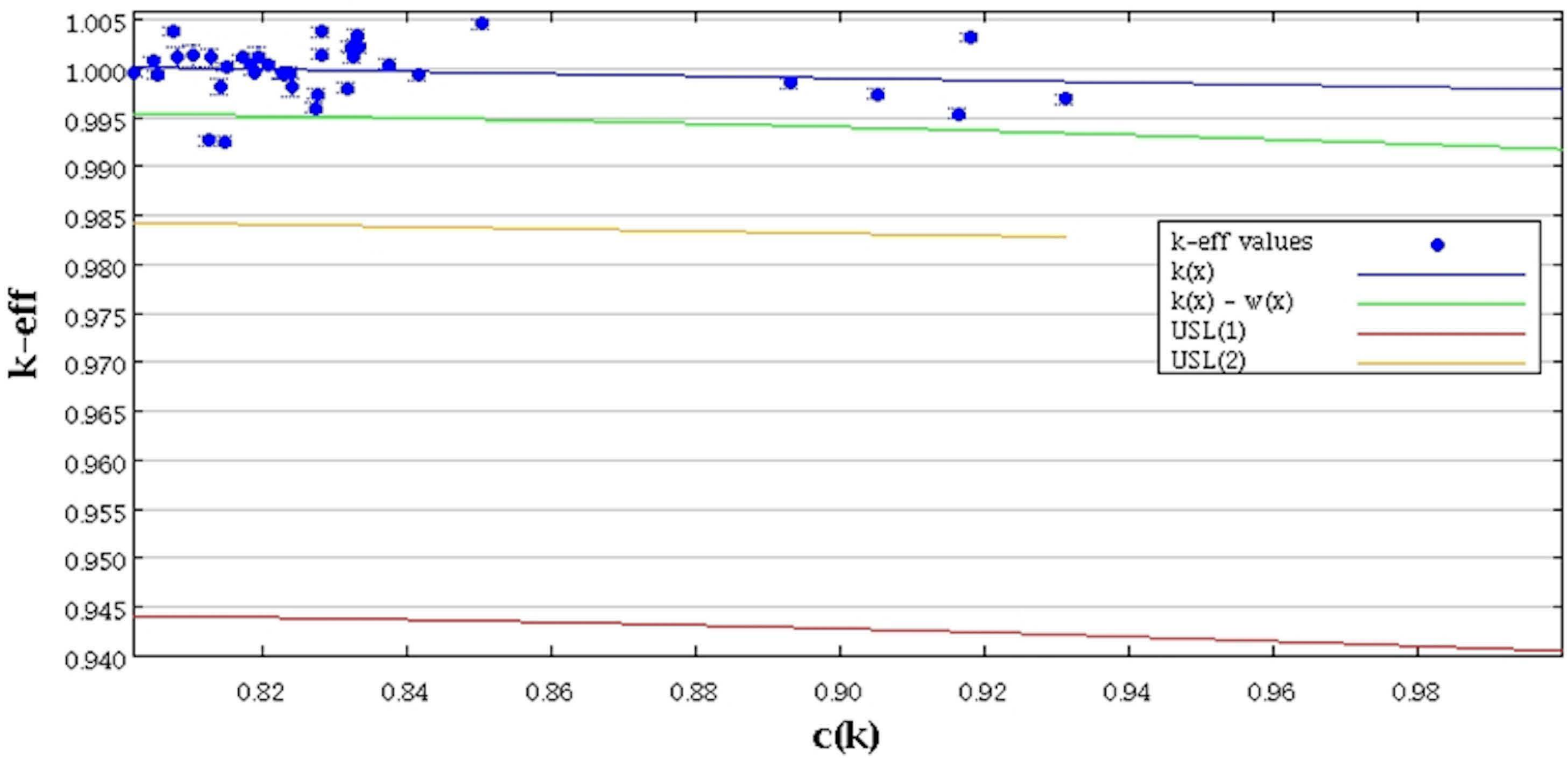

Figure 6-21 USLSTATS Evaluated Limits for an Individual Package, Containing Fuel Rods

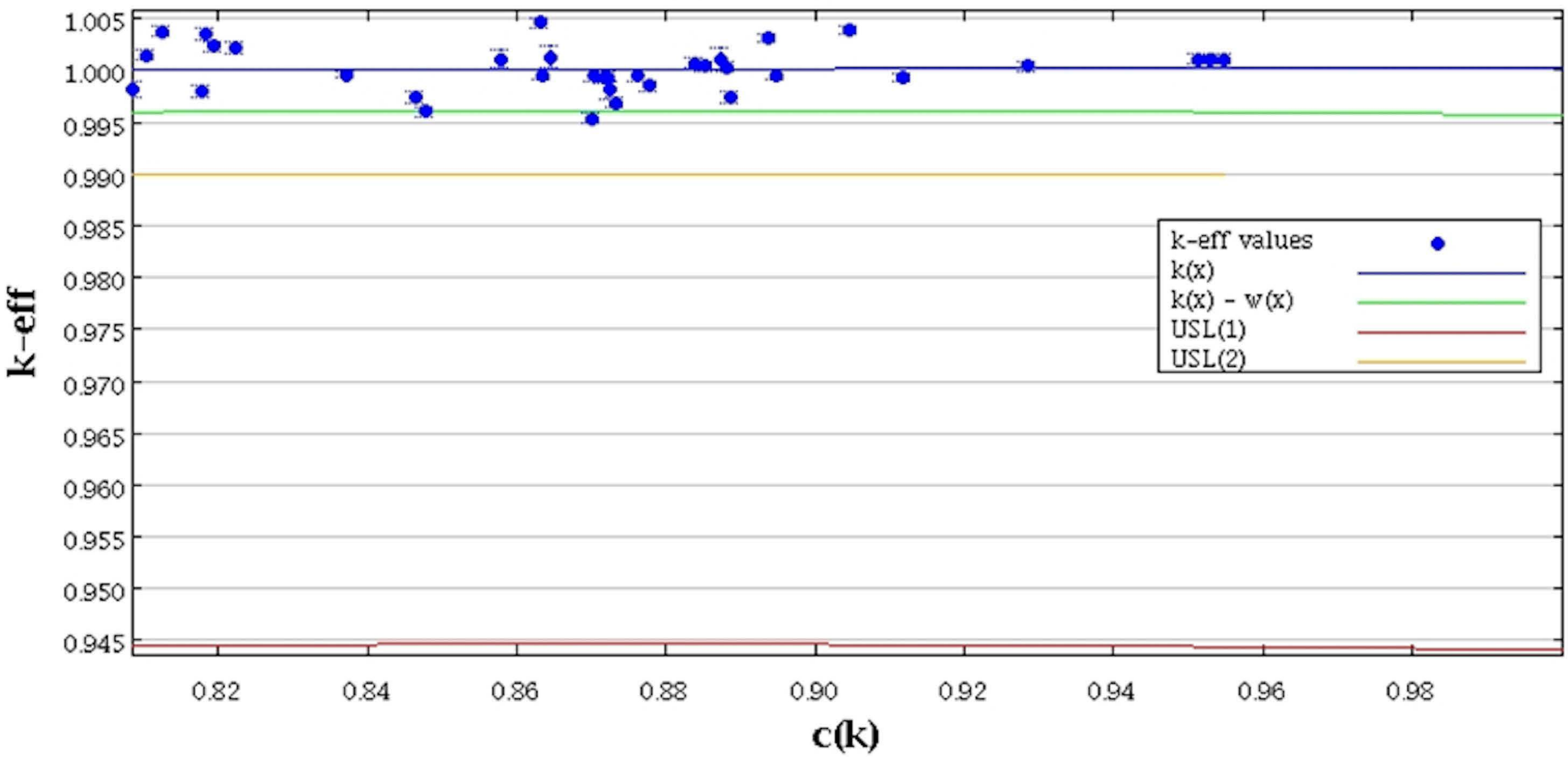

Figure 6-22 USLSTATS Evaluated Limits for a Package Array, Containing Fuel Rods

6.9 APPENDIX

6.9.1 References

1. ANSI/ANS-8.17-2004: "Nuclear Criticality Safety in Operations with Fissionable Materials Outside Reactors," American Nuclear Society, La Grange Park, Illinois.

2. ASTM 996-04, "Standard Specification for Uranium Hexafluoride Enriched to Less Than 5% ^{235}U," ASTM International, West Conshohocken, PA.

3. SCALE: *A Modular Code System for Performing Standardized Computer Analyses for Licensing Evaluations*, ORNL/TM-2005/39, Version 6, Vols. I–III, January 2009. Available from Radiation Safety Information Computational Center at Oak Ridge National Laboratory as CCC-750.

4. NUREG/CR-6686, ORNL/TM-1999/322, "*Experience with the SCALE Criticality Safety Cross Section Libraries*," 1997.

5. ASTM A480 / A480M-10, "Standard Specification for General Requirements for Flat-Rolled Stainless and Heat-Resisting Steel Plate, Sheet, and Strip."

6. NUREG/CR-6361, ORNL/TM-13211, "Criticality Benchmark Guide for Light-Water-Reactor Fuel in Transportation and Storage Packages," March 1997.

7. J. Zino, V. Mills, D. Dixon, "Low Enriched UO_2 Pin Lattice in Water Critical Benchmark Evaluations with ENDF/B-VII Nuclear Data," *ANS Topical Meeting on Advances in Reactor Physics*, PHYSOR2006, Vancouver, BC (September 2006).

8. NUREG 5661, ORNL/TM-11936, "Recommendations for the Criticality Safety Evaluation for Transportation Packages," April 1997.

9. Evaluated Nuclear Data File Version B [ENDF/B]-VII.1 Nuclear Data for Science and Technology: Cross Sections, Covariances, Fission Product Yields and Decay Data, *Nucl. Data Sheets*, 112, 2887-2996 (2011)., http://www.nndc.bnl.gov/exfor/endf00.jsp

10. "Safety Analysis Report for the Model Number RAJ-II Package," J/143/AF-96, Global Nuclear Fuel-Japan, April 2002.

6.9.2 Input Files

All input and output files are provided to NRC for review. This method has been discussed and approved by NRC staff.

6.9.3 Gad Worth Evaluation and Pattern Selection Specifications

A set of BA rod locations is chosen to demonstrate the maximum credible reactivity for each fuel design. Constraints are placed on possible BA rod locations that will force the choice of other fuel lattice locations where the BA rod is a more effective neutron absorber. These constraints are consistent with actual fuel design objectives, and as such recognize that certain arrangements are not allowed in the actual fuel bundle designs. In addition to fuel design constraints, lattice locations at the edge of the fuel bundle are not considered as possible BA rod locations due to transport conditions resulting in partial moderation in the fuel lattice. These constraints result in a demonstration of a maximum reactivity configuration for credible fuel designs only, not every conceivable arrangement of BA rods in the fuel lattice. The constraints that are considered in selecting the BA rod locations for the purpose of the criticality assessment are summarized as the following rules with reference to Figure 6-23:

1. Rule of symmetry: BA rods shall be in positions that are symmetric across the geometric major diagonal (defined from the control blade corner of position A1)

    a. Along the diagonal corresponds to a single position
    b. Off the diagonal corresponds to a pair of two rod positions.

2. No BA rod shall be located in the outermost edge or corner location of the fuel lattice

3. Partial length fuel rods shall not be BA rods

4. At least one BA rod shall be located in three of the four fuel bundle quadrants

5. At least eight (8) BA rods must be located in each fuel lattice (the fuel bundle design defines the axial lattices in a bundle)

6. No BA rods are required in fuel lattices (i.e., axial zones) that do not have fissile material or have uranium enriched in ^{235}U to a maximum of 1.0% by weight.

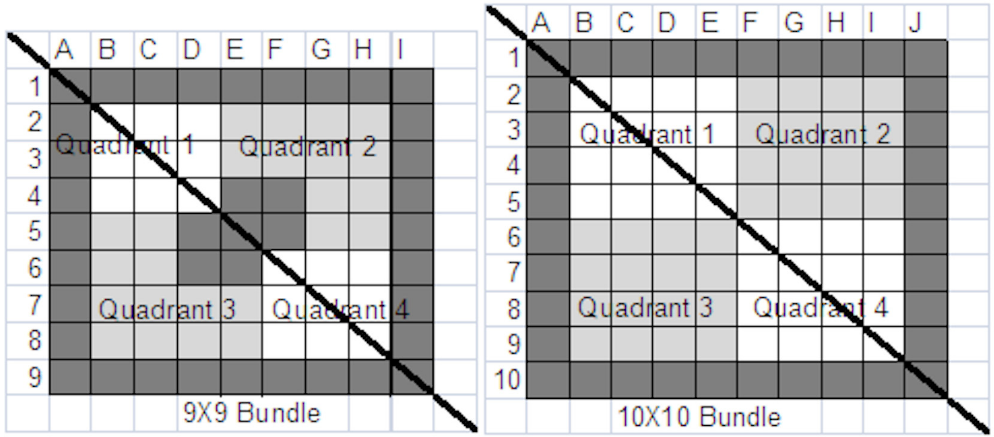

Figure 6-23 Fuel Lattice Description

A fuel lattice quadrant is defined by the symmetry across the major diagonal from the control blade corner of position A1, as shown in Figure 6-23. For a 9X9 fuel lattice, there are not equal number of rods in each quadrants, however the quadrants are symmetric and allow for fuel design flexibility. Three rod zones are defined by the four quadrants, as follow for the purpose of selecting the allowable BA rod positions:

ZONE A Allowable rods in QUADRANT 1

ZONE B Allowable rod pairs in QUADRANT 2 and QUADRANT 3, as defined by the rule of symmetry

ZONE C Allowable rods in QUADRANT 4

Constraints are placed on possible BA rod locations such that the locations chosen for the package evaluation are not necessarily the least worth BA rod locations. In general, the least worth BA rod locations are located furthest from the water moderated regions. For BA rods to occupy at least three quadrants and meet the rule of symmetry, these criterion force selection of increased worth positions that may result in a decreased k_{inf}. Additionally, clumping of BA rods in a single quadrant results in BA rods that are face adjacent; face adjacent rods result in spatial shielding that decreases the individual BA rod worth resulting in an increased k_{inf}. The constraints imposed by rules for the selection of BA rods result in selecting face adjacent BA rods and BA rods that are not the least worth. While, actual BWR bundle designs rarely have face-adjacency, the combination effects will increase criticality for transport calculations. The final constraint states lattice locations at the edge of the fuel bundle are not allowed, since these BA locations would be ineffective for transport conditions resulting in partial moderation in the fuel lattice.

The pattern selection process begins with categorizing the allowable BA rod pairs by Zone A, B and C. The term “rod pairs” is used to represent both a single BA rod on the diagonal (in either

Zone A or C) and a pair of two rods that are in symmetric locations across the major diagonal (in Zone B). The BA rod "worth" means the sensitivity, $\Delta k_{inf}/\Delta N_{Gd}$. The "worth of a rod pair" is therefore either the average of two BA rod positions or, in the case of a rod on the major diagonal, the worth of a single BA rod position. The rule that requires only 3 of the 4 quadrants to have BA rods may eliminate either Zone A or C from the selection process. Both Zone A and C are symmetric in the lattice arrangement. The second step is to sort the BA rod pairs in Zones A, B, and C by their worth. The top least worth rods will define the Zone along the major diagonal to be eliminated from the selection process. Then the BA rod pairs in Zone B and either one of Zone A or Zone C are sorted by their worth. The first 8 BA rods are selected. If no rods in Zone B are in the 8 least worth BA rods, then the highest worth rod pair in the group of 8 is replaced by the next least worth rod pair in Zone B. This process results in a pattern of 8 BA rods that follow the selection rules.

As an example, the SVEA design is utilized here to demonstrate the application of the BA rod pattern selection process, through evaluation of the ^{157}Gd sensitivity coefficients of the infinite array results (displayed at the end of this section). Each rod position is associated with a material identification number assigned by the computer model (SCALE6/CSAS6).

Step 1. Categorize the allowable BA rod pairs by Zone A, B and C and calculate worth

From the fuel bundle the rod pairs are matched and categorized by Zone. The term "rod pairs" is used to represent both a single BA rod on the diagonal (in either Zone A or C) and a pair of two rods that are in symmetric locations across the major diagonal (in Zone B). The average worth of the rod pairs is calculated.

Zone	Material ID	Bundle Location	Average Worth
B	22*99	I2*B9	-2.4949E-03
B	23*89	H2*B8	-2.0807E-03
B	24*79	G2*B7	-2.1369E-03
B	25*69	F2*B6	-2.8627E-03
A	26*59	E2*B5	-2.7787E-03
A	27*49	D2*B4	-2.1770E-03
A	28*39	C2*B3	-2.1183E-03
A	29*	B2	-2.4449E-03
B	32*98	I3*C9	-2.1144E-03
B	33*88	H3*C8	-1.7314E-03
B	34*78	G3*C7	-2.0330E-03
B	35*68	F3*C6	-3.0013E-03
A	36*58	E3*C5	-2.9933E-03
A	37*48	D3*C4	-2.0080E-03
A	38*	C3	-1.7348E-03

Zone	Material ID	Bundle Location	Average Worth
B	42*97	I4*D9	-2.1412E-03
B	43*87	H4*D8	-2.0421E-03
B	44*77	G4*D7	-3.0736E-03
A	47*	D4	-3.0994E-03
B	52*96	I5*E9	-2.8087E-03
B	53*86	H5*E8	-3.0181E-03
C	62*95	I6*F9	-2.7684E-03
C	63*85	H6*F8	-3.0566E-03
C	72*94	I7*G9	-2.1439E-03
C	73*84	H7*G8	-2.0319E-03
C	74*	G7	-2.9188E-03
C	82*93	I8*H9	-2.0653E-03
C	83*	H8	-1.7885E-03
C	92*	I9	-2.4611E-03

Step 2. Sort the BA rod pairs in Zones A, B, and C by their worth

Pairs are ranked based on average worth, with the least average worth (i.e., largest negative value) ranking number one. Zones A and C lie on the major diagonal each containing a single quadrant, while Zone B lies across the major diagonal and includes two quadrants.

Zone	Material ID	Bundle Location	Average Worth	Rank
B	33*88	H3*C8	-1.73E-03	1
A	38*	C3	-1.73E-03	2
C	83*	H8	-1.79E-03	3
A	37*48	D3*C4	-2.01E-03	4
C	73*84	H7*G8	-2.03E-03	5
B	34*78	G3*C7	-2.03E-03	6
B	43*87	H4*D8	-2.04E-03	7
C	82*93	I8*H9	-2.07E-03	8
B	23*89	H2*B8	-2.08E-03	9
B	32*98	I3*C9	-2.11E-03	10
A	28*39	C2*B3	-2.12E-03	11
B	24*79	G2*B7	-2.14E-03	12
B	42*97	I4*D9	-2.14E-03	13

Zone	Material ID	Bundle Location	Average Worth	Rank
C	72*94	I7*G9	-2.14E-03	14
A	27*49	D2*B4	-2.18E-03	15
A	29*	B2	-2.44E-03	16
C	92*	I9	-2.46E-03	17
B	22*99	I2*B9	-2.49E-03	18
C	62*95	I6*F9	-2.77E-03	19
A	26*59	E2*B5	-2.78E-03	20
B	52*96	I5*E9	-2.81E-03	21
B	25*69	F2*B6	-2.86E-03	22
C	74*	G7	-2.92E-03	23
A	36*58	E3*C5	-2.99E-03	24
B	35*68	F3*C6	-3.00E-03	25
B	53*86	H5*E8	-3.02E-03	26
C	63*85	H6*F8	-3.06E-03	27
B	44*77	G4*D7	-3.07E-03	28
A	47*	D4	-3.10E-03	29

Both Zone A and C are symmetric along the major diagonal in the lattice arrangement, therefore one zone may be eliminated in the selection process while maintaining BA rods in 3 quadrants. In this example, the BA rod pairs in Zone C are eliminated, since the rod pairs of Zone A rank higher (i.e., have a lower worth position), as shown in the above table. Therefore, Zone A and Zone B rod pairs are carried to the next step.

Step 3. Sort selected Zones and select BA rod pattern

The BA rod pairs in Zone B and either one of Zone A or Zone C are sorted by their worth. In this example, Zone A and Zone B are re-ranked by least average worth.

Zone	Material ID	Bundle Location	Average Worth	Rank
B	33*88	H3*C8	-1.73E-03	1
A	38*	C3	-1.73E-03	2
A	37*48	D3*C4	-2.01E-03	4
B	34*78	G3*C7	-2.03E-03	6
B	43*87	H4*D8	-2.04E-03	7
B	23*89	H2*B8	-2.08E-03	9
B	32*98	I3*C9	-2.11E-03	10

Zone	Material ID	Bundle Location	Average Worth	Rank
A	28*39	C2*B3	-2.12E-03	11
B	24*79	G2*B7	-2.14E-03	12
B	42*97	I4*D9	-2.14E-03	13
A	27*49	D2*B4	-2.18E-03	15
A	29*	B2	-2.44E-03	16
B	22*99	I2*B9	-2.49E-03	18
A	26*59	E2*B5	-2.78E-03	20
B	52*96	I5*E9	-2.81E-03	21
B	25*69	F2*B6	-2.86E-03	22
A	36*58	E3*C5	-2.99E-03	24
B	35*68	F3*C6	-3.00E-03	25
B	53*86	H5*E8	-3.02E-03	26
B	44*77	G4*D7	-3.07E-03	28
A	47*	D4	-3.10E-03	29

The final step is the selection of the top ranked pair. The first 8 BA rods are selected. If no rods are in Zone B within the 8 least worth BA rods, then the highest worth rod pair in the group of 8 is replaced by the next least worth rod pair in Zone B. This process results in a pattern of 8 BA rods that follow the selection rules.

For this example, the top four lowest ranked pairs contain only 7 rods. In this case, the next least worth single rod is selected, which is rod rank 16 in the table above. Often in the ranking of two zones a single rod on the diagonal is highly ranked, while another single rod is ranked lower. For verification, a pattern is analyzed that removes the single rod from the top 8 selected BA rods, and adds the next ranked pair to the selection of BA rods. In this example, the secondary pattern would result in rod pair ranked values 1, 4, 6, and 7 of the above table.

Since BA rod placement effects system multiplication, through competing effects of self-shielding and absorption, both the patterns are evaluated in an infinite bundle array at 2wt% Gd_2O_3. The most reactive BA pattern specification is carried forward to the package analyses for transport. Often a pattern k_{inf} is within two sigma of other patterns, and hence are statistically the same value. Comparison of pattern results shows that k_{eff} is not particularly sensitive to the applied constraints in the BA rod selection process. Therefore, there is no significant uncertainty associated with the selected least worth BA rod patterns and constraints for most reactive package contents with credited BA rods.

The resultant eight BA rod locations selected based on the constraints for BA rod pattern selection for the SVEA fuel design are B2, C3, D3, G3, H3, C4, C7, and C8, shown in Figure 6-24 in the circled positions.

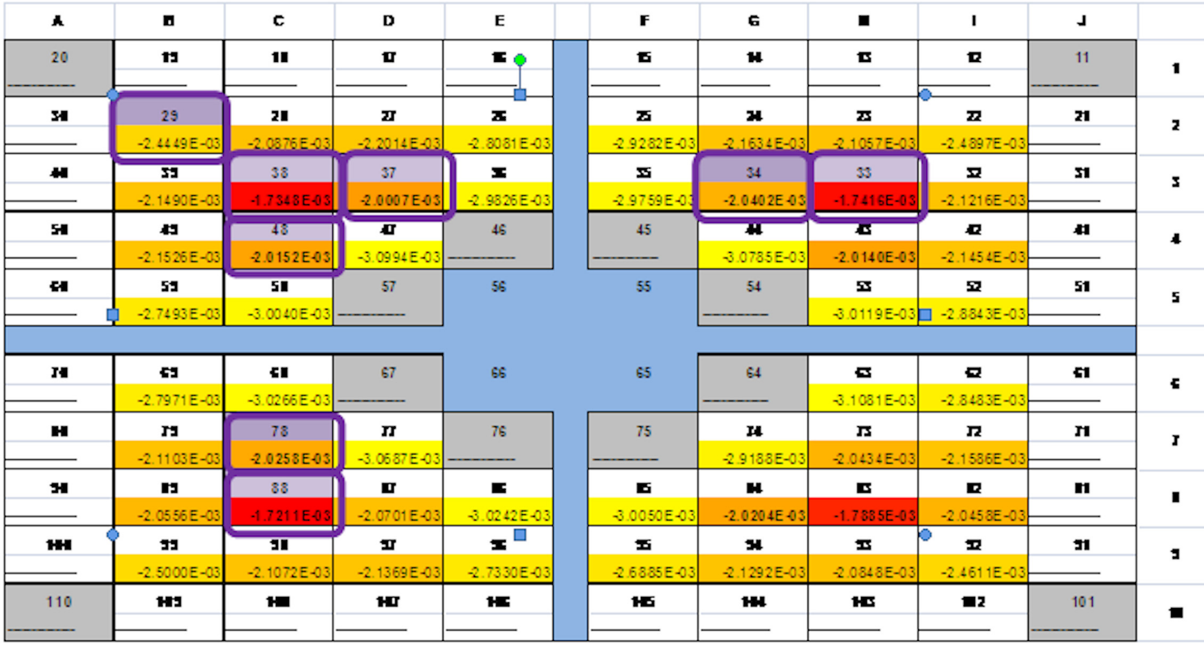

Figure 6-24 SVEA ^{157}Gd Sensitivity Results for Demonstration of Gad Pattern Selection

The following figures display the infinite array calculation results as Gad worth mapping for each rod position used to determine the BA rod positions. The locations are determined for an infinite array of fuel bundles to represent the package array. Figures display the ^{157}Gd relative worth for each viable BA rod position for each fuel design, respectively. The numeric values shown in the figures for each rod position represent an associated material identification number assigned in the computer model (SCALE6/CSAS6) and the ^{157}Gd relative worth value (below in the same box).

The color key below applies to the following figures. The grey colored boxes represent partial length rods and along with the outer edge boxes/rods no burnable absorbers are allowed. The purple colored rod positions represent BA rod selection defined in this calculation note.

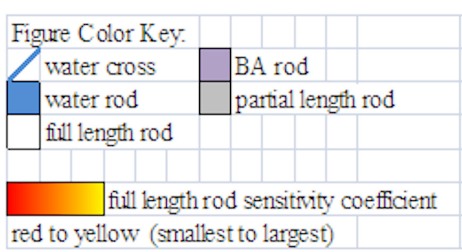

A	B	C	D	E	F	G	H	I	
30 ---------	29 ---------	28 ---------	27 ---------	26 ---------	25 ---------	24 ---------	23 ---------	21 ---------	1
40 ---------	39 ---------	38 -2.9089E-03	37 -2.9974E-03	36 ---------	35 -2.9106E-03	34 -3.0438E-03	33 ---------	31 ---------	2
50 ---------	49 -2.9605E-03	48 -2.4253E-03	47 -2.8297E-03	46 -4.3476E-03	45 -3.9473E-03	44 -2.8421E-03	43 -3.0776E-03	41 ---------	3
60 ---------	59 -2.9896E-03	58 -2.9604E-03	57 -5.2278E-03	56	55	54 -3.9859E-03	53 -3.1175E-03	51 ---------	4
70 ---------	69 ---------	68 -4.3623E-03	67	66	65	64 -4.2982E-03	63 ---------	61 ---------	5
80 ---------	79 -3.1027E-03	78 -3.9418E-03	77	76	75 -5.3780E-03	74 -2.9218E-03	73 -3.0322E-03	71 ---------	6
90 ---------	89 -3.1032E-03	88 -2.9064E-03	87 -4.1097E-03	86 -4.4686E-03	85 -3.0337E-03	84 -2.5217E-03	83 -3.0011E-03	81 ---------	7
100 ---------	99 ---------	98 -3.0937E-03	97 -3.1306E-03	96 ---------	95 -2.9772E-03	94 -3.0529E-03	93 ---------	91 ---------	8
110 ---------	109 ---------	108 ---------	107 ---------	106 ---------	105 ---------	104 ---------	103 ---------	101 ---------	9

Figure 6-25 GE11 Infinite Array ^{157}Gd Worth Mapping

A	B	C	D	E	F	G	H	I	
30 ---------	29 ---------	28 ---------	27 ---------	26 ---------	25 ---------	24 ---------	23 ---------	21 ---------	1
40 ---------	39 ---------	38 -3.0123E-03	37 -2.9993E-03	36 ---------	35 -3.1250E-03	34 -3.1267E-03	33 ---------	31 ---------	2
50 ---------	49 -2.9700E-03	48 -2.4485E-03	47 -2.9018E-03	46 -4.3425E-03	45 -3.9386E-03	44 -2.8075E-03	43 -3.0586E-03	41 ---------	3
60 ---------	59 -3.0602E-03	58 -2.9990E-03	57 -5.2830E-03	56	55	54 -4.0790E-03	53 -3.1568E-03	51 ---------	4
70 ---------	69 ---------	68 -4.3642E-03	67	66	65	64 -4.5328E-03	63 ---------	61 ---------	5
80 ---------	79 -3.0777E-03	78 -3.9329E-03	77	76	75 -5.2902E-03	74 -2.9728E-03	73 -2.9977E-03	71 ---------	6
90 ---------	89 -3.0467E-03	88 -2.8409E-03	87 -3.9192E-03	86 -4.3590E-03	85 -2.9796E-03	84 -2.3670E-03	83 -2.9975E-03	81 ---------	7
100 ---------	99 ---------	98 -3.0577E-03	97 -3.0778E-03	96 ---------	95 -3.0124E-03	94 -2.9172E-03	93 ---------	91 ---------	8
110 ---------	109 ---------	108 ---------	107 ---------	106 ---------	105 ---------	104 ---------	103 ---------	101 ---------	9

Figure 6-26 GE13 Infinite Array ^{157}Gd Worth Mapping

A	B	C	D	E	F	G	H	I	J	
20 ———	19 ———	18 ———	17 ———	16 ———	15 ———	14 ———	13 ———	12 ———	11 ———	1
30 ———	29 ———	28 -2.5465E-03	27 ———	26 -2.3873E-03	25 -2.4431E-03	24 ———	23 -2.6628E-03	22 ———	21 ———	2
40 ———	39 -2.6031E-03	38 -1.9221E-03	37 -2.0113E-03	36 -2.1917E-03	35 -3.0357E-03	34 -3.3329E-03	33 -2.3828E-03	32 -2.7493E-03	31 ———	3
50 ———	49 ———	48 -2.0298E-03	47 -2.1760E-03	46 -3.3988E-03	45	44	43 -3.3755E-03	42 ———	41 ———	4
60 ———	59 -2.4011E-03	58 -2.3277E-03	57 -3.6013E-03	56 ———	55	54	53 -3.0567E-03	52 -2.4269E-03	51 ———	5
70 ———	69 -2.5309E-03	68 -3.1653E-03	67	66	65 ———	64 -3.6893E-03	63 -2.3152E-03	62 -2.4269E-03	61 ———	6
80 ———	79 ———	78 -3.4146E-03	77	76	75 -3.4792E-03	74 -2.1487E-03	73 -2.0281E-03	72 ———	71 ———	7
90 ———	89 -2.6548E-03	88 -2.4165E-03	87 -3.2914E-03	86 -3.0864E-03	85 -2.2811E-03	84 -2.0598E-03	83 -1.9793E-03	82 -2.5112E-03	81 ———	8
100 ———	99 ———	98 -2.5912E-03	97 ———	96 -2.5429E-03	95 -2.3315E-03	94 ———	93 -2.5810E-03	92 ———	91 ———	9
110 ———	109 ———	108 ———	107 ———	106 ———	105 ———	104 ———	103 ———	102 ———	101 ———	10

Figure 6-27 GE12B Infinite Array ^{157}Gd Worth Mapping

A	B	C	D	E	F	G	H	I	J	
20 ———	19 ———	18 ———	17 ———	16 ———	15 ———	14 ———	13 ———	12 ———	11 ———	1
30 ———	29 ———	28 -2.5761E-03	27 ———	26 -2.3813E-03	25 -2.4991E-03	24 ———	23 -2.6644E-03	22 ———	21 ———	2
40 ———	39 -2.6021E-03	38 -1.9106E-03	37 -1.9612E-03	36 -2.2673E-03	35 -3.1841E-03	34 -3.3213E-03	33 -2.3531E-03	32 -2.6903E-03	31 ———	3
50 ———	49 ———	48 -2.1283E-03	47 -2.1858E-03	46 -3.5151E-03	45	44	43 -3.2917E-03	42 ———	41 ———	4
60 ———	59 -2.3882E-03	58 -2.3151E-03	57 -3.7021E-03	56 ———	55	54	53 -3.0332E-03	52 -2.4122E-03	51 ———	5
70 ———	69 -2.5133E-03	68 -3.1680E-03	67	66	65 ———	64 -3.6251E-03	63 -2.3041E-03	62 -2.4122E-03	61 ———	6
80 ———	79 ———	78 -3.3897E-03	77	76	75 -3.5820E-03	74 -2.1583E-03	73 -2.0681E-03	72 ———	71 ———	7
90 ———	89 -2.7234E-03	88 -2.4706E-03	87 -3.4355E-03	86 -3.0918E-03	85 -2.3240E-03	84 -2.0419E-03	83 -1.9794E-03	82 -2.5100E-03	81 ———	8
100 ———	99 ———	98 -2.7003E-03	97 ———	96 -2.5207E-03	95 -2.3675E-03	94 ———	93 -2.5482E-03	92 ———	91 ———	9
110 ———	109 ———	108 ———	107 ———	106 ———	105 ———	104 ———	103 ———	102 ———	101 ———	10

Figure 6-28 GE14C Infinite Array ^{157}Gd Worth Mapping

A	B	C	D	E	F	G	H	I	J	
20 ———	19 ———	18 ———	17 ———	16 ———	15 ———	14 ———	13 ———	12 ———	11 ———	1
30 ———	29 ———	28 -2.5333E-03	27 ———	26 -2.3553E-03	25 -2.4823E-03	24 ———	23 -2.7130E-03	22 ———	21 ———	2
40 ———	39 -2.5707E-03	38 -1.8861E-03	37 -1.9730E-03	36 -2.2319E-03	35 -3.1189E-03	34 -3.3090E-03	33 -2.3501E-03	32 -2.6859E-03	31 ———	3
50 ———	49 ———	48 -1.9881E-03	47 -2.1177E-03	46 -3.4814E-03	45	44	43 -3.3068E-03	42 ———	41 ———	4
60 ———	59 -2.4167E-03	58 -2.3472E-03	57 -3.5194E-03	56 ———	55	54	53 -3.0604E-03	52 -2.5276E-03	51 ———	5
70 ———	69 -2.4851E-03	68 -3.2133E-03	67	66	65 ———	64 -3.6966E-03	63 -2.2915E-03	62 -2.4172E-03	61 ———	6
80 ———	79 ———	78 -3.4220E-03	77	76	75 -3.5775E-03	74 -2.1161E-03	73 -2.0108E-03	72 ———	71 ———	7
90 ———	89 -2.6352E-03	88 -2.3804E-03	87 -3.3465E-03	86 -3.1113E-03	85 -2.3360E-03	84 -2.0473E-03	83 -1.9681E-03	82 -2.5530E-03	81 ———	8
100 ———	99 ———	98 -2.6808E-03	97 ———	96 -2.5302E-03	95 -2.4143E-03	94 ———	93 -2.6357E-03	92 ———	91 ———	9
110 ———	109 ———	108 ———	107 ———	106 ———	105 ———	104 ———	103 ———	102 ———	101 ———	10

Figure 6-29 GE14G Infinite Array ^{157}Gd Worth Mapping

A	B	C	D	E	F	G	H	I	J	
20 ———	19 ———	18 ———	17 ———	16 ———	15 ———	14 ———	13 ———	12 ———	11 ———	1
30 ———	29 -2.3497E-03	28 -2.0903E-03	27 -2.1633E-03	26 -2.2223E-03	25 -2.2335E-03	24 -2.1817E-03	23 -2.1843E-03	22 -2.4803E-03	21 ———	2
40 ———	39 -2.1010E-03	38 -1.7528E-03	37 -1.8877E-03	36 -2.4618E-03	35 -3.1210E-03	34 -2.9431E-03	33 -2.1236E-03	32 -2.1334E-03	31 ———	3
50 ———	49 -2.0438E-03	48 -1.9476E-03	47 -2.8067E-03	46 ———	45	44	43 -3.0692E-03	42 -2.2415E-03	41 ———	4
60 ———	59 -2.1846E-03	58 -2.5770E-03	57 ———	56 ———	55	54	53 -3.1737E-03	52 -2.3137E-03	51 ———	5
70 ———	69 -2.2673E-03	68 -3.2311E-03	67	66	65 ———	64 ———	63 -2.5422E-03	62 -2.2292E-03	61 ———	6
80 ———	79 -2.2135E-03	78 -3.0955E-03	77	76	75 ———	74 -2.8198E-03	73 -1.9589E-03	72 -2.0305E-03	71 ———	7
90 ———	89 -2.1596E-03	88 -2.1021E-03	87 -3.0080E-03	86 -3.2703E-03	85 -2.6442E-03	84 -1.9343E-03	83 -1.7791E-03	82 -2.0626E-03	81 ———	8
100 ———	99 -2.4926E-03	98 -2.1068E-03	97 -2.1311E-03	96 -2.2343E-03	95 -2.1333E-03	94 -2.0724E-03	93 -2.0886E-03	92 -2.4243E-03	91 ———	9
110 ———	109 ———	108 ———	107 ———	106 ———	105 ———	104 ———	103 ———	102 ———	101 ———	10

Figure 6-30 GNF2 Infinite Array ^{157}Gd Worth Mapping

A	B	C	D	E		F	G	H	I	J	
20 ———	19 ———	18 ———	17 ———	16 ———		15 ———	14 ———	13 ———	12 ———	11 ———	1
30 ———	29 -2.4449E-03	28 -2.0876E-03	27 -2.2014E-03	26 -2.8081E-03		25 -2.9282E-03	24 -2.1634E-03	23 -2.1057E-03	22 -2.4897E-03	21 ———	2
40 ———	39 -2.1490E-03	38 -1.7348E-03	37 -2.0007E-03	36 -2.9826E-03		35 -2.9759E-03	34 -2.0402E-03	33 -1.7416E-03	32 -2.1216E-03	31 ———	3
50 ———	49 -2.1526E-03	48 -2.0152E-03	47 -3.0994E-03	46 ———		45 ———	44 -3.0785E-03	43 -2.0140E-03	42 -2.1454E-03	41 ———	4
60 ———	59 -2.7493E-03	58 -3.0040E-03	57 ———	56		55	54 ———	53 -3.0119E-03	52 -2.8843E-03	51 ———	5
70 ———	69 -2.7971E-03	68 -3.0266E-03	67 ———	66		65	64 ———	63 -3.1081E-03	62 -2.8483E-03	61 ———	6
80 ———	79 -2.1103E-03	78 -2.0258E-03	77 -3.0687E-03	76 ———		75 ———	74 -2.9188E-03	73 -2.0434E-03	72 -2.1586E-03	71 ———	7
90 ———	89 -2.0556E-03	88 -1.7211E-03	87 -2.0701E-03	86 -3.0242E-03		85 -3.0050E-03	84 -2.0204E-03	83 -1.7885E-03	82 -2.0458E-03	81 ———	8
100 ———	99 -2.5000E-03	98 -2.1072E-03	97 -2.1369E-03	96 -2.7330E-03		95 -2.6885E-03	94 -2.1292E-03	93 -2.0848E-03	92 -2.4611E-03	91 ———	9
110 ———	109 ———	108 ———	107 ———	106 ———		105 ———	104 ———	103 ———	102 ———	101 ———	10

Figure 6-31 SVEA Infinite Array ^{157}Gd Worth Mapping

6.9.4 Fuel Bundle Lattice Expansion Evaluation

The effect on k_{eff} of increasing the lattice pitch in the fuel bundle is evaluated for a configuration that represents the individual package and package array. The effect is evaluated with and without the normal packing materials. The individual package evaluation is done without BA rods where as the package array evaluation is done with BA rods.

The sensitivity of k_{eff} to changes in lattice pitch is greater for an individual package configuration than for the package array configuration. As the system changes from full leakage in the individual package to no leakage in the infinite page array, the variation in k_{eff} becomes less pronounced or has smaller sensitivity (i.e., lower peaking) over the same range of pitch sizes. As shown in comparing Figure 6-32 to 6-34 or Figure 6-33 to 6-35 for systems with normal packing materials. In addition to the lattice pitch expansion, the difference in sensitivity is also due to the confinement of the lattice expansion to a 50 cm axial length. For the individual package configuration, the expanded lattice accounts for a major portion of the fissions occurring in a fully water reflected system. In the package array configuration, k_{eff} is influenced by the neutron interaction between fuel bundles, where about one fourth of the length (50 cm) is an expanded lattice and the remainder is at nominal pitch.

6.9.4.1 Individual Package

An assessment is done with no burnable absorber rods for the individual package. The optimum k_{eff} occurs in a fuel rod pitch range of 1.9 to 2.3 cm. The optimum pitch corresponds to a packaging dimension that exceeds the dimension of the inner container (Figure 6-32 and 6-33, Tables 6-62 and 6-63). There is no significant effect on the range for optimum pitch due to inclusion of the normal packing material in the individual package. The 10X10 fuel types (GE12B, GE14C, GE14G, GNF2, and SVEA) are the most reactive over the range of lattice expansion. The SVEA, GNF2, and GE14G are the most reactive fuel bundle contents for the individual package.

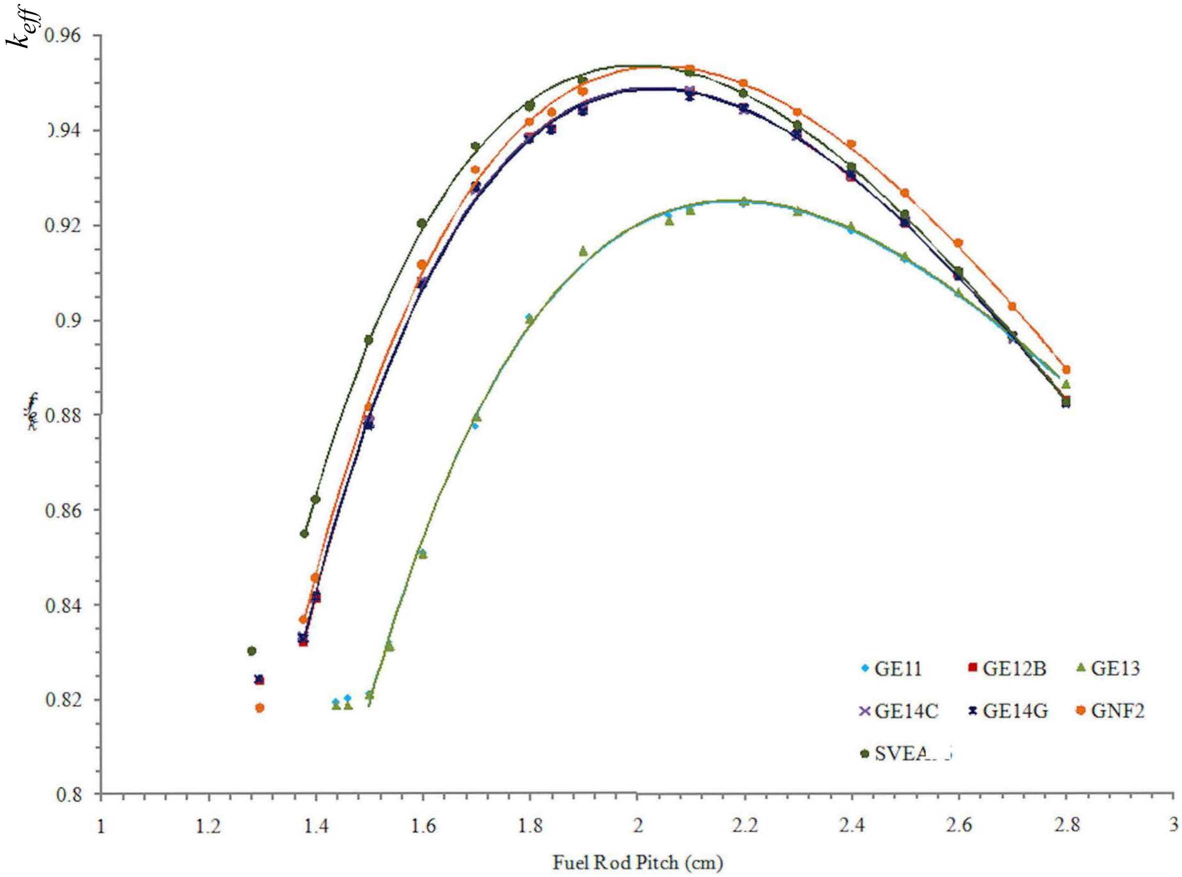

Figure 6-32 Lattice Expansion, Individual Package, without Normal Packing Materials

Table 6-62 Lattice Expansion, Individual Package, without Normal Packing Materials

Fuel Type	GE11		GE12B		GE13		GE14C		GE14G		GNF2		SVEA	
Pitch	k_{eff}	σ	k_{eff}	σ	k_{eff}	σ	k_{eff}	σ	k_{eff}	σ	k_{eff}	σ	k_{eff}	σ
Nominal	0.8195	0.00035	0.8239	0.00038	0.8188	0.00038	0.82447	0.00042	0.8244	0.00038	0.81825	0.00035	0.83026	0.0004
Fuel Channel	0.83223	0.00044	0.83207	0.00035	0.83122	0.00038	0.83322	0.00041	0.83287	0.0004	0.83683	0.00037	0.85492	0.00039
Inner Container	0.92183	0.00037	0.94028	0.00034	0.92069	0.00041	0.94009	0.00041	0.9399	0.00038	0.94373	0.0004	0.94525	0.00033
1.4			0.84136	0.0004			0.84183	0.00044	0.84177	0.00039	0.84553	0.00036	0.86214	0.00042
1.46	0.82043	0.00037			0.81882	0.00034								
1.5	0.82139	0.0004	0.87886	0.00038	0.82107	0.00035	0.8783	0.0004	0.87766	0.00034	0.88167	0.00042	0.89579	0.00035
1.6	0.85092	0.0004	0.9076	0.00049	0.85067	0.0004	0.90794	0.00038	0.90737	0.00039	0.91168	0.00037	0.92024	0.00035
1.7	0.87757	0.0004	0.92775	0.00036	0.87945	0.00037	0.92738	0.00042	0.9279	0.00041	0.93149	0.00043	0.9366	0.00035
1.8	0.90055	0.00035	0.93844	0.00039	0.90006	0.0037	0.93816	0.00047	0.93785	0.00039	0.94164	0.00042	0.94475	0.00035
1.9	0.91429	0.00037	0.94411	0.0004	0.9144	0.00037	0.94439	0.00037	0.94377	0.00039	0.94805	0.00037	0.95022	0.0004
2.1	0.923	0.00036	0.94795	0.00035	0.92287	0.00046	0.94813	0.0004	0.94688	0.0004	0.95271	0.00039	0.95184	0.00043
2.2	0.92426	0.00037	0.94464	0.0004	0.92481	0.00037	0.944	0.00037	0.94448	0.00033	0.94968	0.00036	0.94759	0.00042
2.3	0.92266	0.00037	0.93891	0.00038	0.92268	0.00039	0.93833	0.00035	0.93891	0.00038	0.94347	0.00039	0.9409	0.00039
2.4	0.9187	0.00033	0.92995	0.00033	0.91948	0.00037	0.93006	0.00032	0.93054	0.00033	0.93694	0.00048	0.93218	0.00036
2.5	0.91233	0.00038	0.92022	0.00044	0.9131	0.00047	0.92052	0.00038	0.92029	0.00035	0.92655	0.00032	0.92206	0.0004
2.6	0.90537	0.00045	0.90922	0.00037	0.90559	0.00031	0.9092	0.00036	0.90897	0.00039	0.91587	0.00038	0.91017	0.00035
2.7	0.896	0.00035	0.89648	0.00033	0.89626	0.00039	0.89586	0.00041	0.89622	0.00035	0.90267	0.0004	0.89614	0.00037
2.8	0.88591	0.00032	0.88275	0.00036	0.88606	0.00038	0.88237	0.00031	0.88205	0.00038	0.88913	0.0003	0.8825	0.00033

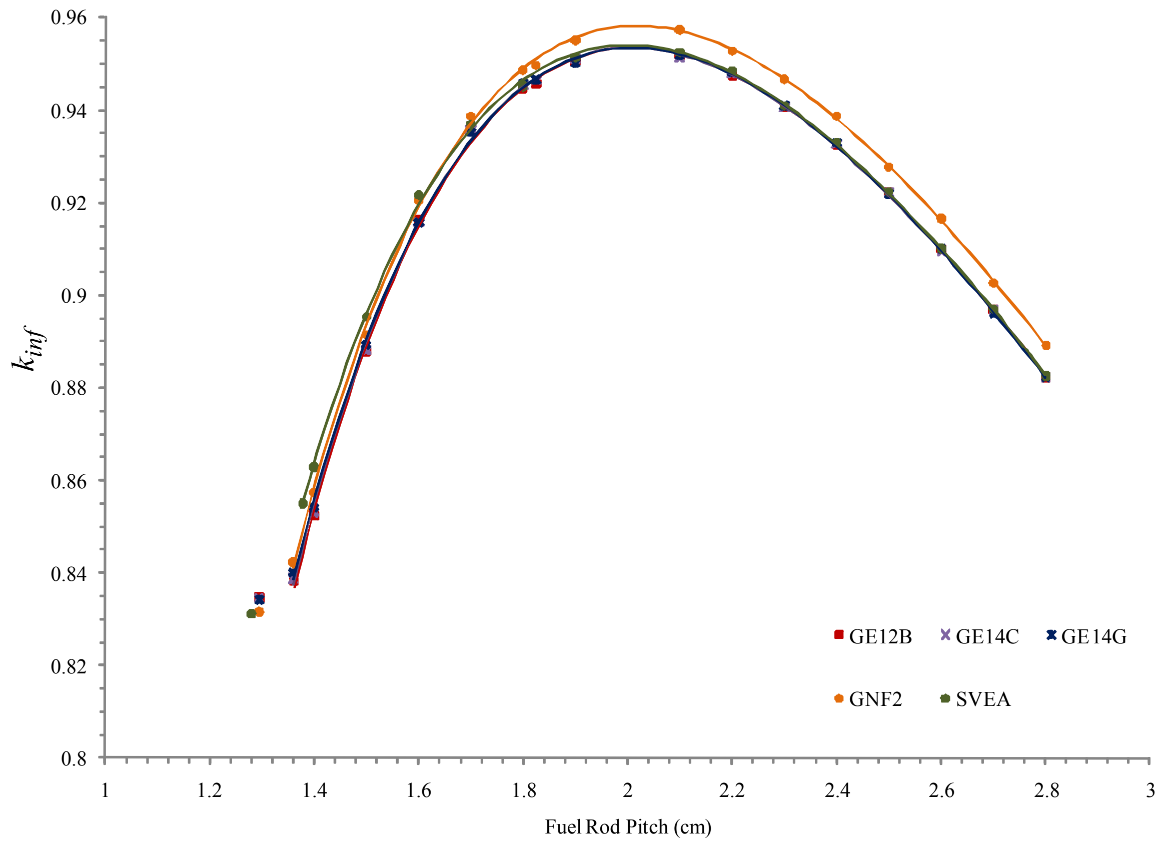

Figure 6-33 Lattice Expansion, Individual Package, with Normal Packing Materials

Table 6-63 Lattice Expansion, Individual Package, with Normal Packing Materials

Fuel Type	GE12B		GE14C		GE14G		GNF2		SVEA	
Pitch	k_{eff}	σ	k_{eff}	σ	k_{eff}	σ	k_{eff}	σ	k_{eff}	σ
Nominal	0.83474	0.00035	0.83477	0.00039	0.83426	0.00035	0.83166	0.00032	0.83121	0.00037
Fuel Channel	0.83817	0.00037	0.83885	0.00037	0.84013	0.00034	0.84232	0.00037	0.85499	0.00038
Inner Container	0.94573	0.00037	0.94631	0.00037	0.9465	0.00037	0.94968	0.00041	0.94491	0.00038
1.4	0.85246	0.00039	0.85318	0.00041	0.85406	0.00037	0.85731	0.0004	0.86285	0.00042
1.5	0.88782	0.00043	0.88819	0.00046	0.88926	0.00039	0.89147	0.0004	0.89524	0.00036
1.6	0.91625	0.00037	0.9158	0.00034	0.91579	0.00043	0.92044	0.00044	0.92157	0.00035
1.7	0.93562	0.00045	0.93568	0.00035	0.93504	0.0004	0.93868	0.00041	0.93685	0.00042
1.8	0.94455	0.00043	0.94523	0.00036	0.94581	0.00042	0.9486	0.00038	0.94541	0.00041
1.9	0.95041	0.00039	0.95099	0.00038	0.94993	0.00043	0.95505	0.00038	0.9512	0.00042
2.1	0.9519	0.00043	0.95132	0.00034	0.95163	0.00033	0.95735	0.00035	0.95232	0.00032
2.2	0.9473	0.00033	0.94782	0.00036	0.94797	0.00032	0.95265	0.00032	0.94839	0.00035
2.3	0.9407	0.00038	0.94047	0.00036	0.94084	0.00037	0.94664	0.00038	0.94095	0.00035
2.4	0.93258	0.00037	0.93266	0.00033	0.93282	0.00034	0.93859	0.00035	0.93298	0.0004
2.5	0.92219	0.00037	0.92208	0.0004	0.92173	0.00035	0.92759	0.00036	0.92226	0.00041
2.6	0.90996	0.00036	0.90953	0.00039	0.91011	0.00035	0.9166	0.00038	0.91008	0.00035
2.7	0.89685	0.00032	0.89687	0.0004	0.89597	0.00034	0.90267	0.00033	0.897	0.00033
2.8	0.88224	0.00039	0.88229	0.00035	0.88226	0.00035	0.88921	0.00036	0.8825	0.00033

6.9.4.2 Package Array

The package array assessment is done with eight, 2 wt% Gd_2O_3 burnable absorber rods in three quadrants. Neutron absorber is most effective at the larger fuel rod pitch and results in the optimum k_{eff} in a fuel rod pitch in a range of 1.5 to 2.0 cm that corresponds to the confinement provided by the inner container (Figures 6-34 and 6-35, Tables 6-64 and 6-65). The presence of BA rod neutron absorber shifts the optimum pitch within the inner container confinement boundaries. The 10X10 fuel types (GE12B, GE14C, GE14G, GNF2, and SVEA) are the most reactive over the range of lattice expansion. The GE and GNF fuel types include more normal packing material than the SVEA, but the SVEA fuel has more moderation with the fuel lattice due to the design of the coolant flow channels within the lattice. These differences result in changes in an increase in k_{eff} for the GE and GNF2 fuel types when the normal packing material is included that is not seen for the SVEA fuel type. The cluster separator packing material is not included when the GE and GNF fuel type contents is shipped as a fuel assembly (fuel bundle with channel installed). SVEA fuel bundles are always shipped with the channel installed. Although there are not large differences in the reactivity of the 10X10 fuel designs, the SVEA, GNF2, and GE14G are the most reactive fuel bundle contents for the package array configuration.

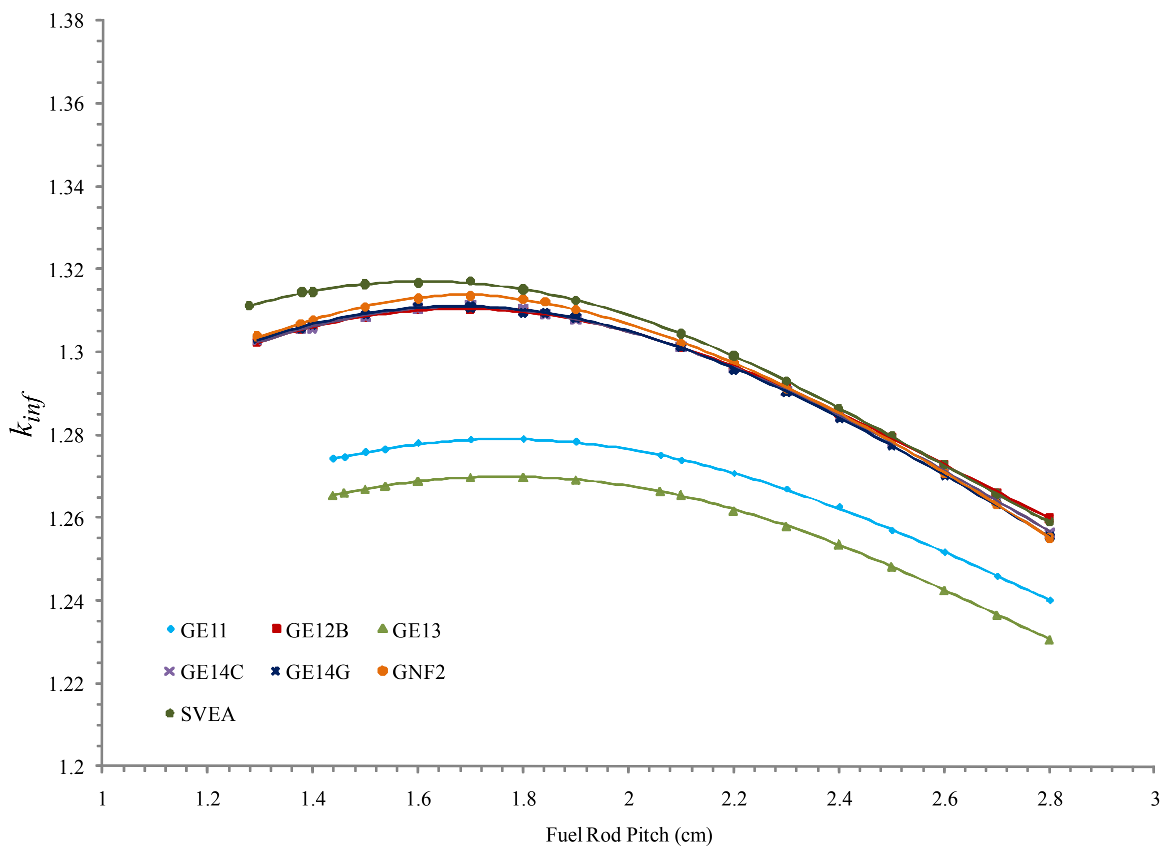

Figure 6-34 Lattice Expansion, Infinite Package Array, without Normal Packing Materials

Table 6-64 Lattice Expansion, Infinite Package Array, without Normal Packing Materials

Fuel Type	GE11		GE12B		GE13		GE14C		GE14G		GNF2		SVEA	
Pitch	k_{inf}	σ	k_{inf}	σ	k_{inf}	σ	k_{inf}	σ	k_{inf}	σ	k_{inf}	σ	k_{inf}	σ
Nominal	1.27444	0.00028	1.30242	0.00031	1.26548	0.00027	1.30279	0.0003	1.30309	0.00028	1.30377	0.00026	1.31122	0.00027
Fuel Channel	1.27663	0.00031	1.30564	0.00027	1.2676	0.00026	1.30577	0.00025	1.30572	0.0003	1.30675	0.00029	1.31454	0.00031
Inner Container	1.27518	0.00027	1.30941	0.00033	1.26639	0.00025	1.30922	0.00027	1.30948	0.0003	1.31218	0.00026	1.3149	0.00028
1.4			1.30623	0.00027			1.30591	0.0003	1.30666	0.00027	1.30784	0.00025	1.31451	0.0003
1.46	1.27468	0.00027			1.26595	0.00028								
1.5	1.27602	0.00031	1.30851	0.00026	1.26692	0.00027	1.30861	0.00026	1.30908	0.00026	1.31089	0.00031	1.31642	0.00027
1.6	1.27807	0.00026	1.31018	0.0003	1.26894	0.00027	1.31061	0.00029	1.31107	0.00026	1.31294	0.0003	1.31668	0.00029
1.7	1.27891	0.00028	1.31038	0.0003	1.26971	0.00027	1.31146	0.00031	1.31094	0.00029	1.31361	0.00029	1.31725	0.00029
1.8	1.27906	0.00028	1.30993	0.00027	1.2697	0.0003	1.31043	0.00029	1.30938	0.00032	1.3127	0.00028	1.31511	0.00026
1.9	1.27835	0.00035	1.30802	0.00029	1.26917	0.00027	1.30783	0.00028	1.30833	0.00027	1.31028	0.00029	1.31256	0.00026
2.1	1.27393	0.00028	1.30116	0.00029	1.26552	0.00028	1.30135	0.0003	1.30126	0.00029	1.30214	0.00029	1.30449	0.00026
2.2	1.27078	0.00026	1.29625	0.00027	1.26171	0.00029	1.29646	0.00029	1.29582	0.0003	1.29739	0.00026	1.29913	0.00027
2.3	1.26693	0.00027	1.29162	0.00026	1.25797	0.00028	1.2906	0.00027	1.29049	0.00026	1.29119	0.00027	1.29288	0.00027
2.4	1.26267	0.00026	1.28522	0.0003	1.25358	0.00029	1.28432	0.00028	1.28409	0.0003	1.28543	0.00026	1.28629	0.00029
2.5	1.2569	0.00029	1.27954	0.00028	1.24822	0.00027	1.27828	0.00026	1.27753	0.00026	1.27854	0.00028	1.27973	0.0003
2.6	1.25169	0.00027	1.27272	0.00027	1.24241	0.00027	1.27112	0.00026	1.27013	0.00029	1.27081	0.00028	1.27294	0.00036
2.7	1.24592	0.00028	1.26587	0.00026	1.23656	0.00026	1.26421	0.00028	1.26322	0.00029	1.26331	0.00027	1.26579	0.00029
2.8	1.24006	0.00028	1.25986	0.00028	1.23057	0.00025	1.25647	0.00032	1.25554	0.00029	1.25512	0.00027	1.25897	0.00026

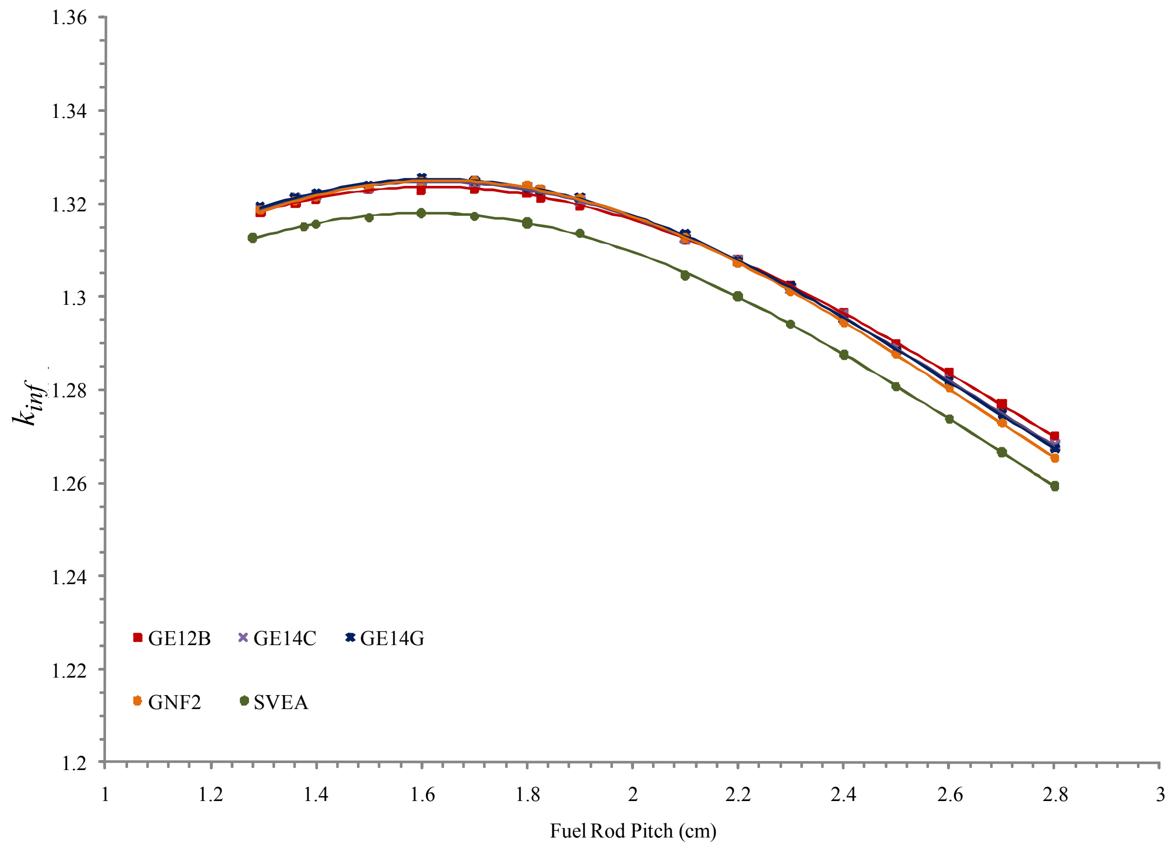

Figure 6-35 Lattice Expansion, Infinite Package Array, with Normal Packing Materials

Table 6-65 Lattice Expansion, Infinite Package Array, with Normal Packing Materials

Fuel Type	GE12B		GE14C		GE14G		GNF2		SVEA	
Pitch	k_{inf}	σ	k_{inf}	σ	k_{inf}	σ	k_{inf}	σ	k_{inf}	σ
Nominal	1.31829	0.00033	1.31883	0.00029	1.31934	0.00028	1.31874	0.00027	1.31264	0.00026
Fuel Channel	1.32024	0.00028	1.3212	0.00029	1.32129	0.00031	1.32057	0.00029	1.31497	0.00028
Inner Container	1.32136	0.00028	1.32279	0.00026	1.32286	0.00027	1.32309	0.00027	1.31604	0.00026
1.4	1.32097	0.00028	1.32175	0.00026	1.32211	0.00027	1.32146	0.00029	1.31555	0.00026
1.5	1.32312	0.00027	1.32341	0.0003	1.32391	0.00031	1.32353	0.0003	1.31703	0.00026
1.6	1.32298	0.00029	1.3246	0.0003	1.32554	0.0003	1.32487	0.00027	1.318	0.00028
1.7	1.32326	0.00027	1.32434	0.00026	1.32489	0.00029	1.32495	0.0003	1.31723	0.00028
1.8	1.32231	0.00029	1.32343	0.00028	1.3233	0.00027	1.3238	0.00027	1.31558	0.00027
1.9	1.31943	0.00027	1.32043	0.00025	1.32117	0.00029	1.32114	0.0003	1.31364	0.00027
2.1	1.31229	0.00028	1.31237	0.00027	1.31355	0.00026	1.31265	0.00028	1.3046	0.0003
2.2	1.30805	0.00026	1.30775	0.00028	1.30762	0.00032	1.30718	0.00027	1.30011	0.00028
2.3	1.30253	0.00026	1.3017	0.00028	1.30223	0.00027	1.30125	0.00028	1.29415	0.00028
2.4	1.29644	0.00028	1.29601	0.00025	1.29514	0.00028	1.29452	0.00027	1.28758	0.00027
2.5	1.28997	0.00026	1.28881	0.00028	1.2884	0.00027	1.2877	0.0003	1.28072	0.00032
2.6	1.28359	0.00031	1.28232	0.00027	1.28204	0.00027	1.28056	0.00027	1.27378	0.00027
2.7	1.27693	0.00025	1.2749	0.00035	1.27484	0.00033	1.27296	0.0003	1.26664	0.0003
2.8	1.27002	0.00032	1.2681	0.00028	1.26743	0.00028	1.26529	0.00027	1.25937	0.00027

6.9.5 Fuel Rod Contents Evaluation

The fuel rod contents are evaluated by calculating an infinite k_{eff} for a range of fuel rod pitches that encompasses peak reactivity to determine a maximum reactivity. The pitch type is defined by triangular configuration to optimize rod stacking. The fuel rod designs are categorized by cylindrical dimensions and evaluated based on category dimensions, as shown in Table 6-66. The longest fuel length of the fuel types per category is used to represent that particular fuel rod category. An optimum configuration of fuel rod pitch and diameter as determined by this evaluation, along with the minimum (PWR_W5) and maximum (PWR_W3) fuel rod categories as based on fuel pellet diameter, are used in the package assessment for transport of fuel rods. The package assessment considers the rod container and pitch type in determining the most reactive configuration for fuel rod transport.

Table 6-66 Fuel Rod Parameters

Fuel Category	Fuel OR	Gap OR	Clad OR	Fuel Length	Fuel Types
BWR_W1	0.424	0.4315	0.492	390	SVEA
BWR_G1	0.478	0.4875	0.599	370.84	GE11, GE13
BWR_G2	0.438	0.447	0.513	405.5	GE12B, GE14C, GE14G
BWR_G3	0.444	0.453	0.513	381	GNF2
PWR_W1	0.4374	0.4463	0.508	365.76	14OFA
PWR_W2	0.4647	0.4742	0.5359	365.76	14STD, 15OFA
PWR_W3	0.4839	0.4928	0.5588	347.218	CE14
PWR_W4	0.4096	0.4178	0.475	381	16STD, CE16 NGF, 17STD
PWR_W5	0.3922	0.4001	0.4572	365.76	16NGF, 17OFA, VV6
PWR_W6	0.4128	0.4216	0.4851	381	CE16NVA
PWR_W7	0.4128	0.4216	0.4851	381	CE16VA, CE16

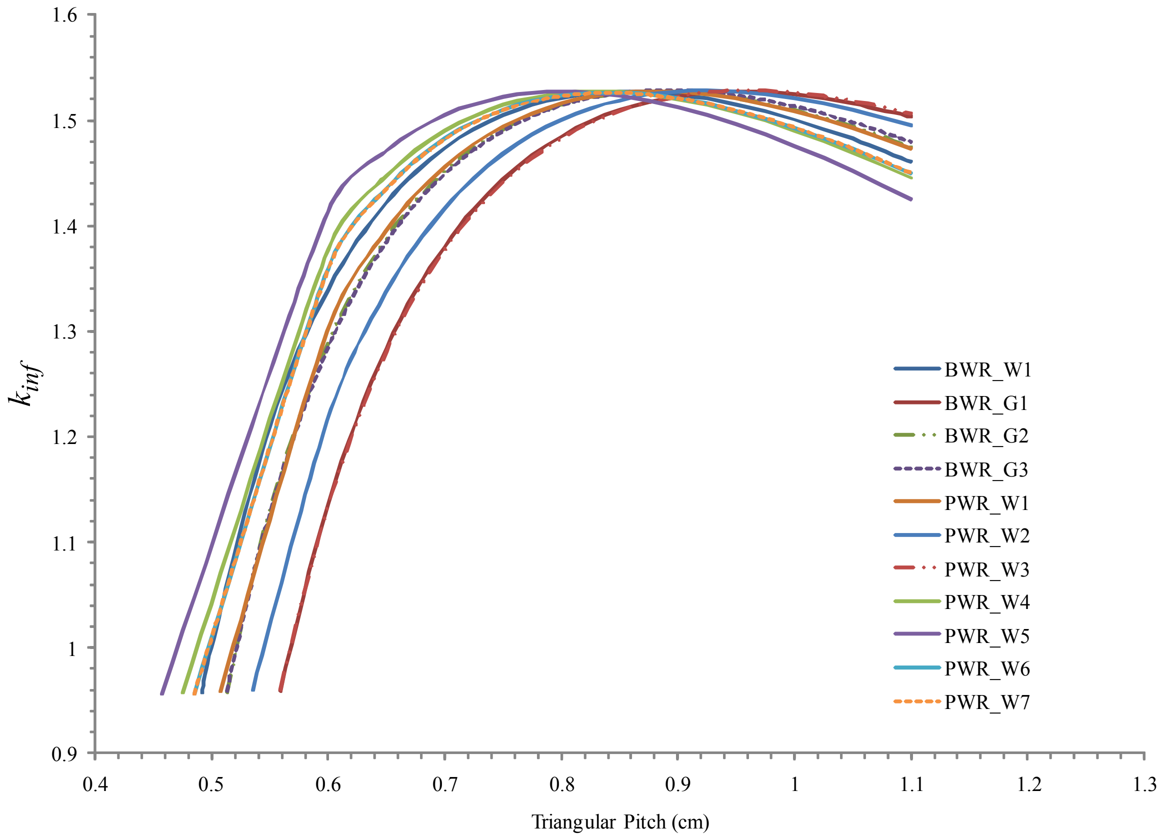

Figure 6-36 Rod Fuel Infinite Array Comparison

Table 6-67 Fuel Rod Infinite Array Comparison (k_{inf})

Fuel Type	BWR_W1	BWR_G1	BWR_G2	BWR_G3	PWR_W1	PWR_W2	PWR_W3	PWR_W4	PWR_W5	PWR_W6	PWR_W7
Rod OR	0.95768	0.95902	0.95792	0.95939	0.9587	0.9602	0.96001	0.95801	0.957	0.95708	0.95684
0.6	1.33954	1.13639	1.28849	1.28455	1.29977	1.2151	1.13445	1.37752	1.41322	1.35947	1.3589
0.65	1.42166	1.28401	1.38782	1.38419	1.39485	1.33633	1.2807	1.44705	1.47046	1.43558	1.43512
0.7	1.47346	1.38005	1.4512	1.4484	1.45572	1.4155	1.37682	1.48985	1.5041	1.48263	1.4823
0.75	1.5047	1.44317	1.49085	1.48906	1.49376	1.46717	1.44055	1.51424	1.52127	1.50999	1.50979
0.8	1.52113	1.48405	1.51385	1.5131	1.51565	1.49976	1.48222	1.52531	1.52641	1.52326	1.52318
0.85	1.52685	1.50908	1.52463	1.52489	1.52563	1.51847	1.5081	1.52624	1.5225	1.52604	1.52608
0.9	1.52411	1.52194	1.52616	1.52738	1.52656	1.52672	1.52182	1.51983	1.51164	1.52083	1.52097
0.95	1.51487	1.52663	1.52052	1.52264	1.52046	1.52689	1.52731	1.50729	1.49537	1.5094	1.50964
1.0	1.5005	1.52387	1.50925	1.51219	1.50882	1.5207	1.52532	1.49006	1.47486	1.49308	1.49341
1.05	1.48206	1.51554	1.49349	1.4972	1.49276	1.50943	1.51771	1.4691	1.45101	1.4729	1.47331
1.1	1.46038	1.50273	1.47415	1.47857	1.47318	1.49408	1.50556	1.4452	1.42456	1.44966	1.45015

6.9.6 Effect of Packaging Materials

The effect of packaging materials is evaluated by calculating the effect that the material has on k_p relative to a reference configuration as follows:

Individual package	Water in all void space and water in regions normally filled with thermal insulator, foam cushion, and impact limiter. Establishes a reference value for k_{eff} that maximizes neutron reflection for the confinement system.
Package array	Void in regions normally filled with thermal insulator, foam cushion, and impact limiter. Water filled in the fuel region. Establish a reference value for k_{eff} for neutron interaction between packages.

For both the individual package and package array the fuel bundle is moderated with full density water and polyethylene representing the cluster separators and plastic sheath is always present in Region 3 for the evaluations.

The packaging configurations are described as follows:

Water	Full density water in all spaces inside packaging that is normally void, thermal insulator, packing material, or impact limiter. Reference package configuration for individual package is described as Water (1,2,3,4)
Void	Void in all spaces inside packaging that is normally thermal insulator, packing material, or impact limiter. Reference package configuration for package array is described as Void (1,2,4).
AlSi (1)	Thermal insulator between the inner and outer walls of the inner container
Poly (2)	Foam cushion is intact and limits the expansion of fuel rods inside the inner container.
Pack Material (3)	Cluster separators and plastic sheath plus the melted foam cushion in the fuel bundle.
Char (4)	Char in regions normally occupied by impact limiter material (balsa wood or cardboard) in the outer container.

The effect of the packaging material is characterized by the statistical error propagation of k_p and σ_p for the configuration as compared to the representative package base case.

6.9.6.1 Individual Package

The effect of the packaging material for an individual package is evaluated using GE14C, GNF2, and SVEA fuel bundle contents without BA rods as this allows the most flexibility for shipment of an individual package. Tables 6-69, 6-70, and 6-71 show the effects of the packaging materials on an individual package for each fuel design with the following packaging material configurations:

AlSi(1), Water (2,3,4)
Poly(2), Water (1,3,4)
Pack Material (3), Water (1,2,4)
Char (4), Water(1,2,3)

The effects of the packaging materials as summarized in Table 6-68 have some dependence on the fuel rod pitch associated with the confinement boundary dimension. All configurations with exception of the foam cushion redistribution to the fuel rod, *Pack Material (3), Water (1,2,4),* result in a decrease in k_p.

Table 6-68 Packaging Material Effects, Individual Package

		Confinement Boundary		
	Packaging Configuration	Nominal	Fuel Channel	Inner Container
Fuel Type	**Material (Region)**	$\Delta k_u(x)$	$\Delta k_u(x)$	$\Delta k_u(x)$
GE14C	AlSi (1) Water (2,3,4)	-0.02812	-0.03203	-0.06007
	Poly (2), Water (1,3,4)	-0.03721	-0.03970	-0.14066
	Pack Material (3), Water (1,2,4)	0.00595	0.00504	0.00375
	Char (4), Water (1,2,3)	-0.00106	-0.00125	-0.00381
CNF2	AlSi (1) Water (2,3,4)	-0.02854	-0.03224	-0.05962
	Poly (2), Water (1,3,4)	-0.03923	-0.04530	-0.14176
	Pack Material (3), Water (1,2,4)	0.00743	0.00407	0.00364
	Char (4), Water (1,2,3)	-0.00055	-0.00127	-0.00265
SVEA	AlSi (1) Water (2,3,4)	-0.03163	-0.03689	-0.06182
	Poly (2), Water (1,3,4)	-0.04375	-0.05134	-0.14096
	Pack Material (3), Water (1,2,4)	0.00643	0.00342	0.00248
	Char (4), Water (1,2,3)	-0.00179	-0.00083	-0.00361
AVERAGE of Fuel Designs	AlSi (1) Water (2,3,4)	-0.02943	-0.03372	-0.06050
	Poly (2), Water (1,3,4)	-0.04006	-0.04545	-0.14113
	Pack Material (3), Water (1,2,4)	0.00660	0.00418	0.00329
	Char (4), Water (1,2,3)	-0.00113	-0.00112	-0.00335

Table 6-69 Packaging Material Effects, Individual Package, GE14C

Packaging Configuration	Confinement Boundary					
	Nominal		Fuel Channel		Inner Container	
Material (Region)	k_{eff}	σ	k_{eff}	σ	k_{eff}	σ
Water (1,2,3,4)	0.80397	0.00041	0.80825	0.00035	0.92011	0.00039
AlSi (1) Water (2,3,4)	0.77532	0.00034	0.77575	0.00031	0.85952	0.00034
Poly (2), Water (1,3,4)	0.76623	0.00034	0.76803	0.00039	0.77892	0.00036
Pack Material (3), Water (1,2,4)	0.80939	0.00033	0.81278	0.00037	0.92333	0.00036
Char (4), Water (1,2,3)	0.80238	0.00034	0.80652	0.00033	0.91578	0.00035

Table 6-70 Packaging Material Effects, Individual Package, GNF2

Packaging Configuration	Confinement Boundary					
	Nominal		Fuel Channel		Inner Container	
Material (Region)	k_{eff}	σ	k_{eff}	σ	k_{eff}	σ
Water (1,2,3,4)	0.80009	0.00032	0.81203	0.0004	0.92442	0.00047
AlSi (1) Water (2,3,4)	0.77108	0.00034	0.7792	0.00043	0.86415	0.00045
Poly (2), Water (1,3,4)	0.76041	0.00032	0.76617	0.00039	0.78207	0.00035
Pack Material (3), Water (1,2,4)	0.80702	0.00039	0.81556	0.00036	0.92742	0.00044
Char (4), Water (1,2,3)	0.79906	0.00036	0.81021	0.00038	0.92119	0.00034

Table 6-71 Packaging Material Effects, Individual Package, SVEA

Packaging Configuration	Confinement Boundary					
	Nominal		Fuel Channel		Inner Container	
Material (Region)	k_{eff}	σ	k_{eff}	σ	k_{eff}	σ
Water (1,2,3,4)	0.80053	0.00038	0.82325	0.00043	0.91905	0.00039
AlSi (1) Water (2,3,4)	0.76838	0.00036	0.7858	0.00036	0.85668	0.00039
Poly (2), Water (1,3,4)	0.75624	0.00039	0.77132	0.0004	0.77753	0.0004
Pack Material (3), Water (1,2,4)	0.80640	0.00041	0.82609	0.00039	0.921	0.00036
Char (4), Water (1,2,3)	0.79819	0.0004	0.82179	0.00046	0.9149	0.00038

6.9.6.2 Package Array

The effect of the packaging material for the package array is evaluated using a GNF2, GE14G, and SVEA fuel bundle contents with BA rods, as this represents the most common configuration for shipment of a package array. Tables 6-73, 6-74, and 6-75 show the effects of the packaging materials on a package array for each fuel design with the following packaging material configurations:

AlSi (1) Void (2,4)
Poly (2), Void (1,4)
Pack Material (3), Void (1,2,4)
Char (4), Void (1,2)

The effects of the packaging materials as summarized in Table 6-72 have some dependence on the fuel rod pitch associated with the confinement boundary dimension. All configurations with exception of the foam cushion redistribution to the fuel rod, *Pack Material (3), Void (1,2,4),* result in a decrease in k_p.

Table 6-72 Packaging Material Effects, Package Array

		Confinement Boundary		
	Packaging Configuration	Nominal	Fuel Channel	Inner Container
Fuel Type	**Material (Region)**	$\Delta k_u(x)$	$\Delta k_u(x)$	$\Delta k_u(x)$
GNF2	AlSi (1) Void (2,4)	-0.00286	-0.00296	-0.00280
	Poly (2), Void (1,4)	-0.01451	-0.01423	-0.01679
	Pack Material (3), Void (1,2,4)	0.00365	0.00328	0.00261
	Char (4), Void (1,2)	-0.00685	-0.00636	-0.00604
GE14G	AlSi (1) Void (2,4)	-0.00295	-0.00285	-0.00194
	Poly (2), Void (1,4)	-0.01380	-0.01271	-0.01425
	Pack Material (3), Void (1,2,4)	0.00441	0.00471	0.00383
	Char (4), Void (1,2)	-0.00651	-0.00624	-0.00519
SVEA	AlSi (1) Void (2,4)	-0.00298	-0.00278	-0.00287
	Poly (2), Void (1,4)	-0.01203	-0.01170	-0.01275
	Pack Material (3), Void (1,2,4)	0.00306	0.00281	0.00285
	Char (4), Void (1,2)	-0.00602	-0.00586	-0.00557
AVERAGE of Fuel Designs	AlSi (1) Void (2,4)	-0.00293	-0.00286	-0.00254
	Poly (2), Void (1,4)	-0.01345	-0.01288	-0.01460
	Pack Material (3), Void (1,2,4)	0.00371	0.00360	0.00310
	Char (4), Void (1,2)	-0.00646	-0.00615	-0.00560

Table 6-73 Packaging Material Effect, Package Array (Infinite), GNF2

Packaging Configuration Material (Region)	Confinement Boundary					
	Nominal		Fuel Channel		Inner Container	
	k_{eff}	σ	k_{eff}	σ	k_{eff}	σ
Void (1,2,4)	1.13173	0.00028	1.13417	0.00026	1.13883	0.00026
AlSi (1) Void (2,4)	1.12846	0.0003	1.13085	0.00025	1.13563	0.0003
Poly (2), Void (1,4)	1.11682	0.00028	1.11954	0.0003	1.12167	0.00027
Pack Material (3), Void (1,2,4)	1.13497	0.0003	1.13709	0.00025	1.14104	0.0003
Char (4), Void (1,2)	1.12448	0.00029	1.12741	0.00031	1.13241	0.00028

Table 6-74 Packaging Material Effect, Package Array (Infinite), GE14G

Packaging Configuration Material (Region)	Confinement Boundary					
	Nominal		Fuel Channel		Inner Container	
	k_{eff}	σ	k_{eff}	σ	k_{eff}	σ
Void (1,2,3,4)	1.12557	0.00027	1.12700	0.00026	1.13012	0.00028
AlSi (1) Void (2,3,4)	1.12221	0.00031	1.12378	0.00026	1.12780	0.00026
Poly (2), Void (1,3,4)	1.11139	0.00027	1.11391	0.00028	1.11548	0.00027
Pack Material (3), Void (1,2,4)	1.12959	0.00028	1.13134	0.00027	1.13357	0.00026
Char (4), Void (1,2,3)	1.11868	0.00027	1.12039	0.00026	1.12453	0.00029

Table 6-75 Packaging Material Effect, Package Array (Infinite), SVEA

Packaging Configuration Material (Region)	Confinement Boundary					
	Nominal		Fuel Channel		Inner Container	
	k_{eff}	σ	k_{eff}	σ	k_{eff}	σ
Void (1,2,3,4)	1.12906	0.0003	1.13163	0.00029	1.1336	0.00028
AlSi (1) Void (2,3,4)	1.12566	0.0003	1.12846	0.00026	1.13035	0.00026
Poly (2), Void (1,3,4)	1.11663	0.00027	1.11952	0.00029	1.12043	0.00031
Pack Material (3), Void (1,2,4)	1.13172	0.00026	1.13402	0.00031	1.13606	0.00027
Char (4), Void (1,2,3)	1.12263	0.00028	1.12535	0.0003	1.12764	0.00027

6.9.6.3 Polyethylene Redistribution Evaluation

When the fuel assembly or fuel bundle is packed into the packaging, the polyethylene packing material such as cluster separators, sheathing/bags, and ethafoam cushioning are used for fuel protection during transport. Placement of additional packing materials is not strictly instructed; therefore movement of packing materials is possible during transport accidents. An evaluation of polyethylene packing materials on the criticality analysis is conducted. The calculation is performed to determine the effect of polyethylene material position variations for a set of damaged packages.

As a result of the fire test of the RAJ-II package, the melting of the fuel assembly packing materials and the cushioning materials within the inner container had been observed [Ref. 10]. Inspection of the contents after cooling had shown melting of the polyethylene parts and attachment of the molten polyethylene on the dummy fuel rods [Ref. 10].

The criticality analysis models are established to follow the melting progress of the polyethylene parts in accordance with temperature rising under the fire test conditions. The process of melting and moving of the polyethylene parts is categorized by two melting stages (Stages 2 and 3) and one normal stage (Stage 1). For each melting stage, two cases are evaluated representing horizontal and vertical positioning of the package. The outside region from the internal wall of the inner container out is the same model for each stage.

For an undamaged package model, the polyethylene materials are assumed to be in original shapes and positions. Therefore Stage 1 represents a before melting state where the normal packing materials are inserted between each row of rods and ethafoam cushioning material is positioned on the IC walls.

As for the damaged package model, several cases are evaluated following the polyethylene material variations as a fire may continually melt the material with progressing presence. The volume of polyethylene to be melted or wrapped on rods is evaluated in two stages. Stage 2 represents an intermediate melting phase, where only the ethafoam cushioning material around the assembly in the IC is fully melted. Stage 3 represents full melt, where all polyethylene materials in the IC including ethafoam cushioning and normal packing materials are fully melted. Based on stage, the volume of melted polyethylene is calculated, defined at the weighted average packing material density of 0.947 g/cm^3. The volume of polyethylene to melt is smeared over the defined IC space (minus the occupying rod space), fully filling a uniform level in the IC.

There are two base cases; one for individual package and one for package array. Base cases for comparison represents the most reactive, damaged fuel contents for HAC, determined by evaluations described in Section 6.6 for package array and Section 6.4 for individual package. The model is the GNF2 fuel bundle with lattice expansion to the inner container for HAC. The package array is 9X9 with moderation maintained in the fuel envelop only and BA rods present in the fuel bundle. The individual package is evaluated with moderation maintained in the fuel envelop only, as a fire is to cause melting of the polyethylene, and inclusion of water would allow resistance to melting. Polyethylene in the fuel bundle is a uniform wrap of the normal packing materials (i.e., cluster separator and sheathing bag) described in Section 6.3.4.1.2 for NCT.

Resulting effects of the polyethylene modeling, including several melting stages and packaging representation, were evaluated for HAC. The largest positive reactivity from any polyethylene redistribution stage is statistically combined as additional uncertainty to the total uncertainty, Δk_u, due to modeling and geometric representations.

The volume of each melting material is calculated and then adjusted to conform to the calculated weighted packing material density of 0.947 g/cm^3. The two melting materials are the ethafoam cushioning and normal packing materials. The ethafoam represents a volume of 53189.6 cm^3 at the specification density of 0.08 g/cm^3, adjusting to the packing material density the volume becomes 4494.51 cm^3. The conversion is calculated by setting the mass of each model equal and solving for the volume at the adjusted density (e.g., $\rho 1 * V_1 = \rho_2 * V_2$, where V_2 is unknown). The normal packing materials is the combination of the sheathing bag and cluster separators, as defined in Table 6-15.

Redistribution Cases

1. Stage 1: normal, before melting model

Representing a normal condition of transport, prior to melting, Stage 1 is modeled with normal packing materials and ethafoam cushioning material in the nominal position. Additionally, the fuel bundle is modeled at the normal pitch without an expanded bottom lattice region. Cluster separators or inserts are placed into the assembly, between the rods at designated positions. For modeling, these pieces are assumed to be uniform polyethylene plates between each row of rods over the effective fuel length. The polyethylene plates are composed of the cluster separators and the sheathing bag, as the bag represents a small fraction of the volume, this allows a simplified model, see Figure 6-37a. For comparison, there are two stage 1 cases; one with the ethafoam is modeled nominally on the IC walls, and one case without ethafoam, since the packaging materials evaluation in Section 6.9.6.1 and 6.9.6.2 showed a negative impact of k_{eff}.

Separator plate thickness calculation is based on an estimated total mass of the cluster separators, as defined in Section 6.3.2.5. The single plate thickness calculated as 0.087cm is distributed over the length of the fuel between each row of rods in the assembly including the outer edge. There are two single plates for each rod cell, hence a total plate thickness 0.174cm between each row of rods and a single plate thickness on the outer edge of the lattice; this results in a conservative overestimation of the polyethylene by approximately 23g. Polyethylene materials properties are defined in Table 6-14.

$$t_{plate} = \frac{M}{\rho \cdot N \cdot m \cdot p \cdot L}$$

where,

t_{plate} = polyethylene plate thickness
M = mass of packing
ρ = density of packing
N = # of rods in a row
m = # of plates (2 per rod cell) = 2N
p = pitch
L = active fuel length

2. Stage 2, ethafoam melt

The inner container ethafoam packaging materials are completely melted for stage 2. Hence ethafoam material nominally positioned on the bottom, four sides and upper lid are accumulated at the bottom part of the inner container, whether the model is oriented vertically or horizontally. The ethafoam volume of 4494.5cm^3 at 0.947 g/ cm^3 is melted for stage 2. Due to melting of material, the fuel assemblies are moved downward and in contact with the bottom wall of the inner container. Therefore, the fully melted material fills part of the assembly and inner container evenly. Fuel rods are now covered with a uniform poly wrap composed of the packing materials, defined by Table 6-14.

For the horizontal model, fuel rods of the bottom row of the assembly are submerged in polyethylene, where the height of the polyethylene is defined by the nominal pitch of the assembly. However, for the expanded lattice the polyethylene fills the first row at the expanded lattice pitch. To calculate the height of the polyethylene in the package, the available space is calculated based on full row heights. The available space is defined by the internal wall of the IC minus any space occupied by fuel bundle components. A volume greater than the polyethylene melt volume is determined, and the next full row height is used to set the polyethylene melt level in the horizontal package. This method allows the inclusion of additional polyethylene; however this is a conservative modeling method. For simpler modeling, the addition of 2395 cm^3 of poly is added to the melt material to fully fill the bottom row of the assembly, and create a uniform polyethylene level in the IC for the height of the first row of rods at the normal pitch, see Figure 6-37b.

For the vertical model, the poly melt height is calculated based on available space within the assembly to match the volume of melted material rounded to the nearest whole number. Hence a height of 22 cm is filled in with polyethylene, with the addition of 116 cm^3 of polyethylene for simpler modeling to the nearest whole number. The model is oriented with the expanded lattice at the bottom, so the polyethylene material fills in the expanded lattice region first, see Figure 6-37b. The expanded lattice represents a more optimal moderator-to-fuel ratio; hence the inclusion of material more moderating than water will have a greater impact on k_{eff}.

For both package orientations, exposed fuel rods are still covered with a uniform poly wrap composed of the normal packing materials, as defined by Table 6-14.

3. Stage 3: full melt

With extended time, the materials are assumed to fully melt and accumulate at the bottom of the inner container, filling a potion of the assembly and uncovering the upper portion of the assembly from any polyethylene. Due to melting of material, the fuel assemblies are moved downward and in contact with the bottom wall of the inner container. Therefore, the fully melted material fills part of the assembly and inner container evenly. Stage 3 is represented by the assembly covered with melted ethafoam and normal packing materials with a combined total volume of 13056.3 cm^3 at weighted packing material density of 0.947g/ cm^3.

For the horizontal model, fuel rods of the bottom two rows of the assembly are submerged in polyethylene, where the height of the polyethylene is defined by the nominal pitch of the assembly. However, for the expanded lattice the polyethylene fills two rows at the expanded lattice pitch. For simpler modeling, the addition of 456 cm^3 of poly is added to the melt material to fully fill two rows of the assembly and create a uniform level in the IC for the height of two rows of rods at the normal pitch, see Figure 6-37c.

For the vertical model, the poly melt height is calculated to match the volume of melted material to the nearest whole number. Hence a height of 63 cm is filled in with polyethylene, with the addition of 146 cm^3 of polyethylene for simpler modeling. The model is oriented with the expanded lattice at the bottom, so the polyethylene material fills in the expanded lattice region first, see Figure 6-37c.

Results of the polyethylene redistribution stages are shown in Table 6-77 for NCT and Table 6-76 for HAC. The Δk_u is the combination of k_{eff} and sigma by the error propagation method. Results show that an increase in hydrogenous material in the lattice expanded region has the greatest impact on k_{eff}, this due to a optimization of the moderator-to-fuel ratio. While increasing the hydrogenous material in the horizontally positioned package has a minimal impact of k_{eff}. The largest positive reactivity from any polyethylene redistribution stage will be added as additional uncertainty due to modeling and geometric representations to the total uncertainty, k_u. For package arrays, the positive impact on k_{eff} due to polyethylene redistribution is 1.87% for NCT and 2.79% for HAC. For the individual package, the positive impact on k_{eff} due to polyethylene redistribution is 1.15% for NCT only, as the HAC moderation shifts in the package the reduction of neutron interaction reduces k_{eff}.

Table 6-76 HAC, Polyethylene Redistribution Comparison

		Fuel Bundle		
Analysis Condition	**Analysis Model**	k_{EFF}	σ	$\Delta k_u(x)$
HAC package array	Full wrap Horizontal / vertical	0.87473	0.00044	–
HAC package array (Intermediate state)	Stage 2: initial melt Horizontal	0.88072	0.00037	0.00656
HAC package array (Intermediate state)	Stage 2: initial melt Vertical	0.88610	0.00042	0.01198
HAC package array (Intermediate state)	Stage 3: full melt Horizontal	0.87410	0.00034	-0.00007
HAC package array (Intermediate state)	Stage 3: full melt Vertical	0.90206	0.00034	0.02789
HAC individual package	Full wrap Horizontal / vertical	0.91476	0.00037	–
HAC individual package (Intermediate state)	Stage 2: initial melt Horizontal	0.75803	0.00036	-0.15621
HAC individual package (Intermediate state)	Stage 2: initial melt Vertical	0.78768	0.00038	-0.12655
HAC individual package (Intermediate state)	Stage 3: full melt Horizontal	0.75752	0.00048	-0.15663
HAC individual package (Intermediate state)	Stage 3: full melt Vertical	0.8366	0.0004	-0.07762

Table 6-77 NCT, Polyethylene Modeling Comparison

		Fuel Bundle		
Analysis Condition	**Analysis Model**	k_p	σ_p	Δk_p
NCT package array	Full wrap Horizontal / vertical	0.82792	0.00036	–
NCT package array	Stage 1: nominal – plates +ethafoam Horizontal / vertical	0.84605	0.00033	0.01862
NCT package array	Stage 1: nominal – plates Horizontal / vertical	0.82581	0.00031	-0.00163
NCT individual package Void	Full wrap Horizontal / vertical	0.53882	0.00028	–
NCT individual package Void	Stage 1: nominal – plates +ethafoam Horizontal / vertical	0.54980	0.00034	0.01142
NCT individual package Void	Stage 1: nominal – plates Horizontal / vertical	0.53801	0.00031	-0.00039

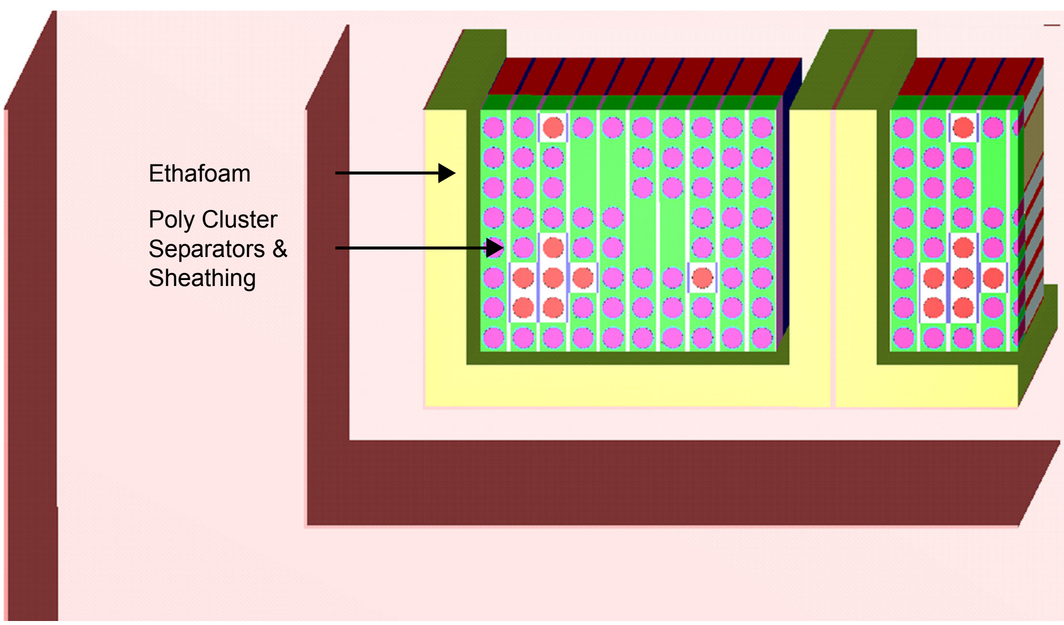

Figure 6-37a Stage 1, NCT

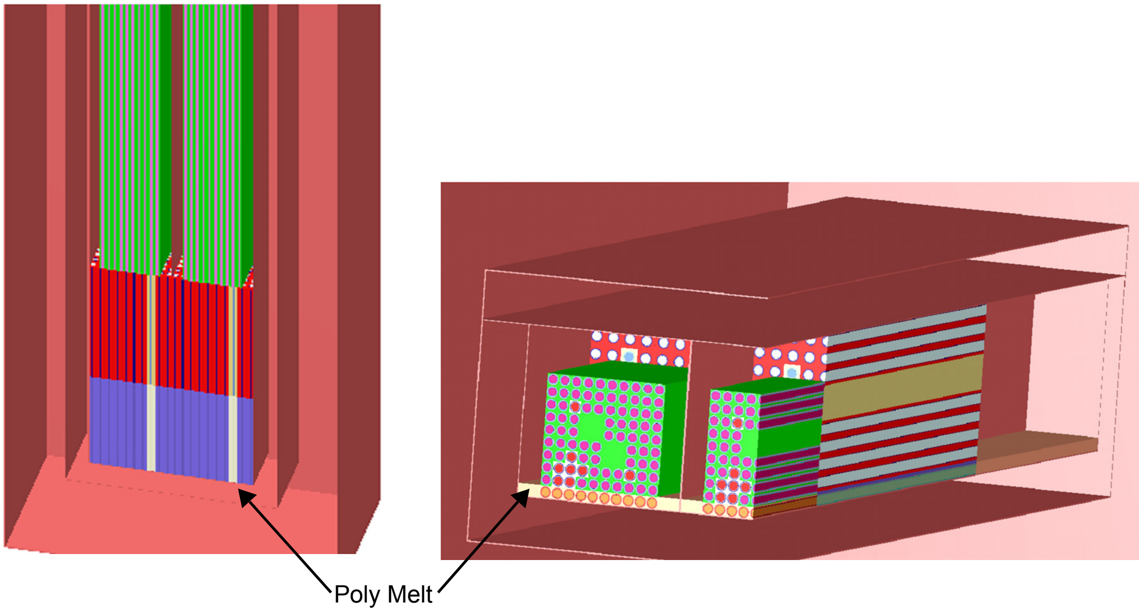

Figure 6-37b Stage 2 Partial Melt, HAC (Left – Vertical, Right – Horizontal)

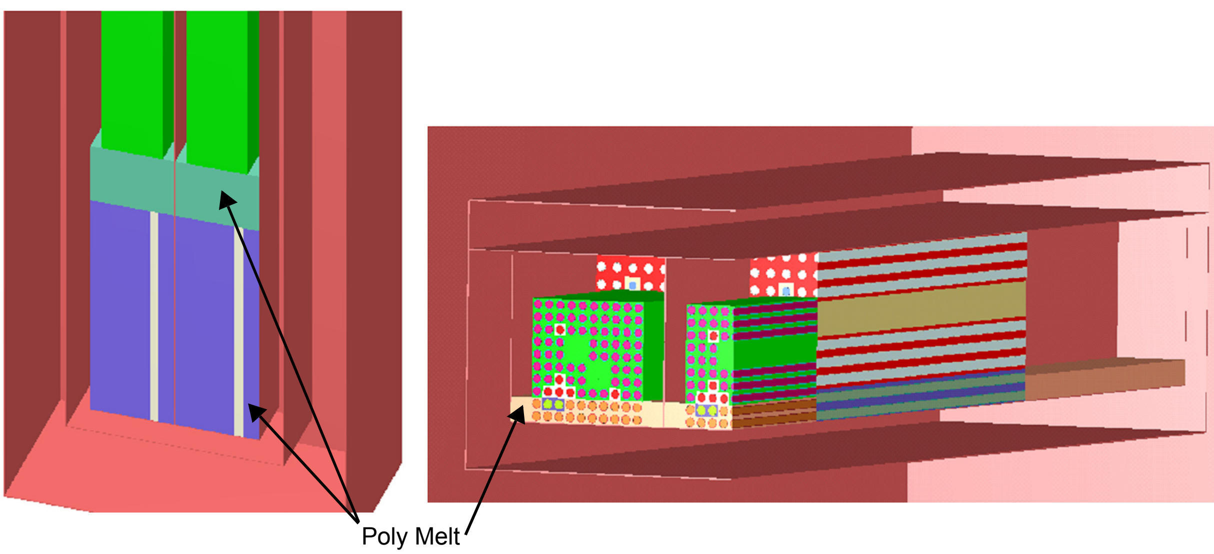

Figure 6-37c Stage 3 Full Melt, HAC (Left – Vertical, Right – Horizontal)

6.9.7 Validation Details

Case No	Case Name	k_{eff}	± s	Enr. (wt%)	Ref.	AEG	EALF(ev)	Pitch (cm)	H_2O/ fuel vol.	H/X	Plate matl.	Boron concen. (wt%)	Plate thick (cm)	No. of holes/ pin	Clad	Assembly separ. (cm)	Dancoff factor
1	ANS33AL1	1.0067	0.0029	4.74	5	199	0.2243	1.35	2.302	138.4	AL	-	.30	-	AL	5.0	0.20091
2	ANS33AL2	1.0168	0.0029	4.74	5	201	0.1913	1.35	2.302	138.4	AL	-	.30	-	AL	2.5	0.20091
3	ANS33AL3	1.0006	0.0029	4.74	5	202.2	0.1721	1.35	2.302	138.4	AL	-	.30	-	AL	10.0	0.20091
8	ANS33SLG	0.9932	0.0029	4.74	5	201	0.1903	1.35	2.302	138.4	-	-	-	-	AL	5.0	0.20091
20	BW1484C1	0.9966	0.0029	2.46		201.3	0.1853	1.636	1.84	204.5	-	-	-	-	AL	1.636	0.190713
21	BW1484C2	0.9983	0.0029	2.46		204.2	0.1466	1.636	1.84	204.5	-	-	-	-	AL	4.908	0.190713
24	BW1484SL	0.9992	0.0029	2.46	6	205	0.1365	1.636	1.841	216.1	-	-	-	-	AL	6.54	0.190713
32	BW1810B	0.9948	0.0029	2.46		198.3	0.2396	1.636	1.84	204.5	-	0.1171	-	0.032	AL	-	0.19044
33	BW1810CR	0.984	0.0029	4.02		194.2	0.3377	1.636	1.84	125.1	-	0.1499	-	0.039	AL	-	0.18662
34	BW1810D	0.9975	0.0005	4.02		194.5	0.3291	1.636	1.84	125.1	-	0.1653	-	0.032	AL	-	0.18662
35	BW1810E	0.9926	0.0029	4.02		194.5	0.3287	1.636	1.84	125.1	-	0.1579	-	0.034	AL	-	0.18662
45	EPRU65	1.0036	0.0029	2.35	7	197.7	0.2483	1.562	1.196	163.6	-	-	-	-	AL	-	0.277268
47	EPRU75	0.9994	0.0029	2.35	7	207.2	0.112	1.905	2.408	329.4	-	-	-	-	AL	-	0.116741
49	EPRU87	1.0027	0.0029	2.35	7	210.8	0.0823	2.210	3.687	504.2	-	-	-	-	AL	-	0.057303
	NC1_K6	0.999	0.013	3.00		2.00E+02	0.203	1.52	1.49	135.7	-	-	-	-	AL		0.243215
	NC10_K6	1.0094	0.0029	3.00		1.98E+02	0.2442	1.52	1.49	135.7	-	-	-	-	AL		0.243215
	NC11_K6	1.0024	0.0029	3.00		1.98E+02	0.2453	1.52	1.49	135.7	-	-	-	-	AL		0.243215
	NC12_K6	0.0125	0.0029	3.00		1.98E+02	0.2269	1.52	1.49	135.7	-	-	-	-	AL		0.243215
	NC13_K6	1.0071	0.0029	3.00		1.99E+02	0.2268	1.52	1.49	135.7	-	-	-	-	AL		0.243215
	NC14_K6	1.0071	0.0029	3.00		1.99E+02	0.2333	1.52	1.49	135.7	-	-	-	-	AL		0.243215
	NC15_K6	0.996	0.016	3.00		1.99E+02	0.2072	1.52	1.49	135.7	-	-	-	-	AL		0.243215
	NC2_K6	1.008	0.014	3.00		2.00E+02	0.2061	1.52	1.49	135.7	-	-	-	-	AL		0.243215
	NC3_K6	0.98	0.013	3.00		2.00E+02	0.2662	1.52	1.49	135.7	-	-	-	-	AL		0.243215
	NC4_K6	0.959	0.014	3.00		1.97E+02	0.2666	1.52	1.49	135.7	-	-	-	-	AL		0.243215
	NC5_K6	0.0966	0.013	3.00		1.97E+02	0.2547	1.52	1.49	135.7	-	-	-	-	AL		0.243215
	NC6_K6	1.0019	0.0029	3.00		1.97E+02	0.2286	1.52	1.49	135.7	-	-	-	-	AL		0.243215

Case No	Case Name	k_{eff}	± s	Enr. (wt%)	Ref.	AEG	EALF(ev)	Pitch (cm)	H_2O/ fuel vol.	H/X	Plate matl.	Boron concen. (wt%)	Plate thick (cm)	No. of holes/ pin	Clad	Assembly separ. (cm)	Dancoff factor
	NC7_K6	1.0008	0.0029	3.00		1.98E+02	0.2327	1.52	1.49	135.7	-	-	-	-	AL		0.243215
	NC8_K6	0.9991	0.0029	3.00		1.99E+02	0.232	1.52	1.49	135.7	-	-	-	-	AL		0.243215
	NC9_K6	1.0138	0.0029	3.00		1.99E+02	0.2428	1.52	1.49	135.7	-	-	-	-	AL		0.243215
54	NSE71SQ	0.9969	0.0053	4.74	8	201.2	0.1879	1.26	1.823	110.0	-	-	-	-	AL	-	0.25704
55	NSE71W1	1.0082	0.0029	4.74	8	198.2	0.2398	1.26	1.823	110.0	-	-	-	.054	AL	-	0.25704
56	NSE71W2	0.9937	0.0051	4.74	8	199.3	0.2183	1.26	1.823	110.0	-	-	-	.152	AL	-	0.25704
	NSE71W2+FOD	1.0563	0.0007	4.74		200.1	0.2056	1.26	1.71	98.4	-	-	-	.152	AL	-	0.262591
	NSE71W2+H2O	1.0139	0.0053	4.74		201.6	0.181	1.26	1.82	105.0	-	-	-	.152	AL	-	0.25704
57	P2438AL	0.9931	0.0029	2.35	9	209.2	0.09545	2.032	2.918	398.7	AL	-	.625	-	AL	8.67	0.08633
58	P2438BA	0.9968	0.0029	2.35	9	208.8	0.09873	2.032	2.918	398.7	B	28.7	.713	-	AL	5.05	0.08633
60	P2438SLG	0.9968	0.0029	2.35	9	209.2	0.09541	2.032	2.918	398.7	-	-	-	-	AL	8.39	0.08633
61	P2438SS	0.9965	0.0029	2.35	9	209.1	0.09625	2.032	2.918	398.7	SS	-	.485	-	AL	6.88	0.25704
63	P2615AL	1.0007	0.0029	4.31	19	207.7	0.1129	2.540	3.883	256.1	AL	-	.625	-	AL	10.72	0.038898
64	P2615BA	1.0016	0.0029	4.31	19	207.6	0.1144	2.540	3.883	256.1	B	28.7	.713	-	AL	6.72	0.038898
68	P2615SS	0.9995	0.0029	4.31	19	207.6	0.1137	2.540	3.883	256.1	SS	-	.485	-	AL	8.58	0.038898
74	P2827SLG	0.985	0.012	2.35	10	209.2	0.09535	2.032	2.918	398.7	-	-	-	-	AL	8.31	0.08633
79	P3314AL	0.9985	0.0029	4.31	11	199	0.2299	1.892	1.60	105.4	AL	-	.625	-	AL	9.04	0.172843
80	P3314BA	1.0004	0.0029	4.31	11	195.1	0.3134	1.892	1.60	105.4	B	28.7	.713	-	AL	4.80	0.172843
81	P3314BC	0.9983	0.0029	4.31	11	202.7	0.1655	1.892	1.60	105.4	B	31.9	.231	-	AL	3.53	0.172843
82	P3314BF1	0.9949	0.0029	4.31	11	197.9	0.251	1.892	1.60	105.4	BF	-	.546	-	AL	3.60	0.172843
83	P3314BF2	0.9965	0.0029	4.31	11	198.5	0.2392	1.892	1.60	105.4	BF	-	.772	-	AL	4.94	0.200956
84	P3314BS1	0.9932	0.0029	2.35	11	198	0.2503	1.684	1.60	218.6	SS	1.1	.298	-	AL	3.86	0.200956
85	P3314BS2	0.9937	0.0029	2.35	11	199	0.2314	1.684	1.60	218.6	SS	1.6	.298	-	AL	3.46	0.200956
86	P3314BS3	0.986	0.017	4.31	11	199.2	0.2274	1.892	1.60	105.4	SS	1.1	.298	-	AL	7.23	0.200956
87	P3314BS4	0.9942	0.0029	4.31	11	196.2	0.2889	1.892	1.60	105.4	SS	1.6	.298	-	AL	6.63	0.200956
96	P3314SLG	0.9928	0.0029	4.31	11	196.2	0.2869	1.892	1.60	105.4	-	-	-	-	AL	10.86	0.172843
97	P3314SS1	0.9895	0.0029	4.31	11	202.1	0.7936	1.892	1.60	105.4	SS	-	.302	-	AL	3.38	0.200956
98	P3314SS2	0.9949	0.0029	4.31	11	202.2	0.1727	1.892	1.60	105.4	SS	-	.302	-	AL	11.55	0.200956

Case No	Case Name	k_{eff}	± s	Enr. (wt%)	Ref.	AEG	EALF(ev)	Pitch (cm)	H_2O/ fuel vol.	H/X	Plate matl.	Boron concen. (wt%)	Plate thick (cm)	No. of holes/ pin	Clad	Assembly separ. (cm)	Dancoff factor
99	P3314SS3	0.9962	0.0029	4.31	11	195.2	0.3122	1.892	1.60	105.4	SS	-	.485	-	AL	4.47	0.200956
100	P3314SS4	1.0054	0.0029	4.31	11	195.4	0.305	1.892	1.60	105.4	SS	-	.485	-	AL	8.36	0.200956
101	P3314SS5	1.004	0.0029	2.35	11	195.4	0.307	1.684	1.60	218.6	SS	-	.302	-	AL	7.80	0.200956
102	P3314SS6	1.0006	0.0029	4.31	11	196.9	0.273	1.892	1.60	105.4	SS	-	.302	-	AL	10.52	0.172843
103	P3314W1	1.0057	0.0056	4.31	11	201.1	0.1941	1.892	1.60	105.4	-	-	-	.149	AL	-	0.172543
104	P3314W2	1.0032	0.0048	2.35		204.1	0.1471	1.684	1.60	185.9	-	-	-	0.051	AL	-	0.201854
138	P3926SL1	0.975	0.015	2.35	12	203.2	0.1576	1.684	1.60	218.6	-	-	-	-	AL	6.59	0.201854
139	P3926SL2	0.995	0.018	4.31	12	197.1	0.2696	1.892	1.60	105.4	-	-	-	-	AL	12.97	0.132077
151	P4267SL1	1.025	0.019	4.31		196.5	0.2819	1.89	1.59	100.9	-	-	-	-	AL	-	0.173697
152	P4267SL2	0.996	0.16	4.31		188.8	0.5186	1.715	1.09	69.1	-	-	-	-	AL	-	0.270303
154	P62FT231	0.9984	0.0029	4.31		193.8	0.3481	1.891	1.59	101.1	B	-	0.683	-	AL	3.824	0.173383
158	P71F214R	1.0049	0.0029	4.31		193.6	0.353	1.891	1.59	101.1	B	-	0.673	-	AL	3.844	0.173383
170	W3269W1	1.0045	0.0054	5.70	15	196	0.2915	1.524	1.495	156.1	-	-	-	-	ZR	-	0.25704
171	W3269W2	1.008	0.0056	5.70		195.6	0.2968	1.4224	1.93	92.6	-	-	-	0.013	SS	-	0.186409

7.0 PACKAGE OPERATIONS

This chapter provides general instructions for loading and unloading and operation of the RAJ-II package. Specific detailed procedures based on and consistent with this application are used for the operation of the package. These procedures are maintained by the user of the package and may provide additional detail regarding the handling and operation of the package. Due to the low specific activity and low abundance of gamma emitting radionuclides, dose rates from the contents of the package when used as a Type A or Type B package are minimal. As a result of the low dose rates, there are no special handling requirements for radiation protection.

7.1 PACKAGE LOADING

This section delineates the procedures for loading a payload into the RAJ-II packaging. Hereafter, reference to specific RAJ-II packaging components may be found in Section 1.3.

7.1.1 Preparation for Loading

Prior to loading the RAJ-II with fuel, the packaging is inspected to ensure that it is in unimpaired physical condition. The inspection looks for damage, dents, corrosion, and missing hardware. Acceptable conditions are defined by the drawings in Section 1.3.2 as described in Section 8.1. Acceptance criteria and detailed loading procedures derived from this application are specified in user written procedures. These user procedures are specific to the authorized content of the package. Since the primary containment is the sealed fuel rod, radiation and contamination surveys are not required prior to loading. There is no required moderator, neutron absorbers or gaskets that require testing or inspection.

Defects that require repair will be fixed prior to shipping in accordance with approved procedures consistent with the quality program.

When used as a Type B package, verification that the primary containment (i.e., fuel rods have been leak checked) will be performed prior to shipping.

7.1.2 Loading of Contents

7.1.2.1 Outer Container Lid Removal

1. Remove the lid bolts.

2. Attach slings to the four lid lift attachment points on the lid.

3. Remove the outer lid.

7.1.2.2 Inner Container Removal

1. Release the inner clamp by removing the eight clamp bolts.

2. Remove the inner container from the outer container, and move it onto the packing table. Ensure that the inner container is lifted using the inner container handles and not the inner container lid handles.

3. Remove the bolts of the inner container lid and take the lid off.

7.1.2.3 Loading Fuel Assemblies into the RAJ-II

1. Clamp the inner container body to the packing table or up righting device, and remove the end lid.

2. Ensure that the following preparation work for packing has been completed if required.

    - The separators have been inserted.
    - The finger spring protectors have been attached.
    - The foam has been put in place.
    - The fuel assemblies have been covered with poly bags.

3. Stand the packing table upright. (The inner container body is fixed with clamps.)

4. Lift one fuel assembly and pack it in the inner container.

5. After packing one fuel assembly into the inner container, fit the securing fixtures of the fuel assembly. Then pack the other fuel assembly in the inner container

6. Lower the packing table back to the horizontal position from the upright position.

7. Attach the end lid of the inner container.

8. Check to ensure that the fuel assemblies are packaged in the container properly.

9. Attach the inner container lid and tighten the bolts securely (wrench tight or as defined in user procedures).

10. Place the inner container into the outer container.

11. Put on hold down clamps and tighten bolts.

12. Place the outer container lid on the package, and tighten the bolts securely (wrench tight or as defined in user procedures).

13. Install tamper-indicating devices on the outer container ends.

7.1.2.4 Loading Loose Rods in the Protective Case into the RAJ-II

1. Insert poly endcap spacers over each end or the fuel rod endcap (optional).
2. Sleeve (optional) each rod to be packed with a maximum of 5 mil polyethylene sleeve/tubing.
3. Insert up to 30, 10x10 design rods, 26, 9x9 design rods or 22, 8x8 design rods into the protective case and fill any empty space with empty tubing.
4. Place cushioning foam pads in protective case as needed to prevent sliding during shipment (optional).
5. Close the protective case and tighten bolts wrench tight.

7.1.2.5 Loading the Protective Case into the RAJ-II

1. Loose rods may be loaded in the protective case while either in the inner container or while removed from the inner container.
2. After packing the protective case(s) into the inner container, fit the securing fixtures for the case.
3. Check to ensure that the protective cases are packaged in the container properly.
4. Attach the inner container lid and tighten the bolts securely (wrench tight or as defined in user procedures).
5. Put on hold down clamps and tighten bolts.
6. Place the outer container lid on the package, and tighten the bolts securely (wrench tight or as defined in user procedures).
7. Install tamper-indicating devices on the outer container ends.
8. It is allowable to ship only one protective case in an RAJ-II inner.

7.1.2.6 Loading Loose Rods in the 5-Inch Stainless Steel Pipe into the RAJ-II

1. Sleeve (optional) each rod to be packed with a maximum of 5 mil polyethylene sleeve/tubing. The ends of the sleeves should be closed in a manner such as knotting or taping with the excess polyethylene trimmed away.
2. Place a cushioning foam pad in the capped end of the pipe (optional).

3. Insert up to 30, 10x10 design rods, 26, 9x9 design rods or 22, 8x8 design rods into the pipe and fill the empty space with empty zircaloy tubing with welded end plugs on both ends.

4. Place cushioning foam pads against the rod ends to block the rods from sliding during shipment (optional).

5. Close pipe with end cap.

6. Lift each 5-inch stainless steel pipe and pack it in the inner container.

7. Check to ensure that the 5-inch stainless steel pipe(s) is packaged in the container properly.

8. Attach the inner container lid and tighten the bolts securely (wrench tight or as defined in user procedures).

9. Place the outer container lid on the package, and tighten the bolts securely (wrench tight or as defined in user procedures).

10. Install tamper-indicating devices on the outer container ends.

11. It is allowable to ship one or two 5-inch pipes containing rods in an RAJ-II inner.

7.1.2.7 Loading Loose Rods (25 Maximum Per Side) into the RAJ-II

1. Sleeve (optional) each rod to be packed with a maximum of 5 mil polyethylene sleeve/tubing. The ends of the sleeves should be closed in a manner such as knotting or taping with the excess polyethylene trimmed away.

2. When only one rod per side is to be packed, no clamps are required. Block the rod in the lower corner of the container by evenly spacing 10 or more notched foam pads the length of the rod.

3. When 2 rods up to a maximum of 25 rods are to be packed, banding with steel clamps is not required for criticality safety purposes. If banding is chosen, position 10 or more open steel clamps evenly in each side of the inner container in which loose rods are place.

4. Place foam pads on top of the open clamps, lay the rods on top of the foam.

5. Close and tighten the clamps so the foam surrounds the array of rods. Tighten each clamp until the foam collapses slightly.

6. Place foam pads against the ends of the rods, above the rods and beside the rods to block the rods from moving during shipment.

7. Repeat the above steps for the other side of the inner container, if required.

8. Fill each side (if used) with foam pads so as to minimize movement during shipment.

9. Attach the inner container lid and tighten the bolts securely (wrench tight or as defined by user procedure).

10. Place the outer container lid on the package, and tighten the bolts securely (wrench tight as defined by user procedure).

11. Install tamper-indicating devices on the outer container ends.

7.1.3 Preparation for Transport

When used as a type B package leak testing of the rods (primary containment) is performed during the manufacturing process. Verification of successful leak testing is done prior to shipment. There are no surface temperature measurements required for this package.

Procedure: (These steps may be performed in any sequence.)

1. Complete the necessary shipping papers in accordance with Subpart C of 49 CFR 172.

2. Ensure that the RAJ-II package markings are in accordance with 10 CFR 71.85(c) and Subpart D of 49 CFR 172. Package labeling shall be in accordance with Subpart E of 49 CFR 172. Package placarding shall be in accordance with Subpart F of 49 CFR 172.

3. Survey the surface of the package for potential contamination and dose rates.

4. Transfer the package to the conveyance and secure using tie-downs secured to the package.

7.2 PACKAGE UNLOADING

7.2.1 Receipt of Package from Carrier

Radiation and contamination surveys are performed upon receipt of the package and the packages are inspected for significant damage. There are no fission gases, coolants or solid contaminants to be removed.

7.2.2 Removal of Contents

After freeing the tie downs, the RAJ-II package is lifted from the carrier either by fork lift or by the use of lifting slings placed around the package. If lifted by forklift, the forks are placed at the designated lift locations and the package is lifted. If slings lift the package, a sling is placed under each end of the package at the lifting angles that prevent the sling from sliding. Care should be taken to ensure that the slings are placed in the correct location depending on whether the package is loaded or empty.

7.2.2.1 Outer Container Lid Removal

1. Remove the lid bolts.
2. Attach slings to the four sling fittings on the lid.
3. Remove the outer lid.

7.2.2.2 Inner Container Removal

1. Release the inner clamp by removing the eight clamp bolts.
2. Remove the inner container from the outer container, and move it onto the packing table. Ensure that the inner container is lifted using the appropriate inner container handles and not the inner container lid handles.
3. Remove the bolts of the inner container lid and take the lid off.

7.2.2.3 Unloading Fuel Assemblies from the RAJ-II

1. Clamp the inner container body to the packing table or up righting device, and remove the end lid.
2. Stand the packing table upright. (The inner container body is fixed with clamps.)
3. Attach the lifting device to the assembly and remove the securing fixture.
4. Lift one fuel assembly at a time from the package.
5. Repeat for other assembly.

7.2.2.4 Removing / Unloading Protective Case or 5-Inch Stainless Steel Pipe from the RAJ-II

1. Remove the outer container and inner container lids as described in Sections 7.2.2.1 and 7.2.2.2.

2. The inner container may be removed or left in place while removing the protective case or 5-inch pipe.

3. Remove the 5-inch stainless steel pipe with a sling or remove the cover from the protective case.

4. Remove the rods from the 5-inch pipe or protective case.

7.3 PREPARATION OF EMPTY PACKAGE FOR TRANSPORT

Empty RAJ-II's are prepared and transported per the requirements of 49 CFR 173.428. Prior to shipping as an empty RAJ-II, the packaging is surveyed to assure that contamination levels are less than the 49 CFR 173.433(a) limit. The RAJ-II is visually verified as being empty. The packaging is inspected to assure that it is in an unimpaired condition and is securely closed so that there will be no leakage of material under conditions normally incident to transportation.

Any labels previously applied in conformance with subpart E of part 172 of this subchapter are removed, obliterated, or covered and the "Empty" label prescribed in 49 CFR 172.450 of this subchapter is affixed to the packaging.

7.4 OTHER OPERATIONS

The following are considered normal routine maintenance items and do not require QA or Engineering evaluation for replacement. Material must be of the same type as original equipment parts.

- Wooden Bolster Assemblies
- Bolster Bolting
- Delrin Inserts
- Polyethylene Container Guides
- Gaskets
- Shock Absorbers (Paper Honeycomb)
- Fork Pocket Rubber Protective Pads
- Outer Container Stopper #2 (Rubber Pad)
- Safety Walk
- Plastic Plugs
- Lid Tightening Bolts (Outer, Inner and End Lid)

- Inner Container End Face Lumber (Upper)
- Inner Container End Face Lumber (Lower “Y” Block)
- Inner Container Polyethylene Foam
- Heliserts

When deviations to items other than those listed above are identified, the RAJ-II shall be removed from service, and the item(s) shall be identified as non-conforming material, and dispositioned in accordance with written procedures including the 10 CFR 71, Subpart H approved QA Plan.

7.5 APPENDIX

No additional information is required. Loading and unloading this package is a relatively simple and routine operation. The weights, contamination levels and radiation dose rates do not impose significant hazards or operations outside normal material handling.

Note: The regulatory provided, such as 49 CFR and 10 CFR, are the current requirements. If regulatory change, the new are applicable. This applies throughout the SAR.

8.0 ACCEPTANCE TESTS AND MAINTENANCE PROGRAM

8.1 ACCEPTANCE TESTS

Per the requirements of subpart G of 10 CFR 71, this section discusses the inspections and tests to be performed prior to first use of the RAJ-II. The RAJ-II is to be manufactured under a Quality Assurance Program meeting the requirements of 10 CFR 71 subpart H and 10 CFR 21.

8.1.1 Visual Inspections and Measurements

Prior to the first use of the RAJ-II for the shipment of licensed material, the RAJ-II will be inspected to ensure that it is conspicuously and durably marked with its model number, serial number, gross weight and package identification number assigned by NRC. Prior to applying the model number, it will be determined that the RAJ-II was fabricated in accordance with the drawings reference in the NRC Certificate of Compliance.

Critical dimensions related to quality are those with tolerances on the drawings called out in Section 1.3.2. Data for these dimensions shall be recorded and verified in accordance with the quality plan. Dimensions are to be taken in an unloaded, horizontal condition. Documentation of these measurements is to be compiled in a data pack. This data pack will be checked for completeness for each RAJ-II as part of the acceptance program. Dimensions without tolerances may vary to ensure form, function and fit by the fabricator.

RAJ-II's are inspected to ensure that there are no missing parts (nuts, bolts, shock absorbers, gaskets, plugs, etc.) or components and that there is no shipping damage on receipt.

The inner and outer container shall be weighed and recorded in the data pack to verify compliance to the maximum weights as called out on the drawings in Section 1.3.2.

8.1.2 Weld Examinations

RAJ-II packaging materials of construction and welds shall be examined in accordance with requirements delineated on the drawings in Section 1.3.2, per the requirements of 10 CFR 71.85(a). This includes 100% VT and liquid penetrant (LP) examination of the horizontal (loaded position – 4 places) lifting lugs and the vertical lifting lugs (2 places) for the inner container, and both outer container sling hold angles (4 places). All such required VT and LP examinations shall occur after the double load test (below).

The non-destructive examination personnel qualification and certification shall be in accordance with either The American Society for Non-destructive Testing (ASNT) SNT-TC-1A (recommended practice) or Japanese Society for Non-destructive Inspection (JSND) Japanese Industrial Standard (JIS) JIS Z 2305 latest revision.

8.1.3 Structural and Pressure Tests

The RAJ-II is not pressurized and is structurally the same as the test units.

All outer and inner containers shall be load tested at twice their maximum design weight. The maximum design weight for the inner container is 992 kg, and that for the outer is 1614 kg. Each shall be tested by an approximately equally distributed weight, and shall be held for a minimum of 2 minutes. Afterwards the affected welds shall have a VT and LP examination, per the above.

The inner container shall be tested horizontally only at the loaded (outside) lifting lugs. The vertical lugs can be tested in either the horizontal position (via hydraulics) or vertically.

The outer container shall be checked by fork lift or other suitable device at the fork lift pockets, and then again via slings at the two sling hold angle positions (three tests total).

Record of load tests and VT and PT examinations shall be in the data packs.

8.1.4 Leakage Tests

No leak tests of the packaging are required. The fuel rod weld joints are examined at the time of fuel fabrication and leak tested to ensure they are sealed. The welding and leak testing of fuel rods is performed during manufacturing using a qualified process. This process assures that the fuel is acceptable for use in a nuclear reactor core and is tightly controlled. The acceptable leak rate is less than 1×10^{-7} atm-cc/s. The inner and outer container are not relied on for containment, and do not require leak testing.

8.1.5 Component and Material Tests

The RAJ-II packaging does not contain gaskets that perform a safety function or pressure boundary, and as such, do not require testing. Neither the inner nor outer container lids are required to provide an air or water tight seal.

The packaging does not contain neutron absorbers that would require testing. No component tests are required.

Material testing or certifications from the suppliers of material for this container must show compliance to the properties found in Tables 2-2 and 2-3, or to other properties that satisfactorily indicate compliance to the properties found in these tables and that are approved by the licensee.

8.1.6 Shielding Tests

The RAJ-II packaging does not contain shielding and therefore shielding tests are not required.

8.1.7 Thermal Tests

The alumina silicate thermal properties will be assured by procuring this material with a certified pedigree that shows compliance to the properties in Table 3-1. This procurement is done consistent with the QA program.

8.1.8 Miscellaneous Tests

There are no additional or miscellaneous tests are required prior to the use of the RAJ-II packaging.

8.2 MAINTENANCE PROGRAM

8.2.1 Structural and Pressure Tests

Prior to each use of the RAJ-II, the packaging is visually inspected to assure that the packaging is not damaged and that the components parts are in place. The containers are constructed primarily from stainless steel making it corrosion resistant. Since the packaging is not relied on for containment, there are no pressure test requirements for the inner or outer containers that comprise the packaging. When used as a Type B package, each fuel rod is leak checked and the successful results of the test are checked before shipment.

The RAJ-II packaging is maintained consistent with a 10 CFR 71 subpart H QA program. Containers that do not conform to the license drawings are removed from service until they are brought back into compliance. Repairs are performed in accordance with the approved procedures and consistent with the quality assurance program.

Leakage Tests

Containment is provided by the fuel rod for Type B shipments. Each loaded fuel rod is leak checked to assure that the rod is leak tight. Neither the inner or outer container is credited with providing leak protection. Therefore, no leak test of the packaging is required.

8.2.2 Component and Material Tests

There are no prescribed component tests or replacement requirements for this packaging. The packaging does not use neutron absorbers or shielding that would require testing or maintenance. Replacement parts shall meet the requirements in Table 2-3 by either testing or certifications from suppliers. The compressive strength of any replacement balsa wood shall be no less than 10.8MPa, and the compressive strength of any replacement foam polyethylene shall be no greater than +/-25% from nominal. The density of the paper honeycomb shall be no greater than +/- 25% from nominal. The density of the foam polyethylene shall be no greater than +10/-25% from nominal.

8.2.3 Thermal Tests

The alumina silicate thermal material is sealed within the stainless steel plates of the container wall. The packaging is visually inspected prior to use to assure that the alumina silicate is contained. No thermal testing is required.

8.2.4 Miscellaneous Tests

There are no additional or miscellaneous tests are required for the use of this packaging. The RAJ-II packaging is inspected prior to each use and maintained consistent with the license drawings. The package is inspected to verify that there are no missing parts or handling damage prior to shipping. As noted on the drawings localized deformation in the shell is permitted up to 25.4 mm and the lids of both containers need not provide an air tight seal. The packaging is repaired in accordance with drawings found in Section 1.3.2 under a Quality Assurance Program meeting 10 CFR 71 subpart H. Rework does not need to meet the 10CFR71 requirement, as long as any replacement parts meet the requirements in Table 2-3.

Foam cushioning material may have up to 5% of the total volume removed for packing purposes, handling or as a result of tears or punctures to the foam.

Small dents, tears and rounding (or damage) of corners on paper honeycomb are acceptable providing the volume of material missing or damaged is less than 10% for the individual piece.

8.3 APPENDIX

No appendix for this section.